POLITECNICO DI MILANO

School of Industrial and Information Engineering
Master of Science Degree in Mechanical Engineering

Numerical Simulation of the Span-wise Coherence of Aerodynamic Forces for a Long-Span Bridge under Turbulent Wind Action

Supervisor:
Prof. Daniele ROCCHI

Co-Supervisor:
Prof. Tommaso ARGENTINI

Dissertation of:

Francesco CORDARO 881430

Academic Year 2019 –2020

Politecnico di Milano:
www.polimi.it

Scuola di Ingegneria Industriale e dell'Informazione:
www.ingindinf.polimi.it

E come il vento
odo stormir tra queste piante, io quello
infinito silenzio a questa voce
vo comparando:
e mi sovvien l'eterno,
e le morte stagioni, e la presente
e viva, e il suon di lei.
Così tra questa
immensità s'annega il pensier mio:
e il naufragar m'è dolce in questo mare.

Contents

List of Figures

List of Tables

Abstract

The wind induced loads caused by the buffeting actions of the turbulent wind on long-span bridges are the object of this thesis, in particular the Braila bridge, which is under construction in Romania. Starting from a *Fourier Transform* (FFT) frequency domain approach, it has been developed a numerical model that works by means of *Power Spectral density* (PSD), both for the generation of the PSD of the lagrangian component of the wind (Input), and the PSD of the response of bridge deck itself (Output).

In previous years different researchers in the world have pointed out that the computation of the buffeting forces considering the *strip assumption* provides an important underestimation of these forces. The current buffeting theory based on the *strip* assumption did not suffice to represent the measured wind loading. A review of the models available in literature of span-wise coherence of the aerodynamic forces is provided in chapter 2.

At this point, it has been introduced in this frequency representation the span - wise coherence of the buffeting forces based on adapted models of Larose G. and Jakobsen J. The response of the Braila bridge deck, considering its first thirteen vibration modes, has been compared to the recorrelated case computed with both the models in chapter 3 for three different mean-wind velocities (U = 20 m/s, 50m/s, 65 m/s).

In the end of this work, considerations about how to consider the recorrelation of the buffeting forces in the bridge deck response without computing the span-wise coherence have been made for each wind velocity.

Sommario

I carichi aerodinamici causati dall'azione turbolenta del vento su ponti di lunghezze elevate sono oggetto dello studio fatto in questa tesi. Nello specifico verrà trattato il caso del ponte Braila che è in costruzione in Romania.

Partendo da un approccio in frequenza che usa le trasformate di $Fourier$, è stato sviluppato un programma che lavora mediante densità di potenza spettrale (PSD). Tale approccio è stato seguito sia per la creazione della PSD della lagrangiana del vento in ingresso (Input), che per il calcolo della risposta del deck del ponte Braila in forma di PSD (Output).

Negli anni passati molteplici studiosi hanno evidenziato come il calcolo delle forze indotte dalla turbolenza ($buffeting$) mediante la $strip\ assumption$ causi una importante sottostima di tali forze. Per tale motivo questa assunzione in molti casi non è adeguata per il calcolo di questi contributi.

Una revisione dei modelli di ricorrelazione presenti nella letteratura scientifica è presente nel capitolo 2.

A questo punto è stata introdotta nel modello numerico che fa uso di PSD la ricorrelazione delle forze aerodinamiche, adattando i modelli di Larose G. e Jakobsen J. mediante fitting numerico e processo di adimensionalizzazione.

La risposta del deck del ponte Braila tenendo in considerazione i suoi primi tredici modi di vibrare è stata confrontata con quella calcolata mediante i modelli di ricorrelazione nel capitolo 3 per tre differenti velocità medie del vento ($U = 20m/s$, $50m/s$, $65m/s$).

Alla fine di questo lavoro sono state fatte considerazione su come tenere conto della ricorrelazione numerica delle forze di $buffeting$, considerando un numero di sezioni ridotto rispetto al caso originale.

Introduction

The phenomena concerning wind loads on structures are very complex due to the difficulty in describing the wind itself and the modeling of such structures.
In this work I will only deal with one type of structure: namely the long span Bridges, specifically the Braila bridge, which is still under construction in Romania (1974 m).

Figure 1: 3D Rendering of the Braila Bridge

The Brăila Bridge is a long span suspension bridge that is under construction over the Danube river, between Brăila, a city in the east of Romania, and the opposite bank of the river in Tulcea County. It will be the fourth bridge over the Romanian coast of the river. It will improve the road traffic accessibility and connection to Moldova.
Bridges, in particular large ones, such as Braila have the function of connecting very distant territories. All this has side effects, the greater the distance they connect, the more their stiffness decreases, the natural frequencies become smaller and smaller and consequently more easily excitable by the turbulence of the wind. The interaction between wind and structure can cause very intense vibrations, which can affect the fatigue life of the structure. For this reason it is necessary to have the contributions of stiffness, damping of the wind on its side, in order to avoid problems related to comfort, in the case of intense wind when crossing the bridge, or in the most serious cases real phenomena of instability that can lead to the collapse of the structure itself, as happened with the Takoma bridge.

In addition to these dynamic instability phenomena, these structures must also be able to withstand static loads due to traffic, railways and pedestrians. In this study I will focus on the problems inherent in the action of the wind.
What is the complexity of the wind due to? The wind represents a random completion phenomenon, describable only through statistical parameters.
Geography of the territory, seasons and climatic events associated with them, the buildings present or not present and their dimensions influence the wind measurements, and connected to these, the feasibility study for the construction of a structure.
The analysis of these problems is very relevant both in the design phase and in the various construction phases. The study of the problems related to wind loads on a bridge is articulated both in numerical and experimental fields, in order to have a validation of the numerical model itself, starting from the study of what has been done previously in scientific literature. The experimental part is related to the construction of scale models of the whole bridge or the bridge deck.
These models are created in order to identify the frequencies and modes of vibration and to study the interaction between wind and structure in a controlled wind tunnel environment.
The numerical part can be divided into two macro-areas:

1. Modeling by means of FEM softwares of the bridge structure, of the modes and of the vibration frequencies

2. Simulation of the wind action on the structure and calculation of the response

Numerical models for the buffeting analysis of long-span bridges can be developed in the time and frequency domains. Over time, the models are capable of modeling at best the non-linearities that have an interaction between fluid and structure, but they are very often heavier from the computational point of view. Frequency models are linear models, but they are numerically more fluid, but this depends on the frequency resolution used.

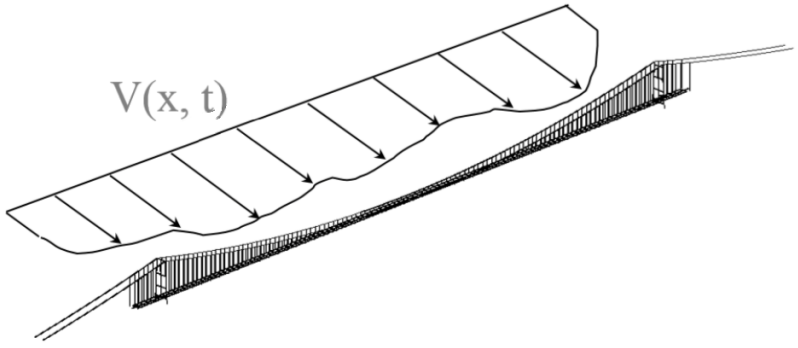

Figure 2: Wind action on a long span bridge

In both cases, the definition of this numerical procedure is quite complex as the aerodynamic forces depend on both the angle of incidence and the reduced speed. These functions vary from bridge to bridge and from the precise conditions of the

site, therefore they must be appropriately identified in wind tunnel.
In the absence of such data, reference is made to the literature, specifically to Davenport for the Admittance Function and the Quasi Steady theory for the flutter derivatives. In this study I will consider only the deck of the Braila bridge, as this is the part most subjected to the action of the wind and specifically the first thirteen modes of vibration will be considered, as they are in the frequency range easily excitable by the action of the wind.
The deck was initially divided into 82 sections, to then consider an increasingly higher number, until obtaining the number of convergent sections, that is, the one for which a further increase always leads to the same response. The bridge, as we well know, is a continuum, but from the numerical point of view it can only be represented as divided into a limited number of sections. For each section, the response to the incoming wind action was calculated, understood as aerodynamic forces. The response of each section correlates with that of the near or distant parts in a different way.
The calculations of bridge buffeting, both in frequency and in time domain, are usually made by means of the strip assumptions, but this assumption is valid only when the incident gusts have much larger scales than the characteristic length of the bridge deck. Based on the strip assumption the coherence among the span of the bridge of the aerodynamic forces can be be represented by the one of the incident wind fluctuations.
Over the years, various researchers have highlighted how the response of the bridge is more correlated with respect to the action of the incoming wind. In order to study this effect, two experimental re-circulation models of Prof. Larose G. [1] and Prof. Jakobsen J. [2] have been adapted, through appropriate fitting and numerical adimensional analysis.
In the final chapter a comparison was made between the two models, which in any case led to a more recurrent response than that of the incoming turbulence.
In addition it has been found the number of sections into divide the Braila bridge deck which is equivalent to implementing the coherence of the two models in the numerical representation.

In order to make the computational part more fluid, starting from a model that works in Fourier transform, I developed one for wind generation and the calculation of the response that works in PSD and this has led to a considerable increase of the computational efficiency.
In order to validate the code that uses the PSDs, the results have been compared with the one that uses the FFTs, already previously validated by wind tunnel testing. Essentially as we expected, using the same frequency resolution both give the same results.

Chapter 1

Numerical Power Spectral Density model

1.1 Introduction

In annex A is described all the theoretical background in order to be able to understand and properly describe the problem of computing the Braila deck response. Starting from this it is necessary to know how the wind generation has been performed, as well as the Braila bridge deck response. I have followed a frequency domain approach in both the cases, in particular using *power spectral densities*. Starting from a code that works by means of $Fourier\ transform$, I have built up a new one that works in PSD and I obtained the subsequent advantages:

1. I have decreased the computational time.

2. The wind generation and the deck's response computation are characterized by the same frequency resolution.

Starting from this, I have implemented in the code the span-wise coherence function for both Larose G. [1] model and Jakobsen J. one [2].

1.2 Response in frequency domain

In annex A, I have described how the aerodynamic forces can be translated in the equivalent stiffness $[K_{aero}]$ and damping $[R_{aero}]$ matrices for a generic deck section and how the buffeting forces $\underline{F}_{buff}$ can be described as function of the wind turbulence. At the beginning the aerodynamic forces are obtained in time domain, then it is convenient to linearise them and solve the problem in frequency domain.

The advantages of the frequency approach are many:

- The computations are performed in a easier way and it doesn't require numerical integration.

- The frequency approach is well appropriated for the determination of extreme responses.

- The characteristics of the the turbulence and deck's transfer function are more suitable to be reported in the frequency domain.

When the wind is generated and the response of the bridge is computed, this is performed on a certain range of frequencies. In my work I have taken into the frequency range f = 0 - 0.4 Hz that covers all the first thirteen vibration modes of Braila bridge deck. Being $[K_{aero}]$, $[R_{aero}]$ and $[A_m]$ function of the reduced frequency f^*, at each step Δf of the frequency vector, all these matrices need to be updated.

1.2.1 Frequency Response function (FRF)

In order to characterize the aerodynamic problem in frequency, we consider for simplicity an harmonic excitation:

$$[M_s]\underline{\ddot{X}} + [R_s + R_{aero}]\underline{\dot{X}} + [K_s + K_{aero}]\underline{X} = \underline{F}e^{i\omega t} \tag{1.1}$$

We consider a solution that has the shape of the excitation (steady state solution):

$$\underline{X}(t) = [H(\omega)]\underline{F}e^{i\omega t} \tag{1.2}$$

Substituting equation 1.2 in 1.1 we have:

$$-\omega^2[M_s][H(\omega)]\underline{F}e^{i\omega t} + i\omega[R_s + R_{aero}][H(\omega)]\underline{F}e^{i\omega t} + [K_s + K_{aero}][H(\omega)]\underline{F}e^{i\omega t} = \underline{F}e^{i\omega t} \tag{1.3}$$

If we isolate in this expression $[H(\omega)]$ we have the complex transfer function, also called *Frequency Response Function* (FRF), between the buffeting force $\underline{F}_{buff}(f)$ and the deck response $\underline{\tilde{X}}(f)$:

$$[H(\omega)] = (-\omega^2[M_s] + i\omega[R_s + R_{aero}(f^*)] + [K_s + K_{aero}(f^*)])^{-1} \tag{1.4}$$

The frequency response function (FRF) is the one that allows to pass from the input $\underline{F}_{buff}$ to the output $\underline{\tilde{X}}(f)$ accordind to:

$$\underline{\tilde{X}}(f) = [H(f)]\underline{F}_{buff}(f) \tag{1.5}$$

Solving the equation 1.5 on the whole frequency range, for each frequency step Δf, it is possible to compute the response of the deck. The matrix inversion in equation 1.4 must be computed at every frequency step Δf. The computation cost of the determination of the FRF rises increasing the number of modes that we are considering.

1.2.2 PSD of the Lagrangian of the Wind

In order to generate the input for study the response of the Braila bridge deck, it has been followed a sectional approach. In this sectional approach the deck that is phisically a continous element has been been divided in sections of equal length (figure 1.1).

For each part the wind has been generated. In my numerical model the wind sections coincide with Braila bridge deck ones.

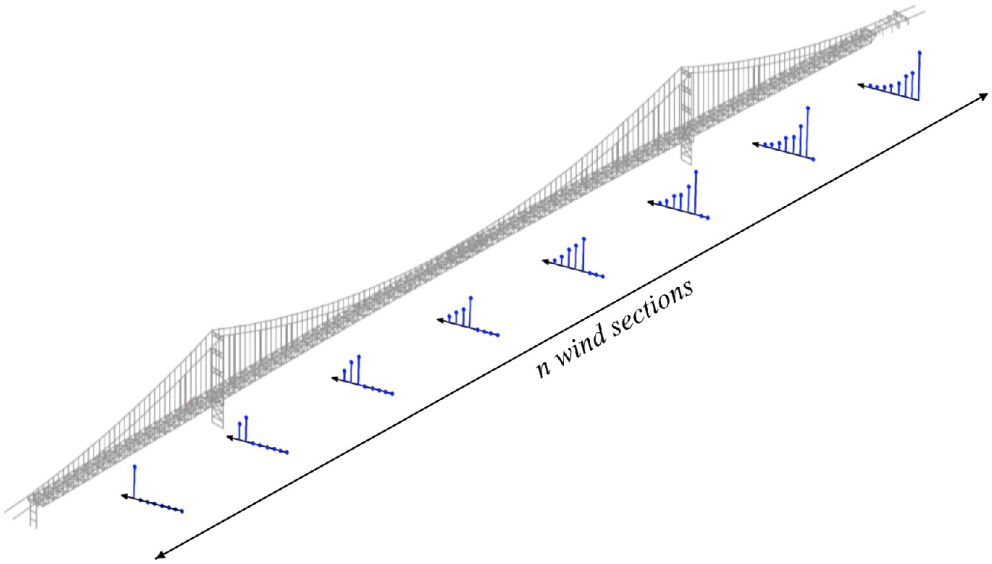

Figure 1.1: Braila bridge deck model divided in sections of equal length

The adopted reference system and the position of sections S_2, S_3 and S_4, whose response will be highlighted in chapter 3 is defined in figure 1.2 and table 1.1.

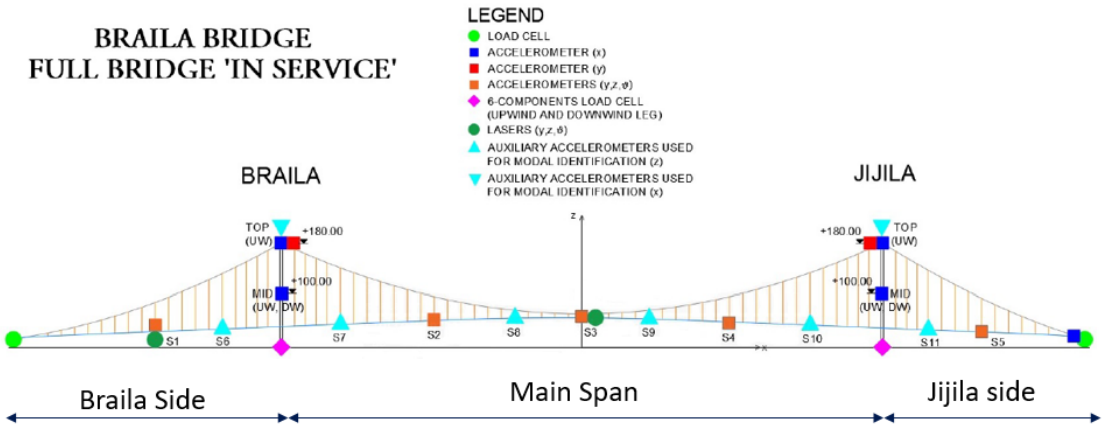

Figure 1.2: Braila bridge reference system with the Cobra probes location

Table 1.1: Braila bridge position of sections $S2$, $S3$ and $S4$

	Position	Length	Reference Length
Main span	Center	1.120 m	1.120 m
Braila side	Left side	489.65 m	489.65 m
Jijila side	Right Side	364.65 m	364.65 m
S2	$\frac{1}{4}$ main span	769.65 m	- 280.35 m
S3	$\frac{1}{2}$ main span	1049.65 m	- 0.3 m
S4	$\frac{3}{4}$ main span	1329.65 m	279.7 m

As I have already mentioned above, the numerical model works in frequency domain, in particular by means of PSD approach. Now I want to enter in details about the generation of the PSD of the Lagrangian of the generated wind. The admittance function is defined by means of Davenport [3] [4] approach in this way and it changes for each frequency step Δf and for each section in which the deck of the Braila bridge is divided. It assumes this form:

$$[A_m(f)] == \frac{1}{2}\rho V^2 BL \begin{bmatrix} Am_{Du} & Am_{Dw} \\ Am_{Lu} & Am_{Lw} \\ Am_{Mu}B & Am_{Mw}B \end{bmatrix} \tag{1.6}$$

Knowing this, it is necessary to define the matrix of the spectra of the generated wind that for two sections at a distance Δy:

$$[S(f)] = \begin{bmatrix} S_{uu}^{ii}(f) & S_{uw}^{ii}(f) & S_{uu}^{ij}(f) & S_{uw}^{ij}(f) \\ S_{uw}^{ii}(f) & S_{ww}^{ii}(f) & S_{uw}^{ij}(f) & S_{ww}^{ij}(f) \\ S_{uu}^{ij}(f) & S_{uw}^{ij}(f) & S_{uu}^{jj}(f) & S_{uw}^{jj}(f) \\ S_{uw}^{ij}(f) & S_{ww}^{ij}(f) & S_{uw}^{jj}(f) & S_{ww}^{jj}(f) \end{bmatrix} \tag{1.7}$$

The reasoning can be extended to all the ij sections in which is divided the deck having a [S(f)] matrix of dimensions $2n$ x $2n$. Since v turbulence component has no effect on the bridge response, it has been neglected. Then it is possible to introduce the matrix that contains all the thirteen modes interpolated in each deck section: [Φ]. Knowing this we can compute the power spectral density (PSD) of the lagrangian of the wind:

$$PSD_{Lagr.}^{Wind} = [\Phi]^T [A_m(f)][S(f)][A_m(f)]^T [\Phi] \tag{1.8}$$

Equation 1.8 represents the input in order to compute the deck response.
While the PSD of the forces of the wind can be introduced as:

$$PSD_{Force}^{Wind} = [A_m(f)][S(f)][A_m(f)]^T \tag{1.9}$$

In equation 1.9, the PSD_{Force}^{Wind} can be expressed as :

$$\begin{bmatrix} {D_u}^2 S_{uu}^{ii} + 2D_u D_w S_{uw}^{ii} + {D_w}^2 S_{ww}^{ii} & D_u L_u S_{uu}^{ii} + D_w L_u S_{uw}^{ii} + D_u L_w S_{uw}^{ii} + D_w L_w S_{ww}^{ii} & D_u M_u S_{uu}^{ii} + D_w M_u S_{uw}^{ii} + D_u M_w S_{uw}^{ii} + D_w M_w S_{ww}^{ii} \\ SYM & {L_u}^2 S_{uu}^{ii} + 2L_u L_w S_{uw}^{ii} + {L_w}^2 S_{ww}^{ii} & L_u M_u S_{uu}^{ii} + L_u M_w S_{uw}^{ii} + + L_w M_u S_{uw}^{ii} + L_w M_w S_{ww}^{ii} \\ SYM & SYM & {M_u}^2 S_{uu}^{ii} + 2M_u M_w S_{uw}^{ii} + {M_w}^2 S_{ww}^{ii} \end{bmatrix} \tag{1.10}$$

This matrix (equation 1.10) could be extended to every ij section of the Braila deck spaced of Δy.

1.2.3 Span - wise coherence of the Aerodynamic force

The span - wise coherence of the aerodynamic buffeting forces has been introduced in equation 1.9 multipling the terms that affects only lift and aerodynamic moment due to turbulence component w for the respective ratios $coh_L^{1/2}/coh_w^{1/2}$ and $coh_T^{1/2}/coh_w^{1/2}$ defined in chapter 3 in the adapted Jakobsen J. and Larose G. representations. This moltiplication has been performed in order to take into account the recorrelation of the buffeting forces with respect to the w gusty wind.

For what regards the cross terms, that are the products between lift and moment because of w turbulence component, they have been multiplied for $\sqrt{\left(\frac{coh_L^{1/2}}{coh_w^{1/2}}\frac{coh_T^{1/2}}{coh_w^{1/2}}\right)}$. This operation has been done in order to produce suitable physical result in the deck response, considering the correlation of the buffeting lift with respect to the buffeting moment with this simplified formulation.

1.2.4 Braila bridge deck response computation

Starting from the PSD_{Lagr}^{Wind} as input it is necessary to define the transfer function [H] in this way:

$$[H(\omega)] = (-\omega^2[M_s + M_{aero}(f^*)] + i\omega[R_s + R_{aero}(f^*)] + [K_s + K_{aero}(f^*)])^{-1} \quad (1.11)$$

Then the PSD of the displacement of the Braila deck $[PSD_{Modal}^{disp.}]$ for each vibration mode and for each frequency step Δf in the frequency range can be introduced as:

$$[PSD_{Modal}^{disp.}] = [H][PSD_{Lagr}^{Wind}][H]^T \quad (1.12)$$

and in a similar way the PSD of the modal acceleration matrix $[PSD_{Modal}^{acc.}]$:

$$[PSD_{Modal}^{acc.}] = [PSD_{Modal}^{disp.}]\omega^4 \quad (1.13)$$

These are the instruments in order to build up the response of the Braila deck in both the cases in which we introduce or not the span - wise coherence of the aerodynamic forces. The models of normalized span wise cross-spectra available in literature will be described extensively in next chapter.

Chapter 2

Span-wise Coherence of the Aerodynamic Forces

2.1 Introduction

The importance of the knowledge of the spatial distribution of the aerodynamic forces induced by turbulent wind is at the basis of the buffeting response of the structure. At the beginning of this work, a comparison was made between the various models available in literature in order to calculate the re-correlation of aerodynamic forces with respect to the turbulent incident wind. This review underlined how the buffeting response computed by means of the *strip assumption* is underestimated compared to the one calculated by means of the experimental re-correlation models present in the literature. These representations were developed through wind tunnel tests on a motionless closed box girder deck. Among all the available models the most promising are those of Larose G. [1] and Jakobsen J. [2].

After having analyzed the representations mentioned above extensively, I have adapted the most promising ones through numerical fitting and dimensionless analysis to the study of the buffeting Response of the full Braila Bridge considering its first thirteen natural frequencies.

2.2 Davenport's spectral approach limitations

The limitations and assumptions of the Davenport's [3] [4] spectral approach are here below presented:

- Wind loading caused by the turbulence is a stochastic process of the stationary random type.

- $Quasi - steady\ assumption$: The instantaneous forces acting on the deck are made equal to the stationary forces caused by a steady wind having the same relative velocity and direction as the instantaneous wind. The static aerodynamic coefficients are considered in order to solve the equation of motion governing the deck dynamics under the action of turbulent wind as described in the first chapter.

- *Strip assumption* The aerodynamic forces acting on one strip are only generated by the turbulent fluctuations on that strip. This means that the coherence of the wind in the space is enough to describe the spatial distribution of the buffeting forces

- Natural frequencies of structure are separated, in this way we cannot have coupling between the different modes of vibration. The study in this way can be done mode by mode and then the overall response can be computed by means of the superposition principle of each single degree-of-freedom system.

- The fluctuations induced by the wind turbulence are considered small enough compared to the mean velocity so that gust loads can be formulated as linear function of the gust velocities

- The direction much more influenced by the action of the wind is considered the one normal to the bridge axis.

- $Cross - spectra$ between u and w turbulence components of the wind are negligible.

- The aerodynamic damping is a linear function of the wind speed and is independent of amplitude, The contribution of the aerodynamic stiffness is not considered.

- The parent distribution of the extreme response is taken as Gaussian.

The *Davenport*'s spectral approach, is assumed to be valid for large reduced velocities V^*.

The limitations imposed by the $quasi - steady$ aerodynamic assumption can be overcome by considering the notion of aerodynamic admittance. Davenport proposed to apply the aerodynamic admittance in order to consider:

- The loss of lift force in correspondence of the small gusts of the turbulence at high frequency

- The variation along the space in the flow, because the aerodynamic forces on one strip are caused, not only,by the fluctuations on that strip but also from ones acting on the region surrounding the considered strip.

2.3 Span-wise coherence and joint acceptance function

The $span - wise\ coherence$ and the $joint\ acceptance\ function$ [5] [6] are the statistical parameters that is necessary to define in order to describe how the aerodynamic forces are correlated along the length of the bridge.

2.3.1 Span-wise coherence

The magnitude squared coherence function can be defined as the modulus squared of the cross spectrum of the considered function (for example the Lift force) measured at two points which are at a distance of Δy:

$$coh(f, \Delta y) = \frac{|C_{o12}(f) + Q_{u12}(f)|^2}{S_{L1}(f) S_{L2}(f)} \tag{2.1}$$

Where:

- $C_{o12}(f)$ represents the real part of the cross spectrum between points one and two
- $Q_{o12}(f)$ represents the imaginary part of the cross spectrum between points one and two
- $S_{L1}(f)$ and $S_{L2}(f)$ are the power spectrum in correspondence of point one and two

The root coherence can be calculated by making the square root of equation(2.1). In the buffeting analysis, the contribution of imaginary part of the cross spectrum $Q_{o12}(f)$ can be considered null. Then it is possible to define the root coherence which can be determined as:

$$coh^{1/2}(f, \Delta y) = \frac{C_{o12}(f)}{\sqrt{S_{L1}(f) S_{L2}(f)}} \tag{2.2}$$

2.3.2 Joint acceptance function

The joint acceptance function $J_L(f^*)$ measures the correlation along space and modes of vibration for that span of the aerodynamic forces. It can be defined as:

$$|J_L(f^*)|^2 = \int_0^l \int_0^l \frac{S_{L1L2}(f^*, \Delta y)}{S_L(f^*)} \mu_j(y_1) \mu_j(y_2) dy_1 dy_2 \tag{2.3}$$

Where:

- μ_j is the j mode shape considered in position in y_1 and y_2
- S_{L1L2} is the cross spectrum of the considered function (in this case the Lift force) between points one and two at a distance Δy

If we know the root coherence of the considered function $coh_L^{1/2}$, then it is possible to rewrite the joint acceptance function as:

$$|J_L(f^*)|^2 = \int_0^l \int_0^l coh_L^{1/2}(f^*, \Delta y) \mu_j(y_1) \mu_j(y_2) dy_1 dy_2 \tag{2.4}$$

This formulation is valid for both the aerodynamic forces and turbulence components.

2.4 Strip assumption

If the *strip assumption* is assumed to be valid, the spatial distribution of the wind velocity fluctuations is sufficient to describe the span-wise coherence of the forces.

$$coh_w^{1/2}(f^*, \Delta y) = coh_L^{1/2}(f^*, \Delta y) \tag{2.5}$$

$$coh_w^{1/2}(f^*, \Delta y) = coh_M^{1/2}(f^*, \Delta y) \tag{2.6}$$

$$coh_w^{1/2}(f^*, \Delta y) = coh_D^{1/2}(f^*, \Delta y) \tag{2.7}$$

This is valid only when the incident gusts have much larger scales than the characteristic length of the bridge deck. Very often this condition is not satisfied and using the spatial coherence of wind in order to describe the buffeting response causes an important underestimation of the response itself. The *strip assumption* could be not valid for closed box girder decks because their width is often characterized by the same dimensions as the scales of the turbulence component w.

2.4.1 Davenport model

Davenport [7] introduced one of the first experimental model in order to describe the coherence of u and w components in the atmospheric boundary layer (ABL):

$$coh_{u,w}^{1/2}(f, \Delta y) \approx \exp\left[\left(-c_1 \frac{f\Delta y}{V}\right)^{c_2}\right] \tag{2.8}$$

Where:

- c_1 is a set of constants that changes, changing the direction and turbulence component considered x, y, z
- V is mean wind speed velocity.
- Δy is the distance between two different points of the deck.
- c_2 is the exponent introduced by Naito [8] in order to consider the sea exposure and it can vary between one and two depending on the specific conditions of the site.

2.5 When the strip assumption is not valid

Several researchers during the years have developed different models for describing the correlation of the aerodynamic forces and the width of the correlation.

2.5.1 Nettleton model

Nettleton [9] was the first to show the importance of the effect of the variations along the span for the lift forces of having gusts passing by a thin airfoil with a larger chord than the vertical length scale of turbulence (the *strip assumption* is not valid). He observed that the forces were more correlated than the incident wind.

The integral length scale of the correlation along y can be represented as :

$$L^y = \int_0^\infty R_{12}(\Delta y) d(\Delta y) \tag{2.9}$$

Where:

- R_{12} is the coefficient related to the cross correlation

During his research Nettleton found that the correlation length of the forces was 3.6 times larger than the one of the incident wind:

$$L_L^y = 3.6 L_w^y \tag{2.10}$$

2.5.2 Melbourne model

Melbourne [10] confirmed the researches developed by Nettleton, by comparing the span-wise coherence of the pressures of the leading edge on the West Gate Bridge and the coherence of turbulence component u.

He conducted experiments both in full scale conditions on the prototype bridge and in wind tunnel simulating the action of the turbulent wind on proper scaled model. The results of the Melbourne's studies displayed a larger coherence of the pressures.

The experimental data was fitted by means of exponential functions. He obtained for the scaled model and the full scale prototype that the coherence of the pressure in correspondence of the leading edge was:

$$coh_{pressure} = exp[-4\frac{f\Delta y}{V}] \tag{2.11}$$

and for the fluctuation due to u turbulence components:

$$coh_u = exp[-16\frac{f\Delta y}{V}] \tag{2.12}$$

The results showed that the pressures in correspondence of the leading edge were much more correlated with respect to the turbulence component u considering the West gate bridge study. During the experiments it was not possible to fix the deck and then its movement could have increased the coherence of the pressures.

Figure 2.1: West Gate bridge

2.5.3 Empirical model of Hjorth-Hansen et al.

Hjorth-Hansen et al. [11] developed an empirical model of the root coherence of the aerodynamic forces that is a decreasing exponential, characterized by an additional term. This additional term has been considered in order to take into account of the absence of correlation at low frequency and large separation.

Hjort-Hansen et al. discovered that the integral length scale of the drag force L_D^y along y direction was found to be from 20% to 200% than the integral length scale of u turbulence component along the same direction L_u^y.

After the experimental measures by means of pressure taps on three strips, the aerodynamic forces were computed by the simultaneous integration of the unsteady pressure distribution experimentally computed.

The root coherence according to Hjorth-Hansen et al. can be defined as:

$$coh_D^{1/2}(f, \Delta y) = \exp\left\{ - \left[c_1 \frac{f \Delta y}{V} + c_2 \left(\frac{\Delta y}{L_D^y} \right)^2 \right] \right\} \tag{2.13}$$

Where:

- $c_1 = 7$, $c_2 = 2$ - 3 are constants obtained by proper fitting of the experimental wind tunnel test for the drag force
- $L_D^y = 0.20$ m experimentally tuned
- $c_1 = 10$, $c_2 = 1$ obtained after the numerical fitting for the u turbulence component

- $L_u^y = 0.10$ m for the u turbulence component

From their experiments Hjorth-Hansen et al. realized that there were lower than anticipated drag forces on a strip when confronted to quasy-steady buffeting theory.

The larger coherence according to the researchers could be compensated by a lower cross-sectional admittance.

2.5.4 Empirical model of Kimura et al.

Kimura et al. [12] performed experiments on flat hexagonal and rectangular cylinders (figure 2.2) in order to clarify the characteristics of the buffeting response.

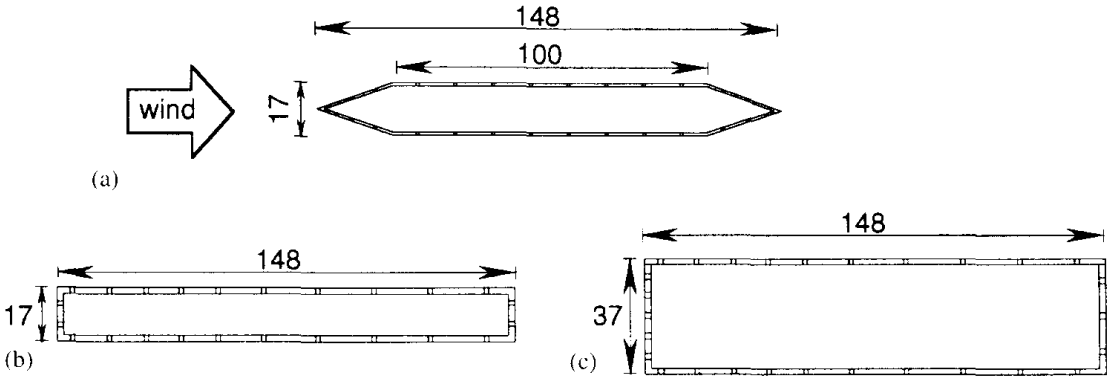

Figure 2.2: Model Cross sections: (a) Flat hexagon B/D = 8.7:1, (b) Rectangular B/D = 8.7:1, (c) Rectangular B/D 4:1

The experiments were conducted considering three different wind speeds, respectively 4 m/s , 8 m/s and 12 m/s and different turbulence conditions as can be observed in figure 2.3. Actually, the length scales of L_w^x, L_u^y, and L_w^x, defined in figure 2.3 correspond to the double of the ones considered for the isotropic turbulence condition.

The effect of the turbulence length scales on the buffeting aerodynamic forces were studied for three different grids resulting from the subsequent L_w^y/B ratios: 0.47, 0.30 and 0.20. Also in this research, the span-wise coherence was found to be higher than that of the turbulence of the wind, which was in accordance with the previous studies. The forces were obtained by integration of the experimental surface pressures recorded during wind tunnel tests.

Coherence of the incident wind field was based on the representation made by Irwin [13] which computed an analytical root coherence function of the w turbulence component based on the Von Kárman spectrum. This exponential function was able to fit well the wind data.

For what concerns the correlation of aerodynamic forces, Kimura et al. developed a new exponential function in order to fit the experimental data based on Von Kárman spectrum.

	Wind speed (m/s)	Turbulence intensity (%)		Turbulence scales (cm)			
				Mean flow direction		Normal to the mean flow direction	
		I_u	I_w	L_u^x	L_w^x	L_u^y	L_w^y
Grid A	4	10.4	8.8	24	14	16	13
	8	10.3	8.7	21	14	16	14
	12	10.2	8.6	21	14	16	14
Grid B	4	10.0	8.6	11	8	10	9
	8	9.9	8.3	13	8	9	9
	12	9.8	8.2	13	8	9	9
Grid C	4	9.9	8.3	7	5	5	5
	8	9.8	8.1	8	5	6	5.5
	12	9.8	7.9	8	5	6	6

Figure 2.3: Flow characteristics according to Kimura et al. experiments

The span-wise coherence of the lift buffeting force can be defined as:

$$coh_L^{1/2}(f\Delta y) = 0.994\left(\eta^{5/6}K_{5/6}(\eta) - \frac{\eta^{11/6}K_{1/6}(\eta)}{1+188.7\left[f^{0.74}(\frac{4.5L_w^y}{V})\right]^2}\right) \tag{2.14}$$

Where η is defined as:

$$\eta = \frac{\Delta y}{4.5L_w^y}0.747\sqrt{1+70.8\left[f^{0.74}(\frac{4.5L_w^y}{V})\right]^2} \tag{2.15}$$

The other parameters inside this formulation are:

- $K_{5/6}$ and $K_{1/6}$ are second kind order modified Bessel functions
- L_w^y is the span wise length scale of wind turbulence w component

The empirical formulation fitted well the correlation of the lift forces for the three cross section examined. Kimura et al. are in accordance with the other researchers in affirming that the buffeting lift is more correlated than the incident wind. For what concerns the drag aerodynamic force, they discovered that in this case the *strip assumption* could be applied, in this way the coherence along the span of the incident gusts is enough to describe the one of the drag force.

In addition they noted a smaller cross-sectional lift than anticipated. This difference according to Kimuta el al. could be led back to secondary flow that decreases the force because an incident gust on the specif strip but increases its influence considering all the span.

This effect is more important lowering the turbulence length scales associated.

In figure 2.4 it is possible to compare the joint acceptance functions for the wind turbulence and the lift. It can be clearly seen that the buffeting lift is much more correlated than the incident wind.

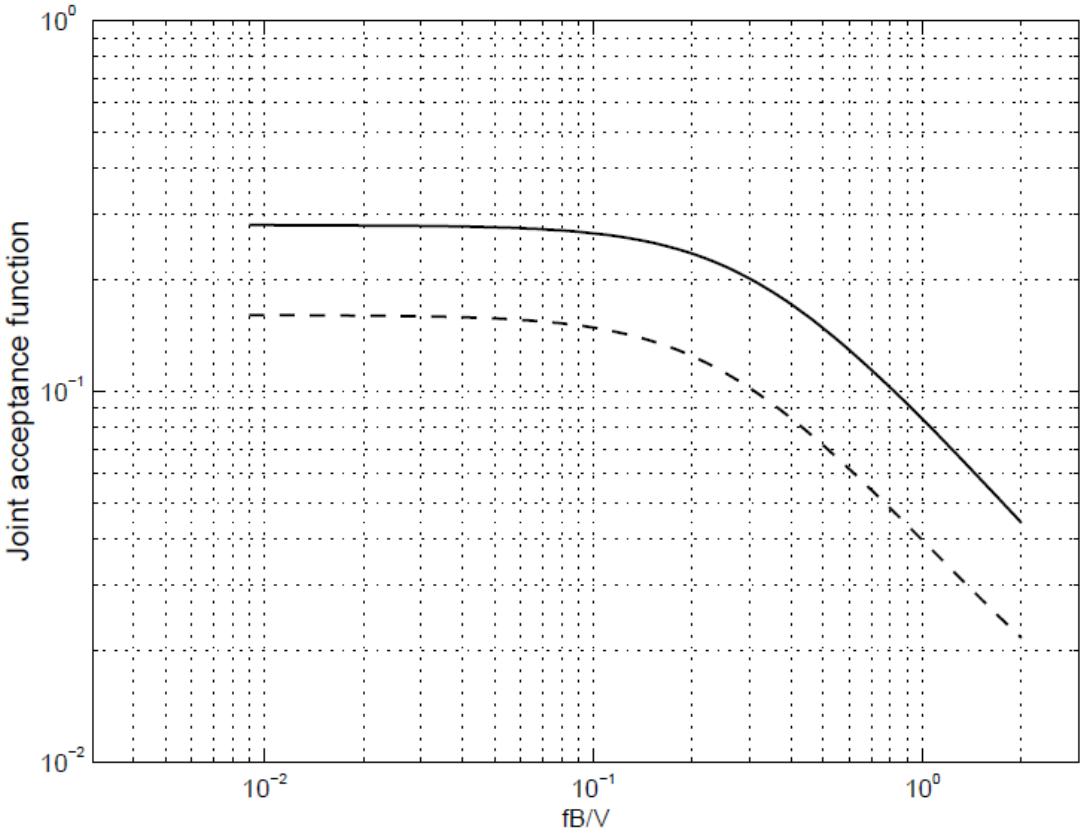

Figure 2.4: Joint acceptance function computed with uniform mode shape ($\mu(y_1) = \mu(y_2) = 1$) for the wind turbulence root coherence (dashed line) and for the one of the lift forces (solid line)

2.5.5 Empirical model of Bogunovic Jakobsen

Jakobsen J. [2] derived experimentally an expression of the span-wise coherence for the buffeting lift and moment and for the w turbulence component. The forces were computed starting from pressure tube measurements with a fixed section model.

Experimental set-up

The model of closed box girder (figure 2.5) deck was in 1:70 scale. It was characterized by:

- A deck span of B = 0.286 m
- The length of the model L = 2.64 m spanning the width of the section chamber of the wind tunnel
- The ratio between the span and the height of the deck B/H = 4.5

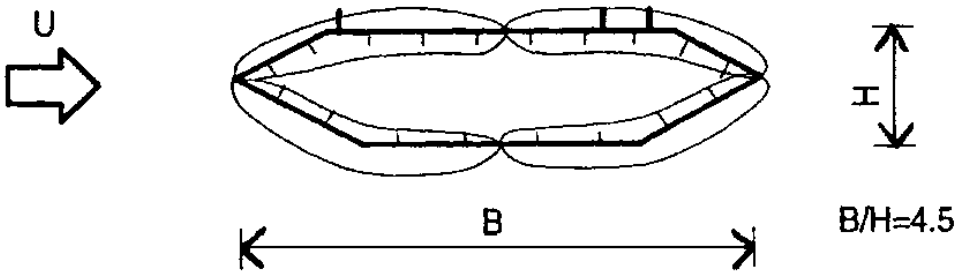

Figure 2.5: Suspension closed box deck equipped with pressure taps

The prototype was vertically and torsionally connected to a pair of stiff rods on each of its ends and attached by drag wires along the wind direction.

Flow conditions

The tests were performed in turbulent flow conditions. Turbulence generation involved a fairly coarse grid consisting of horizontal and vertical bars, that were positioned in correspondence of the entrance of the working section.

Turbulence intensity in correspondence of the model's position, 6.25 m far from the beginning of the working section, was close to 8% both in the along wind and vertical directions. The integral length scales of turbulence were:

- $L_u^y \approx 130$ mm for the u turbulence component along the y direction
- $L_w^y \approx 108$ mm for the w turbulence component along the y direction

The integral length scales derived above are both for a Δy along the prototype of the deck.

Span-wise coherence model

Jakobsen J. made a comparison between the measured buffeting forces and the incident wind and obtained that there was a relation between the correlation width of the lift and of the w turbulence component of the wind:

$$L_L^y = 3.0 L_w^y \tag{2.16}$$

This data is in accordance with the previous studies mentioned before.
The span-wise coherence of the buffeting lift and moment was the result of a fitting by a least square minimization algorithm of the experimental tests.

Jakobsen J. used the same negative exponential function in order to define the coherence of the aerodynamic forces and of the turbulence component w:

$$coh_{L,M,w}^{1/2}(f, \Delta y) = \exp\left\{ - \left[\Delta y \sqrt{c_2^2 + (c_3 f/V)^2} \right]^{c_1} \right\} \tag{2.17}$$

The constants c_1, c_2 and c_3 (table 2.1) take different values passing from the lift to the moment or considering the w gust speed.

Table 2.1: Fitting coefficients c_1, c_2 and c_3 for lift, torsion and w turbulence component

	c_1	c_2 (m^-1)	c_3
Turbulence component w	1.00	4.21	5.47
Buffeting, Lift	1.40	2.11	2.24
Buffeting, Torsion	1.35	2.44	2.15

The frequencies analyzed were in the range 0 - 30 Hz (f^* up to 0.6), considering a mean wind speed U = 15.36 m/s. Very similar coefficients c_1, c_2 and c_3 were derived for U = 9.38 m/s.

The selected frequency range was able to incorporate the main part of the wind loading process on the deck.

Jakobsen J. computed (figure 2.6) the joint acceptance function $|J(f^*)|^2$ of the span-wise coherence of the aerodynamic forces and comparing it to the one of the turbulence wind component w, discovered an important underestimation when the *strip assumption* was assumed to be valid. This suggests that the structure perturbs the oncoming flow in a relevant way.

With respect to Hjorth-Hansen et al. who compared the span wise coherence of the drag force and the one of the along wind component for a rectangular closed box girder deck, Jakobsen J. made the parallel of the root coherence for the lift and the buffeting moment with the one of w turbulence component of the wind.

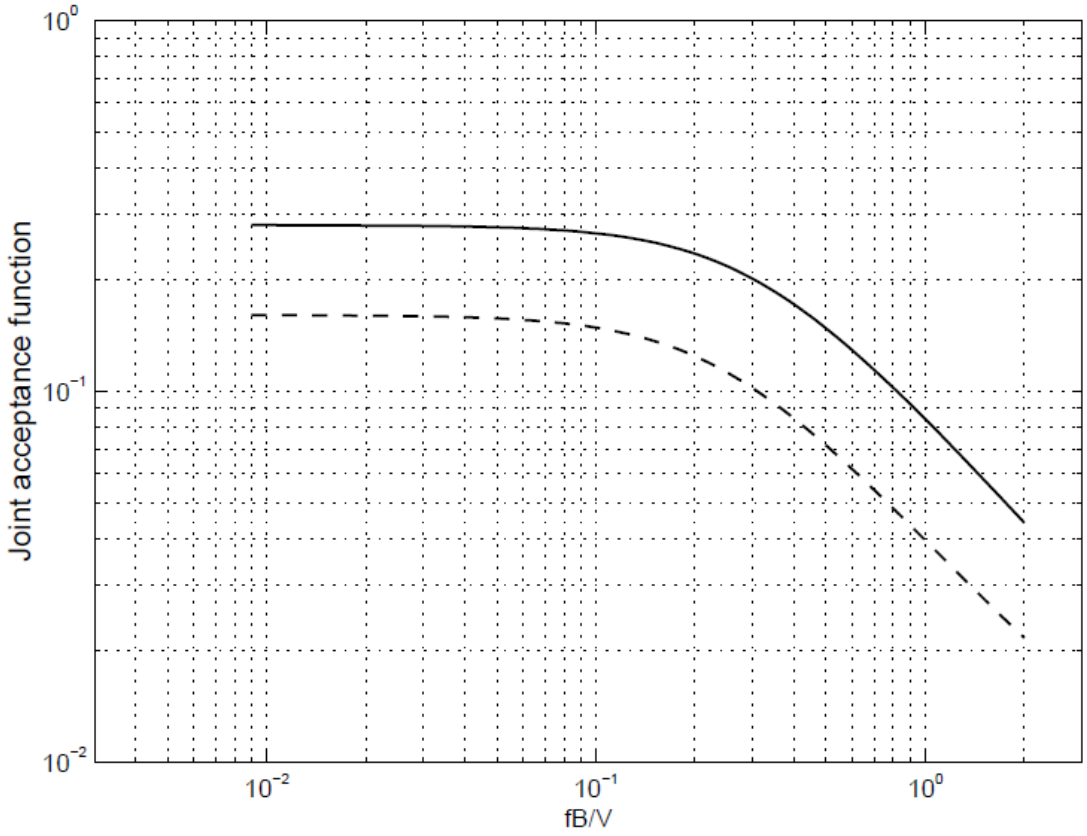

Figure 2.6: Joint acceptance function computed with uniform mode shape ($\mu(y_1) = \mu(y_2) = 1$) for the wind turbulence root coherence (dashed line) and for the one of the lift forces (solid line) according to Jakobsen J.

Experimental results

In the figures below it is possible to observe the normalized co-spectrum of w-fluctuations, for the buffeting lift and aerodynamic moment for four different separations in the range $\Delta y/B = 0.07$ and 0.70, considering the mean wind speed of U = 15.36 m/s and B = 0.286 m.

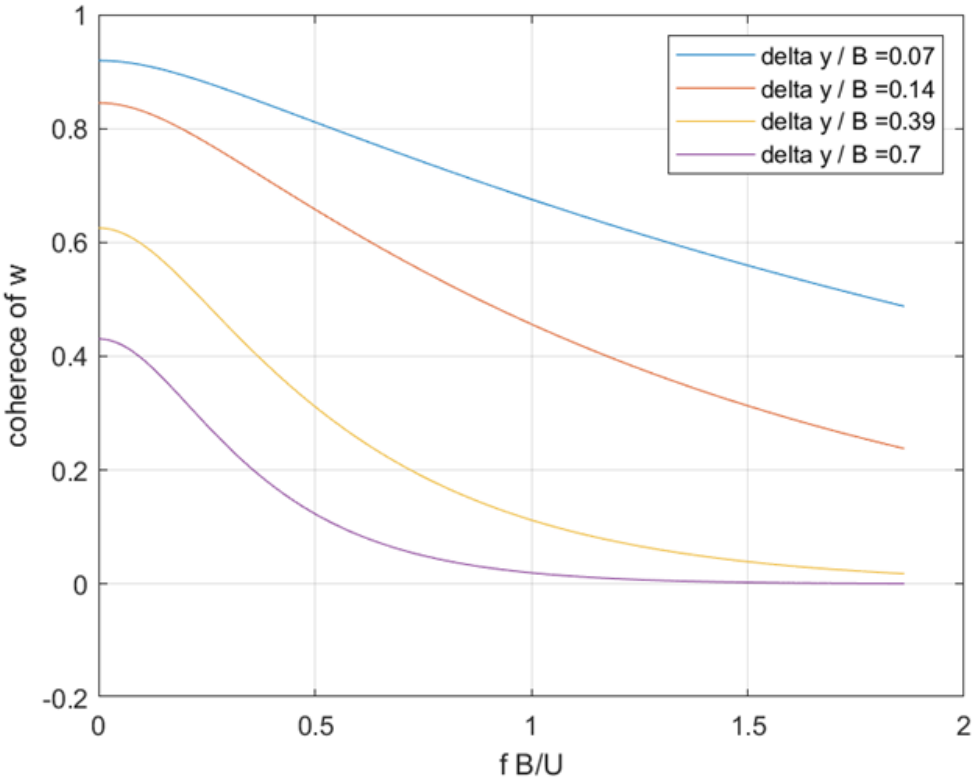

Figure 2.7: Span-wise coherence of w turbulence component of the wind for four different separations $\Delta y/B$.

Is possible to observe in figure 2.7 the span-wise correlation of w for reduced frequencies f^* between 0 and 2 for four different $\Delta y/B$. Increasing the distance between the points considered Δy, as we expected we experience a decrease of the coherence. These plot has been computed for each case, changing the fixed Δy.

At high reduced frequencies f^* and large separations $\Delta y/B$, we have the lowest values of correlation, in a specific case $\Delta y/B = 0.7$ and f^* close to 2 we can experience slightly negative values of coherence. This has not any physical meaning, and it is caused from the numerical fitting of the Jakobsen J. model.

When I have adapted this model to the full Braila bridge case, I have considered a smaller range of f^* in order to do not meet this issue.

In figures 2.8 and 2.9 there is the trend of the buffeting lift and moment for the same case mentioned above. As we expected there is an increase of correlation of the aerodynamic forces with respect the one of the gusty wind. The coherence also in this case decreases increasing the spacing Δy between the considered points.

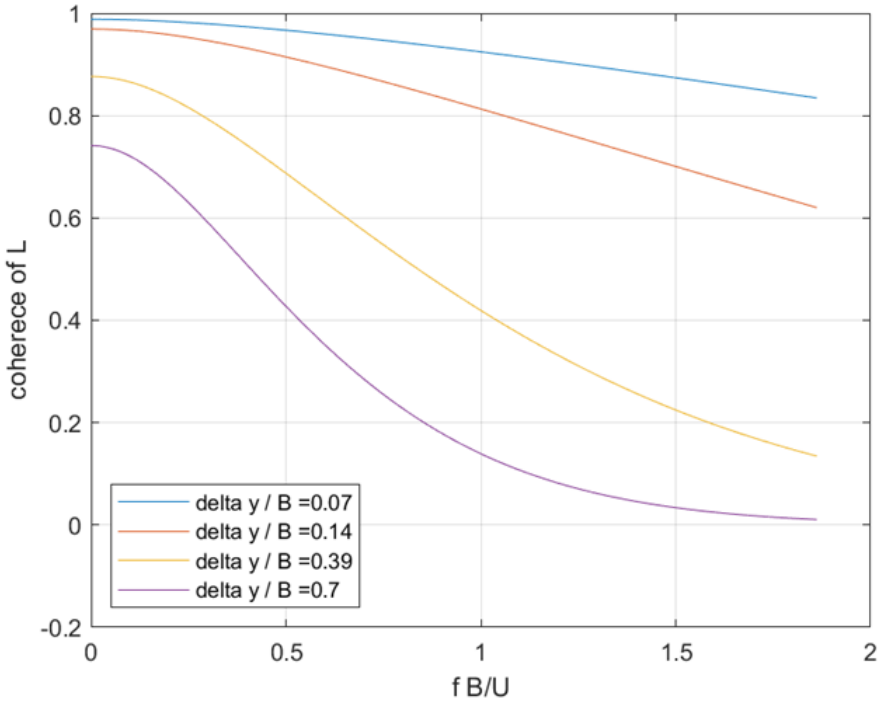

Figure 2.8: Span-wise coherence of the lift for four different separations $\Delta y/B$.

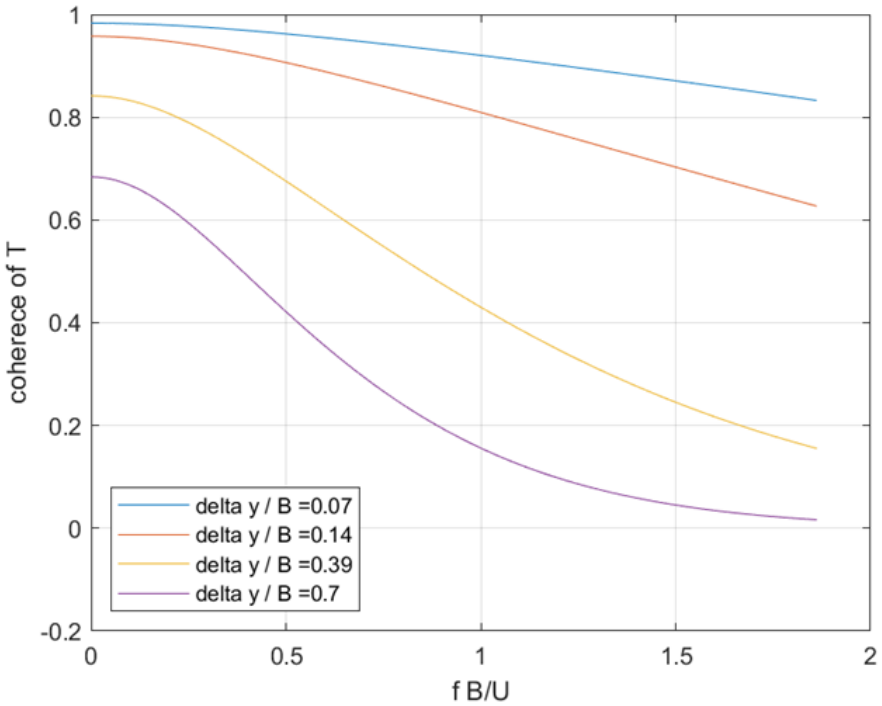

Figure 2.9: Span-wise coherence of the moment for four different separations $\Delta y/B$.

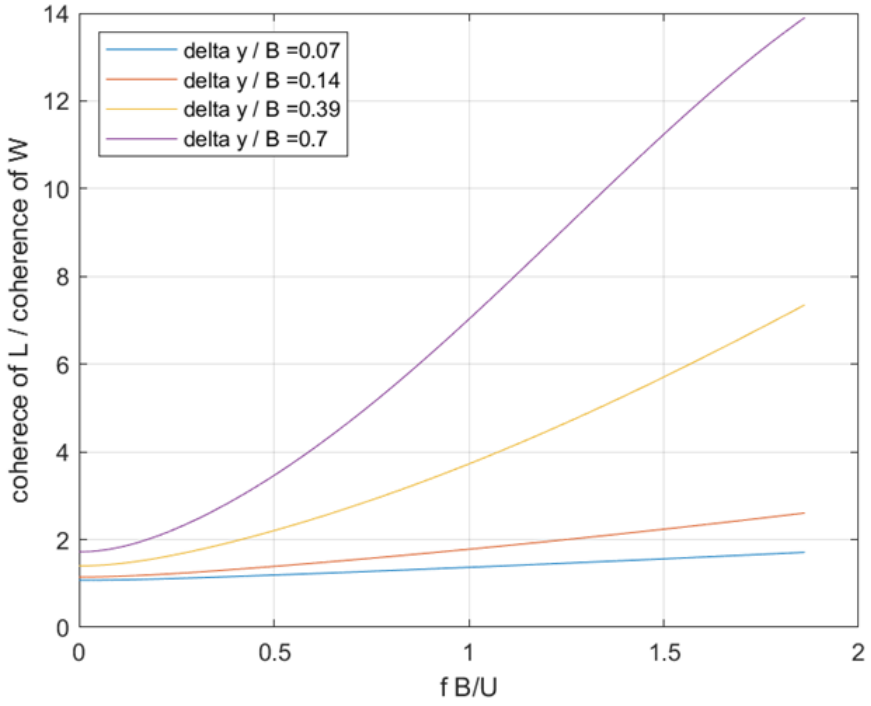

Figure 2.10: Span-wise coherence of the ratio $coh_L^{1/2}/coh_w^{1/2}$ for four different $\Delta y/B$.

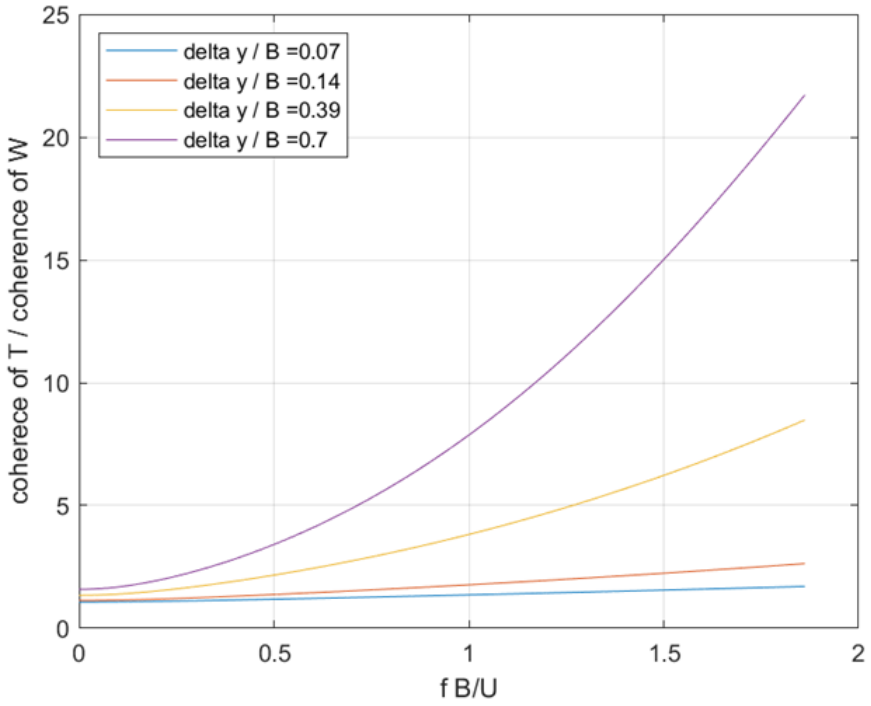

Figure 2.11: Span-wise coherence of the ratio $coh_T^{1/2}/coh_w^{1/2}$ for four different $\Delta y/B$.

In correspondence of high values of reduced frequency f^*, and high Δy we experience too high ratios between $coh_T^{1/2}/coh_w^{1/2}$ and $coh_L^{1/2}/coh_w^{1/2}$ as it is possible to observe in figure 2.10 and 2.11. Having noticed this, in addition to what has been observed for the w span-wise coherence, the model has been adapted to the full case of the Braila bridge for a smaller range of reduced frequencies f^*. In addition, in the Jakobsen J. original representation small negative values of w normalized cross-spectrum in the tail of the raw version of the curves and the subsequent values, either positive or negatives have been substituted by zeros, that is another way to tell that this specific reduced frequency range f^* have not been considered.

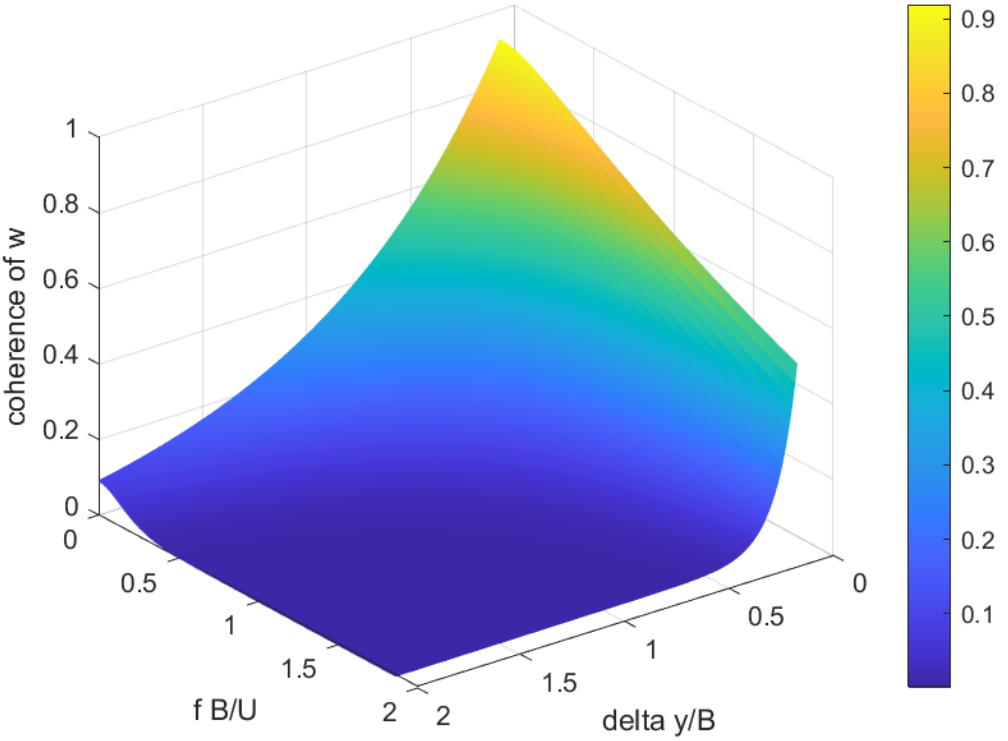

Figure 2.12: Normalized cross-spectrum of w turbulence component for different $\Delta y/B$ and f^*

In figures 2.12, 2.13 and 2.14 it is possible to examine the 3D trend of the span-wise coherence for w gusty wind component and lift and aerodynamic moment, taking into account at the same time the reduced frequency f^* and the normalized distance between two different point $\frac{\Delta y}{B}$. Also these results confirm the underestimation given by the *strip assumption*.

The experimental tests, also in this case have been performed at a mean wind speed $U = 15.16$ m/s, and considering a deck span $B = 0.286$ m.

These 3D curves are the ones that best approximate the experimental results obtained by means of wind tunnel testing.

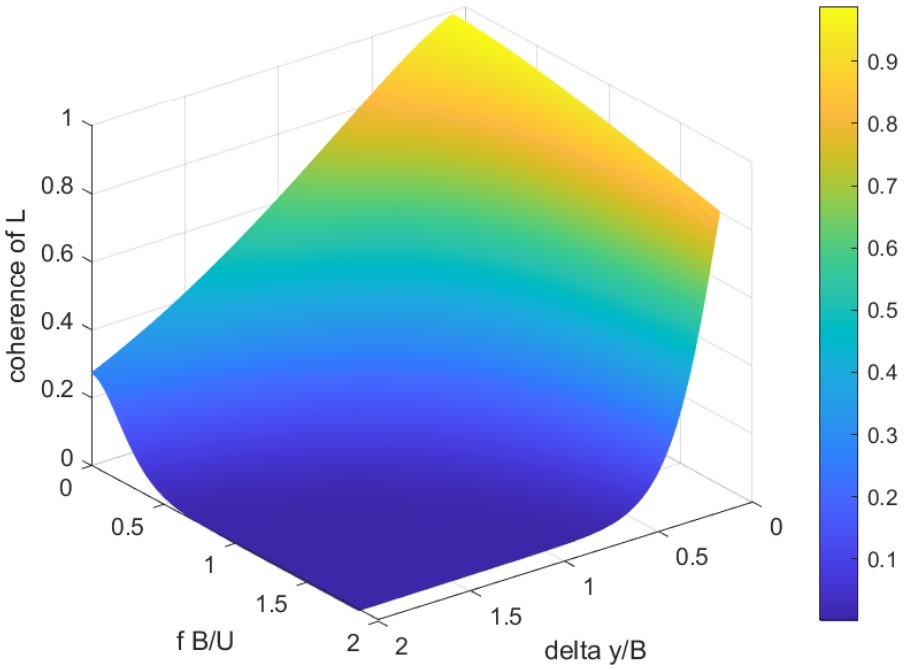

Figure 2.13: Normalized cross-spectrum of the buffeting L for different $\Delta y/B$ and f^*

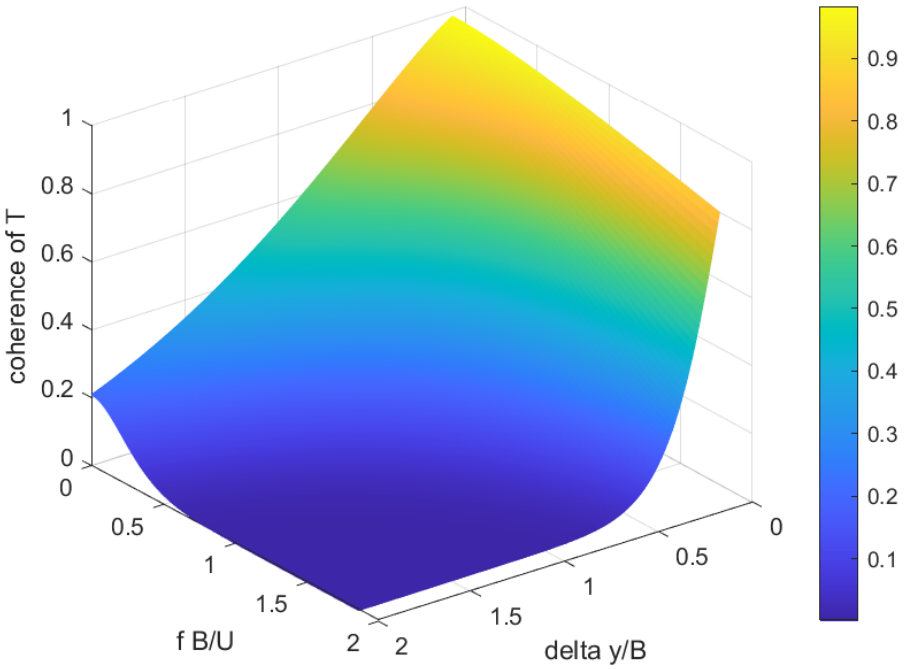

Figure 2.14: Normalized cross-spectrum of the buffeting T for different $\Delta y/B$ and f^*

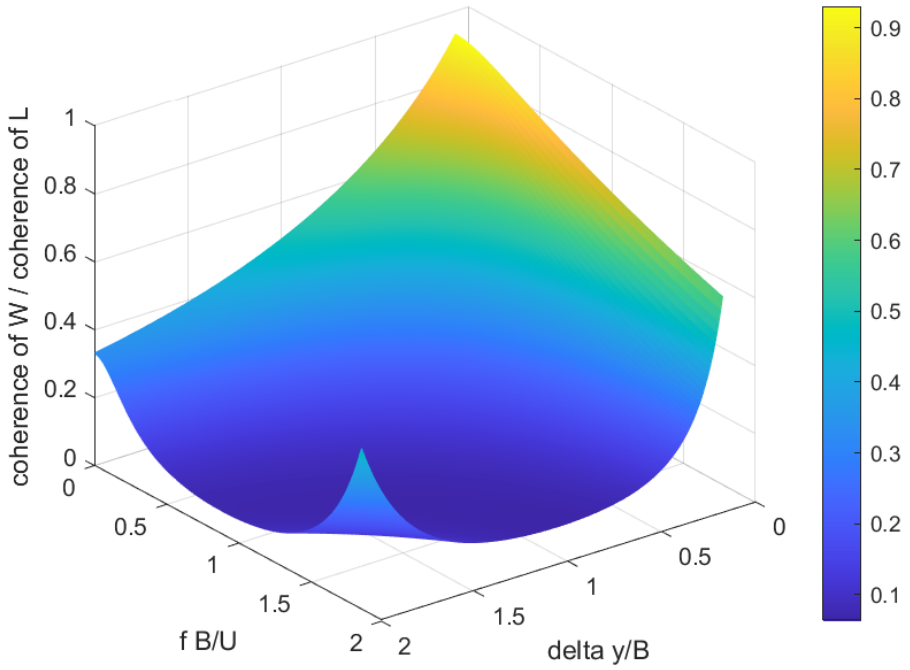

Figure 2.15: Ratio of normalized cross-spectra $coh_w^{1/2}/coh_L^{1/2}$ for different $\Delta y/B$ and f^*

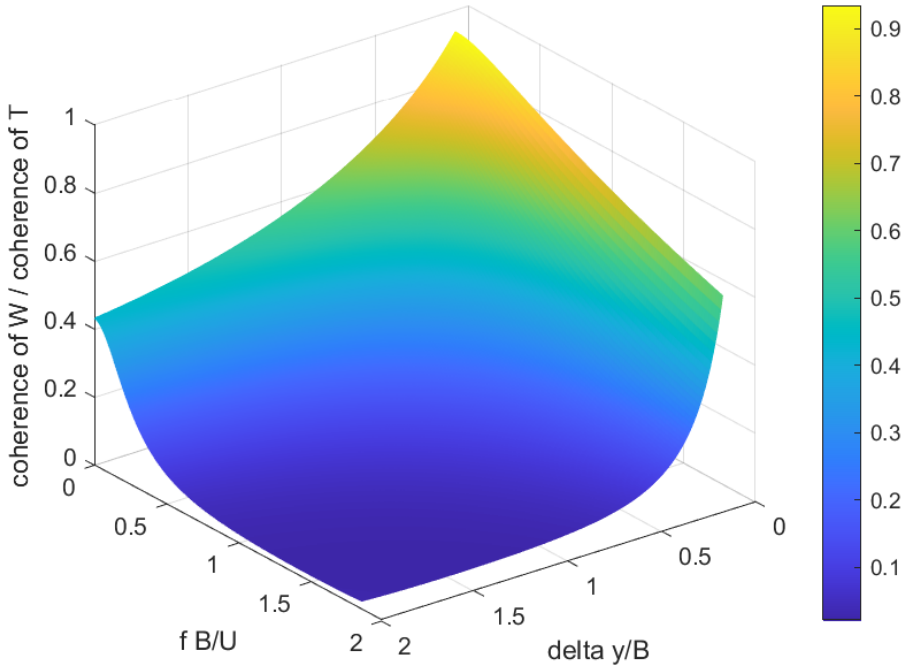

Figure 2.16: Ratio of normalized cross-spectra $coh_w^{1/2}/coh_T^{1/2}$ for different $\Delta y/B$ and f^*

In figures 2.15, 2.16, it is possible to watch the 3D trends of the ratio between $coh_w^{1/2}/coh_L^{1/2}$ and $coh_w^{1/2}/coh_T^{1/2}$ taking into account at the same time the reduced frequency $\frac{fB}{U}$ and the adimensional spacing $\frac{\Delta y}{B}$.

The plots, also in this case, displays an higher recorrelation with respect the one of the turbulent wind. The results at high reduced frequency f^* and big distance Δy have been not considered in the adapted model for the full Braila bridge, for the reasons already mentioned above.

2.5.6 Empirical model of Larose G.

The experimental technique of Larose G. [1] consists in determining the normalized cross-spectra of the buffeting lift and moment starting from measures of the vertical, torsional and lateral forces at the extremities of a deck sectional model.

Wind tunnel tests were made in turbulent flow and the model was fixed in order to not experience any wind induced motion. The method developed by Larose is able to compute the aerodynamic admittance for decks of any cross section. The admittance matrix calculated in this way contains two contributions:

1. Contribution of the cross sectional admittance
2. Contribution because of the spatial distribution along the span of the aerodynamic forces.

Figure 2.17: Höga Kusten Bridge

Experimental Set-up

The sectional model of closed box girder figure (2.18) deck of the Höga Kusten Bridge in its construction stage (60% porous railings, no median divider) was tested in the wind tunnel of the Danish Maritime Institute (DMI). The scale of the model was 1:60.

It was rigidly connected to the force balance. The dimensions of the test rig were: 2.6m wide, 1.8m high and 21m long.

At the two extremities of the sectional prototype were measured drag, lift and pitching moment with a sampling frequency of 200 Hz for a time period of 180 s.

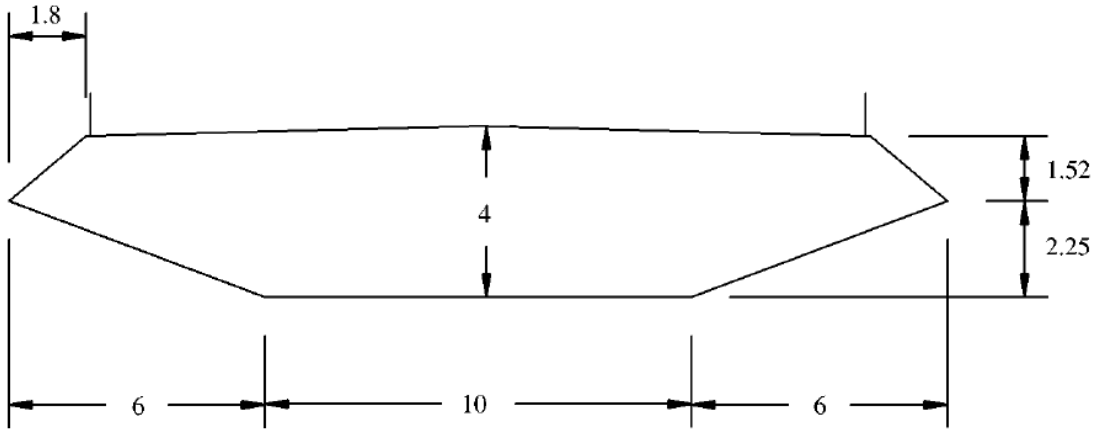

Figure 2.18: Höga Kusten Bridge tested model by Larose G.

In figure 2.18 is possible to observe the tested model and its dimensions:

- A deck span of B = 0.367 m
- The length of the model L = 2.55 m spanning the main part of the width of the section chamber of the wind tunnel
- The ratio between the span and the height of the deck B/D = 5.5

Flow conditions

The tests were performed in turbulent flow conditions. Turbulence generation involved large spires, mounted at the entrance of the wind tunnel, 15 m before than the tested deck working section.

The vertical turbulence intensity in correspondence of the model's position, I_w was 7.3% and vertical turbulence macroscale index $\mathcal{L}$ was 0.22m.

Considering the Von Kárman spectrum $\mathcal{L}_{u,w}$ is linked to the integral length scale by the following relationships:

$$L_u^x \approx 0.92\mathcal{L}_u \tag{2.18}$$

$$L_w^x \approx 0.67\mathcal{L}_w \tag{2.19}$$

Integral length scales of turbulence L_w^x can be derived by means of equation 2.19 and is equal to $L_w^x = 147$ mm. In general the turbulence macroscale index $\mathcal{L}_w$ is defined as the inverse of the wave number $k_1 = \frac{2\pi f}{U}$ corresponding to the peak of the wind spectrum in its $fS_w(f)$ modelling.

During the experiments was observed that the buffeting lift and moment were not linked to the u turbulence component length scales. It is believed that u gusty wind component slightly influences the generations of the two aerodynamic actions mentioned above.

Span-wise coherence model

The span-wise normalized cross spectrum for the w turbulence component can be defined according to Larose in this way:

$$coh_w^{1/2} = \exp\left[-c_1\gamma^{c_2}\right]\cos\left(c_3\gamma\right) \tag{2.20}$$

where:

$$\gamma = k_1\Delta y\sqrt{1+\frac{1}{(k_1L)^2}} \tag{2.21}$$

It is necessary to introduce the subsequent parameters that can be noticed in equations 2.20 and 2.21:

- Wave number : $k_1 = \frac{2\pi f}{\overline{V}}$
- Length scale fitted to the experiments $L_{coh} = 0.27$ that changes, changing the dimension of the spires in the turbulence generation process (medium grid)
- Von Kárman collapsing parameter γ (equation 2.21)
- Fitting constants c_1, c_2 and c_3, where $c_1 = 0.73$, $c_2 = 1.03$ and $c_3 = 0.27$.

In a similar way it is possible to define the co-coherence of the lift [1] and the pitching moment[2]: :

$$coh_L^{1/2} = \exp\left[-c_1\eta^{c_2}\right]\cos\left(c_3\eta\right) \tag{2.22}$$

Where for the lift:

$$\eta = k_1^{a_L}\Delta y\sqrt{1+\frac{1}{(k_1^{a_L}L_L)^2}} \tag{2.23}$$

$$L_L = L\frac{(p+\Delta y/B)^2}{(q+r(\Delta y/B)^2} \qquad p = 1.0,\ q = 0.46,\ r = 1.42,\ L = 0.39\ \text{m} \tag{2.24}$$

$$a_L = \left(\frac{B}{D}\right)^{-0.25}\frac{(p+\Delta y/B)^2}{(q+r(\Delta y/B)^2} \qquad p = 0.160,\ q = 0.088,\ r = 0.935 \tag{2.25}$$

Where:

- Fitting constants c_1, c_2 and c_3, where $c_1 = 0.346$, $c_2 = 1.5$ and $c_3 = 0$.
- Length scale L fitted to the experiments considering lift (medium grid)
- Fitting constants p, q, r assuming different values for a_L and L_L

[1] The exponent of B/D in a_L (equation 2.25) differs from the one presented by Larose in its work because it contained a misprint.

[2] The exponent of B/D in a_T (equation 2.29) differs from the one presented by Larose in its work because it contained a misprint.

And for the pitching moment:

$$coh_T^{1/2} = \exp\left[-c_1\eta^{c_2}\right]\cos\left(c_3\eta\right) \tag{2.26}$$

Where:

$$\eta = k_1^{a_T}\Delta y\sqrt{1+\frac{1}{(k_1^{a_T}L_T)^2}} \tag{2.27}$$

$$L_T = L\frac{(p+\Delta y/B)^2}{(q+r(\Delta y/B)^2} \qquad p=1.0,\ q=0.46,\ r=1.42,\ L=0.39\text{ m} \tag{2.28}$$

$$a_T = \left(\frac{B}{D}\right)^{-0.15}\frac{(p+\Delta y/B)^2}{(q+r(\Delta y/B)^2} \qquad p=0.098,\ q=0.059,\ r=0.970 \tag{2.29}$$

Where:

- Fitting constants c_1, c_2 and c_3, where $c_1 = 0.341$, $c_2 = 1.33$ and $c_3 = 0.22$
- Fitting constants p, q, r assuming different values for a_T and L_T

In figures 2.19 and 2.20 it is possible to see the trend of a_L and a_T as a function of the adimensional spacing $\Delta y/B$ for three different ratios $\left(\frac{B}{D}\right) = 5$, 10 and 12.67. This comparison has been carried out by Larose in his PhD thesis [6], and it is shown in order to have a validation of the coefficients mentioned above.

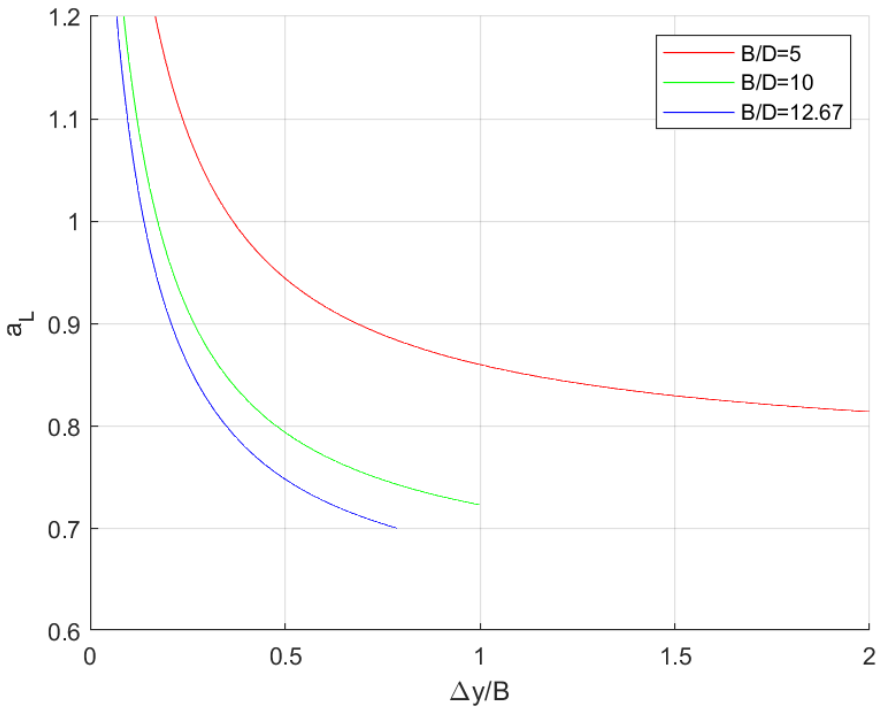

Figure 2.19: a_L coefficient for different ratios $\left(\frac{B}{D}\right) = 5$, 10 and 12.67

The trend of a_L and a_T is similar considering all the B/D ratios and this can be attributed to the similar exponent of B/D in the two formulations (2.25 and 2.29).

The influence of B/D ratios is important in both a_L and a_T. In correspondence of the lowest one ($B/D = 5$) we meet the highest values of the two coefficients as we expected. The decks examined in these experiments were characterized always by the same D, with changing B. The shape of the cross section in all cases was the same.

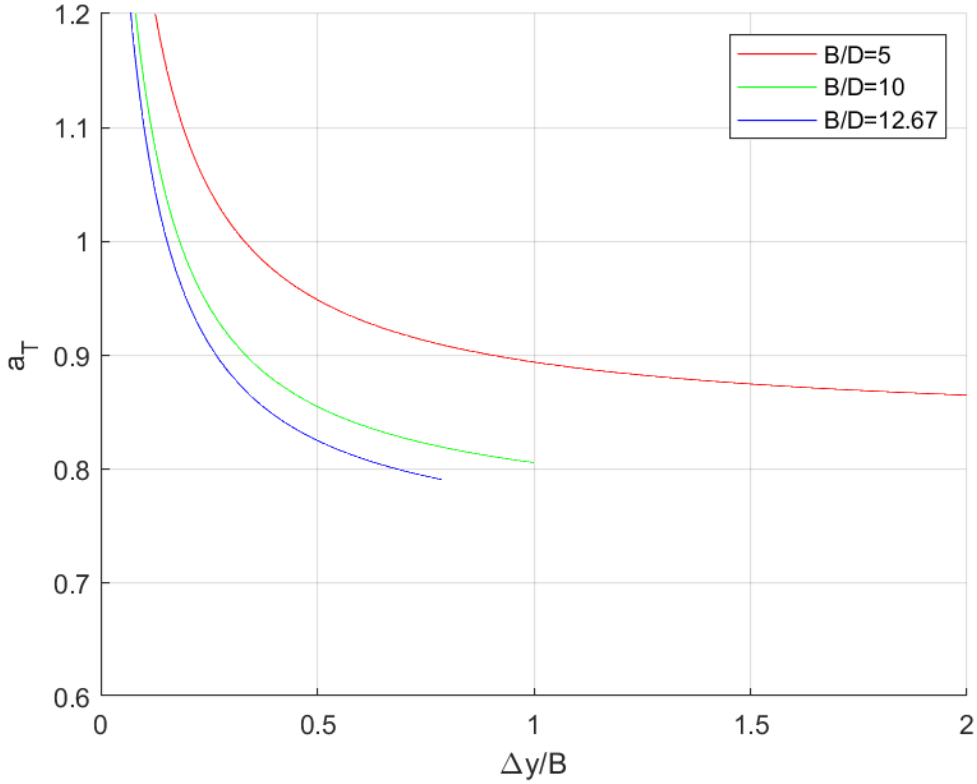

Figure 2.20: a_T coefficient for different ratios $\left(\frac{B}{D}\right) = 5$, 10 and 12.67

In figures 2.21 and 2.22 we can look the the trend of a_L and a_T coefficients without the influence of the ratio B/D , as a function of the spacing $\Delta y/B$. As expected the two trends plots are very similar, small differences are because of the different p, q and r coefficients in the two expressions 2.25 and 2.29.

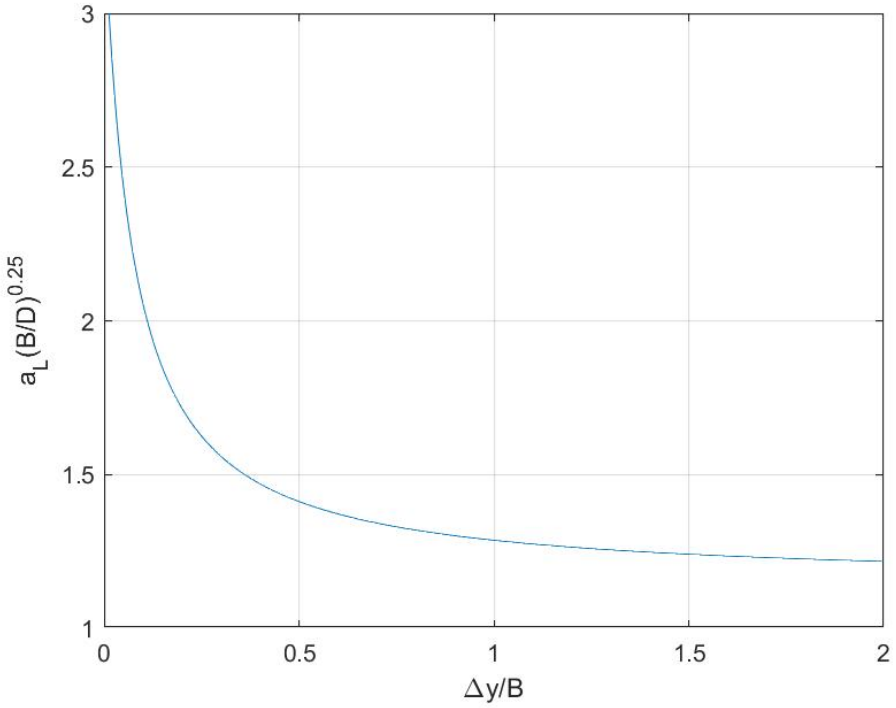

Figure 2.21: Coefficient a_L multiplied by $\left(\frac{B}{D}\right)^{0.25}$ with changing $\frac{\Delta y}{B}$

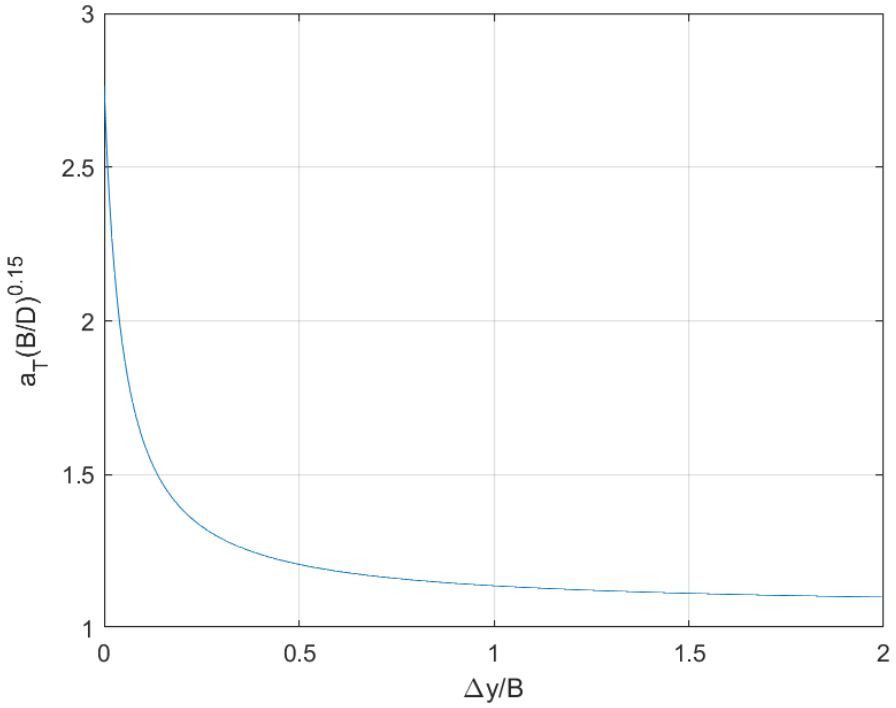

Figure 2.22: Coefficient a_T multiplied by $\left(\frac{B}{D}\right)^{0.15}$ with changing $\frac{\Delta y}{B}$

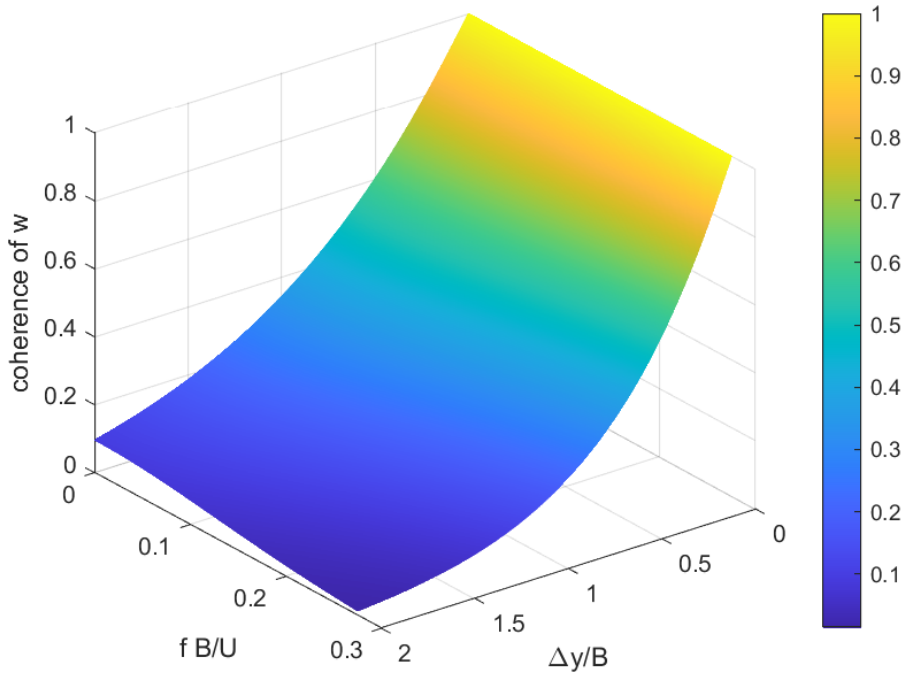

Figure 2.23: Normalized cross-spectrum of w turbulence component for different $\Delta y/B$ and f^*

In figures 2.23, 2.24 and 2.25 it is possible to examine the 3D trend of the span-wise coherence for w gusty wind component and lift and aerodynamic moment, taking into account at the same time the reduced frequency f^* and the normalized distance between two different point $\frac{\Delta y}{B}$. Also considering the Larose model, it confirm the underestimation given by the *strip assumption*.

The experimental tests, also in this case have been performed at a mean wind speed $U = 8$ m/s, and considering a deck span $B = 0.367$ m.

These 3D curves are the ones that best approximate the experimental results obtained by means of wind tunnel testing.

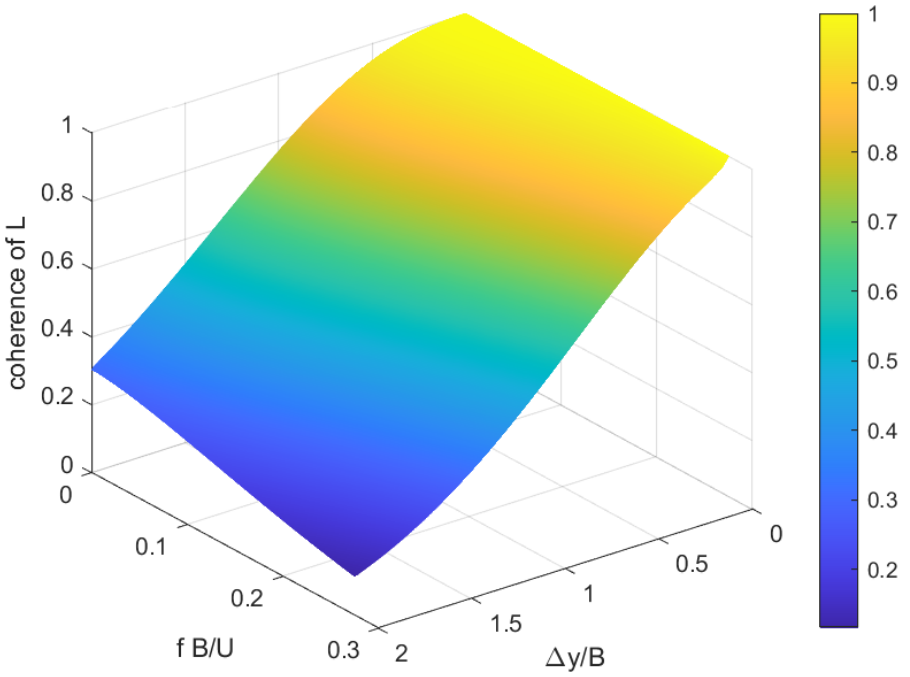

Figure 2.24: Normalized cross-spectrum of the buffeting L for different $\Delta y/B$ and f^*

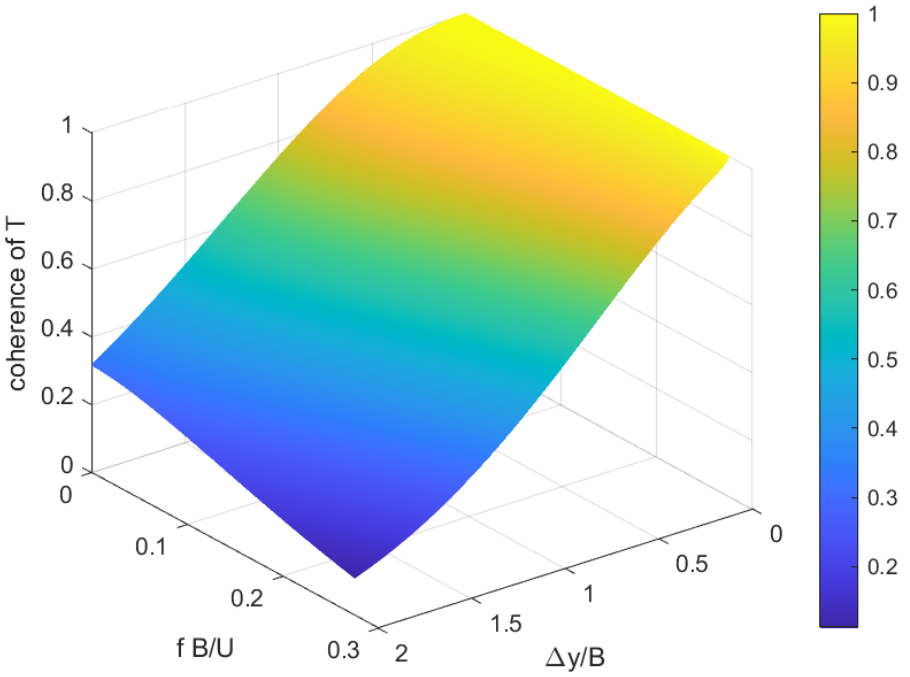

Figure 2.25: Normalized cross-spectrum of the buffeting T for different $\Delta y/B$ and f^*

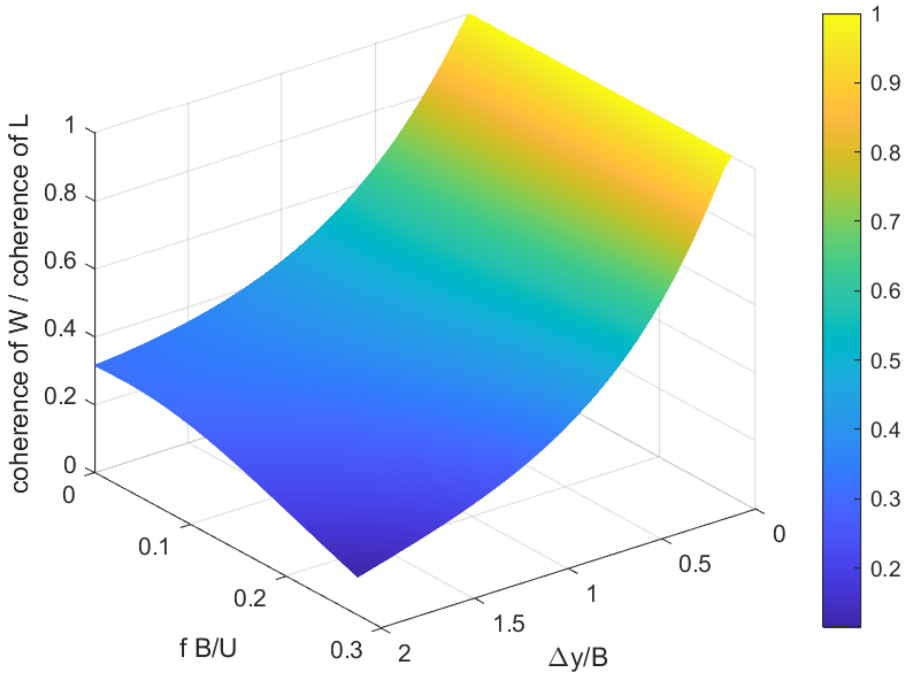

Figure 2.26: Ratio of normalized cross-spectra $coh_w^{1/2}/coh_L^{1/2}$ for different $\Delta y/B$ and f^*

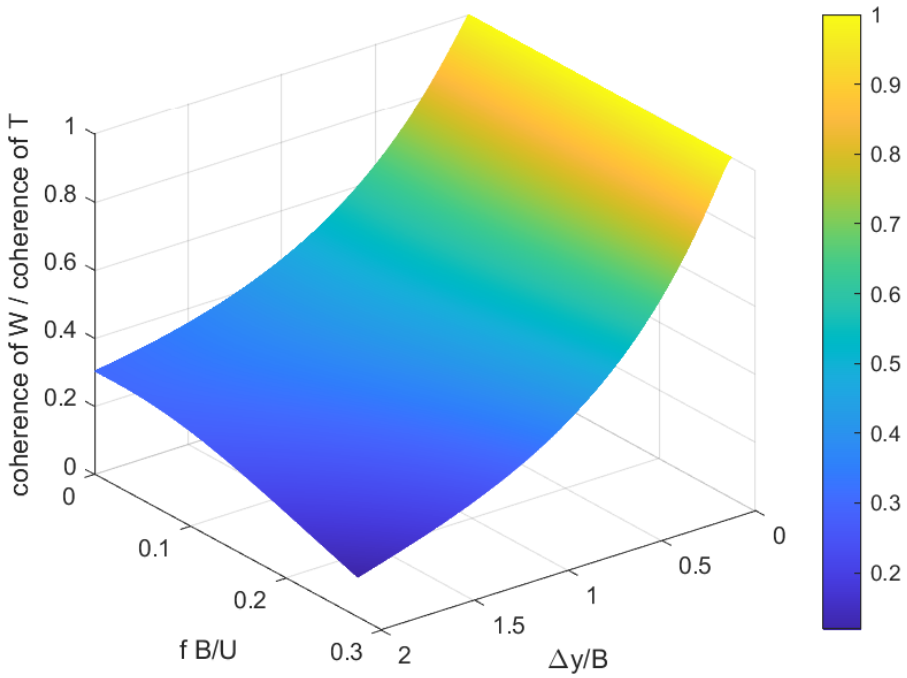

Figure 2.27: Ratio of normalized cross-spectra $coh_w^{1/2}/coh_T^{1/2}$ for different $\Delta y/B$ and f^*

In figures 2.26, 2.27, it is possible to watch the 3D trends of the ratio between $coh_w^{1/2}/coh_L^{1/2}$ and $coh_w^{1/2}/coh_T^{1/2}$ taking into account at the same time the reduced frequency $\frac{fB}{U}$ and the adimensional spacing $\frac{\Delta y}{B}$.

The plots, also in this case, considering the Larose model, display an higher recorrelation with respect the one of the turbulent wind. The results at high reduced frequency f^* and big distance Δy have been not considered in the adapted model for the full Braila bridge, because in these cases there was a lower fitting between the experimental curves and the exponential fitting function.

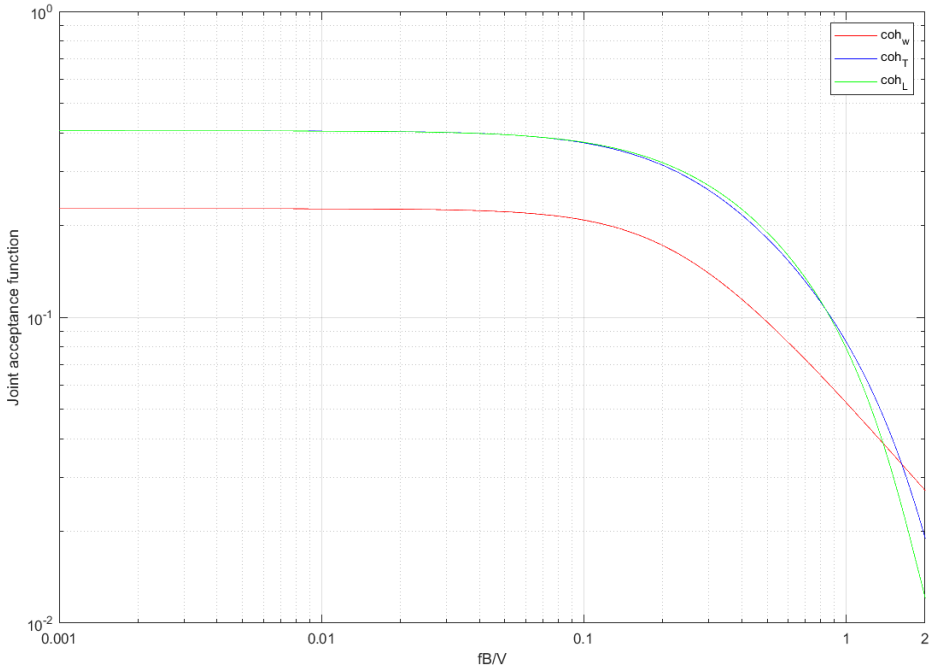

Figure 2.28: Joint acceptance function computed with uniform mode shape ($\mu(y_1) = \mu(y_2) = 1$) for the wind turbulence root coherence (red line), for the lift force (green line) and for the buffeting moment (blue line) according to Larose G.

In figure 2.28 it is possible to look the joint acceptance function[3] $|J(f^*)|^2$ of the span-wise coherence of the aerodynamic forces and of the w component of the turbulent wind. Comparing the green and blue curves to the one of the gusty wind, (red curve), Larose confirmed what was discovered in the previous years by Jakobsen G. and other researchers: there was an important underestimation when the *strip assumption* was assumed to be valid.

[3]This Joint acceptance function has been computed by me considering the Larose G. model described in previous pages.

Chapter 3

Span-wise Coherence of the Aerodynamic Forces for the Braila bridge deck

3.1 Introduction

In this last chapter of my work I am going to introduce the effect of the recorrelation of the aerodynamic forces into the full numerical model of the Braila bridge deck, considering its first thirteen vibration modes.

In order to do this I have adapted through dimensional analysis and numerical fitting the models of Jakobsen J. [2] and Larose G. [1]. For each of the two representations I am going to show how I have obtained the adapted one, and in which way the response of the bridge is affected by the span-wise coherence of the buffeting forces.

In the end of this work I am going to show how is possible to take into account of the recorrelation of the buffeting forces by lowering the number of sections in which is divided the bridge's deck.

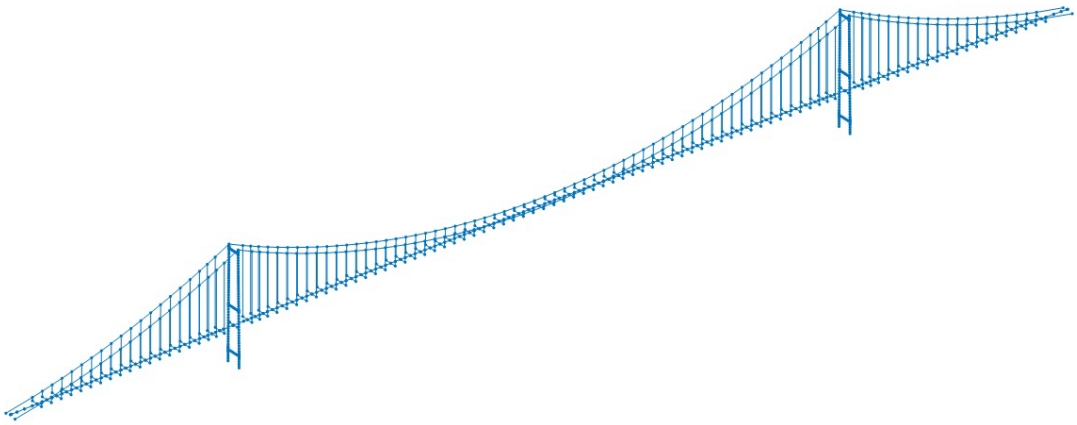

Figure 3.1: Braila bridge FEM model

3.2 Model of Jakobsen J. for Braila Bridge

Starting from the original model I have adapted it by means of non-dimensionalization of c_2 (m^{-1}) constant in this way:

$$coh_{L,M,w}^{1/2}(f,\Delta y) = \exp\left\{ -\left[\frac{\Delta y}{B}\sqrt{(Bc_{2,Braila})^2 + \left(\frac{Bc_3 f}{V}\right)^2}\right]^{c_1}\right\} \tag{3.1}$$

Where the term $c_{2,Braila}$ is obtained by:

$$c_{2,Braila} = \frac{B_{Jakobsen}c_2}{B_{Braila}} \tag{3.2}$$

And the terms in the equation are:

- Fitting coefficient of the Jakobsen J. model c_2 (m^{-1}) that changes passing from w turbulence component to the buffeting lift and moment
- Deck width of the Braila bridge $B_{Braila} = 31.6$ m
- Deck with of the model tested by Jakobsen J. $B_{Jakobsen} = 0.367$ m

The non-dimensionalization process has been done in order to obtain the same non-dimensional groups passing from the original deck section to the Braila one. It has been performed only on the product Bc_2 because c_2 it is the only dimensional (m^{-1}) constant among c_1, c_2 and c_3. In this way the value of c_1 and c_3 remains the same. In the table 3.1 is summarized the value taken by c_1, c_2 and c_3. As expected the value of c_2 constant decreased, taking into account of the ratio between $B_{Jakobsen}$ and B_{Braila}

Simulations have been performed for three different speeds: 20 m/s, 50 m/s and 65 m/s.

Table 3.1: Coefficients c_1, c_2, c_3 of the adapted Jakobsen J. model for the Braila bridge

	c_1	c_2 (m^-1)	c_3
Turbulence component w	1.00	0.049	5.47
Buffeting, Lift	1.40	0.025	2.24
Buffeting, Torsion	1.35	0.028	2.15

Once introduced the adapted model, I am going to show the trends of the functions described above ($coh_w^{1/2}$, $coh_L^{1/2}$ and $coh_w^{1/2}$, $coh_L^{1/2}$) for every wind speed considered (20 m/s, 50 m/s, 65 m/s) and the ratios between $coh_w^{1/2}$ and $coh_L^{1/2}$, $coh_T^{1/2}$. After this I am going to define the input parameters of each numerical simulation that I made. In the end I am going display the effect of the recorrelation on the response of the bridge itself.

3.2.1 Braila bridge deck response for 20 m/s wind velocity

Span-wise coherence for 20 m/s wind velocity

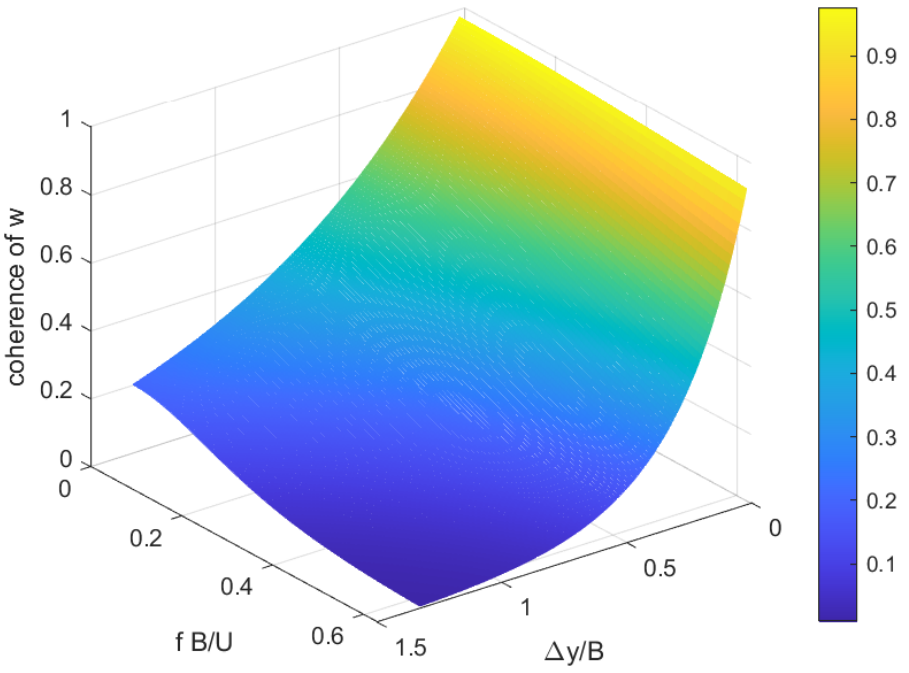

Figure 3.2: Normalized cross-spectrum of the w turbulence component for different $\Delta y/B$ and f^*

In figures 3.2, 3.3 and 3.4 it is possible to examine the 3D trend of the span-wise coherence for w gusty wind component, lift and aerodynamic moment, taking into account at the same time the reduced frequency f^* and the normalized distance between two different point $\frac{\Delta y}{B}$. Also considering the adapted Jakobsen J. representation, as we expected, it confirms the underestimation given by the *strip assumption*. In pictures 3.5, 3.6, it is possible to watch the 3D trends of the ratio between $coh_w^{1/2}/coh_L^{1/2}$ and $coh_w^{1/2}/coh_T^{1/2}$ taking into account at the same time the reduced frequency $\frac{fB}{U}$ and the adimensional spacing $\frac{\Delta y}{B}$.

The plots, also in this case, considering the adapted Jakobsen J. model, display an higher recorrelation with respect the one of the turbulent wind. These functions have been considered in the simulations for all the entire frequency range (f = 0 - 0.4 Hz), but for a reduced spacing between the sections: in the range $\Delta y/B = 0 - 1.52$ for the moment and $\Delta y/B = 0 - 0.76$ for the lift. This has been done in order to cover part of the range of $\Delta y/B$ of Jakobsen J. model and to obtain physical results.

In table 3.2 it is possible to find the parameters concerning the wind generation and the kind of admittance matrix considered in the simulation of the bridge response at 20 m/s.

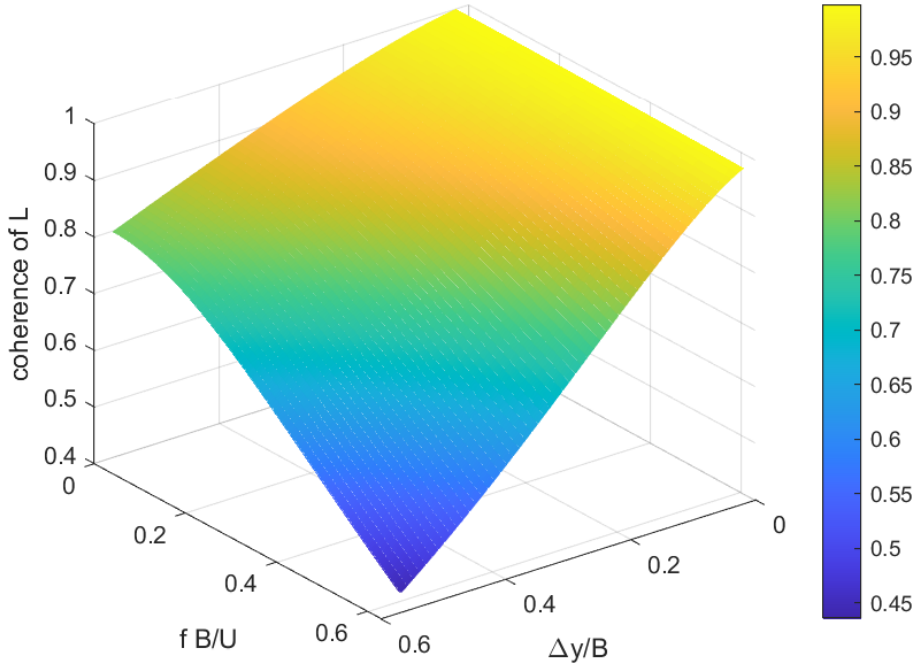

Figure 3.3: Normalized cross-spectrum of the buffeting L for different $\Delta y/B$ and f^*

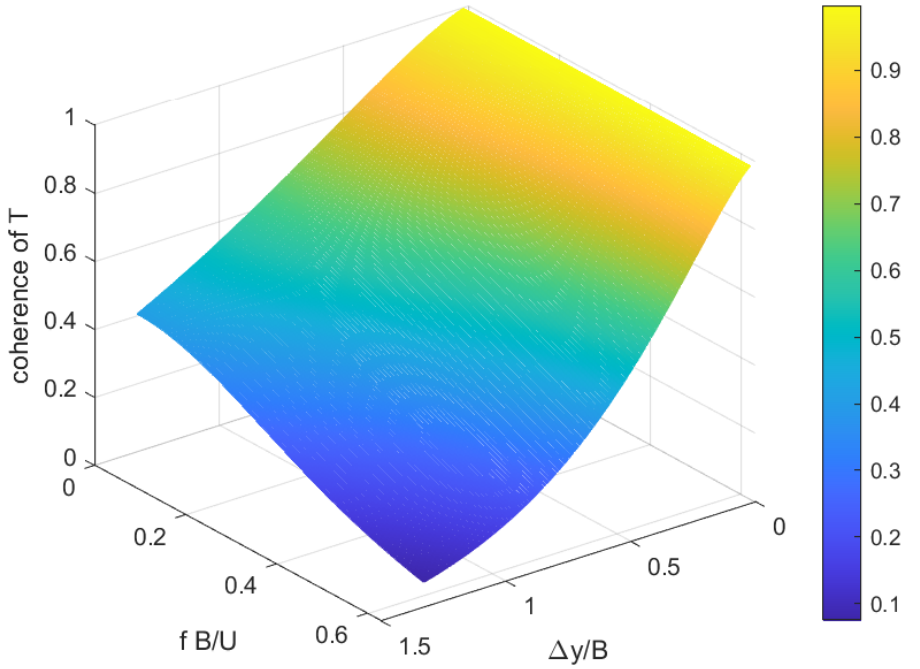

Figure 3.4: Normalized cross-spectrum of the buffeting T for different $\Delta y/B$ and f^*

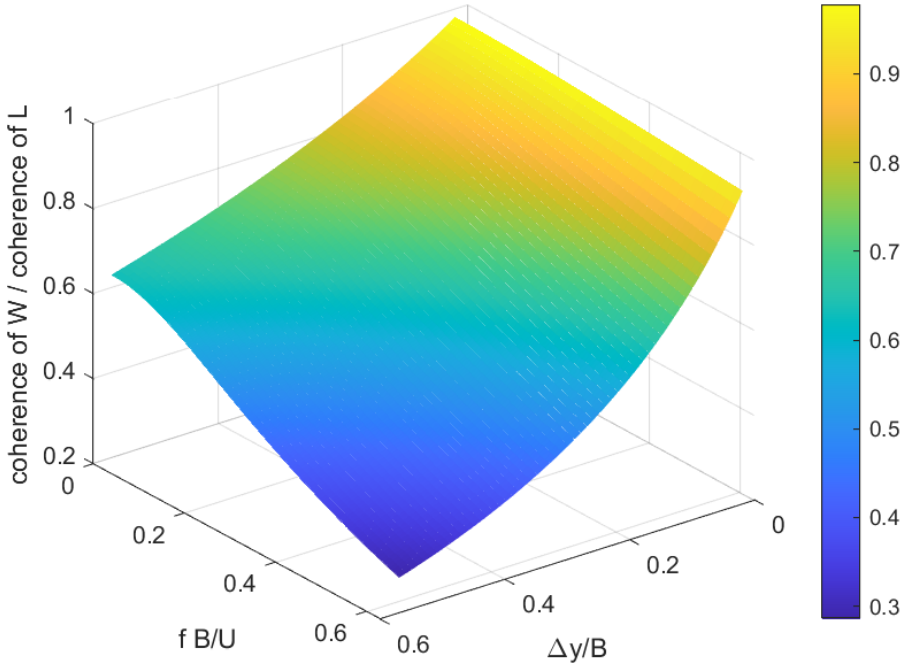

Figure 3.5: Ratio of normalized cross-spectra $coh_w^{1/2}/coh_L^{1/2}$ for different $\Delta y/B$ and f^*

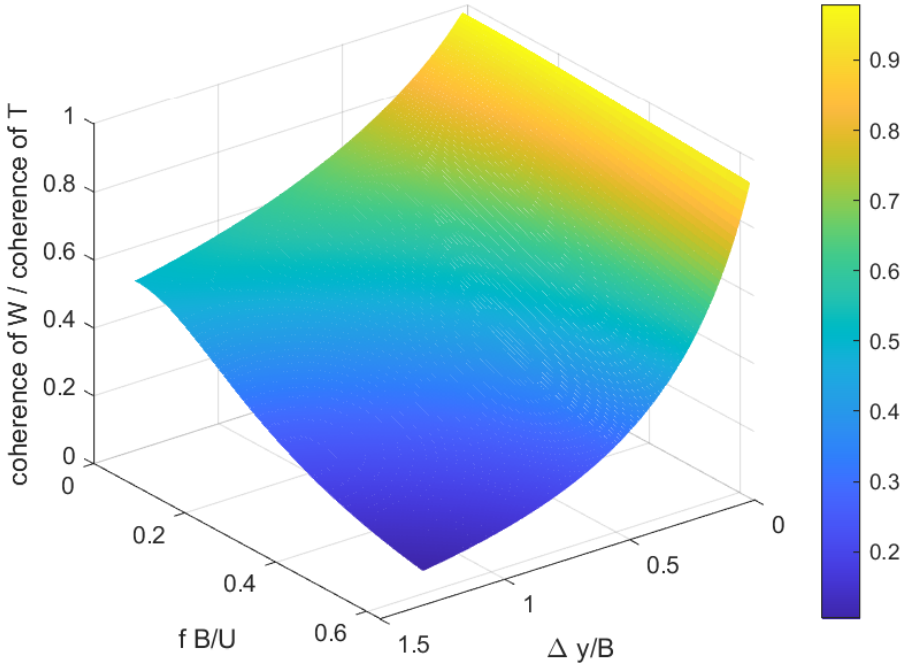

Figure 3.6: Ratio of normalized cross-spectra $coh_w^{1/2}/coh_T^{1/2}$ for different $\Delta y/B$ and f^*

Generation of the PSD of the wind for 20 m/s wind

Table 3.2: Parameters considered for the simulation at 20 m/s

Parameter	Target Value
$\overline{U}$	20 m/s
L_u^x	160 mm
L_w^x	16 mm
I_u	0.143
I_w	0.0715
C_{wx}	0.5
C_{wy}	6.5
C_{wz}	3
C_{ux}	3
C_{uy}	10
C_{uz}	10
C_{vx}	3
C_{vy}	6.5
C_{vz}	6.5
Admittance	Davenport

In figures 3.7, 3.8, 3.9, 3.10, 3.11, 3.12, 3.13 it is possible to observe the PSD of the Lagrangian of the generated wind for each vibration mode. It has been plotted for each of the thirteen modes of the Braila bridge the comparison between the *recorrelated* case (red line) and the *strip assumption* case (blue line).

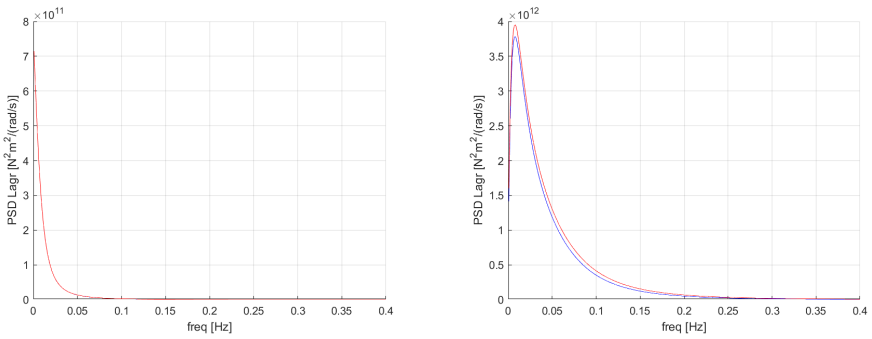

(a) Mode 1H **(b)** Mode 1V

Figure 3.7: PSD of the Lagrangian of the generated wind for mode 1H and 1V

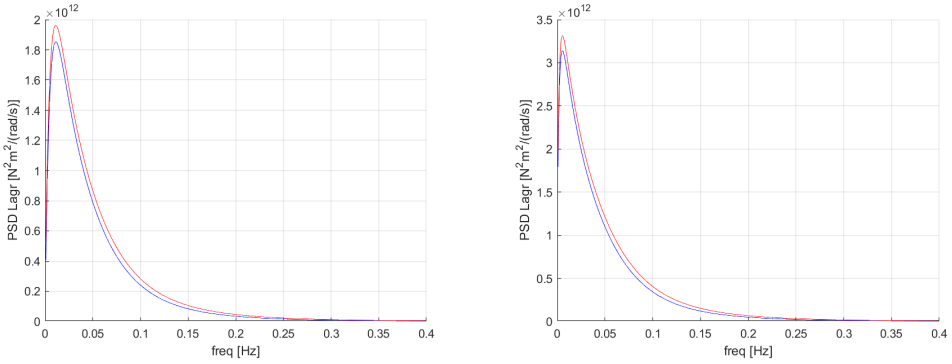

(a) Mode 2A **(b)** Mode 2V

Figure 3.8: PSD of the Lagrangian of the generated wind for mode 2A and 2V

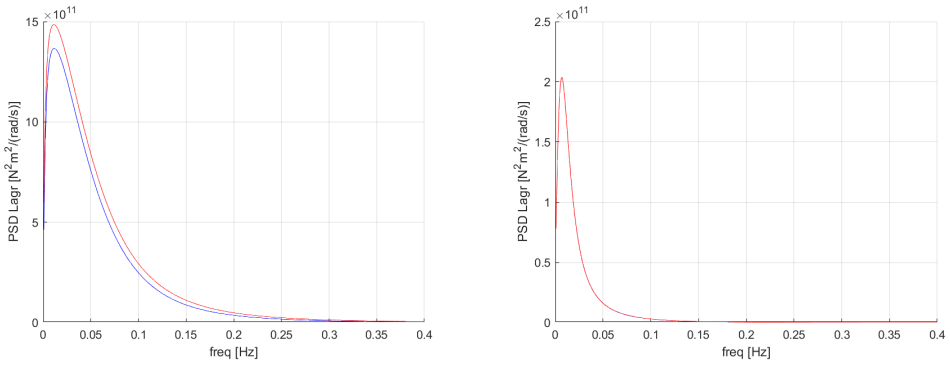

(a) Mode 3V **(b)** Mode 2H

Figure 3.9: PSD of the Lagrangian of the generated wind for mode 3V and 2H

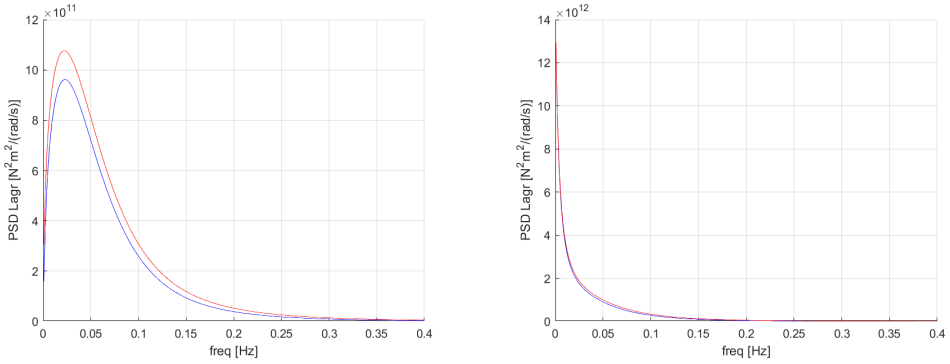

(a) Mode 4V **(b)** Mode 5V

Figure 3.10: PSD of the Lagrangian of the generated wind for mode 4V and 5V

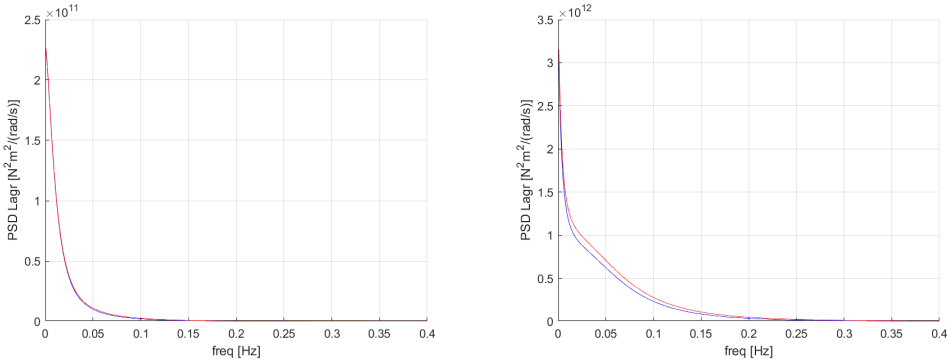

(a) Mode 3H **(b)** Mode 6V

Figure 3.11: PSD of the Lagrangian of the generated wind for mode 3H and 6V

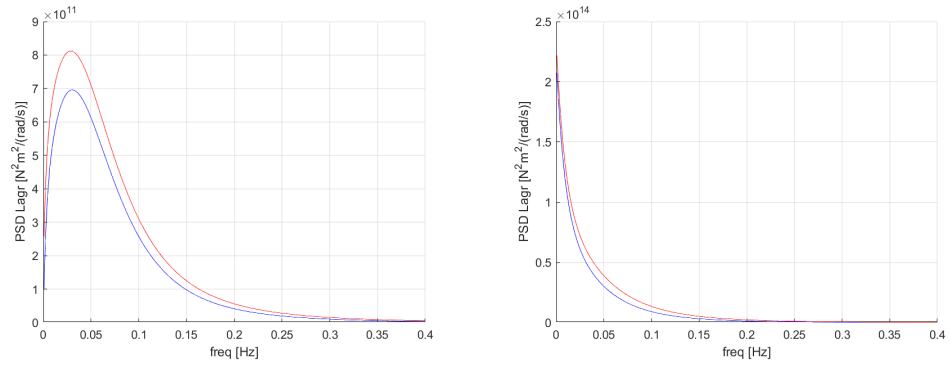

(a) Mode 7V **(b)** Mode 1T

Figure 3.12: PSD of the Lagrangian of the generated wind for mode 7V and 1T

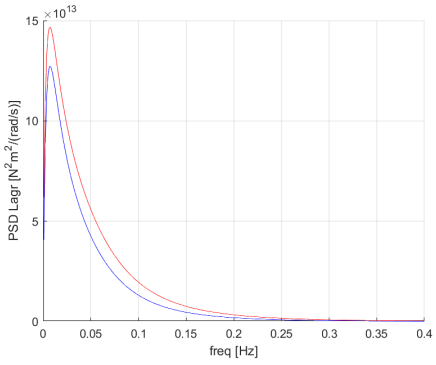

Figure 3.13: PSD of the Lagrangian of the generated wind for mode 2T

As we expected, for each mode, the recorrelated curve is higher in terms of amplitude with respect to the *strip assumption* case in the whole considered frequency range. The modes whose curves are superimposed are the ones that are mainly influenced by the drag contribution, that based on considerations made by previous researchers (i.e. Kimura et al.) have been computed by means of the *strip assumption*.

The convergent number of sections for 20 m/s wind velocity

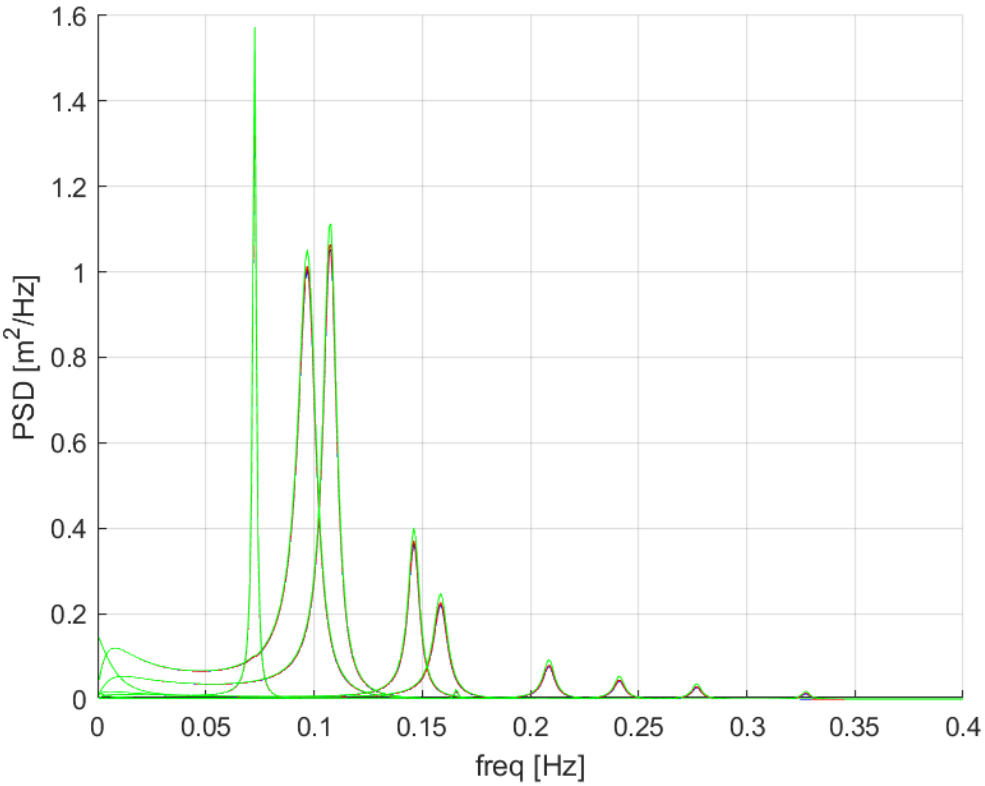

Figure 3.14: PSD of the displacement of the deck for each vibration mode changing number of sections: 82 sections (green line), 164 sections (blue line), 328 sections (red line).

In order to study the dynamic behaviour of the Braila bridge deck, it was initially divided in 82 sections. In order to apply the span - wise coherence function it was necessary to find the number of sections into divide the bridge deck for which the dynamic response did not change. In figures 3.14 and 3.15 it is possible to recognize that the convergent number of sections is 328. In order to have a better representation, in figure 3.15, the contribution of the first mode of vibration has been cancelled.

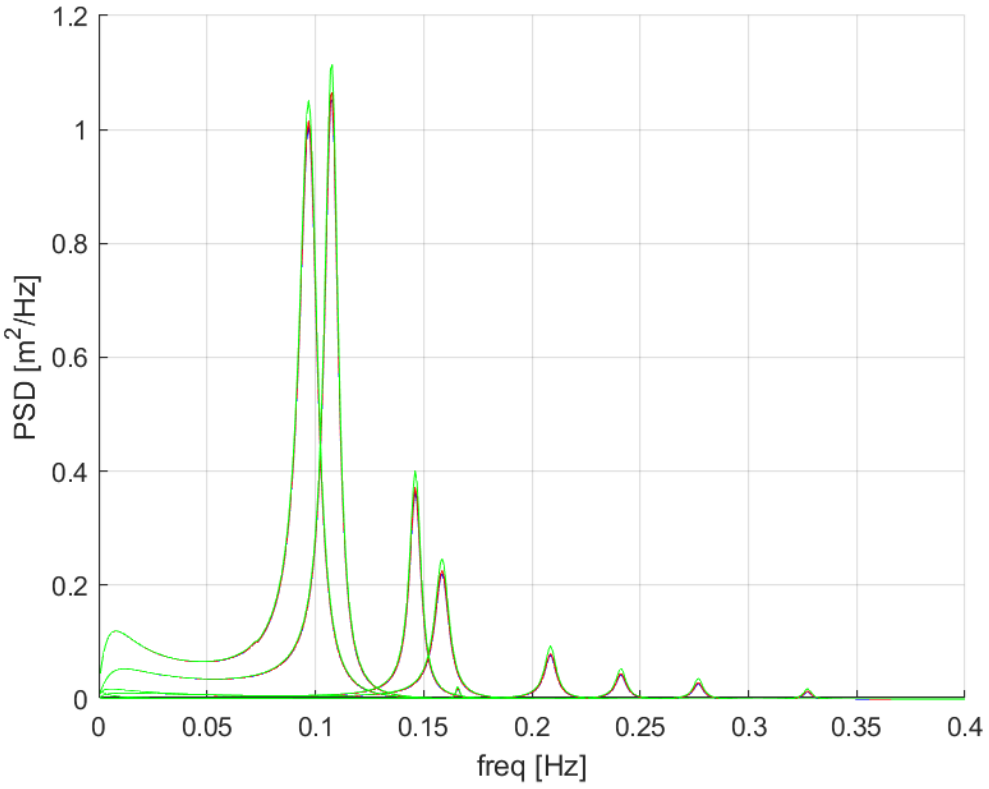

Figure 3.15: PSD of the displacement of the deck for each vibration mode except 1st changing number of sections: 82 sections (green line), 164 sections (blue line), 328 sections (red line).

Effect of the span-wise coherence on the bridge response for 20 m/s wind velocity

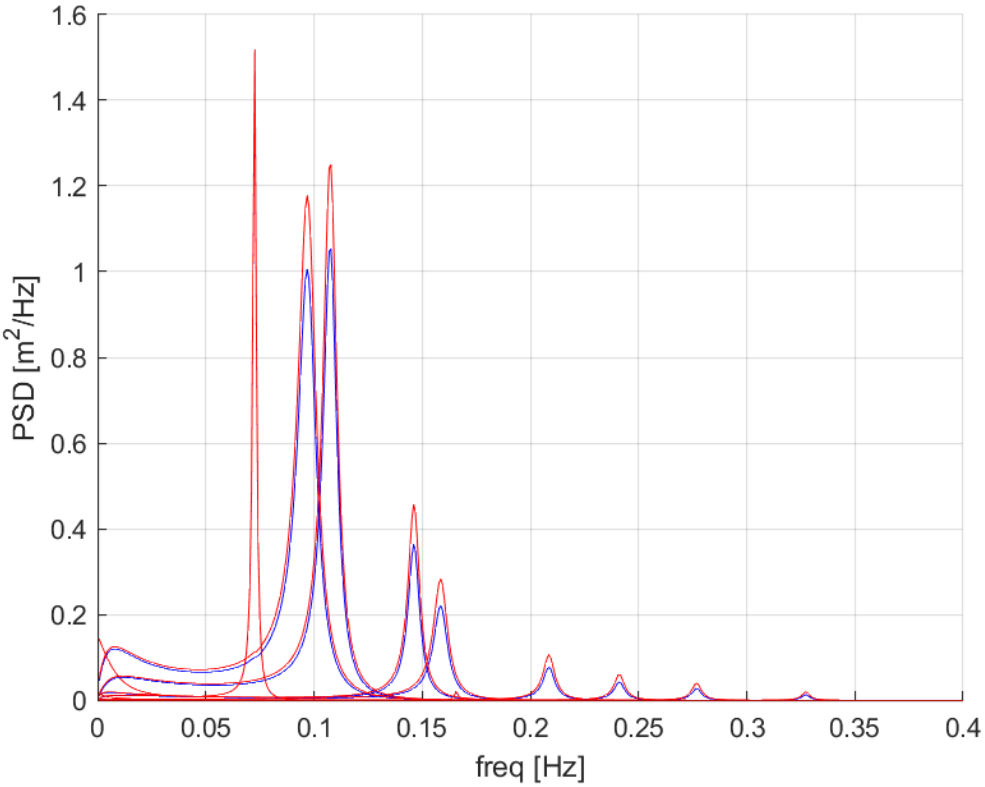

Figure 3.16: PSD of the displacement of the deck for each vibration mode with the span-wise coherence (red line) or the strip assumption (blue line).

In figure 3.16 and 3.17 it is possible to recognize the modal displacement of the Braila deck for each vibration mode. In picture 3.18 it is possible to see the modal acceleration of the deck. In figures 3.19, 3.20, 3.21 we can watch the accelerations along y, z and ϑ for sections $S2$, $S3$, $S4$.

All the plots described above have been performed using a number of sections equal to 328 (convergent number).

It is clear that the effect of recorrelation of buffeting forces is more important in correspondence of the peaks of resonance, then it is an effect that has to be considered during the design of the bridge and in its fatigue life. As we expected in all the cases mentioned above the *strip assumption* produces an underestimation of the results, that in certain cases could be quite big and it has to be taken into account.

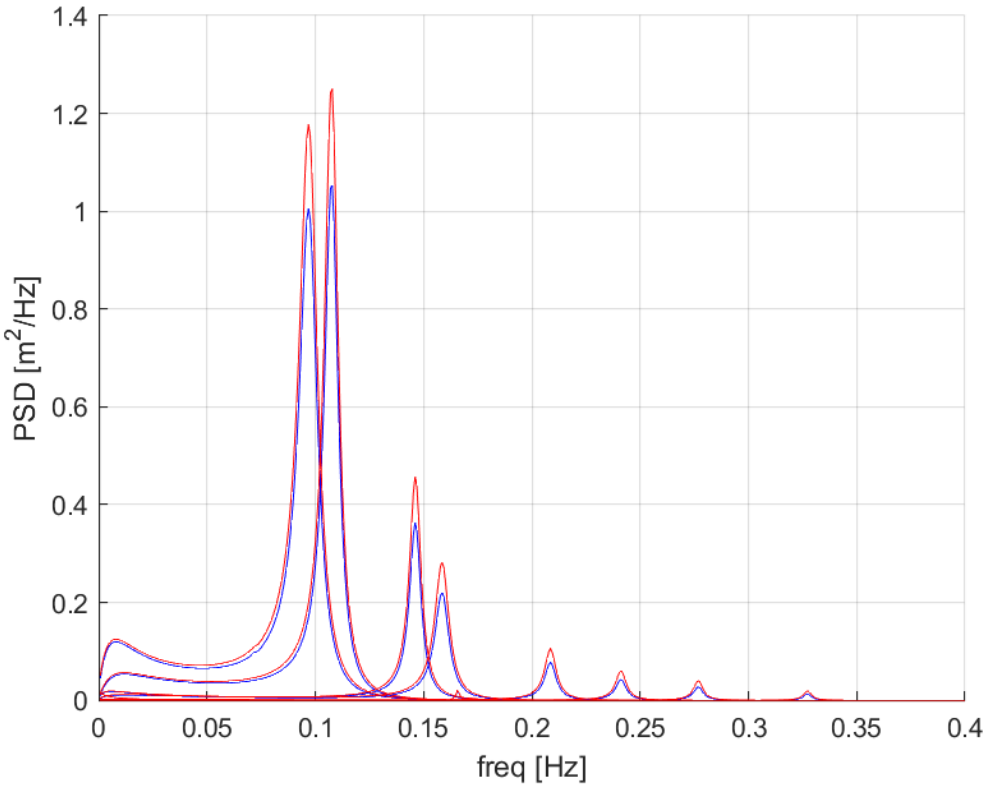

Figure 3.17: PSD of the displacement of the deck for each vibration mode except 1st with the span-wise coherence (red line) or the strip assumption (blue line).

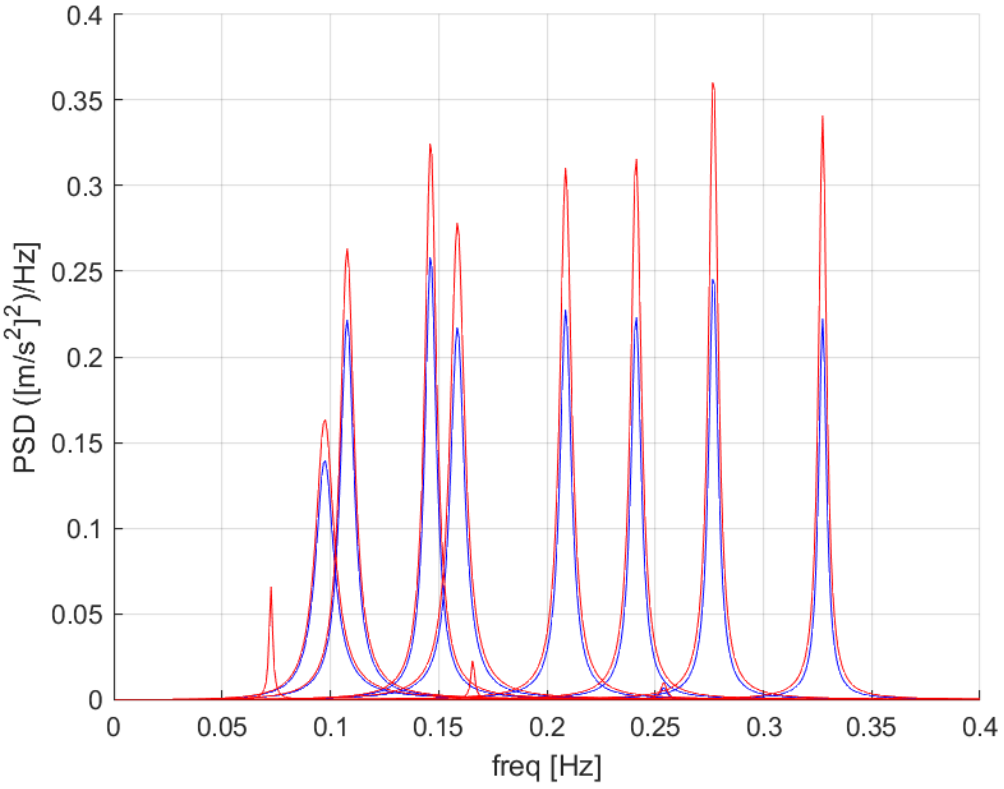

Figure 3.18: PSD of the modal acceleration of the deck with recorrelation (red line) or strip assumption (blue line).

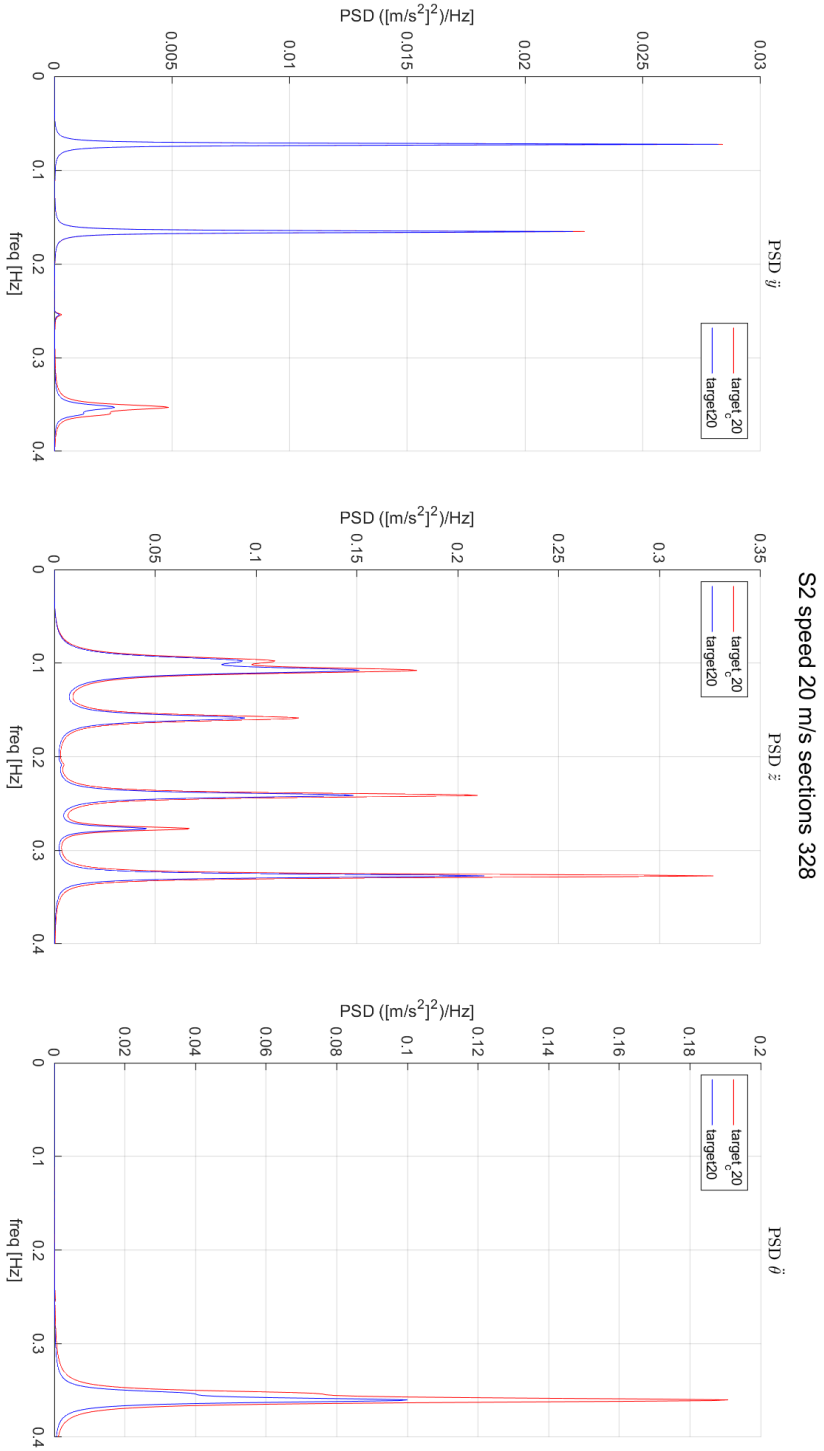

Figure 3.19: PSD of the acceleration along y, z and ϑ for section S2.

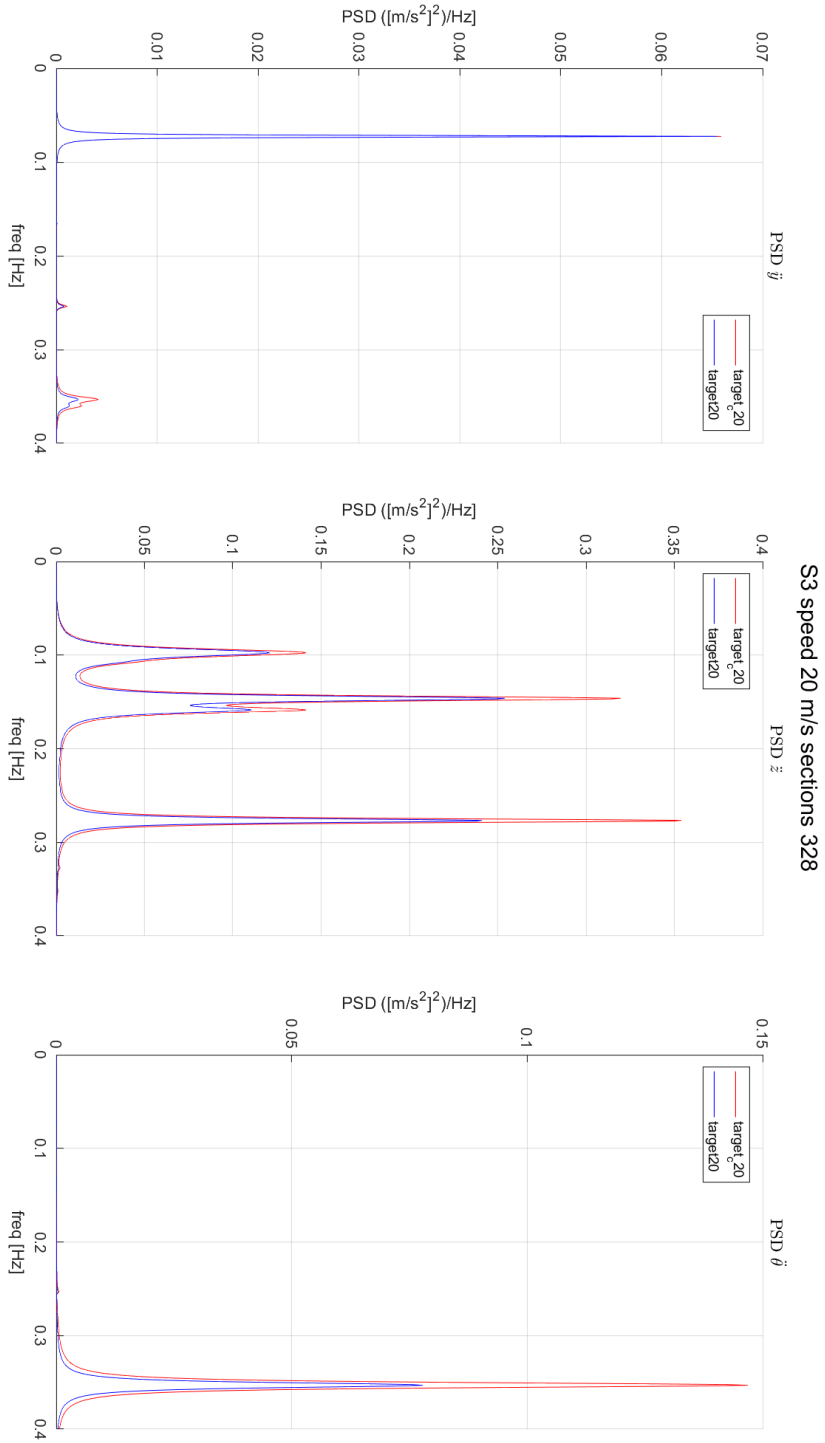

Figure 3.20: PSD of the acceleration along y, z and ϑ for section S3.

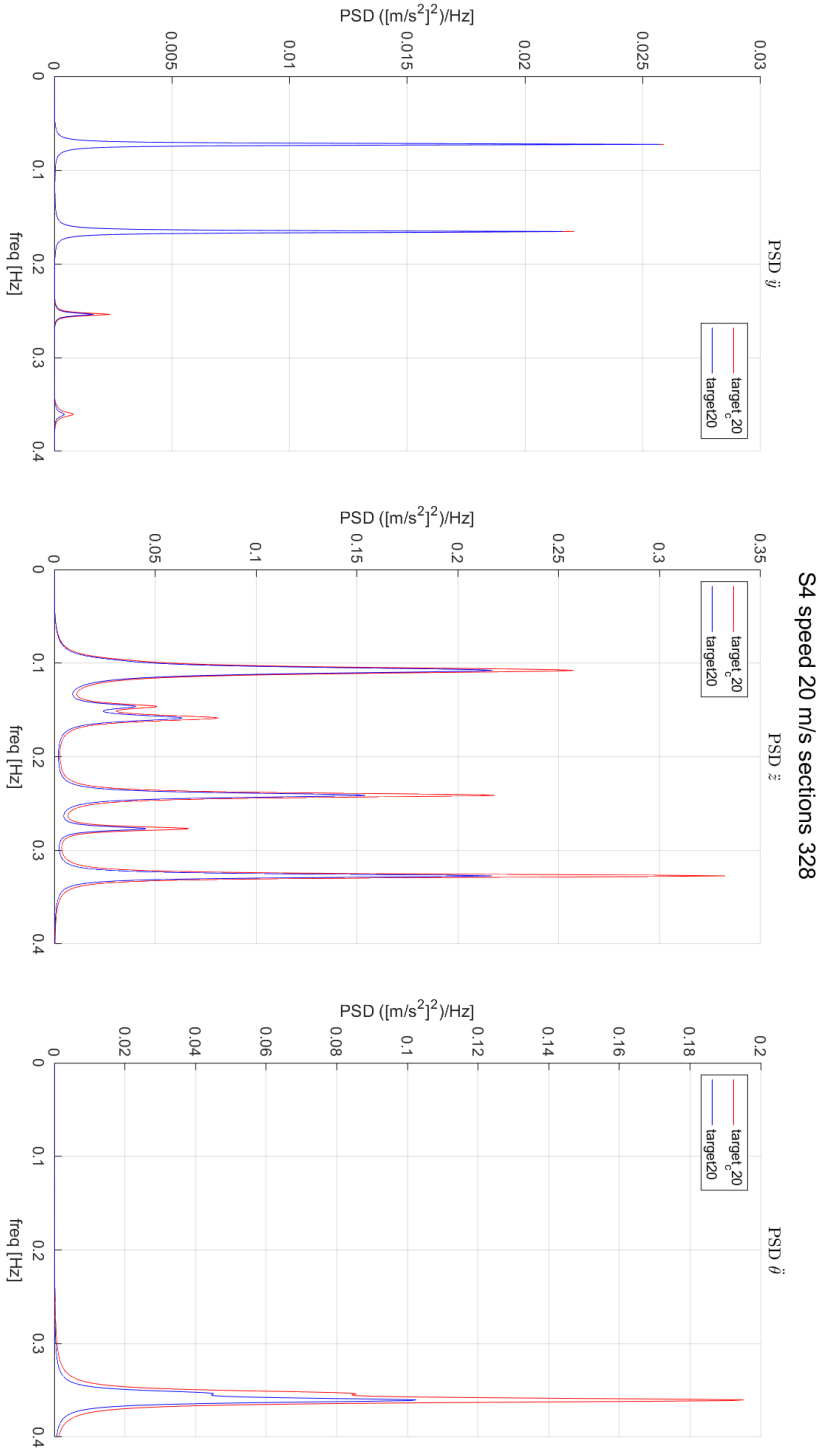

Figure 3.21: PSD of the acceleration along y, z and ϑ for section S4.

3.2.2 Braila bridge deck response for 50 m/s wind velocity

Span-wise coherence for 50 m/s wind velocity

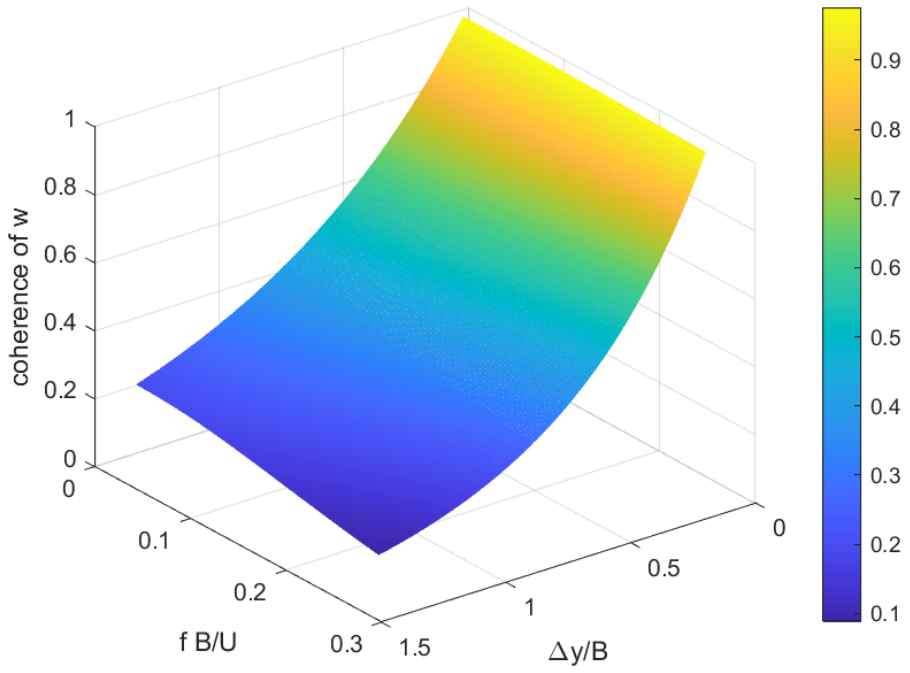

Figure 3.22: Normalized cross-spectrum of the w turbulence component for different $\Delta y/B$ and f^*

In figures 3.22, 3.23 and 3.24 it is possible to examine the 3D trend of the span-wise coherence for w gusty wind component, lift and aerodynamic moment, taking into account at the same time the reduced frequency f^* and the normalized distance between two different point $\frac{\Delta y}{B}$. Also considering the adapted Jakobsen J. representation, as we expected, it confirms the underestimation given by the *strip assumption*. In pictures 3.25, 3.26, it is possible to watch the 3D trends of the ratio between $coh_w^{1/2}/coh_L^{1/2}$ and $coh_w^{1/2}/coh_T^{1/2}$ taking into account at the same time the reduced frequency $\frac{fB}{U}$ and the adimensional spacing $\frac{\Delta y}{B}$.

The plots, also in this case, considering the adapted Jakobsen J. model, display an higher recorrelation with respect the one of the turbulent wind. These functions have been considered in the simulations for all the entire frequency range (f = 0 - 0.4 Hz), but for a reduced spacing between the sections: in the range $\Delta y/B = 0 - 1.52$ for the moment and $\Delta y/B = 0 - 0.76$ for the lift. This has been done in order to cover part of the range of $\Delta y/B$ of Jakobsen J. model and to obtain physical results.

In table 3.3 it is possible to find the parameters concerning the wind generation and the kind of admittance matrix considered in the simulation of the bridge response at 50 m/s.

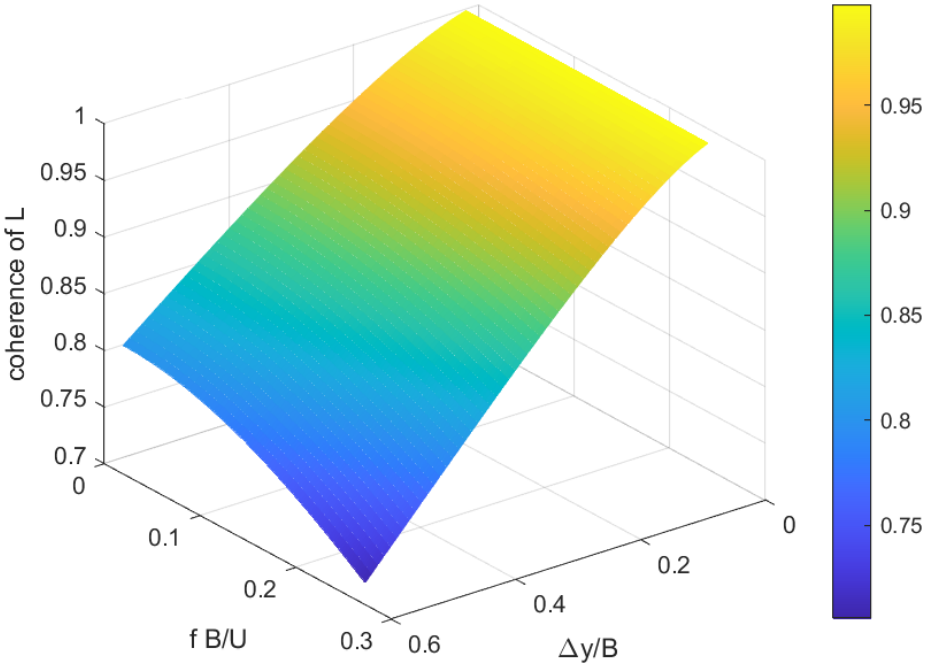

Figure 3.23: Normalized cross-spectrum of the buffeting L for different $\Delta y/B$ and f^*

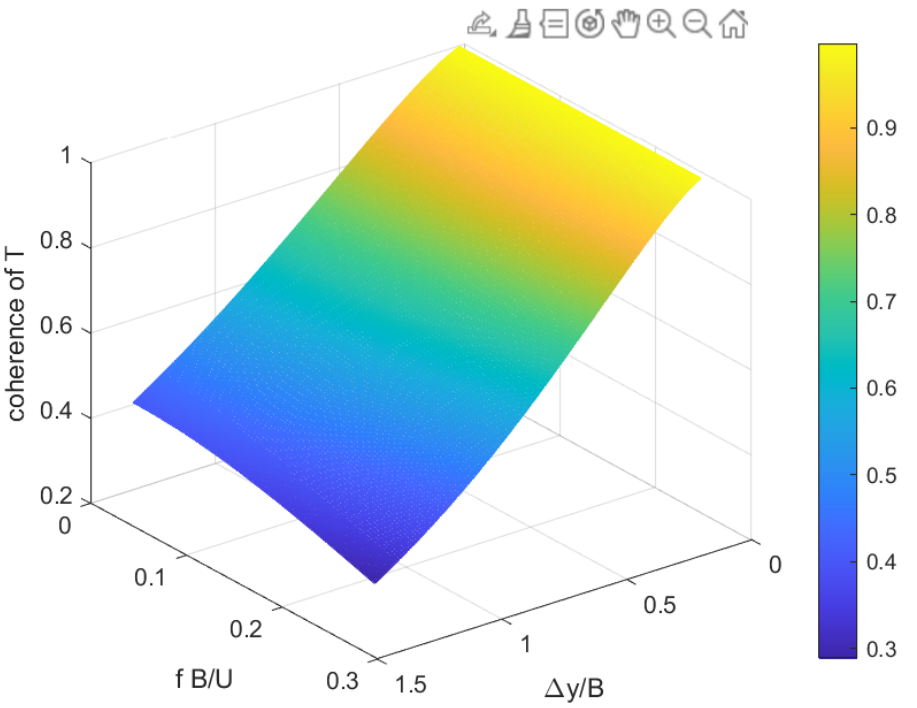

Figure 3.24: Normalized cross-spectrum of the buffeting T for different $\Delta y/B$ and f^*

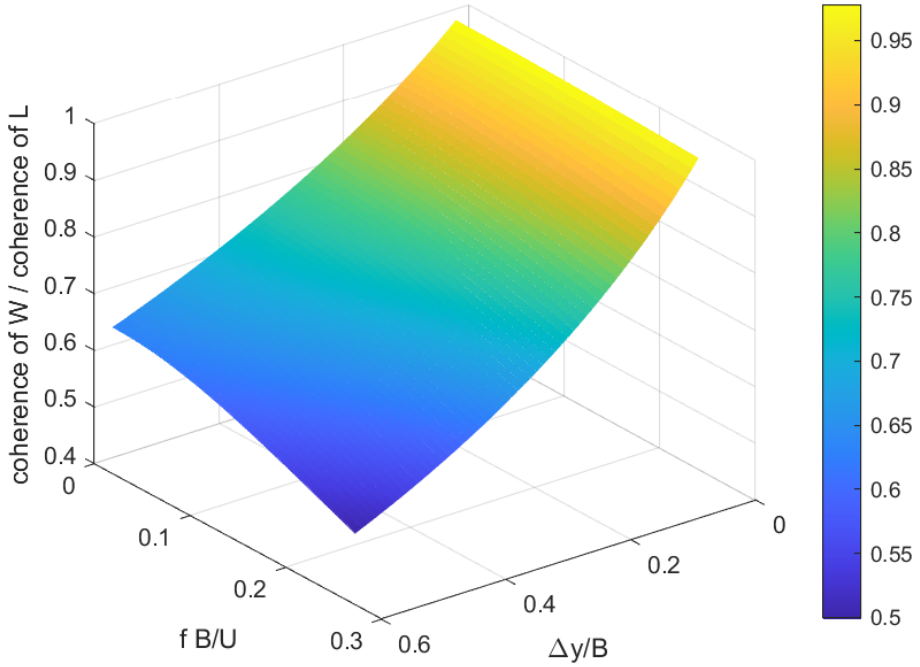

Figure 3.25: Ratio of normalized cross-spectra $coh_w^{1/2}/coh_L^{1/2}$ for different $\Delta y/B$ and f^*

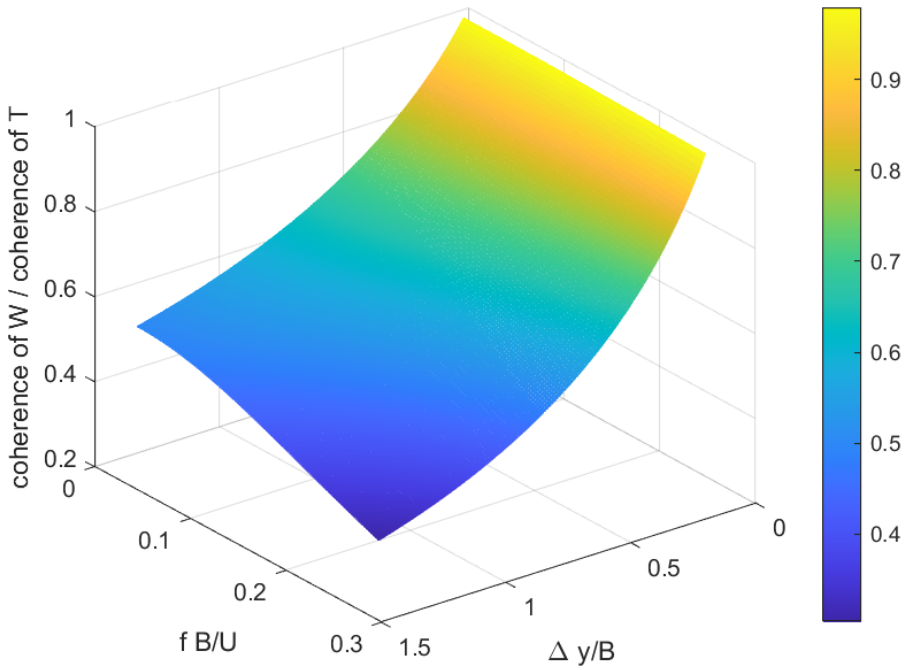

Figure 3.26: Ratio of normalized cross-spectra $coh_w^{1/2}/coh_T^{1/2}$ for different $\Delta y/B$ and f^*

Generation of the PSD of the wind for 50 m/s wind

Table 3.3: Parameters considered for the simulation at 50 m/s

Parameter	Target Value
$\overline{U}$	50 m/s
L_u^x	160 mm
L_w^x	16 mm
I_u	0.143
I_w	0.0715
C_{wx}	0.5
C_{wy}	6.5
C_{wz}	3
C_{ux}	3
C_{uy}	10
C_{uz}	10
C_{vx}	3
C_{vy}	6.5
C_{vz}	6.5
Admittance	Davenport

In figures 3.27, 3.28, 3.29, 3.30, 3.31, 3.32, 3.33 it is possible to observe the PSD of the Lagrangian of the generated wind for each vibration mode. It has been plotted for each of the thirteen modes of the Braila bridge the comparison between the *recorrelated* case (red line) and the *strip assumption* case (blue line).

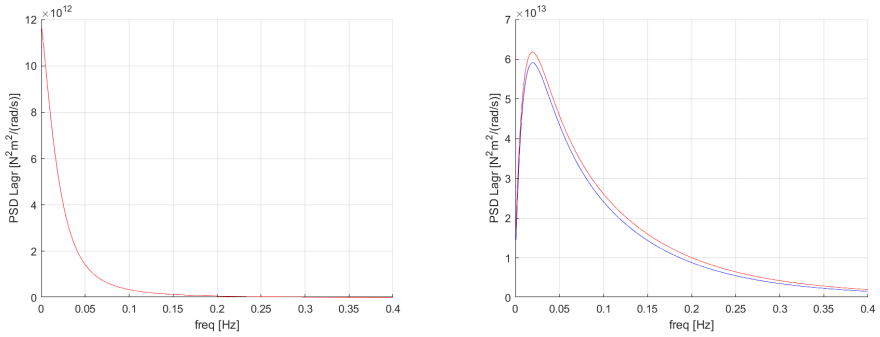

(a) Mode 1H **(b)** Mode 1V

Figure 3.27: PSD of the Lagrangian of the generated wind for mode 1H and 1V

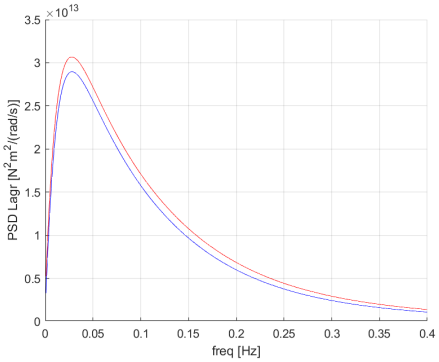

(a) Mode 2A

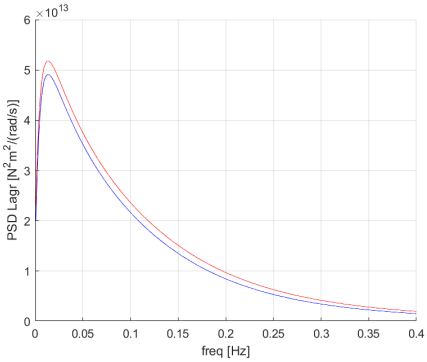

(b) Mode 2V

Figure 3.28: PSD of the Lagrangian of the generated wind for mode 2A and 2V

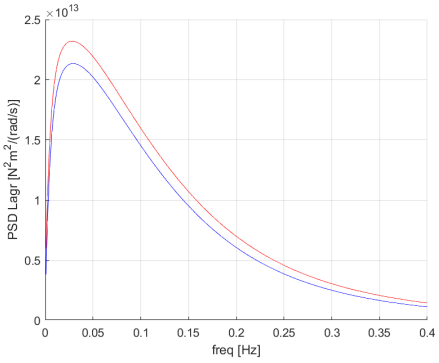

(a) Mode 3V

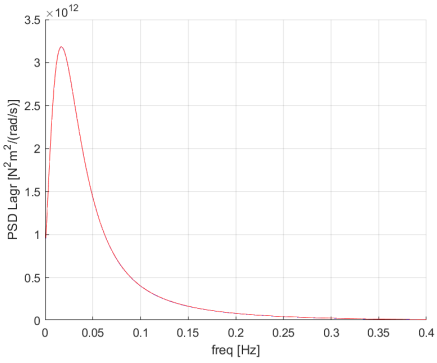

(b) Mode 2H

Figure 3.29: PSD of the Lagrangian of the generated wind for mode 3V and 2H

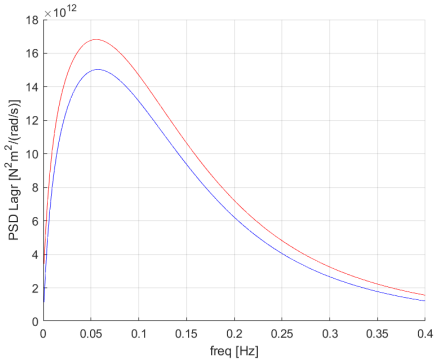

(a) Mode 4V

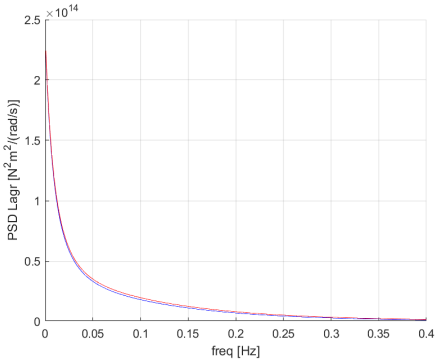

(b) Mode 5V

Figure 3.30: PSD of the Lagrangian of the generated wind for mode 4V and 5V

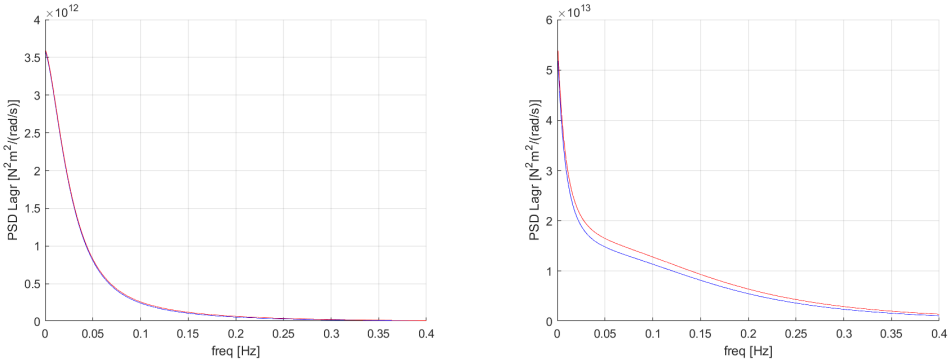

(a) Mode 3H **(b)** Mode 6V

Figure 3.31: PSD of the Lagrangian of the generated wind for mode 3H and 6V

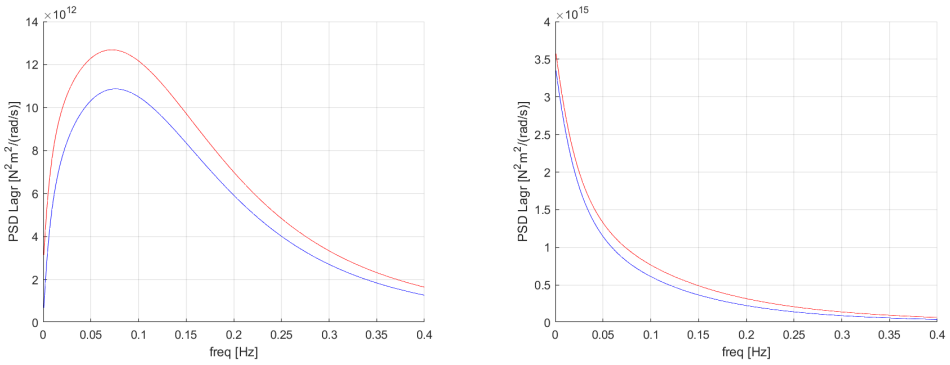

(a) Mode 7V **(b)** Mode 1T

Figure 3.32: PSD of the Lagrangian of the generated wind for mode 7V and 1T

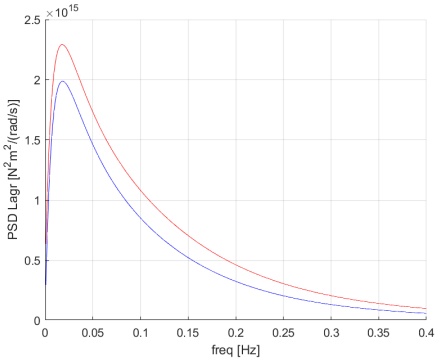

Figure 3.33: PSD of the Lagrangian of the generated wind for mode 2T

As we expected for each mode the recorrelated curve is higher in terms of amplitude with respect to the *strip assumption* case, in the whole considered frequency range. The modes whose curves are superimposed are the ones that are mainly influenced by the drag contribution, that based on considerations made by previous researchers (i.e. Kimura et al.) have been computed by means of the *strip assumption*.

The convergent number of sections for 50 m/s wind velocity

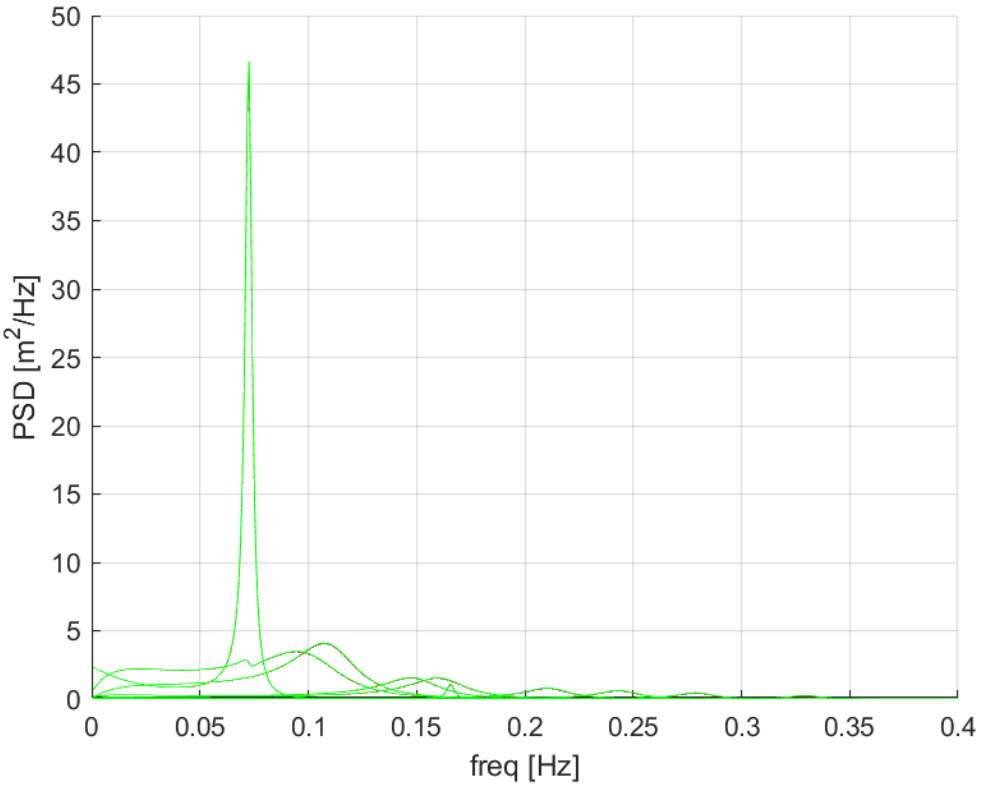

Figure 3.34: PSD of the displacement of the deck for each vibration mode changing number of sections: 82 sections (green line), 164 sections (blue line), 328 sections (red line).

In order to study the dynamic behaviour of the Braila bridge deck, it was initially divided in 82 sections. In order to apply the span - wise coherence function it was necessary to find the number of sections into divide the bridge for which the dynamic response did not change. In figures 3.34 and 3.35 it is possible to recognize that the convergent number of sections is 328. In order to have a better representation, in figure, 3.35, the contribution of the first mode of vibration has been cancelled.

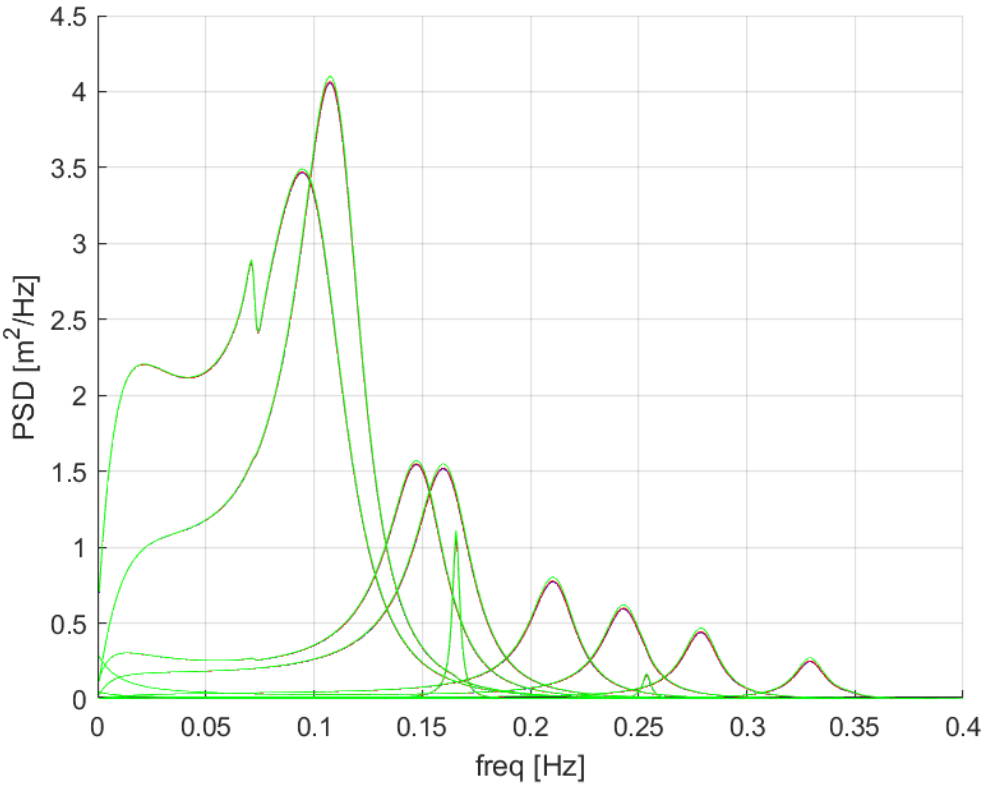

Figure 3.35: PSD of the displacement of the deck for each vibration mode except 1st changing number of sections: 82 sections (green line), 164 sections (blue line), 328 sections (red line).

Effect of the span-wise coherence on the bridge response for 50 m/s wind velocity

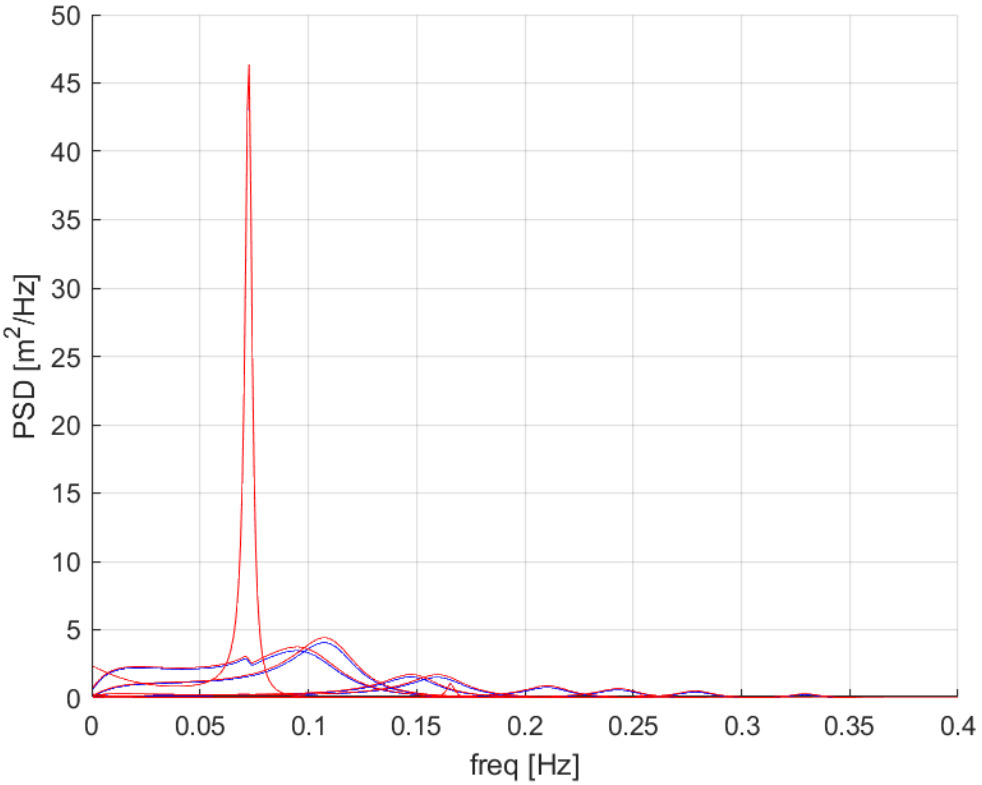

Figure 3.36: PSD of the displacement of the deck for each vibration mode with the span-wise coherence (red line) or the strip assumption (blue line).

In figure 3.36 and 3.37 it is possible to recognize the modal displacement of the Braila deck for each vibration mode. In picture 3.38 it is possible to see the modal acceleration of the deck. In figures 3.39, 3.40, 3.41 we can watch the accelerations along y, z and ϑ for sections $S2$, $S3$, $S4$.

All the plots described above have been performed using a number of sections equal to 328 (convergent number).

It is clear that the effect of recorrelation of buffeting forces is more important in correspondence of the peaks of resonance, than it is an effect that has to be considered during the design of the bridge and in its fatigue life. As we expected in all the cases mentioned above the *strip assumption* produces an underestimation of the results, that in certain cases could be quite big and it has to be taken into account. Passing from 20 m/s to 50 m/s it is possible to see that the effect of recorrelation is decreasing (blue and red curve are closer).

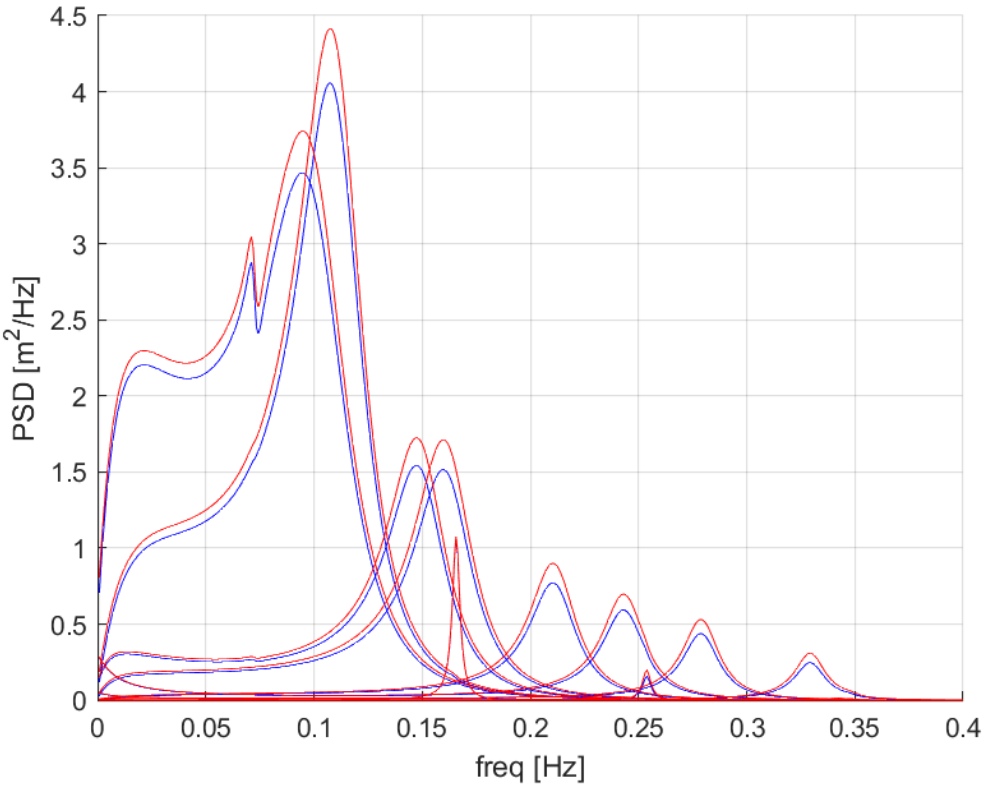

Figure 3.37: PSD of the displacement of the deck for each vibration mode except 1st with the span-wise coherence (red line) or the strip assumption (blue line).

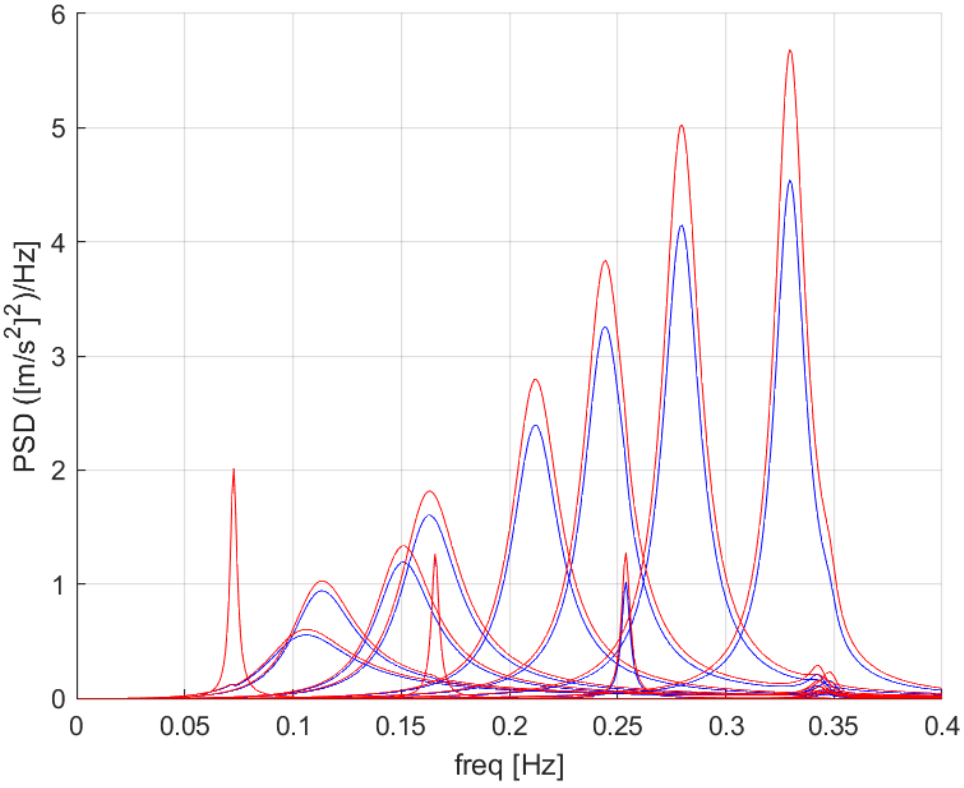

Figure 3.38: PSD of the modal acceleration of the deck with recorrelation (red line) or strip assumption (blue line).

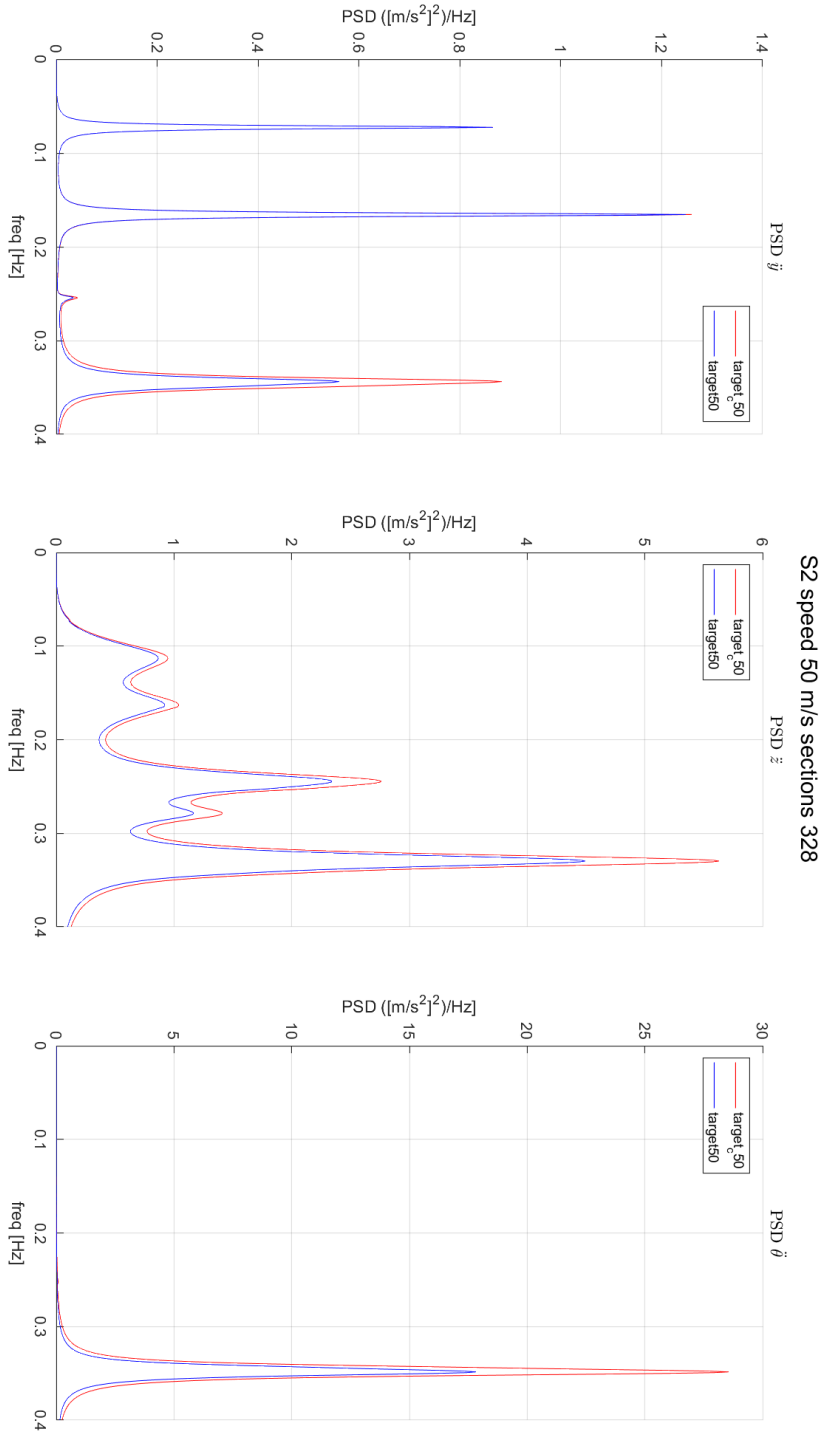

Figure 3.39: PSD of the acceleration along y, z and ϑ for section S2.

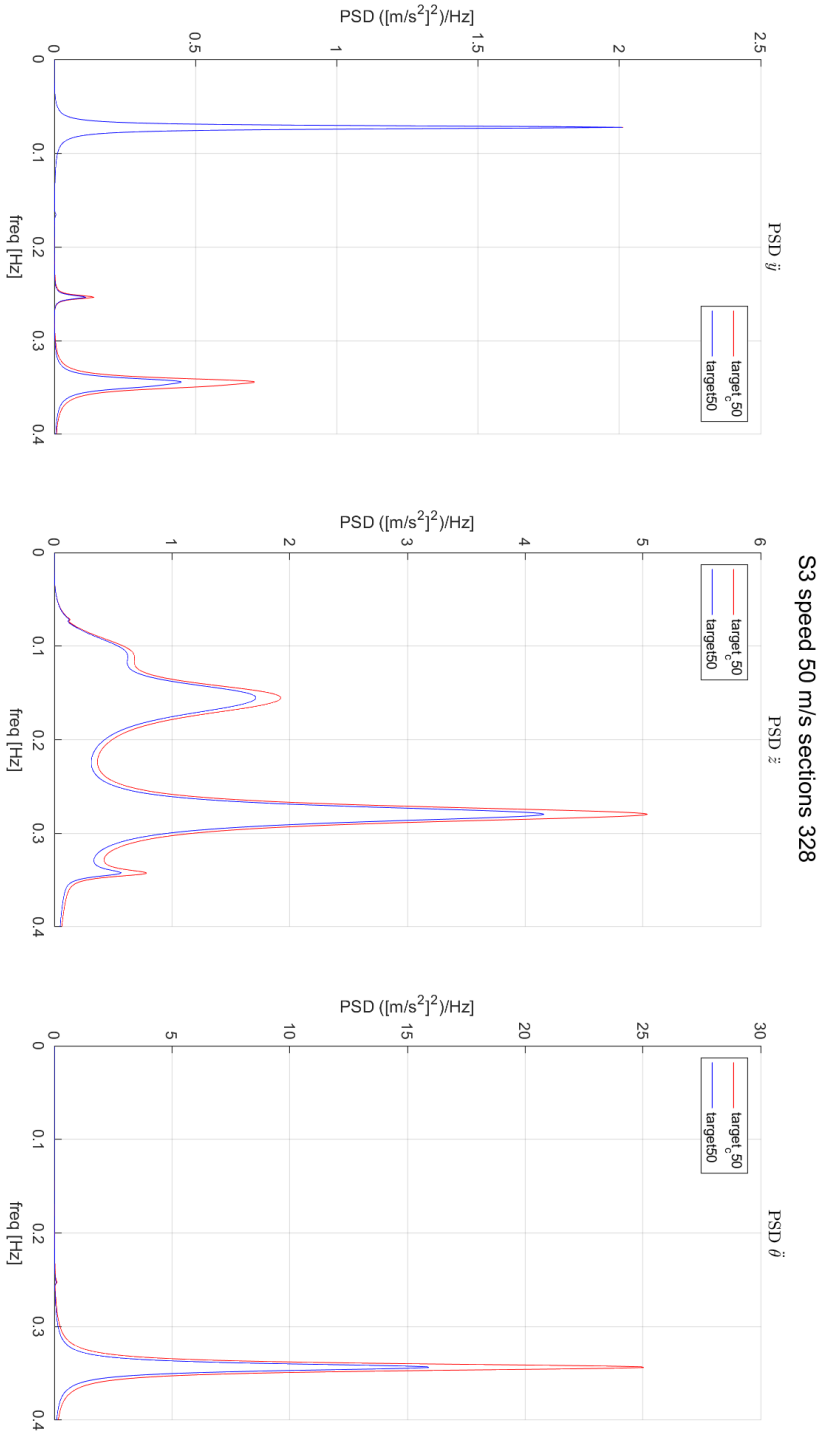

Figure 3.40: PSD of the acceleration along y, z and ϑ for section S3.

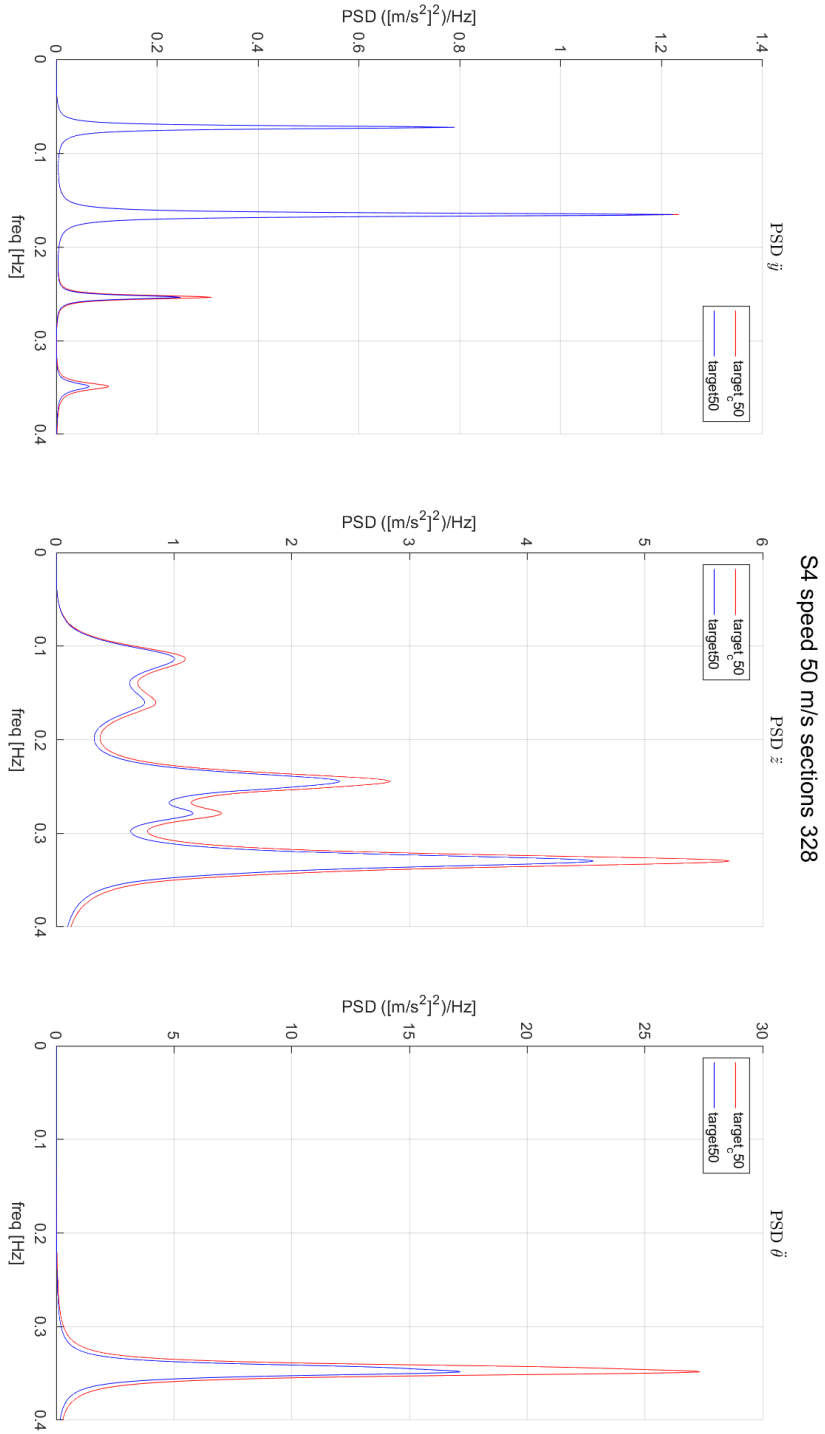

Figure 3.41: PSD of the acceleration along y, z and ϑ for section S4.

3.2.3 Braila bridge deck response for 65 m/s wind velocity

Span-wise coherence for 65 m/s wind velocity

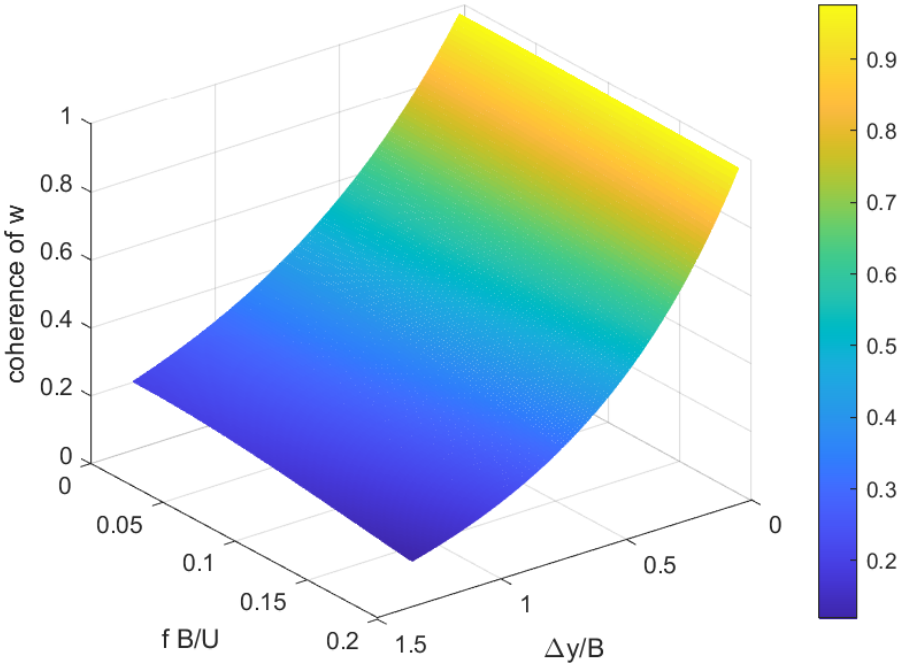

Figure 3.42: Normalized cross-spectrum of the w turbulence component for different $\Delta y/B$ and f^*

In figures 3.42, 3.43 and 3.44 it is possible to examine the 3D trend of the span-wise coherence for w gusty wind component, lift and aerodynamic moment, taking into account at the same time the reduced frequency f^* and the normalized distance between two different point $\frac{\Delta y}{B}$. Also considering the adapted Jakobsen J. representation, as we expected, it confirms the underestimation given by the *strip assumption*. In pictures 3.45, 3.46, it is possible to watch the 3D trends of the ratio between $coh_w^{1/2}/coh_L^{1/2}$ and $coh_w^{1/2}/coh_T^{1/2}$ taking into account at the same time the reduced frequency $\frac{fB}{U}$ and the adimensional spacing $\frac{\Delta y}{B}$.

The plots, also in this case, considering the adapted Jakobsen J. model, display an higher recorrelation with respect the one of the turbulent wind. These functions have been considered in the simulations for all the entire frequency range (f = 0 - 0.4 Hz), but for a reduced spacing between the sections: in the range $\Delta y/B = 0 - 1.52$ for the moment and $\Delta y/B = 0 - 0.76$ for the lift. This has been done in order to cover part of the range of $\Delta y/B$ of Jakobsen J. model and to obtain physical results.

In table 3.4 it is possible to find the parameters concerning the wind generation and the kind of admittance matrix considered in the simulation of the bridge response at 65 m/s.

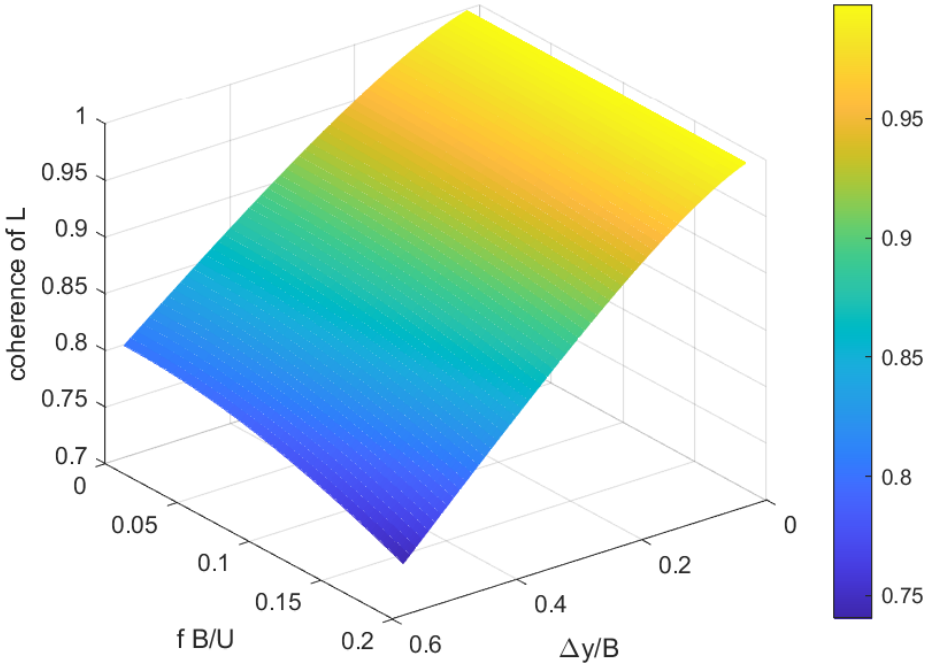

Figure 3.43: Normalized cross-spectrum of the buffeting L for different $\Delta y/B$ and f^*

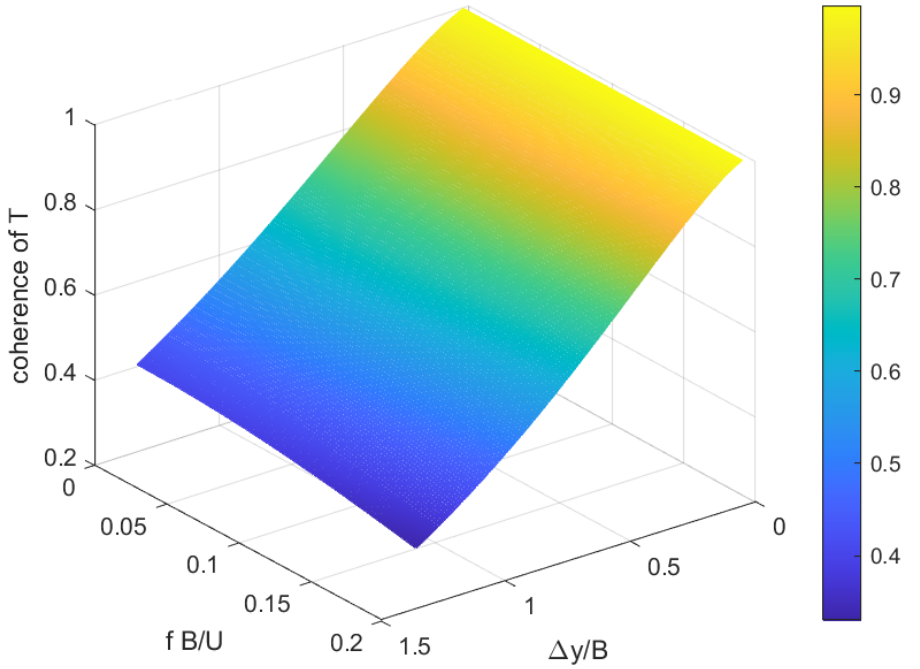

Figure 3.44: Normalized cross-spectrum of the buffeting T for different $\Delta y/B$ and f^*

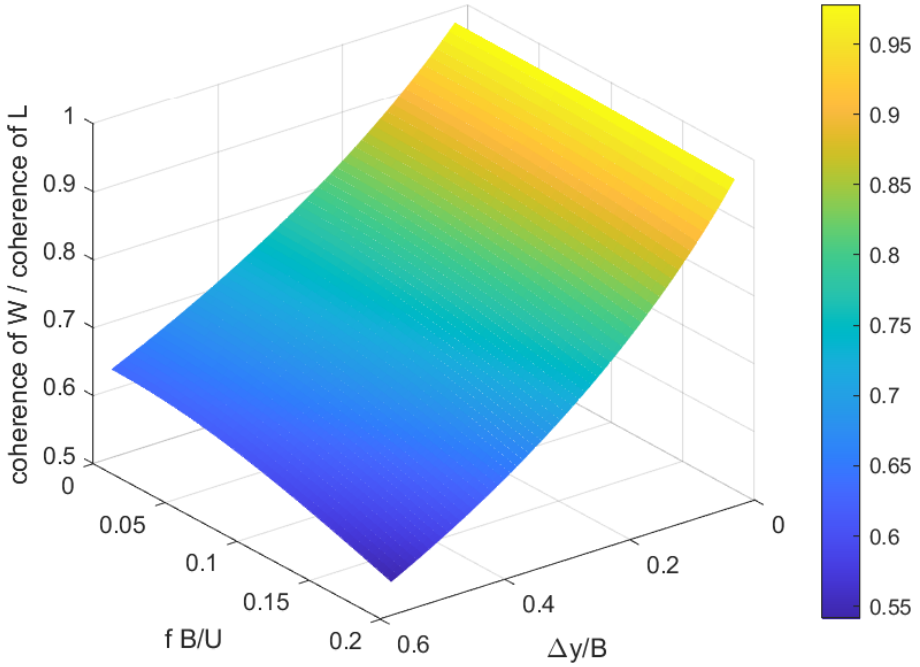

Figure 3.45: Ratio of normalized cross-spectra $coh_w^{1/2}/coh_L^{1/2}$ for different $\Delta y/B$ and f^*

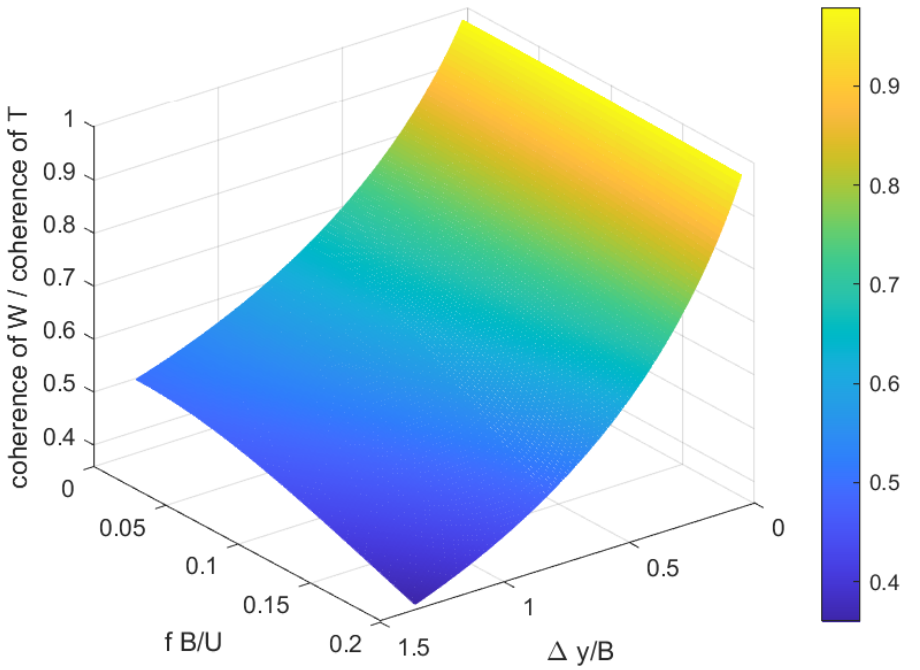

Figure 3.46: Ratio of normalized cross-spectra $coh_w^{1/2}/coh_T^{1/2}$ for different $\Delta y/B$ and f^*

Generation of the PSD of the wind for 65 m/s wind

Table 3.4: Parameters considered for the simulation at 65 m/s

Parameter	Target Value
$\overline{U}$	65 m/s
L_u^x	160 mm
L_w^x	16 mm
I_u	0.143
I_w	0.0715
C_{wx}	0.5
C_{wy}	6.5
C_{wz}	3
C_{ux}	3
C_{uy}	10
C_{uz}	10
C_{vx}	3
C_{vy}	6.5
C_{vz}	6.5
Admittance	Davenport

In figures 3.47, 3.48, 3.49, 3.50, 3.51, 3.52, 3.53 it is possible to observe the PSD of the Lagrangian of the generated wind for each vibration mode. It has been plot for each of the thirteen modes of the Braila bridge the comparison between the *recorrelated* case (red line) and the *strip assumption* case (blue line).

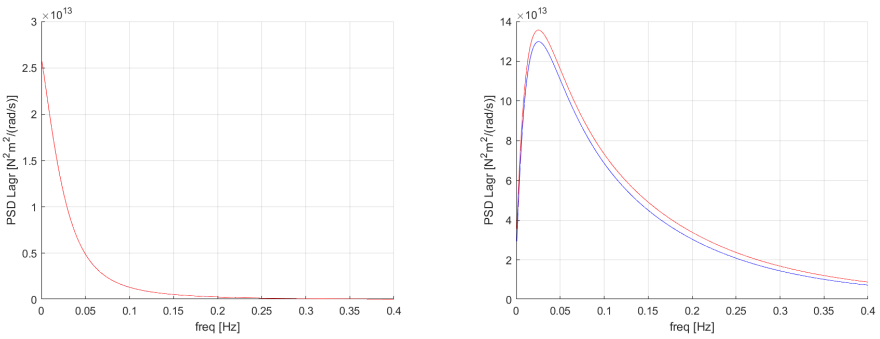

(a) Mode 1H **(b)** Mode 1V

Figure 3.47: PSD of the Lagrangian of the generated wind for mode 1H and 1V

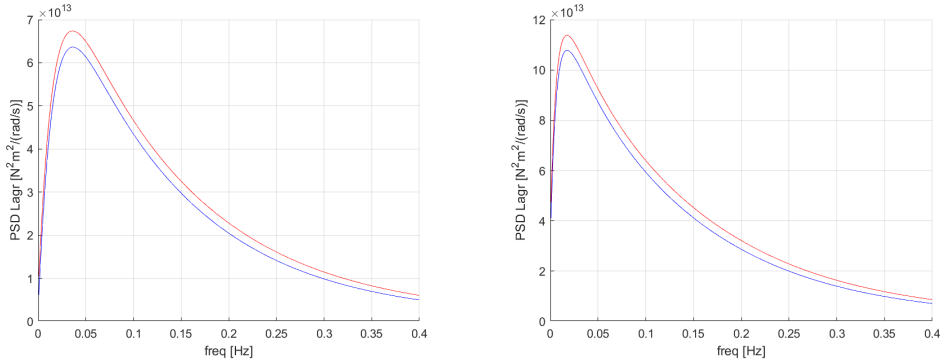

(a) Mode 2A **(b)** Mode 2V

Figure 3.48: PSD of the Lagrangian of the generated wind for mode 2A and 2V

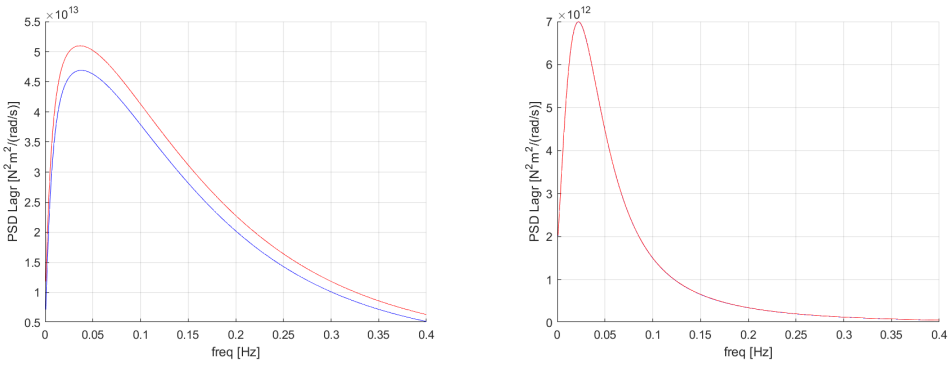

(a) Mode 3V **(b)** Mode 2H

Figure 3.49: PSD of the Lagrangian of the generated wind for mode 3V and 2H

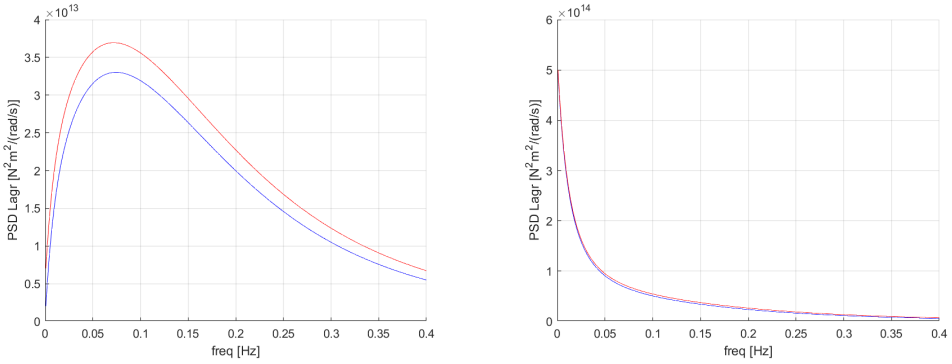

(a) Mode 4V **(b)** Mode 5V

Figure 3.50: PSD of the Lagrangian of the generated wind for mode 4V and 5V

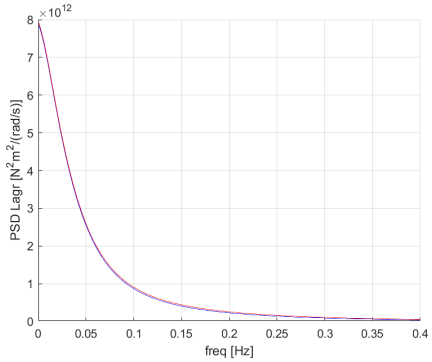

(a) Mode 3H

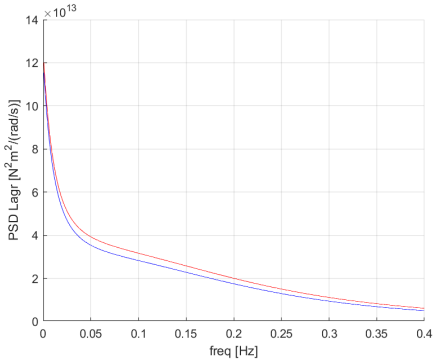

(b) Mode 6V

Figure 3.51: PSD of the Lagrangian of the generated wind for mode 3H and 6V

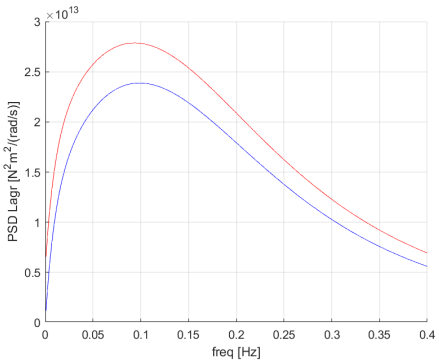

(a) Mode 7V

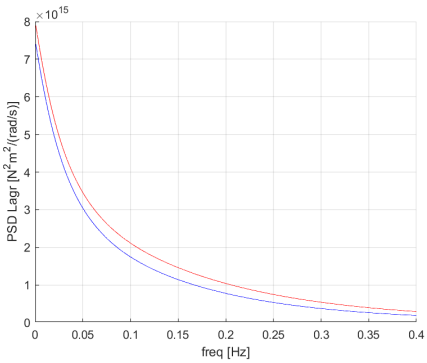

(b) Mode 1T

Figure 3.52: PSD of the Lagrangian of the generated wind for mode 7V and 1T

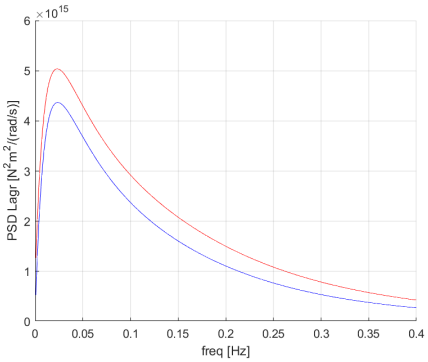

Figure 3.53: PSD of the Lagrangian of the generated wind for mode 2T

As we expected, for each mode, the recorrelated curve is higher in terms of amplitude with respect to the *strip assumption* case in the whole considered frequency range. The modes whose curves are superimposed are the ones that are mainly influenced by the drag contribution, that based on considerations made by previous researchers (i.e. Kimura et al.) have been computed by means of the *strip assumption*.

The convergent number of sections for 65 m/s wind velocity

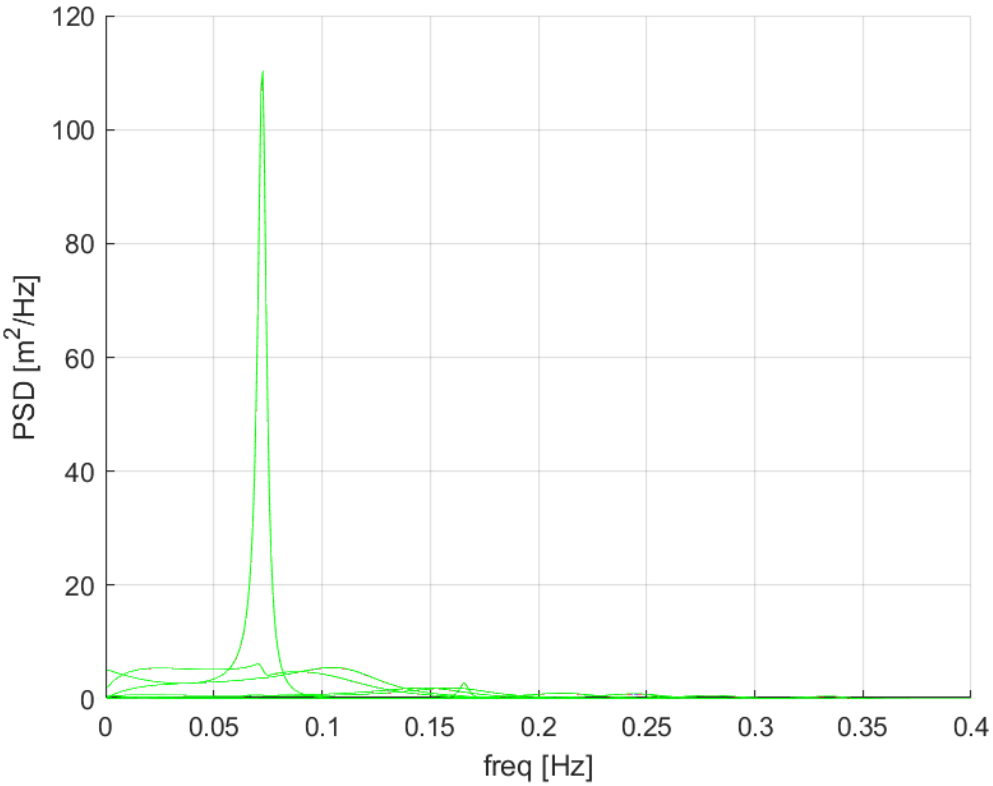

Figure 3.54: PSD of the displacement of the deck for each vibration mode changing number of sections: 82 sections (green line), 164 sections (blue line), 328 sections (red line).

In order to study the dynamic behaviour of the Braila bridge deck, it was initially divided in 82 sections. In order to apply the span - wise coherence function it was necessary to find the number of sections into divide the bridge for which the dynamic response did not change. In figures 3.54 and 3.55 it is possible to recognize that the convergent number of sections is 328. In order to have a better representation, in figure, 3.55, the contribution of the first mode of vibration has been cancelled.

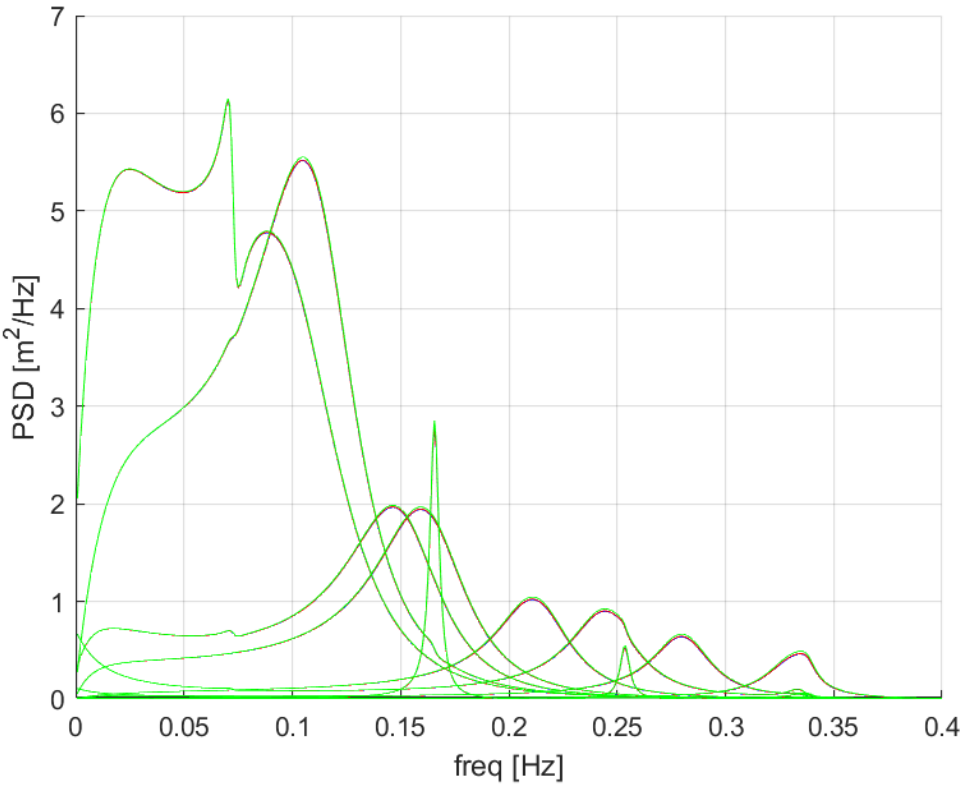

Figure 3.55: PSD of the displacement of the deck for each vibration mode except 1st changing number of sections: 82 sections (green line), 164 sections (blue line), 328 sections (red line).

Effect of the span-wise coherence on the bridge response for 65 m/s wind velocity

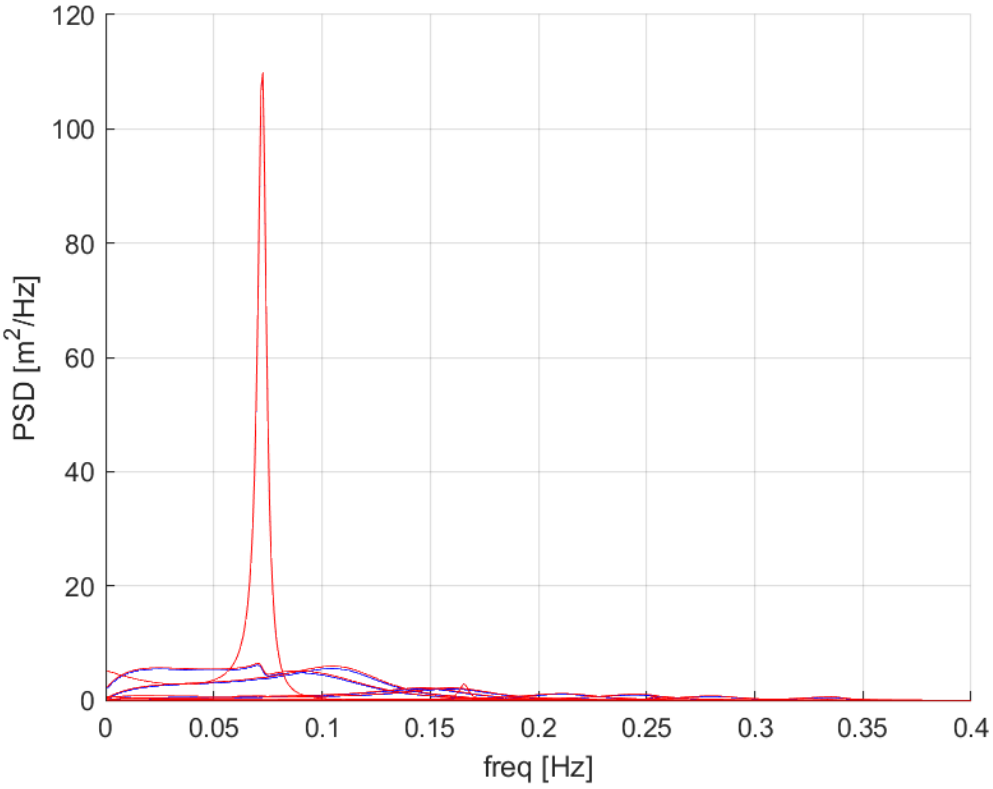

Figure 3.56: PSD of the displacement of the deck for each vibration mode with the span-wise coherence (red line) or the strip assumption (blue line).

In figure 3.56 and 3.57 it is possible to recognize the modal displacement of the Braila deck for each vibration mode. In picture 3.58 it is possible to see the modal acceleration of the deck. In figures 3.59, 3.60, 3.61 we can watch the accelerations along y, z and ϑ for sections $S2$, $S3$, $S4$.

All the plots described above have been performed using a number of sections equal to 328 (convergent number).

It is clear that the effect of recorrelation of buffeting forces is more important in correspondence of the peaks of resonance, than it is an effect that has to be considered during the design of the bridge and in its fatigue life. As we expected in all the cases mentioned above the *strip assumption* produces an underestimation of the results, that in certain cases could be quite big and it has to be taken into account. Passing from 50 m/s to 65 m/s it is possible to see that we have a similar effect of recorrelation between the two speeds. In the conclusion of this work a comparison between the case of 328 sections with span-wise coherence of the buffeting forces and the one characterized by each section of length equal to B (deck width) and 1.5 B considering the *strip assumption* will be made.

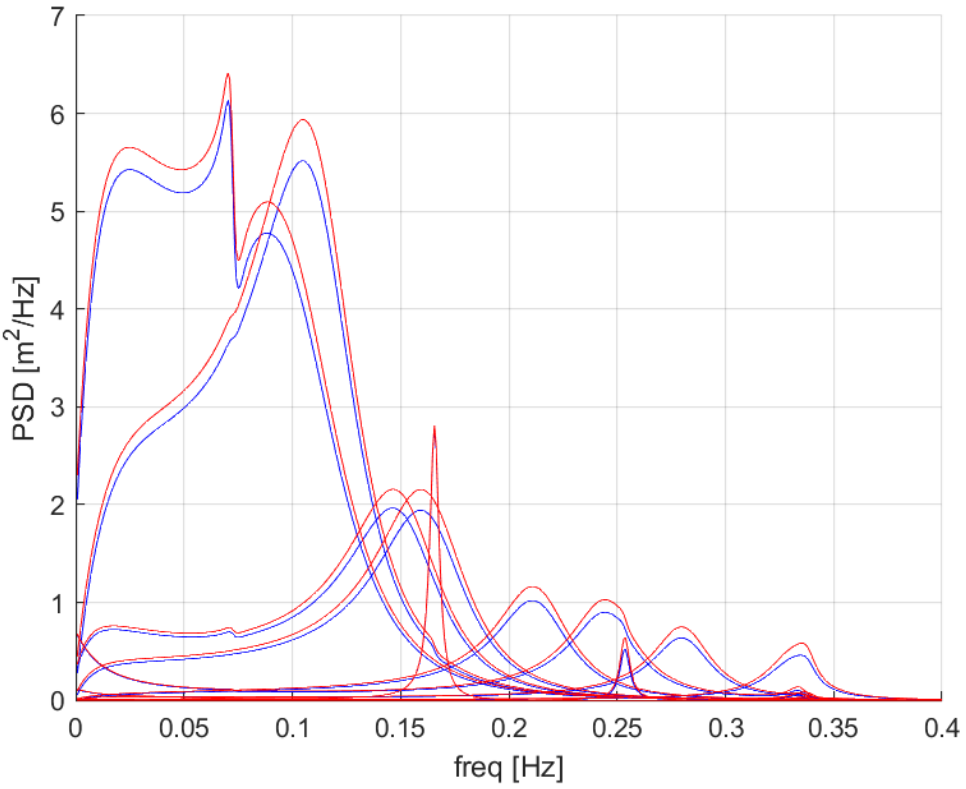

Figure 3.57: PSD of the displacement of the deck for each vibration mode except 1st with the span-wise coherence (red line) or the strip assumption (blue line).

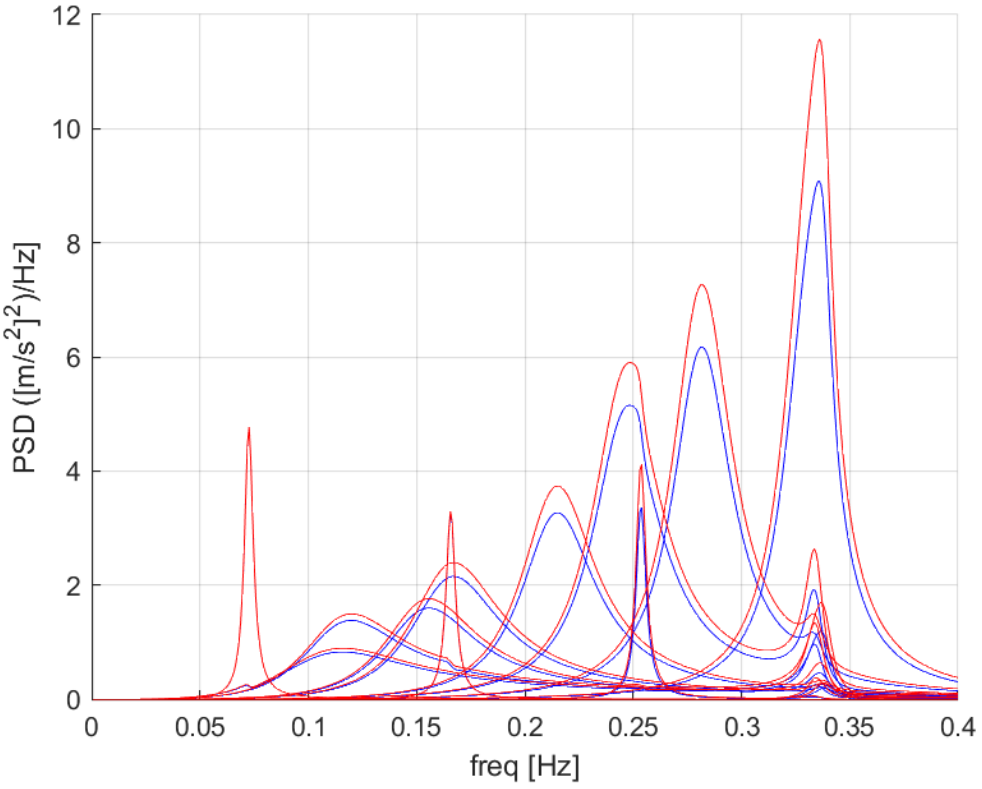

Figure 3.58: PSD of the modal acceleration of the deck with recorrelation (red line) or strip assumption (blue line).

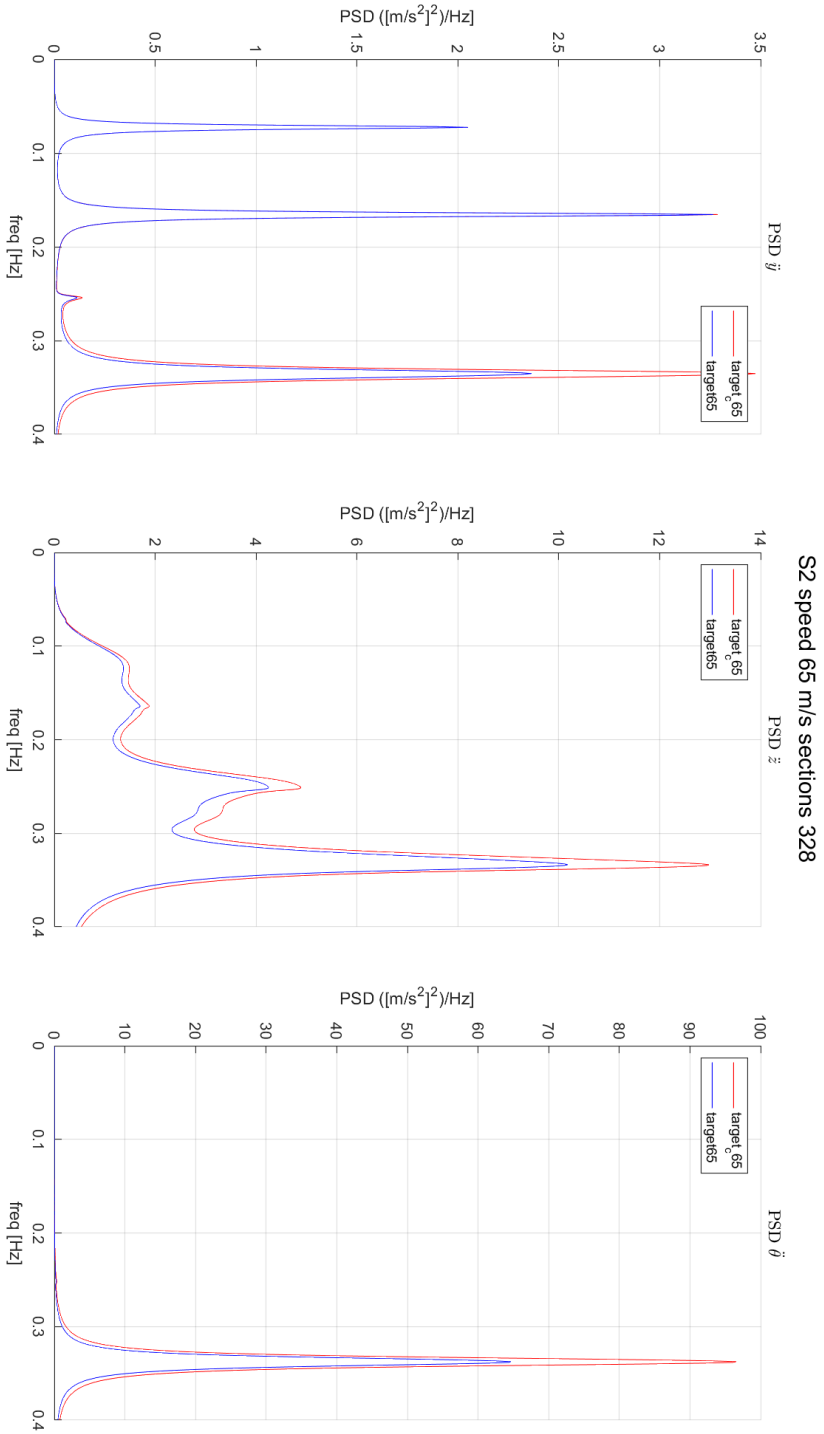

Figure 3.59: PSD of the acceleration along y, z and ϑ for section S2.

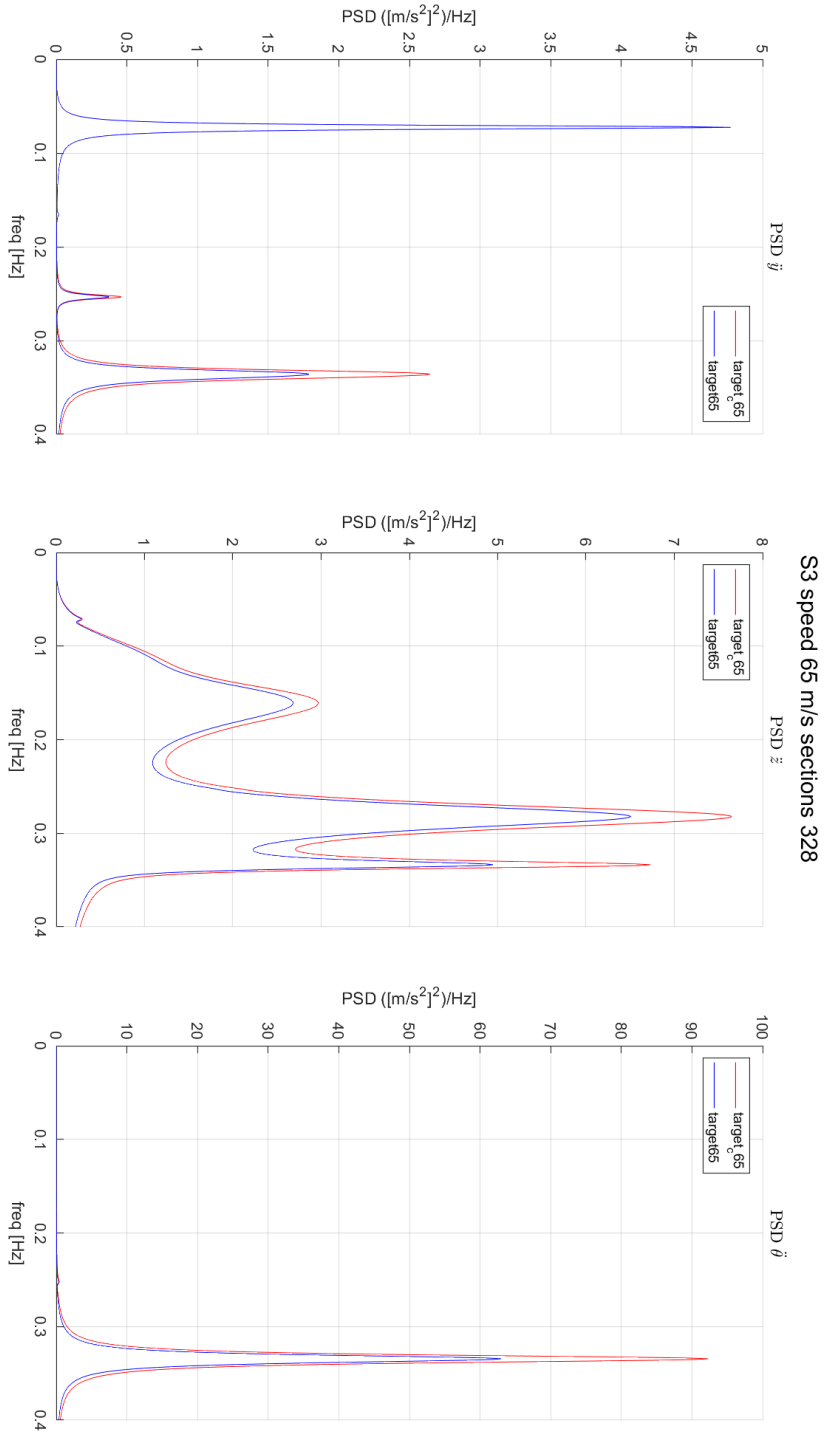

Figure 3.60: PSD of the acceleration along y, z and ϑ for section S3.

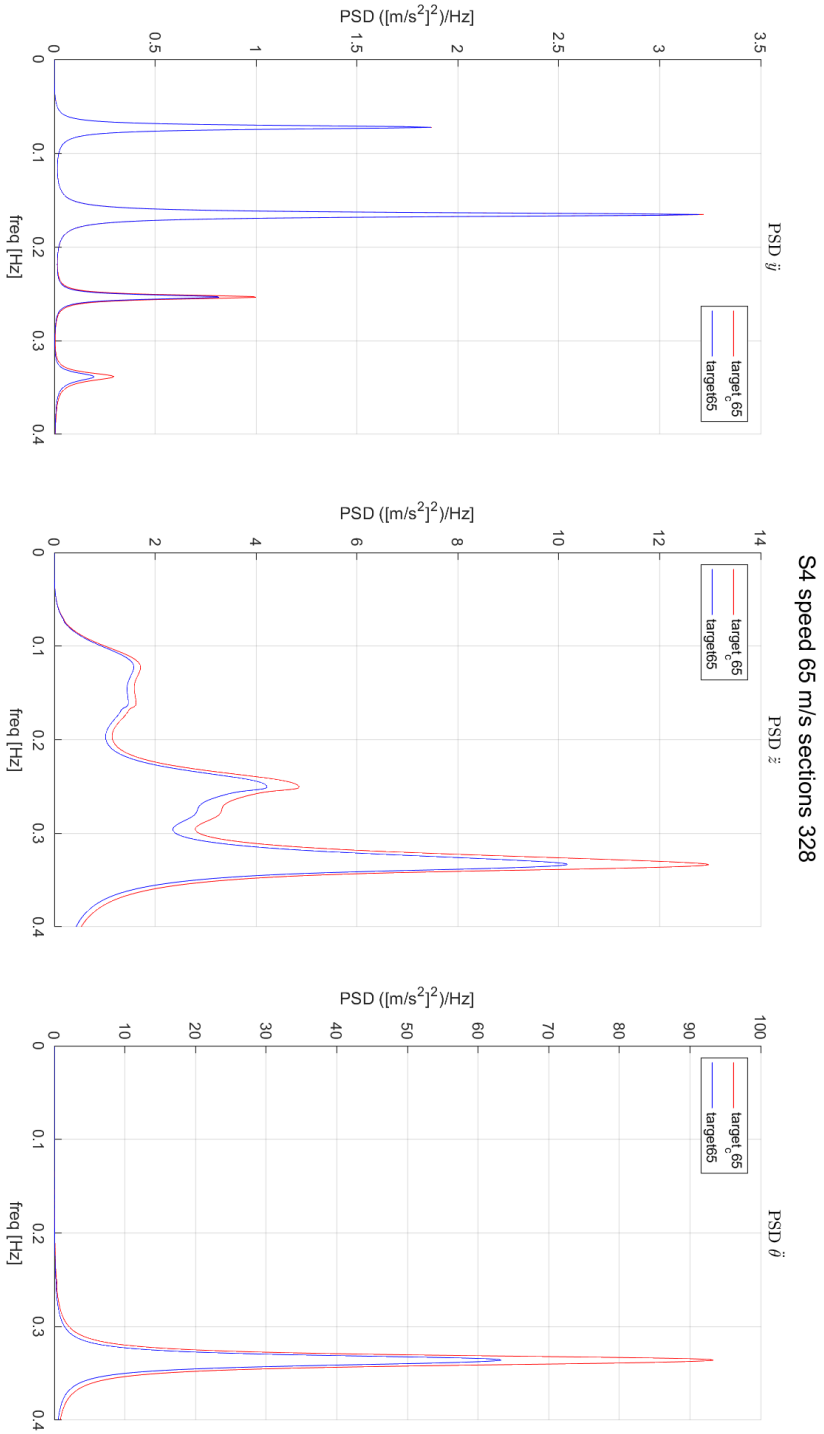

Figure 3.61: PSD of the acceleration along y, z and ϑ for section S4.

3.3 Model of Larose G. for Braila Bridge

Starting from the original Larose G. [1] representation I have adapted it to the Braila deck case, in order to maintain the ratios L/B_{Larose}, L_L/B_{Larose}, L_T/B_{Larose} constant between the two models in equations 3.4, 3.6, 3.10. Another modification is given by the fact that the exponents a_L and a_T in equations 3.6 and 3.10 have been applied not only to k_1 but to k_1 and to all the terms for which it is multiplied both outside the square root and inside. This operation has been performed in order to take into account of the dimensional analysis. I have verified, in addition, to work in a similar range of reduced frequency f^* for each considered wind velocity (20 m/s, 50m/s, 65 m/s).

The formulation of the span-wise normalized cross spectrum of the adapted model of Larose G. for the Braila deck could be schematized in this way:

$$coh_w^{1/2} = \exp\left[-c_1\gamma^{c_2}\right]\cos\left(c_3\gamma\right) \tag{3.3}$$

where:

$$\gamma = k_1 B_{Braila}\frac{\Delta y}{B_{Braila}}\sqrt{1+\frac{1}{(k_1 B_{Braila}\frac{L}{B_{Larose}})^2}} \tag{3.4}$$

It is necessary to introduce the subsequent parameters that can be noticed in equations 3.3 and 3.4:

- Wave number : $k_1 = \frac{2\pi f}{\bar{V}}$
- Length scale fitted to the experiments $L = 0.27$ m that changes, changing the dimension of the spires in the turbulence generation process (medium grid)
- Von Kárman collapsing parameter adapted for the case of the Braila bridge γ (equation 3.4)
- Fitting constants c_1, c_2 and c_3, where $c_1 = 0.73$, $c_2 = 1.03$ and $c_3 = 0.27$, that being not dimensional remained equal to the ones of the original representation

In a similar way it is possible to define the co-coherence of the lift and the pitching moment:

$$coh_L^{1/2} = \exp\left[-c_1\eta^{c_2}\right]\cos\left(c_3\eta\right) \tag{3.5}$$

Where for the lift:

$$\eta = \left(k_1 B_{Braila}\frac{\Delta y}{B_{Braila}}\right)^{a_L}\sqrt{1+\frac{1}{(k_1 B_{Braila}\frac{L_L}{B_{Larose}})^{2a_L}}} \tag{3.6}$$

$$L_L = L\frac{(p+\Delta y/B)^2}{(q+r(\Delta y/B)^2} \qquad p = 1.0,\ q = 0.46,\ r = 1.42,\ L = 0.39\text{ m} \tag{3.7}$$

$$a_L = \left(\frac{B}{D}\right)^{-0.25}\frac{(p+\Delta y/B)^2}{(q+r(\Delta y/B)^2} \qquad p = 0.160,\ q = 0.088,\ r = 0.935 \tag{3.8}$$

Where:

- Fitting constants c_1, c_2 and c_3, where $c_1 = 0.346$, $c_2 = 1.5$ and $c_3 = 0$ that being not dimensional remained equal to the ones of the original representation
- Length scale L fitted to the experiments considering lift (medium grid)
- Fitting constants p, q, r assuming different values for a_L and L_L

And for the pitching moment:

$$coh_T^{1/2} = \exp\left[-c_1\eta^{c_2}\right]\cos\left(c_3\eta\right) \tag{3.9}$$

Where:

$$\eta = \left(k_1 B_{Braila}\frac{\Delta y}{B_{Braila}}\right)^{a_T}\sqrt{1+\frac{1}{(k_1 B_{Braila}\frac{L_T}{B_{Larose}})^{2a_T}}} \tag{3.10}$$

$$L_T = L\frac{(p+\Delta y/B)^2}{(q+r(\Delta y/B)^2} \qquad p = 1.0,\ q = 0.46,\ r = 1.42,\ L = 0.39\text{ m} \tag{3.11}$$

$$a_T = \left(\frac{B}{D}\right)^{-0.15}\frac{(p+\Delta y/B)^2}{(q+r(\Delta y/B)^2} \qquad p = 0.098,\ q = 0.059,\ r = 0.970 \tag{3.12}$$

Where:

- Fitting constants c_1, c_2 and c_3, where $c_1 = 0.341$, $c_2 = 1.33$ and $c_3 = 0.22$, that being not dimensional remained equal to the ones of the original representation
- Length scale L fitted to the experiments considering moment (medium grid)
- Fitting constants p, q, r assuming different values for a_T and L_T

Simulations have been performed for three different speeds: 20 m/s, 50 m/s and 65 m/s. Once introduced the adapted model I am going to show the plots of the functions described above $coh_w^{1/2}$, $coh_L^{1/2}$ and $coh_w^{1/2}$, $coh_L^{1/2}$for every wind speed considered (20 m/s, 50 m/s, 65 m/s) and the ratios between $coh_w^{1/2}$ and $coh_L^{1/2}$, $coh_T^{1/2}$. After this I am going to define the input parameters of each numerical simulation that I made. In the end I am going display the effect of the recorrelation on the response of the bridge deck itself.

3.3.1 Braila bridge deck response for 20 m/s wind velocity

Span-wise coherence for 20 m/s wind velocity

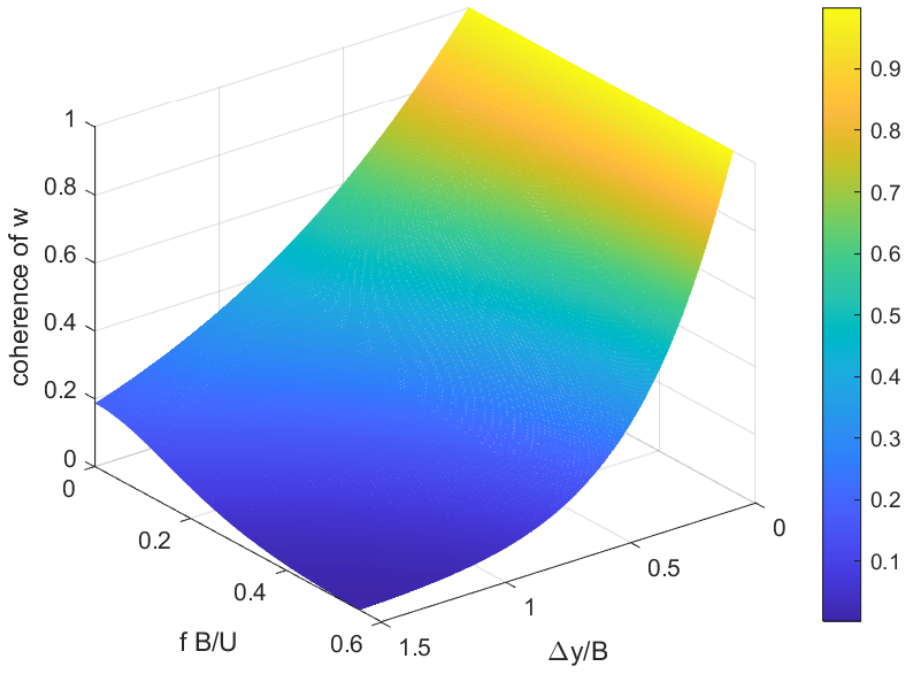

Figure 3.62: Normalized cross-spectrum of the w turbulence component for different $\Delta y/B$ and f^*

In figures 3.62, 3.63 and 3.64 it is possible to examine the 3D trend of the span-wise coherence for w gusty wind component, lift and aerodynamic moment, taking into account at the same time the reduced frequency f^* and the normalized distance between two different point $\frac{\Delta y}{B}$. Also considering the adapted Larose G. representation, as we expected, it confirms the underestimation given by the *strip assumption*. In pictures 3.65, 3.66, it is possible to watch the 3D trends of the ratio between $coh_w^{1/2}/coh_L^{1/2}$ and $coh_w^{1/2}/coh_T^{1/2}$ taking into account at the same time the reduced frequency $\frac{fB}{U}$ and the adimensional spacing $\frac{\Delta y}{B}$.

The plots, also in this case, considering the adapted Larose G. model, display an higher recorrelation with respect the one of the turbulent wind. These functions have been considered in the simulations for all the entire frequency range (f = 0 - 0.4 Hz), but for a reduced spacing between the sections: in the range $\Delta y/B = 0 - 1.52$ for the moment and $\Delta y/B = 0 - 0.76$ for the lift. This has been done in order to obtain physical results and to compare the results with the Jakobsen J. representation, having considered the same $\Delta y/B$ ranges.

In table 3.5 it is possible to find the parameters concerning the wind generation and the kind of admittance matrix considered in the simulation of the bridge response at 20 m/s.

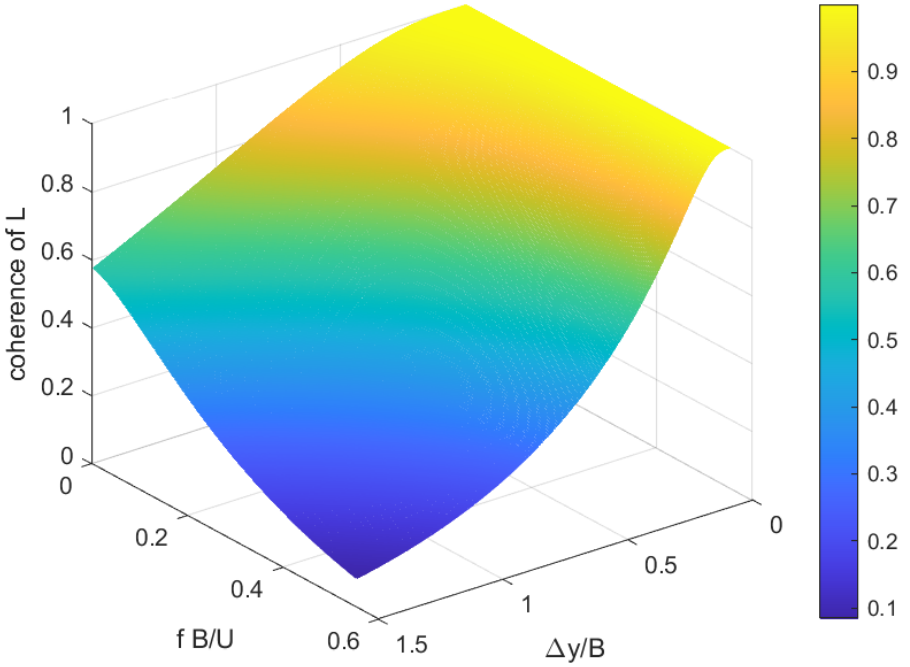

Figure 3.63: Normalized cross-spectrum of the buffeting L for different $\Delta y/B$ and f^*

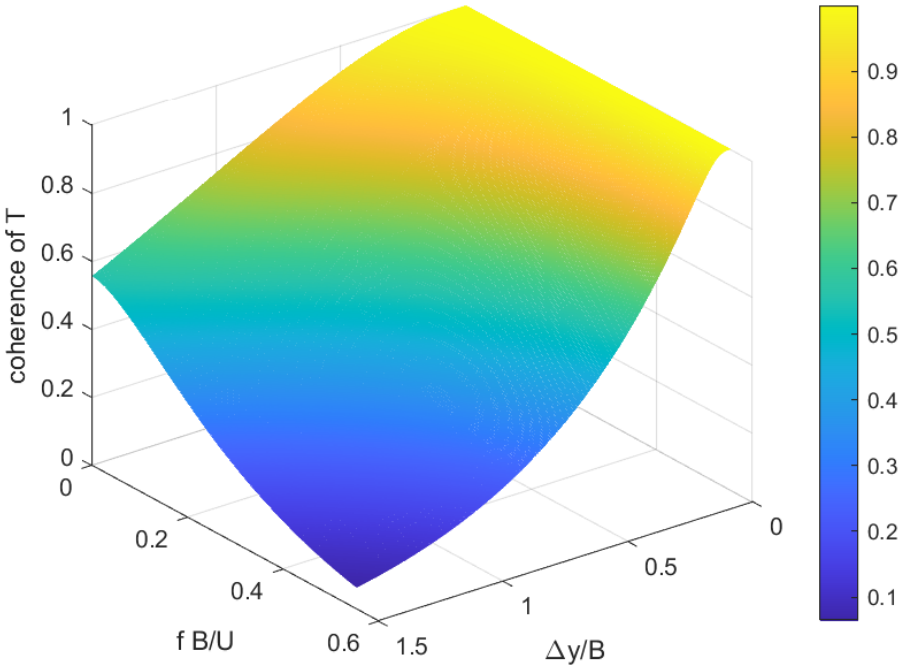

Figure 3.64: Normalized cross-spectrum of the buffeting T for different $\Delta y/B$ and f^*

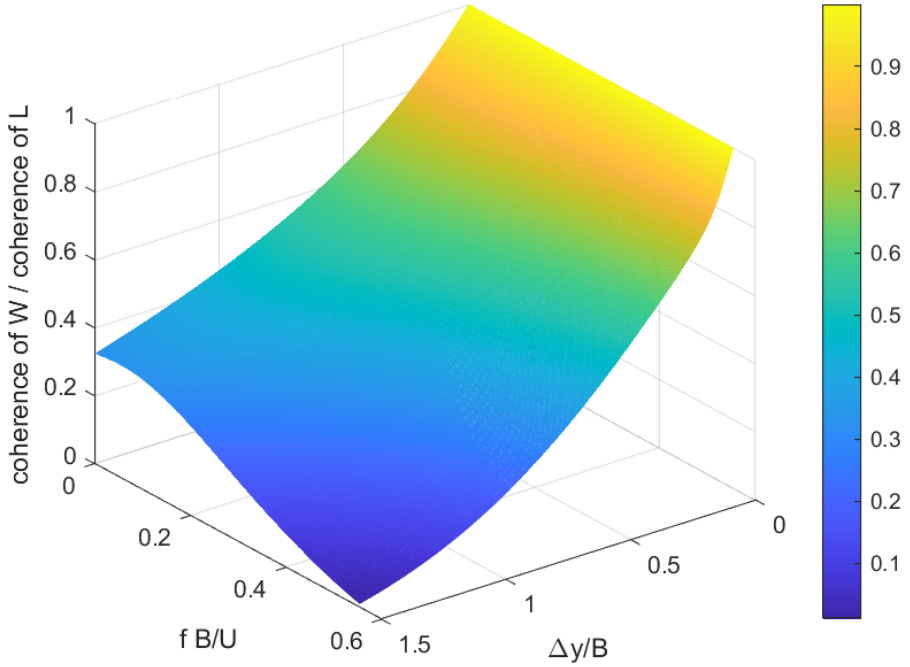

Figure 3.65: Ratio of normalized cross-spectra $coh_w^{1/2}/coh_L^{1/2}$ for different $\Delta y/B$ and f^*

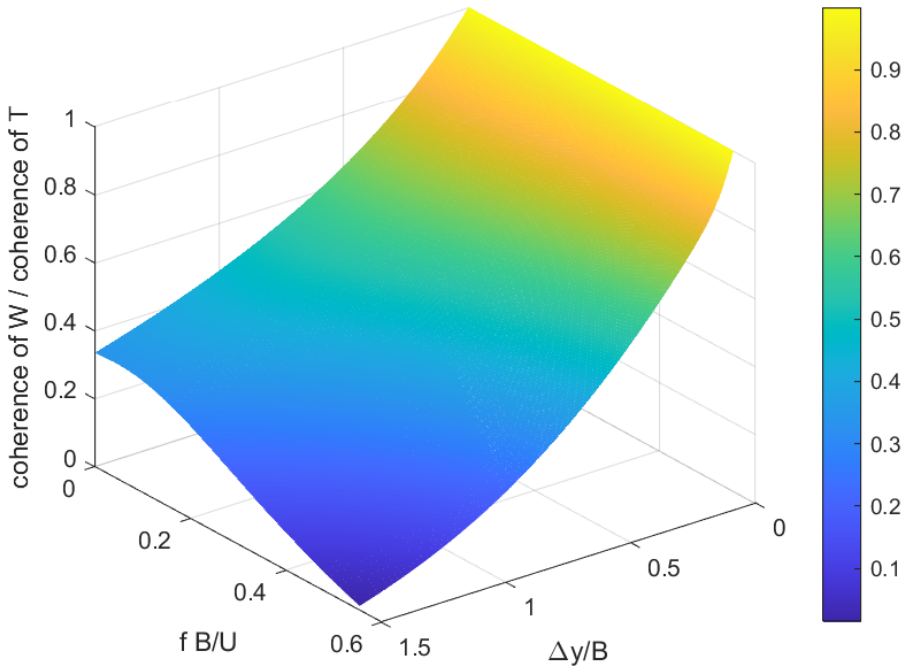

Figure 3.66: Ratio of normalized cross-spectra $coh_w^{1/2}/coh_T^{1/2}$ for different $\Delta y/B$ and f^*

Generation of the PSD of the wind for 20 m/s wind

Table 3.5: Parameters considered for the simulation at 20 m/s

Parameter	Target Value
$\overline{U}$	20 m/s
L_u^x	160 mm
L_w^x	16 mm
I_u	0.143
I_w	0.0715
C_{wx}	0.5
C_{wy}	6.5
C_{wz}	3
C_{ux}	3
C_{uy}	10
C_{uz}	10
C_{vx}	3
C_{vy}	6.5
C_{vz}	6.5
Admittance	Davenport

In figures 3.67, 3.68, 3.69, 3.70, 3.71, 3.72, 3.73 it is possible to observe the PSD of the Lagrangian of the generated wind for each vibration mode. It has been plotted for each of the thirteen modes of the Braila bridge the comparison between the *recorrelated* case (red line) and the *strip assumption* case (blue line).

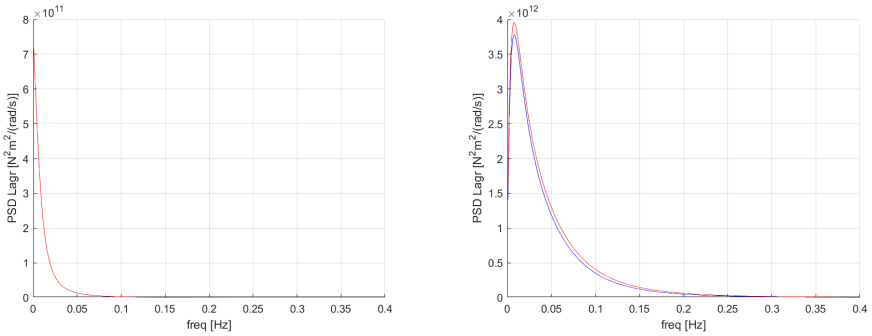

(a) Mode 1H **(b)** Mode 1V

Figure 3.67: PSD of the Lagrangian of the generated wind for mode 1H and 1V

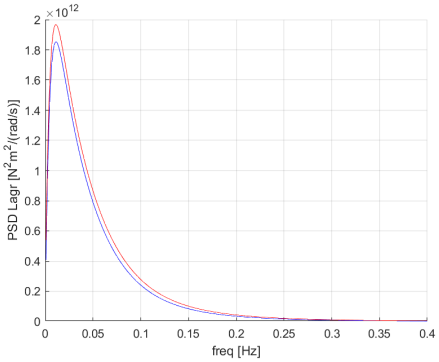

(a) Mode 2A

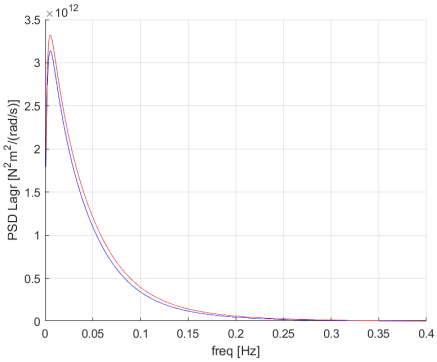

(b) Mode 2V

Figure 3.68: PSD of the Lagrangian of the generated wind for mode 2A and 2V

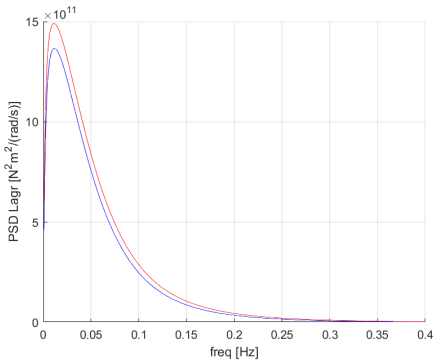

(a) Mode 3V

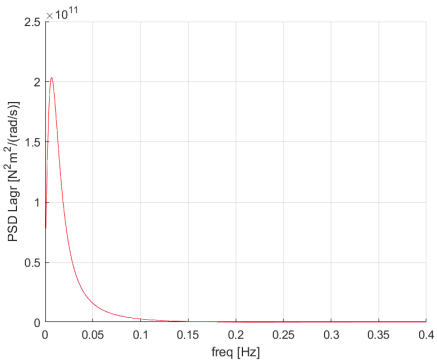

(b) Mode 2H

Figure 3.69: PSD of the Lagrangian of the generated wind for mode 3V and 2H

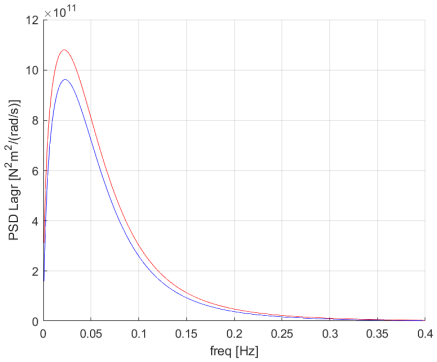

(a) Mode 4V

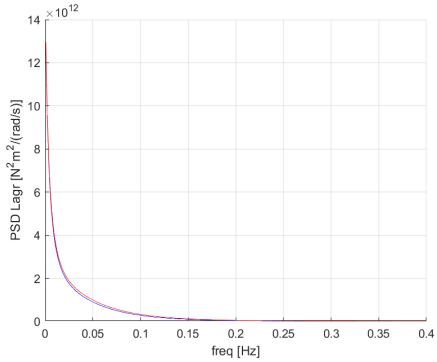

(b) Mode 5V

Figure 3.70: PSD of the Lagrangian of the generated wind for mode 4V and 5V

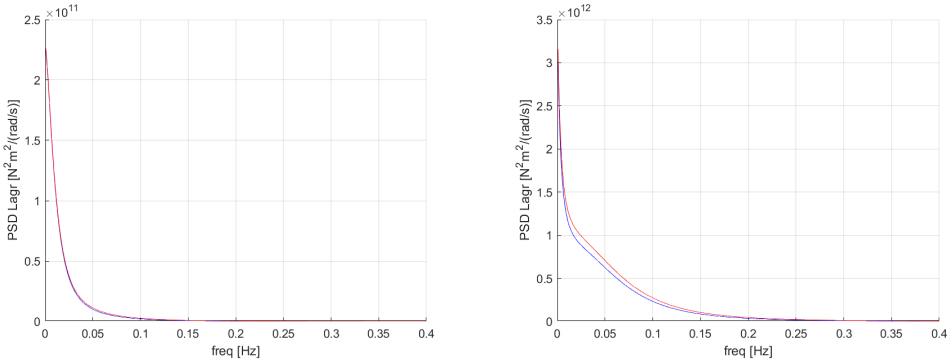

(a) Mode 3H **(b)** Mode 6V

Figure 3.71: PSD of the Lagrangian of the generated wind for mode 3H and 6V

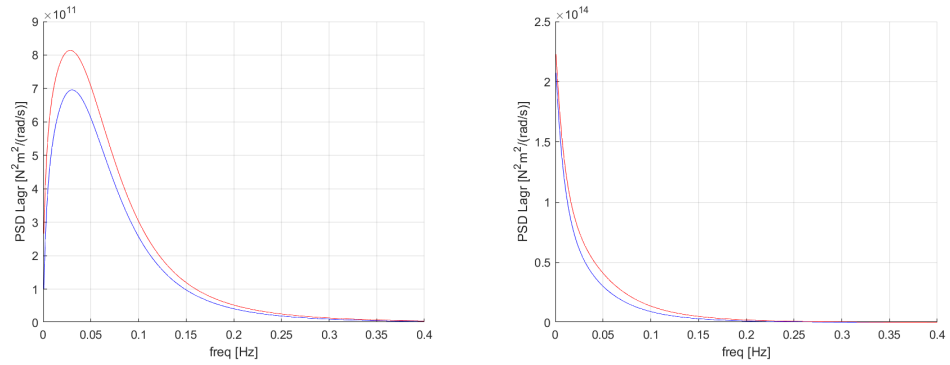

(a) Mode 7V **(b)** Mode 1T

Figure 3.72: PSD of the Lagrangian of the generated wind for mode 7V and 1T

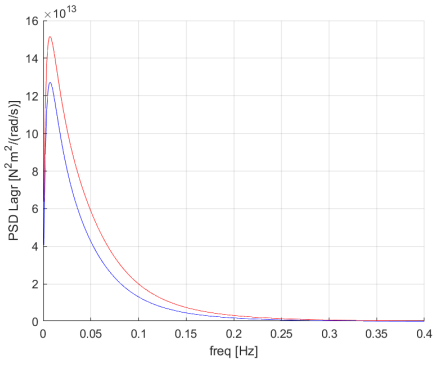

Figure 3.73: PSD of the Lagrangian of the generated wind for mode 2T

As we expected, for each mode, the recorrelated curve is higher in terms of amplitude with respect to the *strip assumption* case in the whole considered frequency range. The modes whose curves are superimposed are the ones that are mainly influenced by the drag contribution, that based on considerations made by previous researchers (i.e. Kimura et al.) have been computed by means of the *strip assumption*.

The convergent number of sections for 20 m/s wind velocity

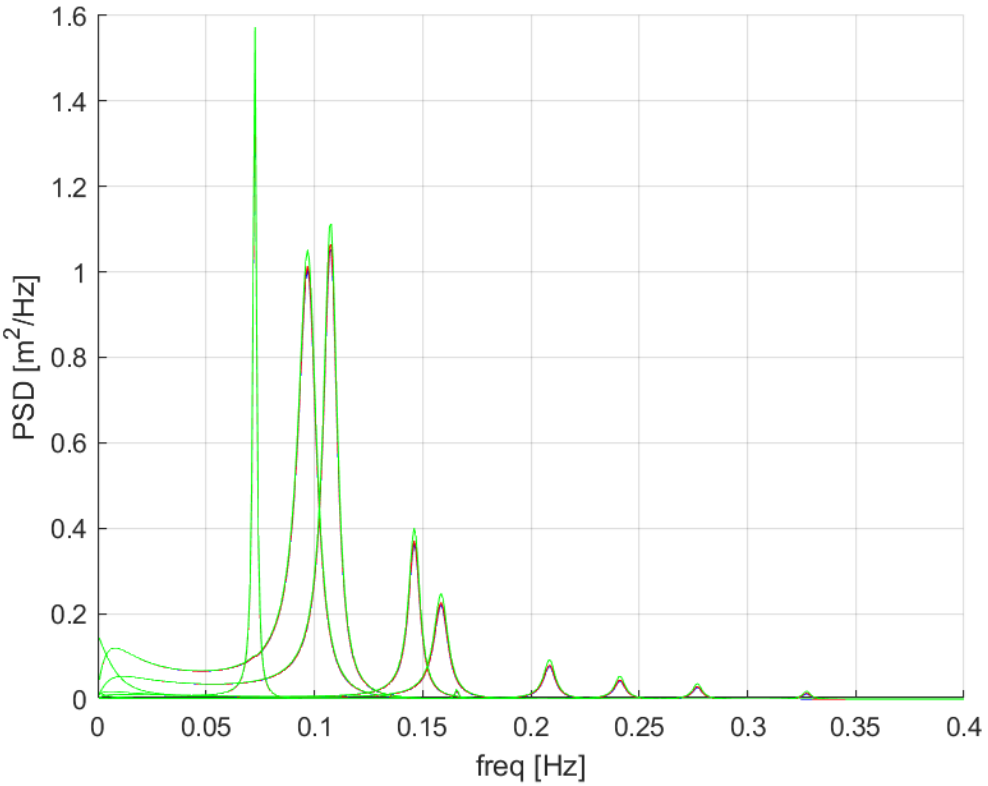

Figure 3.74: PSD of the displacement of the deck for each vibration mode changing number of sections: 82 sections (green line), 164 sections (blue line), 328 sections (red line).

In order to study the dynamic behaviour of the Braila bridge deck, it was initially divided in 82 sections. In order to apply the span - wise coherence function it was necessary to find the number of sections into divide the bridge for which the dynamic response did not change. In figures 3.74 and 3.75 it is possible to recognize that the convergent number of sections is 328. In order to have a better representation, in figure, 3.75, the contribution of the first mode of vibration has been cancelled.

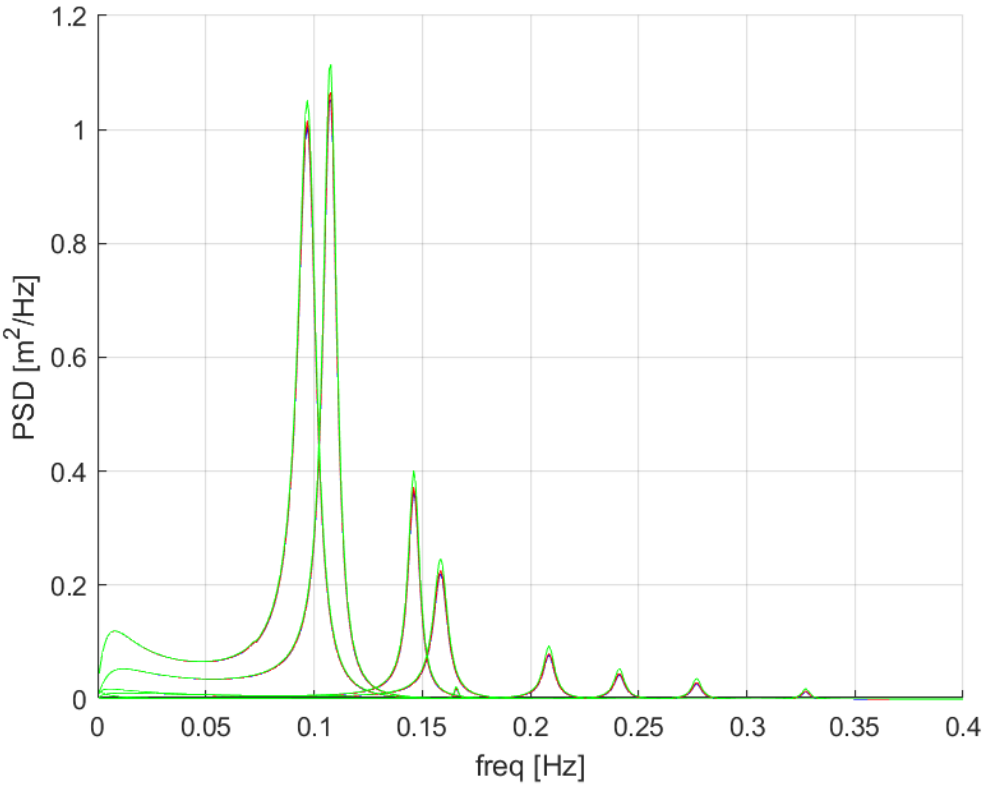

Figure 3.75: PSD of the displacement of the deck for each vibration mode except 1st changing number of sections: 82 sections (green line), 164 sections (blue line), 328 sections (red line).

Effect of the span-wise coherence on the bridge response for 20 m/s wind velocity

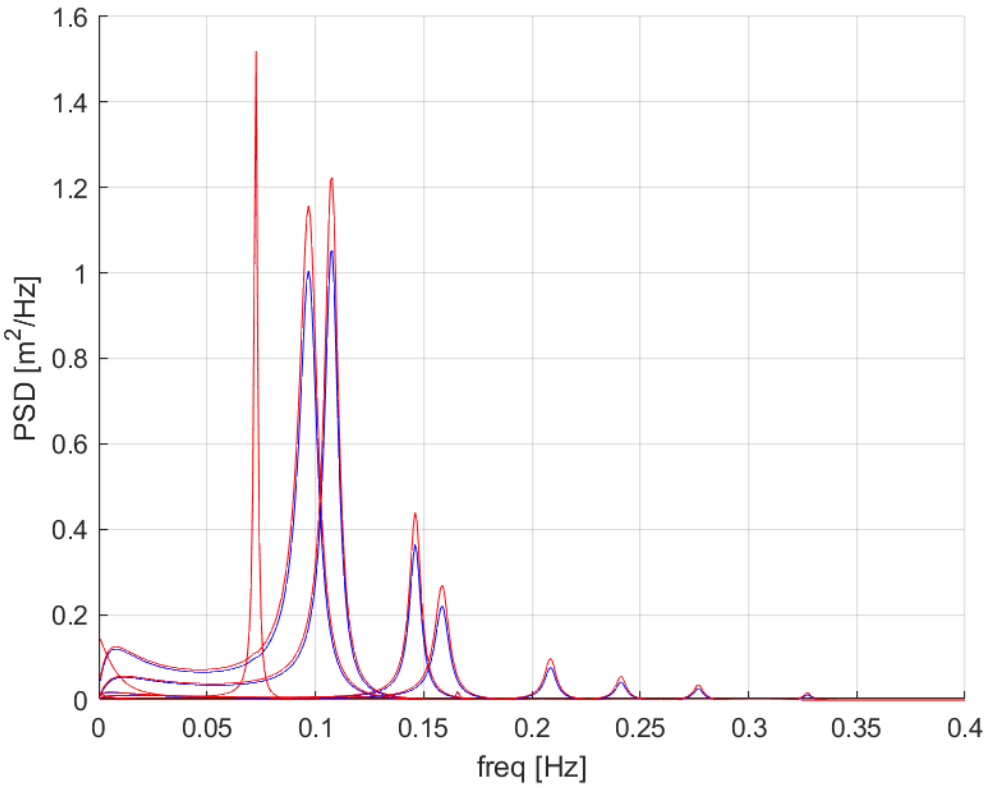

Figure 3.76: PSD of the displacement of the deck for each vibration mode with the span-wise coherence (red line) or the strip assumption (blue line).

In figure 3.76 and 3.77 it is possible to recognize the modal displacement of the Braila deck for each vibration mode. In picture 3.78 it is possible to see the modal acceleration of the deck. In figures 3.79, 3.80, 3.81 we can watch the accelerations along y, z and ϑ for sections $S2$, $S3$, $S4$.

All the plots described above have been performed using a number of sections equal to 328 (convergent number).

It is clear that the effect of recorrelation of buffeting forces is more important in correspondence of the peaks of resonance, than it is an effect that has to be considered during the design of the bridge and in its fatigue life. As we expected in all the cases mentioned above the *strip assumption* produces an underestimation of the results, that in certain cases could be quite big and it has to be taken into account.

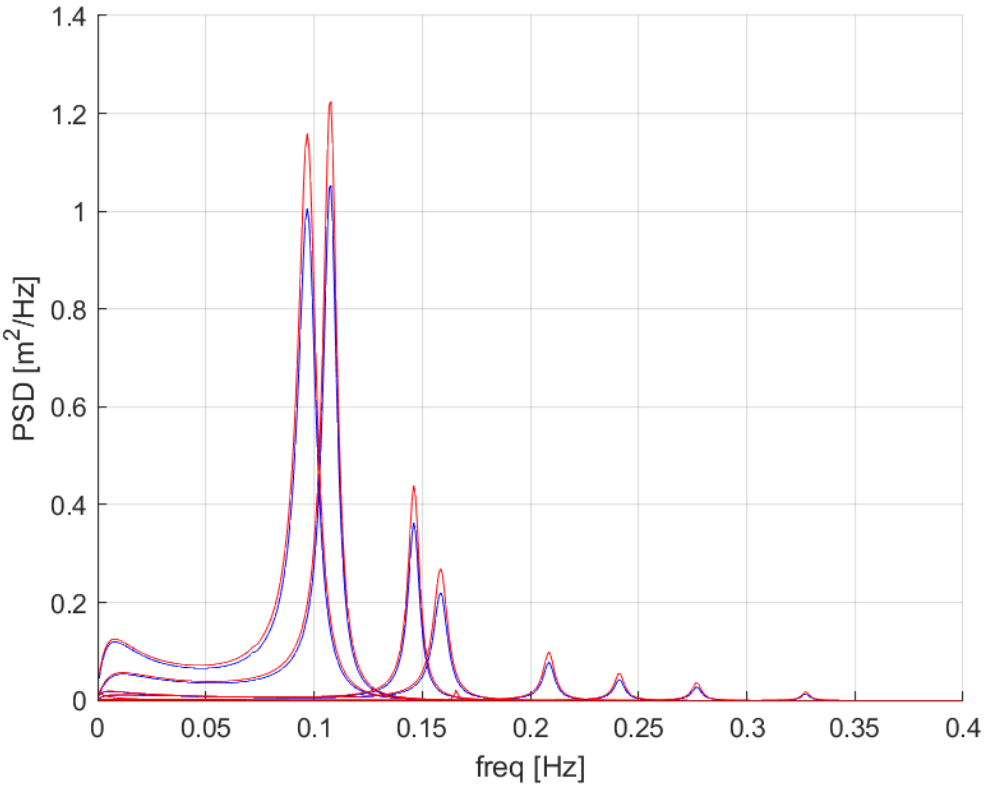

Figure 3.77: PSD of the displacement of the deck for each vibration mode except 1st with the span-wise coherence (red line) or the strip assumption (blue line).

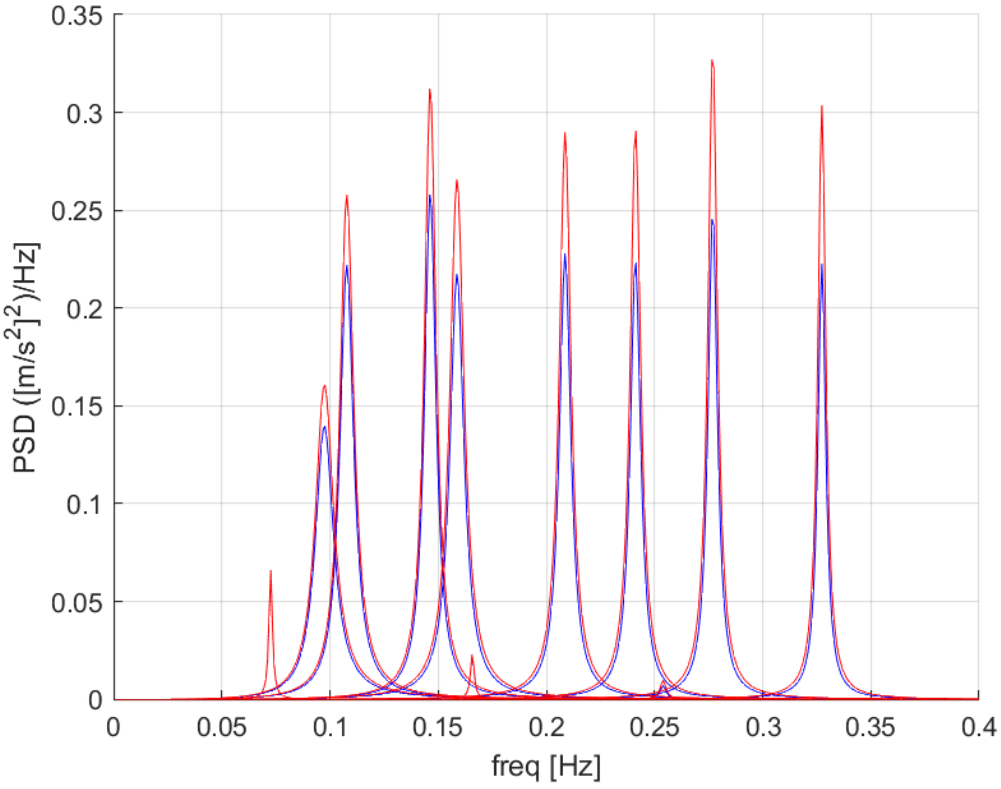

Figure 3.78: PSD of the modal acceleration of the deck with recorrelation (red line) or strip assumption (blue line).

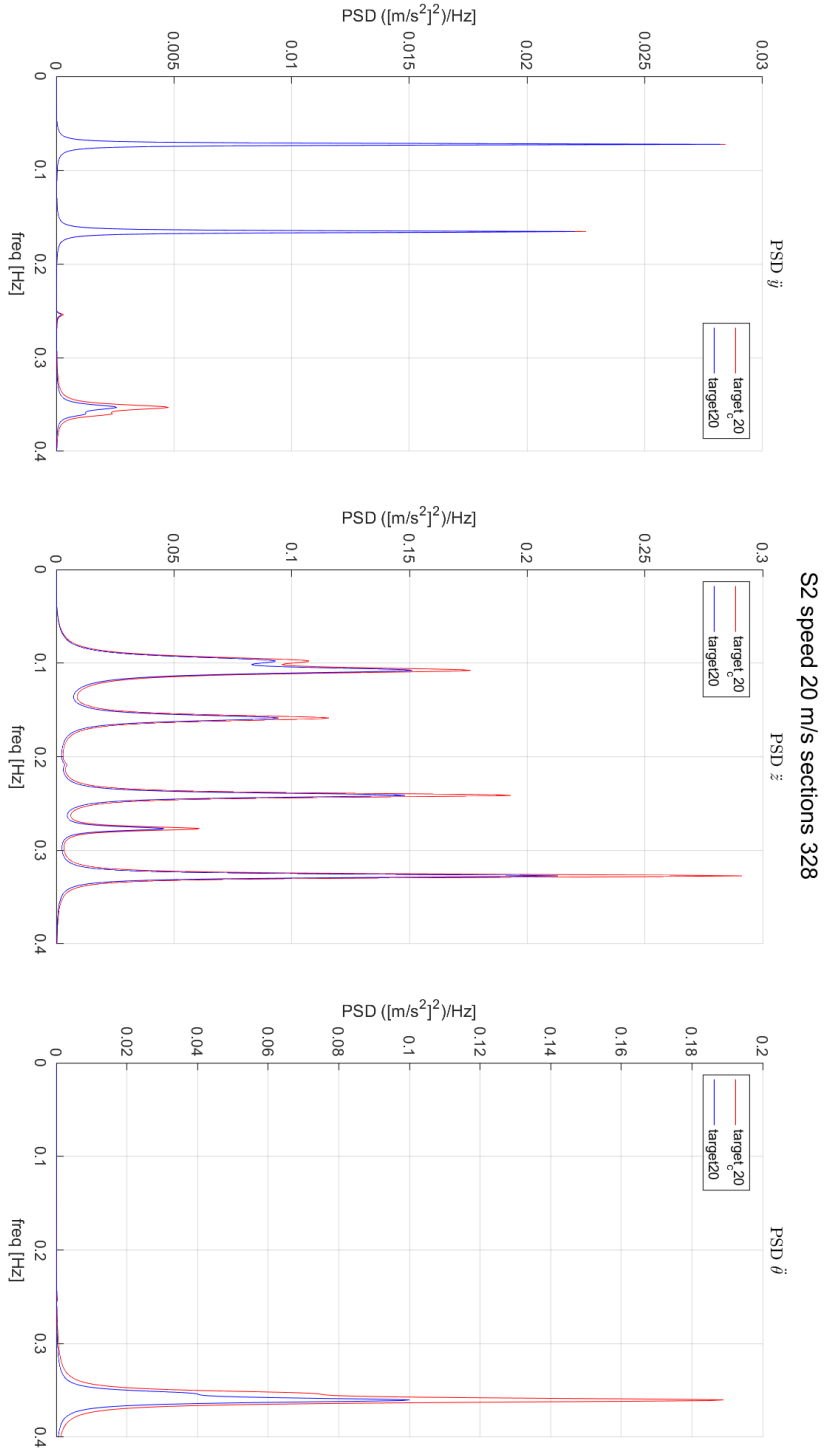

Figure 3.79: PSD of the acceleration along y, z and ϑ for section S2.

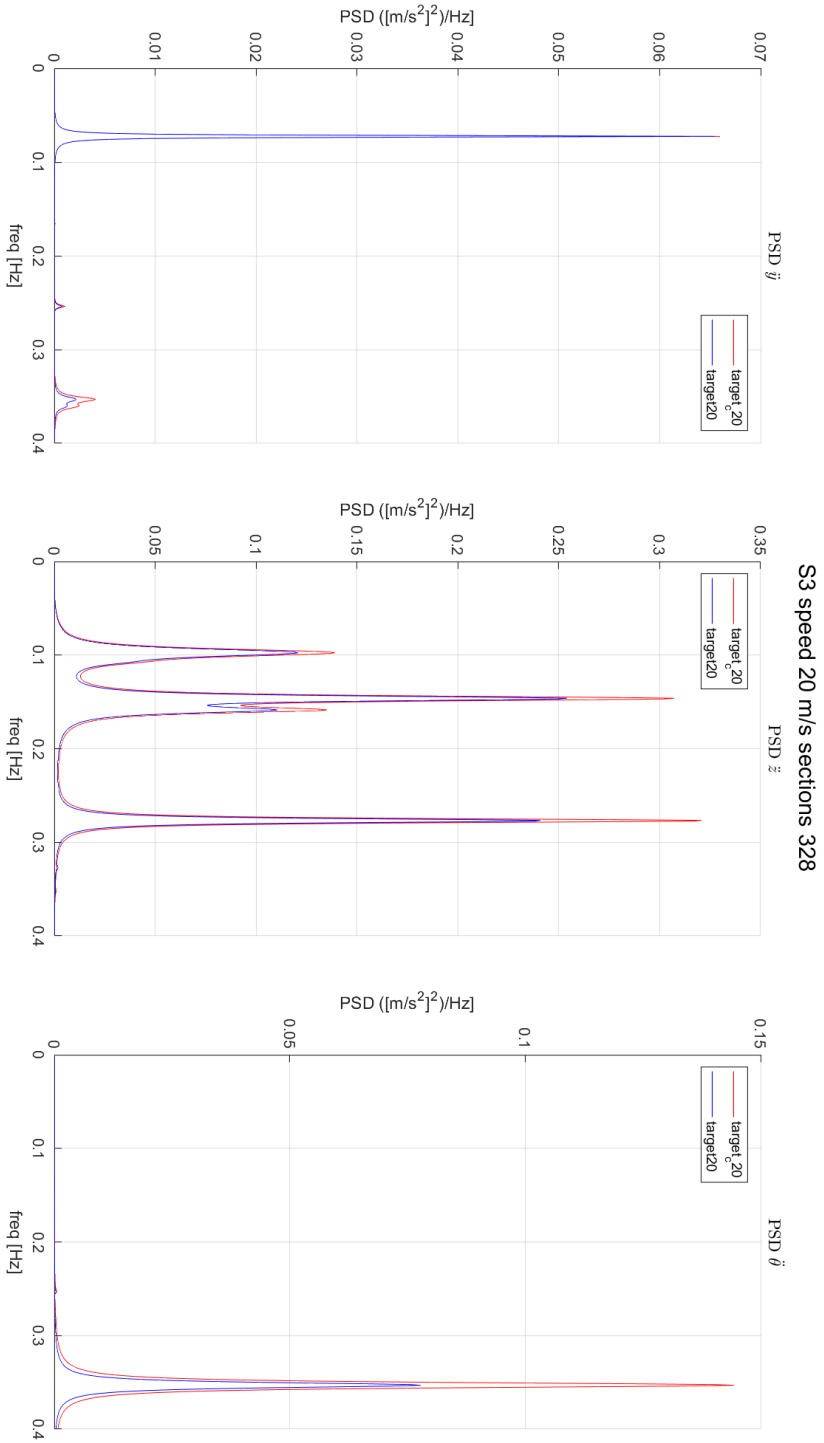

Figure 3.80: PSD of the acceleration along y, z and ϑ for section S3.

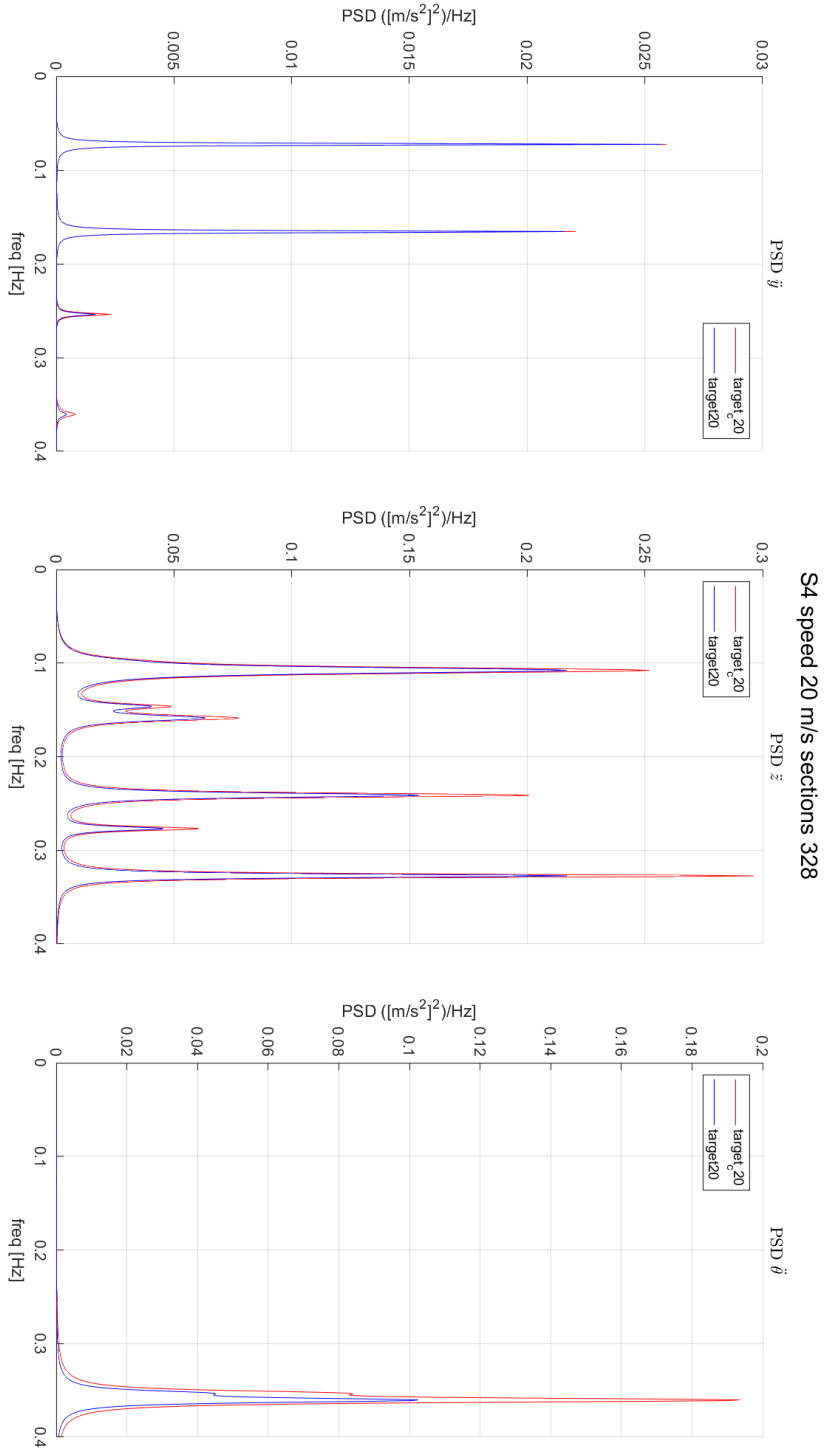

Figure 3.81: PSD of the acceleration along y, z and ϑ for section S4.

3.3.2 Braila bridge deck response for 50 m/s wind velocity

Span-wise coherence for 50 m/s wind velocity

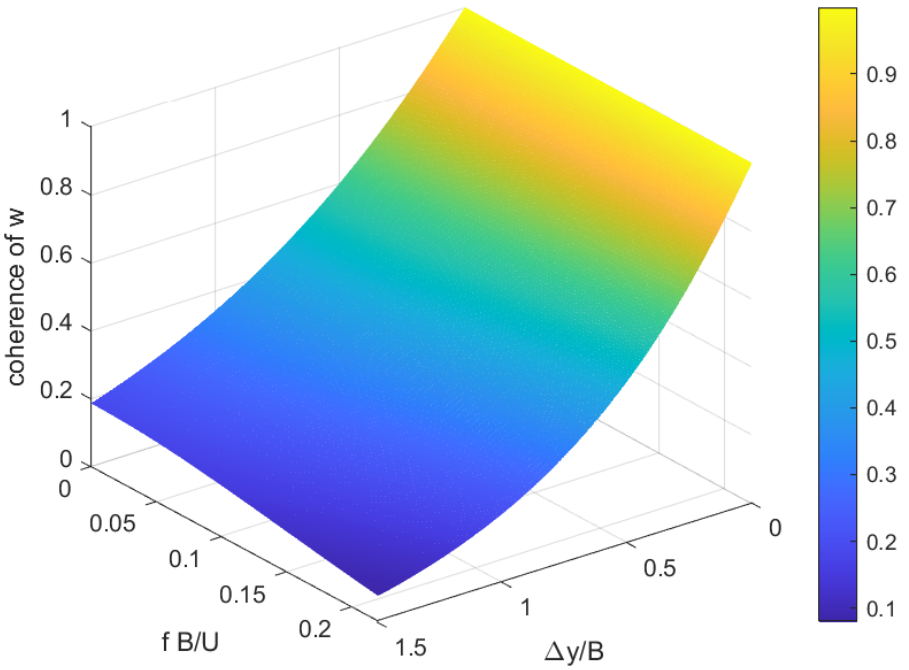

Figure 3.82: Normalized cross-spectrum of the w turbulence component for different $\Delta y/B$ and f^*

In figures 3.82, 3.83 and 3.84 it is possible to examine the 3D trend of the span-wise coherence for w gusty wind component, lift and aerodynamic moment, taking into account at the same time the reduced frequency f^* and the normalized distance between two different point $\frac{\Delta y}{B}$. Also considering the adapted Larose G. representation, as we expected, it confirms the underestimation given by the *strip assumption*. In pictures 3.85, 3.86, it is possible to watch the 3D trends of the ratio between $coh_w^{1/2}/coh_L^{1/2}$ and $coh_w^{1/2}/coh_T^{1/2}$ taking into account at the same time the reduced frequency $\frac{fB}{U}$ and the adimensional spacing $\frac{\Delta y}{B}$.

The plots, also in this case, considering the adapted Larose G. model, display an higher recorrelation with respect the one of the turbulent wind. These functions have been considered in the simulations for all the entire frequency (f = 0 - 0.4 Hz), but for a reduced spacing between the sections: in the range $\Delta y/B = 0 - 1.52$ for the moment and $\Delta y/B = 0 - 0.76$ for the lift. This has been done in order to obtain physical results and to compare the results with the Jakobsen J. representation, having considered the same $\Delta y/B$ ranges.

In table 3.6 it is possible to find the parameters concerning the wind generation and the kind of admittance matrix considered in the simulation of the bridge response at 50 m/s.

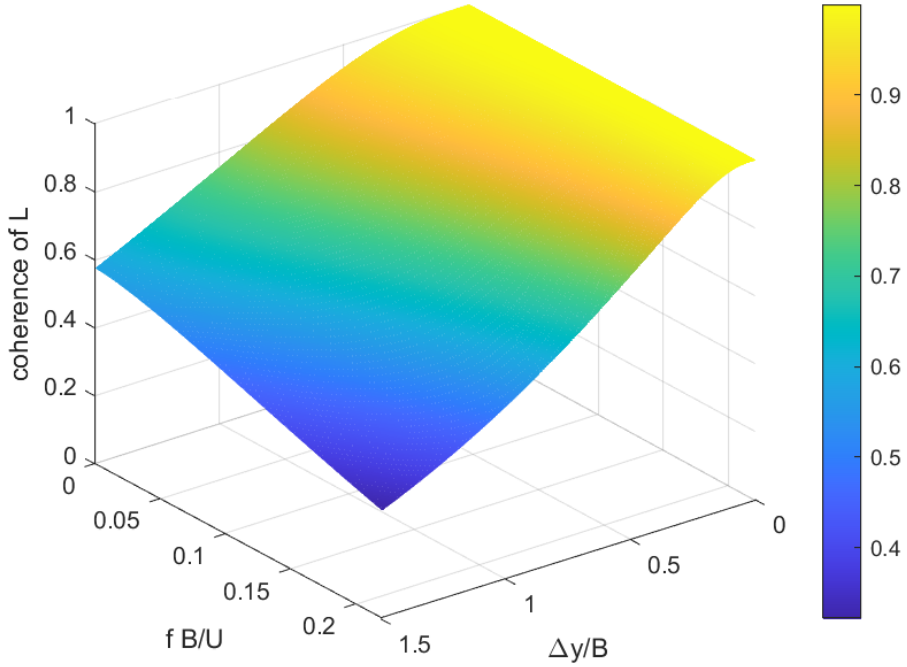

Figure 3.83: Normalized cross-spectrum of the buffeting L for different $\Delta y/B$ and f^*

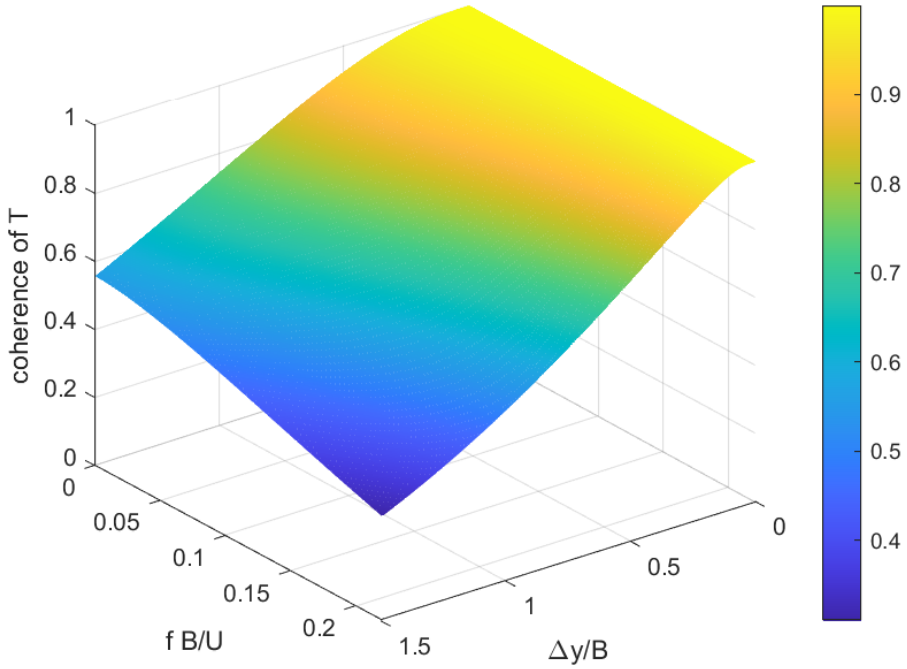

Figure 3.84: Normalized cross-spectrum of the buffeting T for different $\Delta y/B$ and f^*

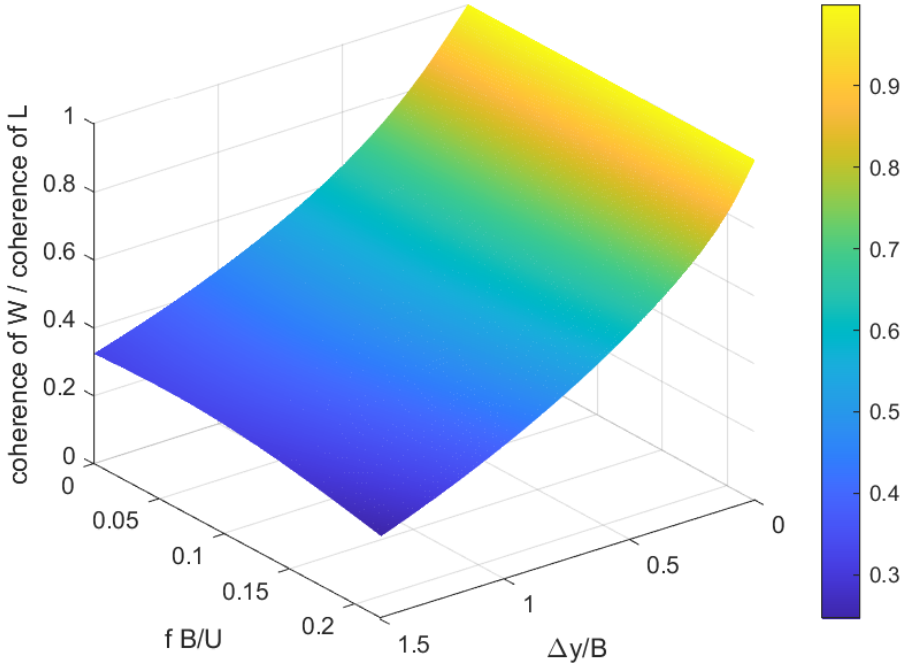

Figure 3.85: Ratio of normalized cross-spectra $coh_w^{1/2}/coh_L^{1/2}$ for different $\Delta y/B$ and f^*

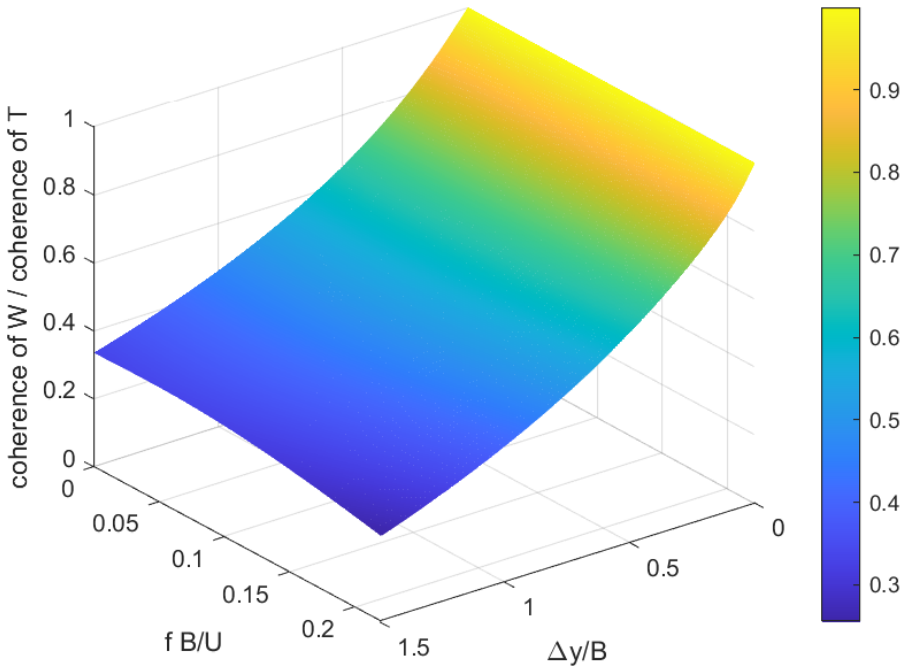

Figure 3.86: Ratio of normalized cross-spectra $coh_w^{1/2}/coh_T^{1/2}$ for different $\Delta y/B$ and f^*

Generation of the PSD of the wind for 50 m/s wind

Table 3.6: Parameters considered for the simulation at 50 m/s

Parameter	Target Value
$\overline{U}$	50 m/s
L_u^x	160 mm
L_w^x	16 mm
I_u	0.143
I_w	0.0715
C_{wx}	0.5
C_{wy}	6.5
C_{wz}	3
C_{ux}	3
C_{uy}	10
C_{uz}	10
C_{vx}	3
C_{vy}	6.5
C_{vz}	6.5
Admittance	Davenport

In figures 3.87, 3.88, 3.89, 3.90, 3.91, 3.92, 3.93 it is possible to observe the PSD of the Lagrangian of the generated wind for each vibration mode. It has been plotted for each of the thirteen modes of the Braila bridge the comparison between the *recorrelated* case (red line) and the *strip assumption* case (blue line).

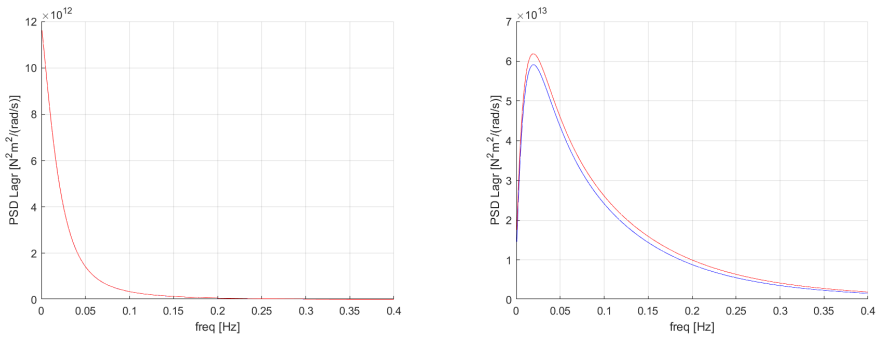

(a) Mode 1H **(b)** Mode 1V

Figure 3.87: PSD of the Lagrangian of the generated wind for mode 1H and 1V

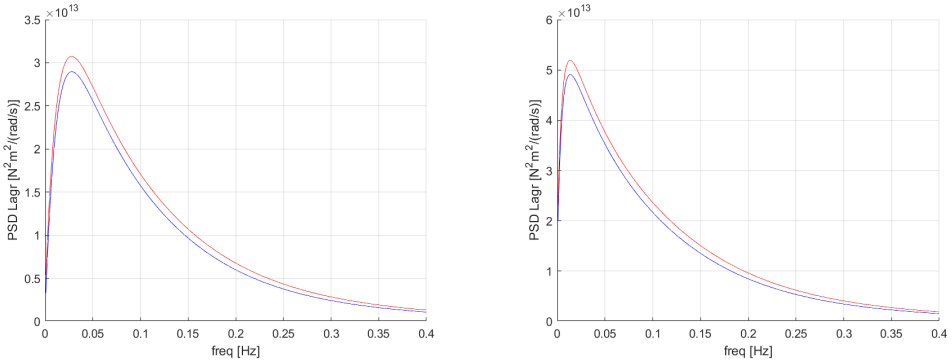

(a) Mode 2A **(b)** Mode 2V

Figure 3.88: PSD of the Lagrangian of the generated wind for mode 2A and 2V

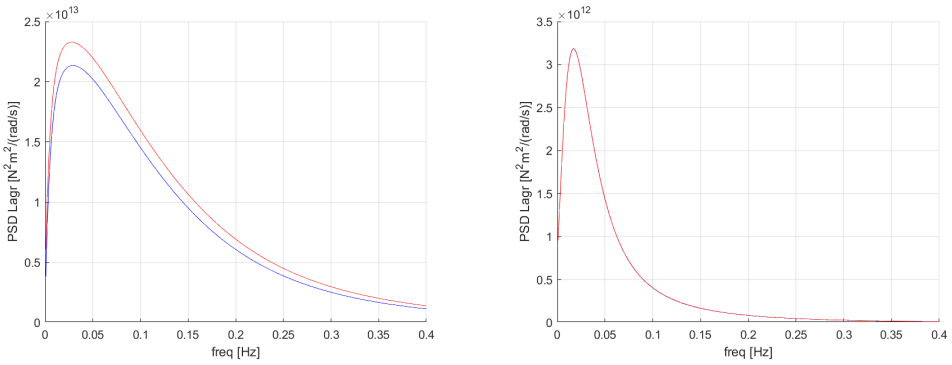

(a) Mode 3V **(b)** Mode 2H

Figure 3.89: PSD of the Lagrangian of the generated wind for mode 3V and 2H

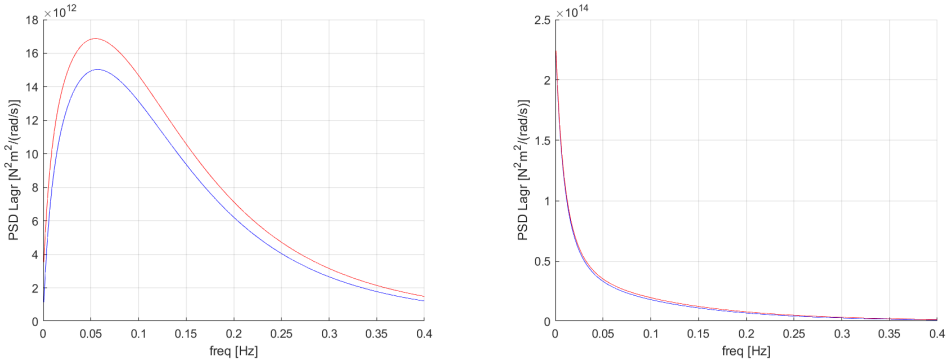

(a) Mode 4V **(b)** Mode 5V

Figure 3.90: PSD of the Lagrangian of the generated wind for mode 4V and 5V

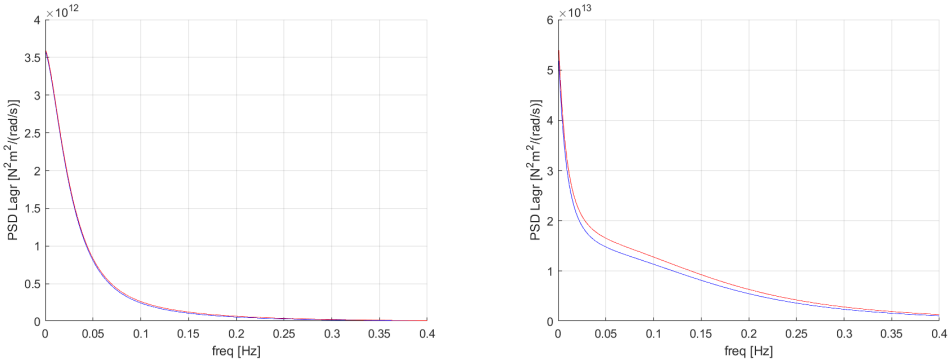

(a) Mode 3H **(b)** Mode 6V

Figure 3.91: PSD of the Lagrangian of the generated wind for mode 3H and 6V

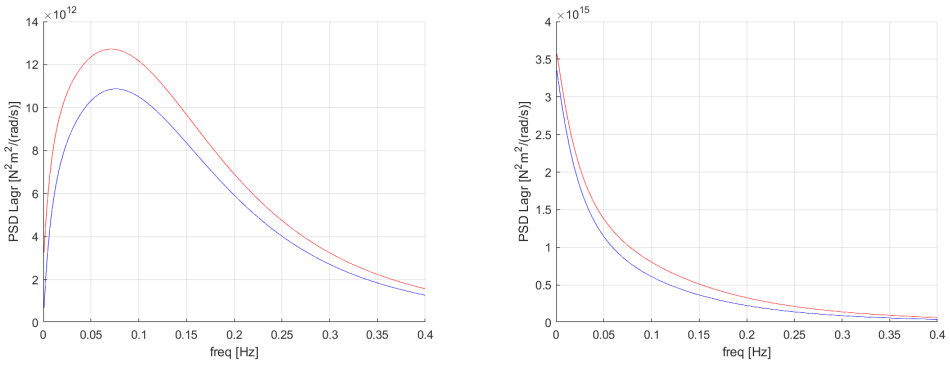

(a) Mode 7V **(b)** Mode 1T

Figure 3.92: PSD of the Lagrangian of the generated wind for mode 7V and 1T

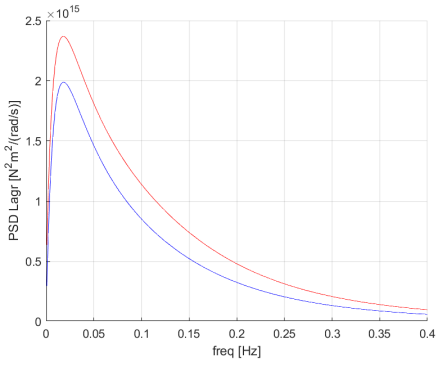

Figure 3.93: PSD of the Lagrangian of the generated wind for mode 2T

As we expected, for each mode, the recorrelated curve is higher in terms of amplitude of respective the *strip assumption* case, in the whole considered frequency range. The modes whose curves are superimposed are the ones that are mainly influenced by the drag contribution, that based on considerations made by previous researchers (i.e. Kimura et al.) have been computed by means of the *strip assumption*.

The convergent number of sections for 50 m/s wind velocity

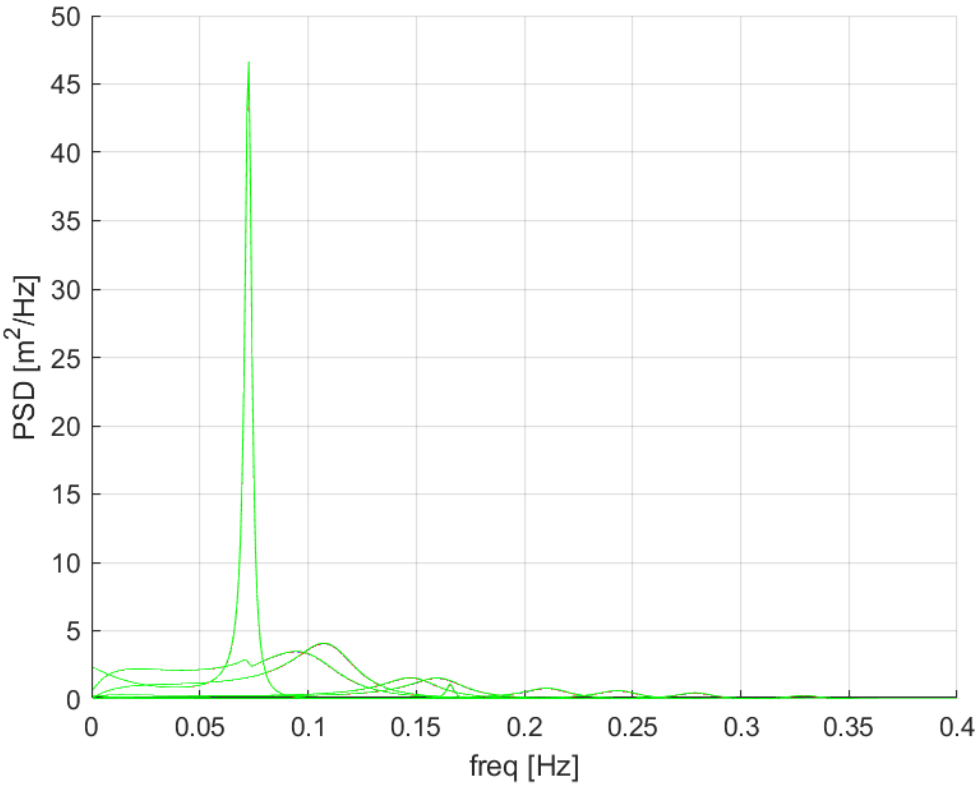

Figure 3.94: PSD of the displacement of the deck for each vibration mode changing number of sections: 82 sections (green line), 164 sections (blue line), 328 sections (red line).

In order to study the dynamic behaviour of the Braila bridge deck, it was initially divided in 82 sections. In order to apply the span - wise coherence function it was necessary to find the number of sections into divide the bridge for which the dynamic response did not change. In figures 3.94 and 3.95 it is possible to recognize that the convergent number of sections is 328. In order to have a better representation, in figure, 3.95, the contribution of the first mode of vibration has been cancelled.

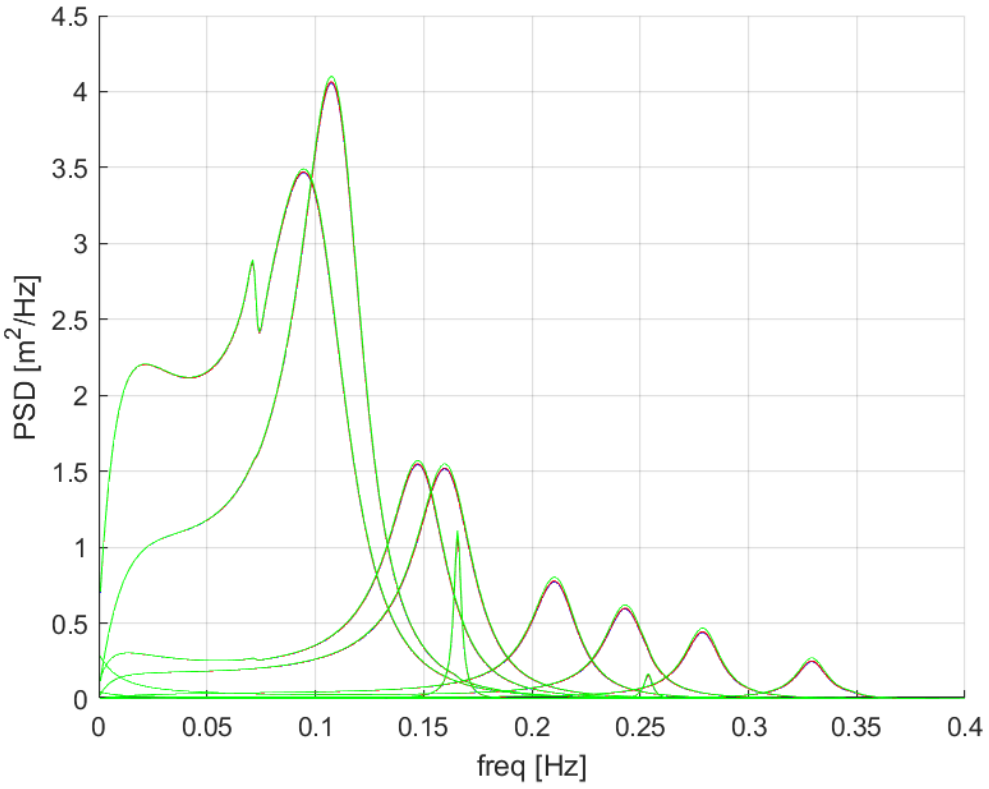

Figure 3.95: PSD of the displacement of the deck for each vibration mode except 1st changing number of sections: 82 sections (green line), 164 sections (blue line), 328 sections (red line).

Effect of the span-wise coherence on the bridge response for 50 m/s wind velocity

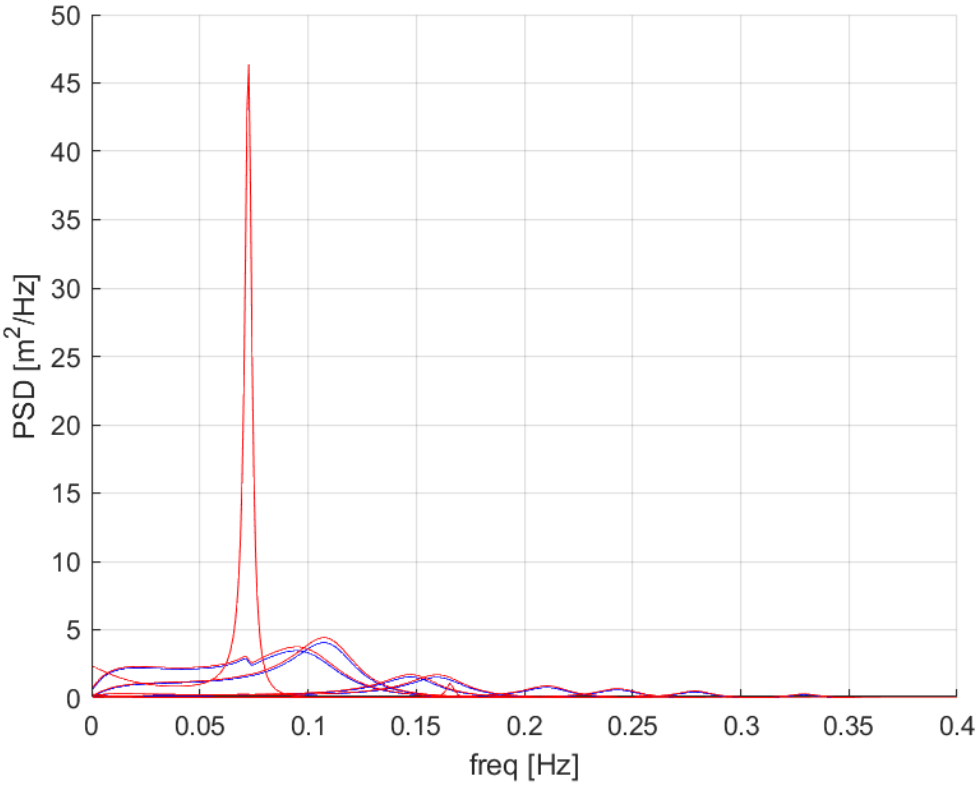

Figure 3.96: PSD of the displacement of the deck for each vibration mode with the span-wise coherence (red line) or the strip assumption (blue line).

In figure 3.96 and 3.97 it is possible to recognize the modal displacement of the Braila deck for each vibration mode. In picture 3.98 it is possible to see the modal acceleration of the deck. In figures 3.99, 3.100, 3.101 we can watch the accelerations along y, z and ϑ for sections $S2$, $S3$, $S4$.

All the plots described above have been performed using a number of sections equal to 328 (convergent number).

It is clear that the effect of recorrelation of the buffeting forces is more important in correspondence of the peaks of resonance, than it is an effect that has to be considered during the design of the bridge and in its fatigue life. As we expected in all the cases mentioned above the *strip assumption* produces an underestimation of the results, that in certain cases could be quite big and it has to be taken into account. Passing from 20 m/s to 50 m/s it is possible to see that the effect of recorrelation is decreasing (blue and red curve are closer).

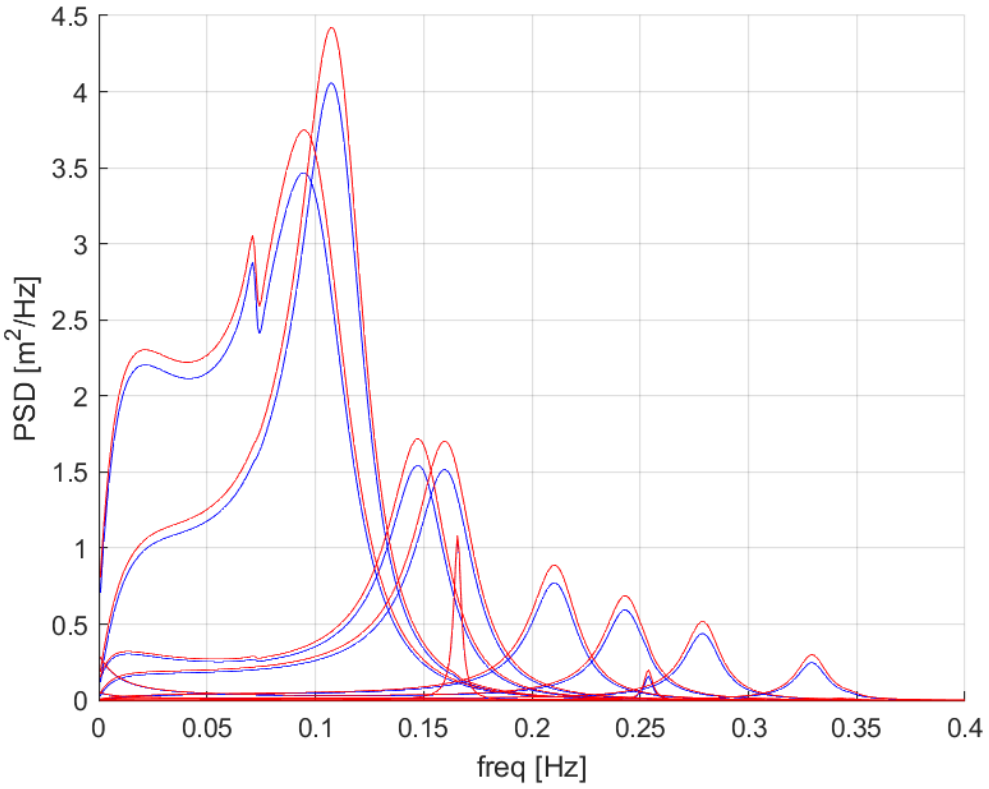

Figure 3.97: PSD of the displacement of the deck for each vibration mode except 1st with the span-wise coherence (red line) or the strip assumption (blue line).

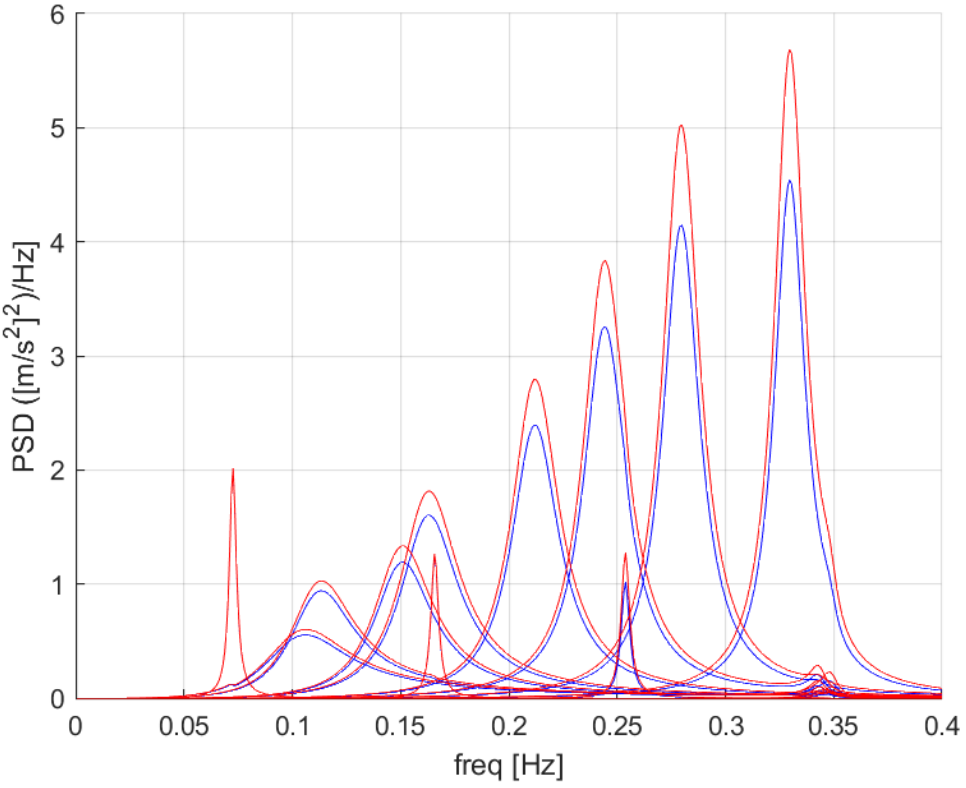

Figure 3.98: PSD of the modal acceleration of the deck with recorrelation (red line) or strip assumption (blue line).

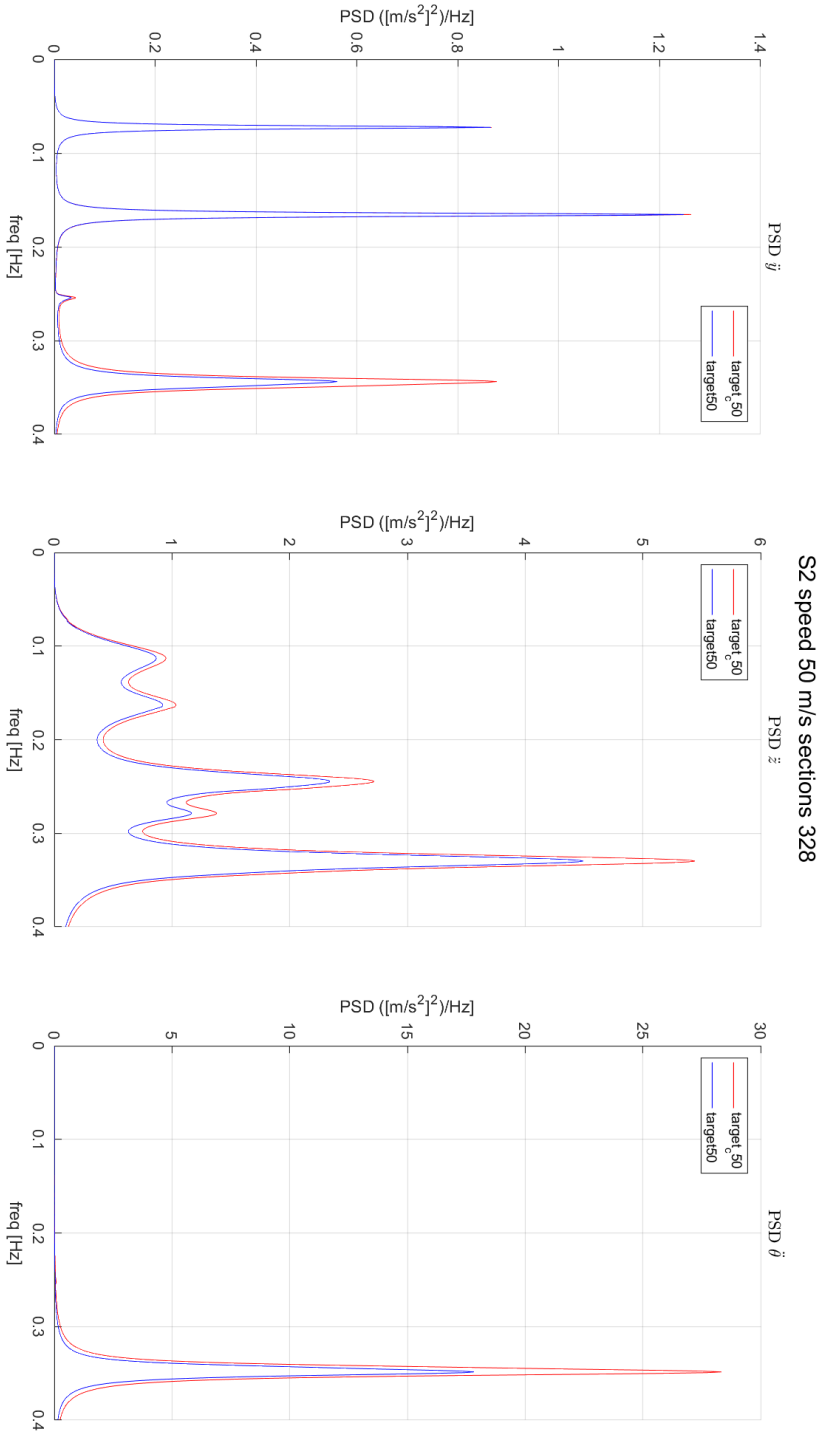

Figure 3.99: PSD of the acceleration along y, z and ϑ for section S2.

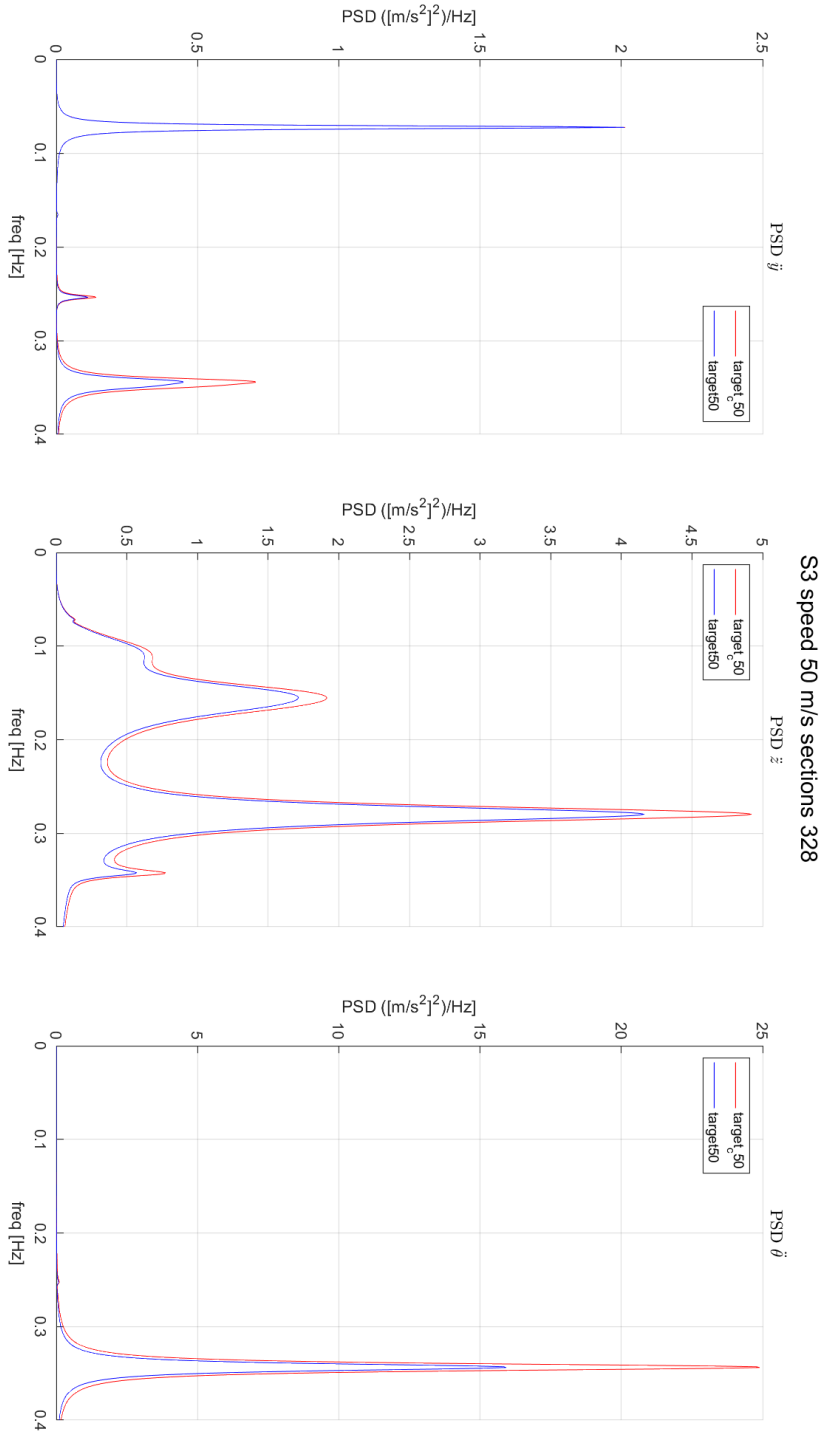

Figure 3.100: PSD of the acceleration along y, z and ϑ for section S3.

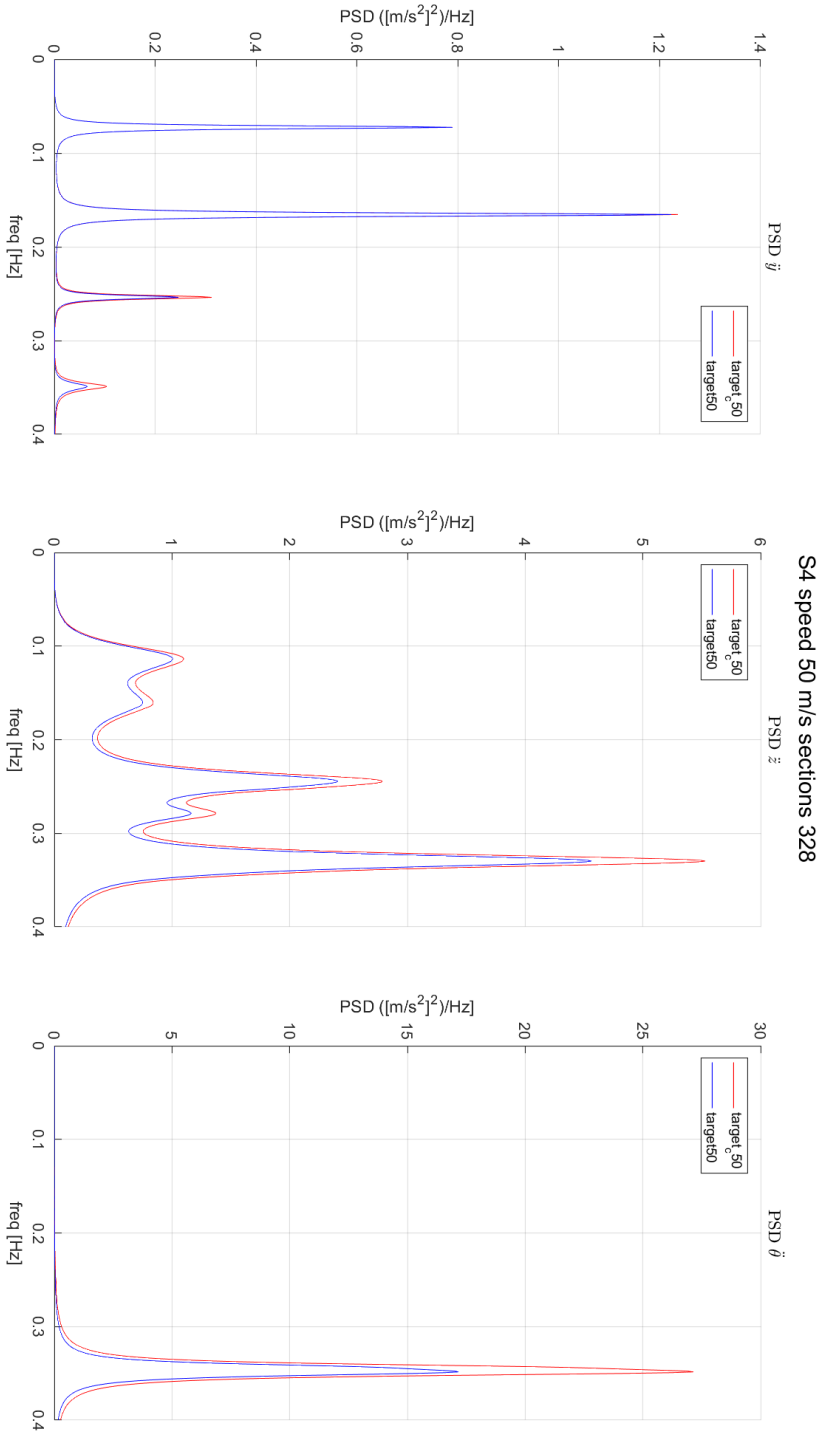

Figure 3.101: PSD of the acceleration along y, z and ϑ for section S4.

3.3.3 Braila bridge deck response for 65 m/s wind velocity

Span-wise coherence for 65 m/s wind velocity

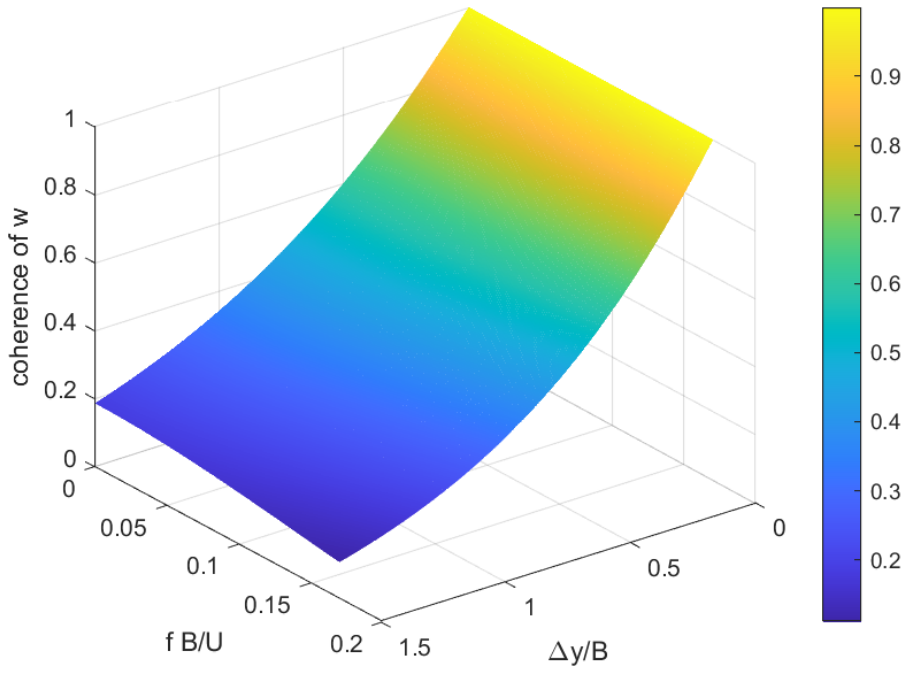

Figure 3.102: Normalized cross-spectrum of the w turbulence component for different $\Delta y/B$ and f^*

In figures 3.102, 3.103 and 3.104 it is possible to examine the 3D trend of the span-wise coherence for w gusty wind component, lift and aerodynamic moment, taking into account at the same time the reduced frequency f^* and the normalized distance between two different point $\frac{\Delta y}{B}$. Also considering the adapted Larose G. representation, as we expected, it confirms the underestimation given by the *strip assumption*. In pictures 3.105, 3.106, it is possible to watch the 3D trends of the ratio between $coh_w^{1/2}/coh_L^{1/2}$ and $coh_w^{1/2}/coh_T^{1/2}$ taking into account at the same time the reduced frequency $\frac{fB}{U}$ and the adimensional spacing $\frac{\Delta y}{B}$.

The plots, also in this case, considering the adapted Larose G. model, display an higher recorrelation with respect the one of the turbulent wind. These functions have been considered in the simulations for all the entire frequency range (f = 0 - 0.4 Hz), but for a reduced spacing between the sections: in the range $\Delta y/B = 0 - 1.52$ for the moment and $\Delta y/B = 0 - 0.76$ for the lift. This has been done in order to obtain physical results and to compare the results with the Jakobsen J. representation, having considered the same $\Delta y/B$ ranges.

In table 3.7 it is possible to find the parameters concerning the wind generation and the kind of admittance matrix considered in the simulation of the bridge response at 65 m/s.

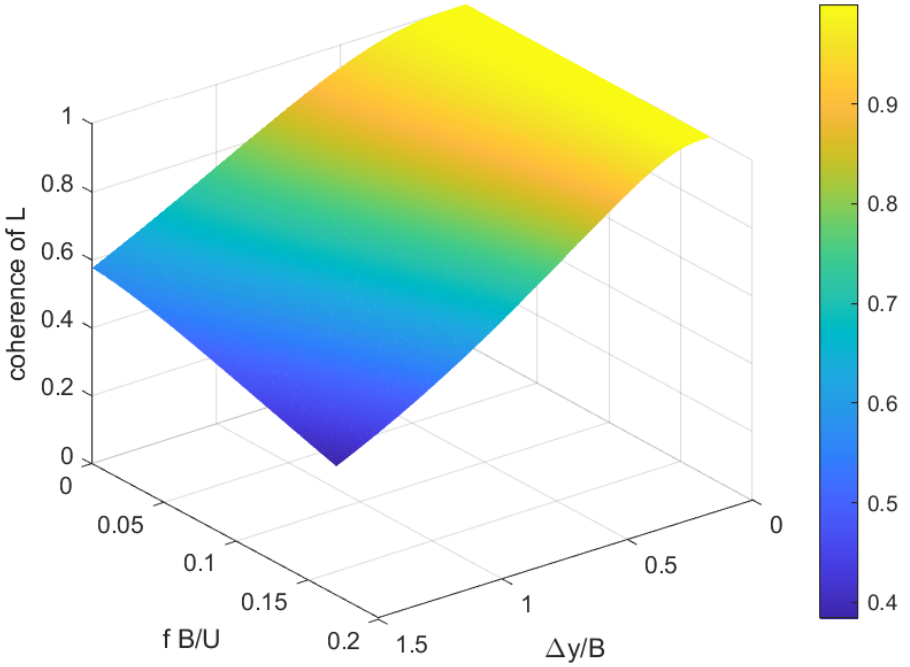

Figure 3.103: Normalized cross-spectrum of the buffeting L for different $\Delta y/B$ and f^*

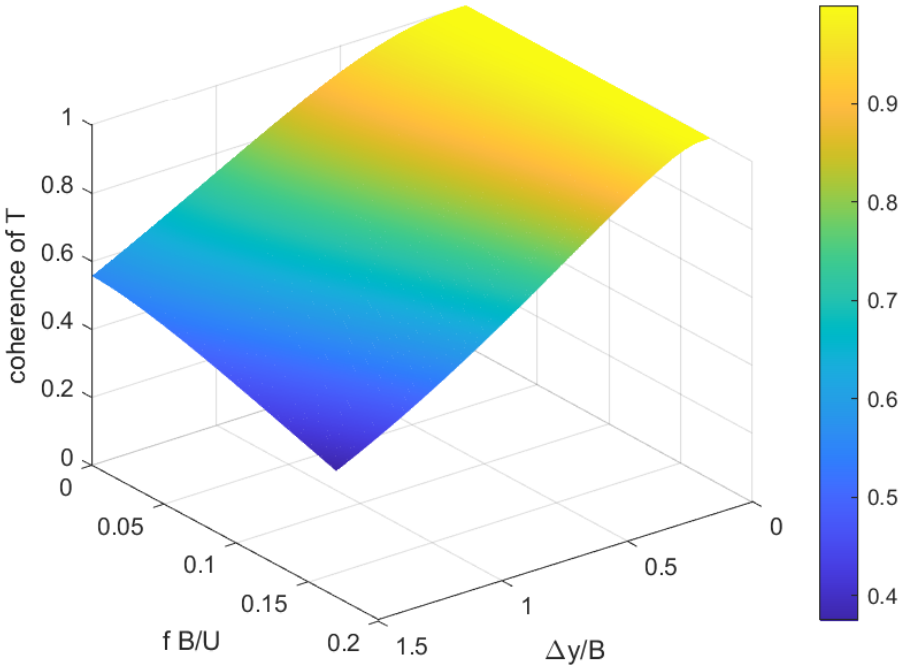

Figure 3.104: Normalized cross-spectrum of the buffeting T for different $\Delta y/B$ and f^*

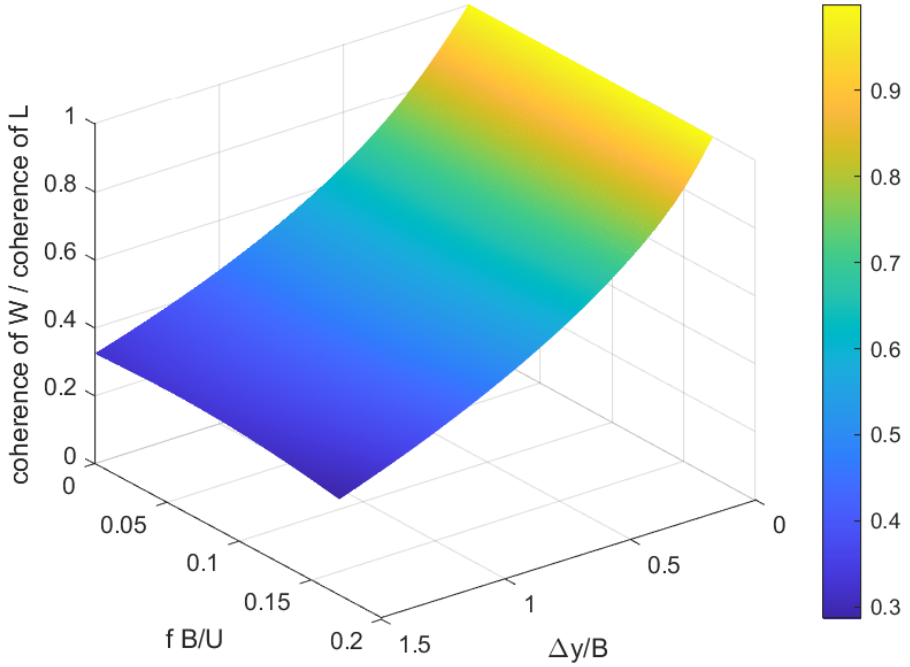

Figure 3.105: Ratio of normalized cross-spectra $coh_w^{1/2}/coh_L^{1/2}$ for different $\Delta y/B$, f^*

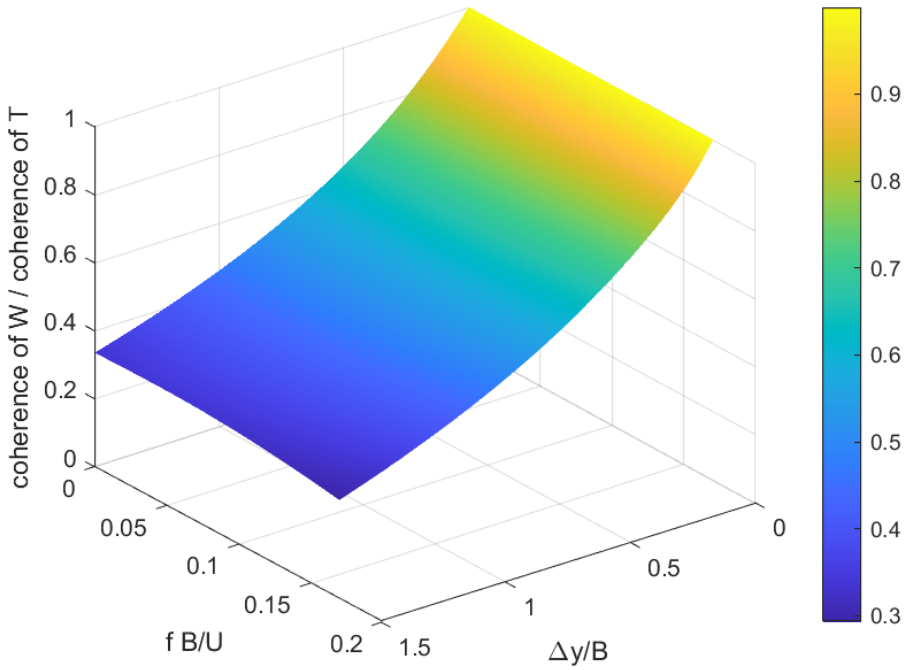

Figure 3.106: Ratio of normalized cross-spectra $coh_w^{1/2}/coh_T^{1/2}$ for different $\Delta y/B$, f^*

Generation of the PSD of the wind for 65 m/s wind

Table 3.7: Parameters considered for the simulation at 65 m/s

Parameter	Target Value
$\overline{U}$	65 m/s
L_u^x	160 mm
L_w^x	16 mm
I_u	0.143
I_w	0.0715
C_{wx}	0.5
C_{wy}	6.5
C_{wz}	3
C_{ux}	3
C_{uy}	10
C_{uz}	10
C_{vx}	3
C_{vy}	6.5
C_{vz}	6.5
Admittance	Davenport

In figures 3.107, 3.108, 3.109, 3.110, 3.111, 3.112, 3.113 it is possible to observe the PSD of the Lagrangian of the generated wind for each vibration mode. It has been plotted for each of the thirteen modes of the Braila bridge the comparison between the *recorrelated* case (red line) and the *strip assumption* case (blue line).

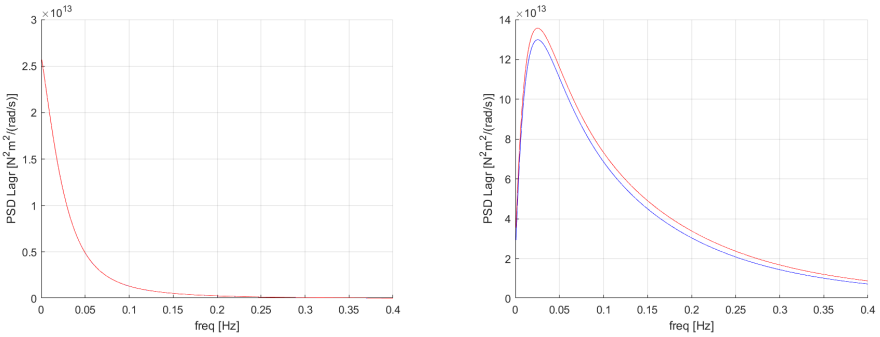

(a) Mode 1H **(b)** Mode 1V

Figure 3.107: PSD of the Lagrangian of the generated wind for mode 1H and 1V

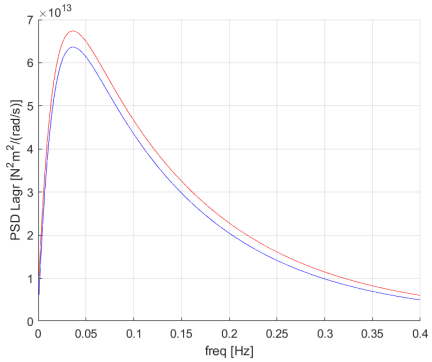

(a) Mode 2A

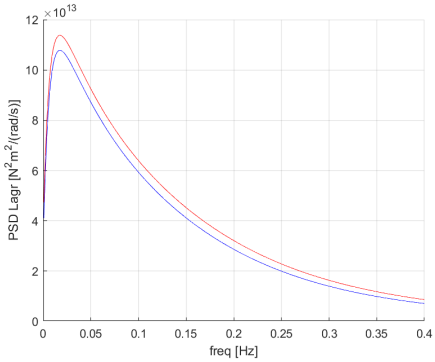

(b) Mode 2V

Figure 3.108: PSD of the Lagrangian of the generated wind for mode 2A and 2V

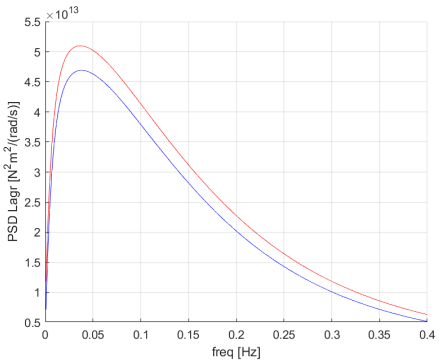

(a) Mode 3V

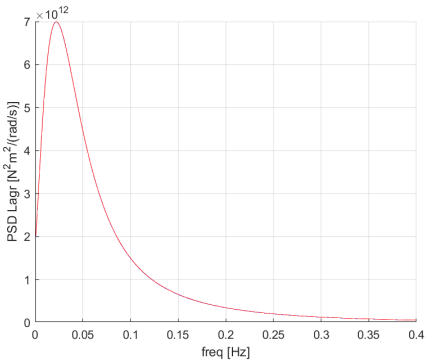

(b) Mode 2H

Figure 3.109: PSD of the Lagrangian of the generated wind for mode 3V and 2H

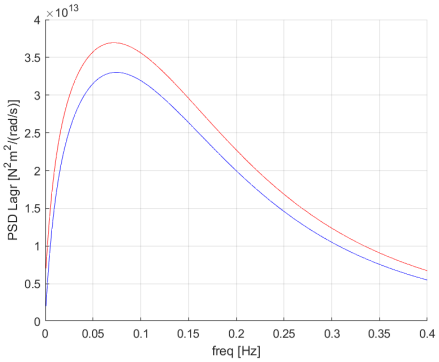

(a) Mode 4V

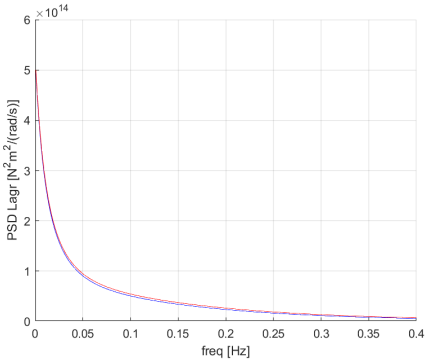

(b) Mode 5V

Figure 3.110: PSD of the Lagrangian of the generated wind for mode 4V and 5V

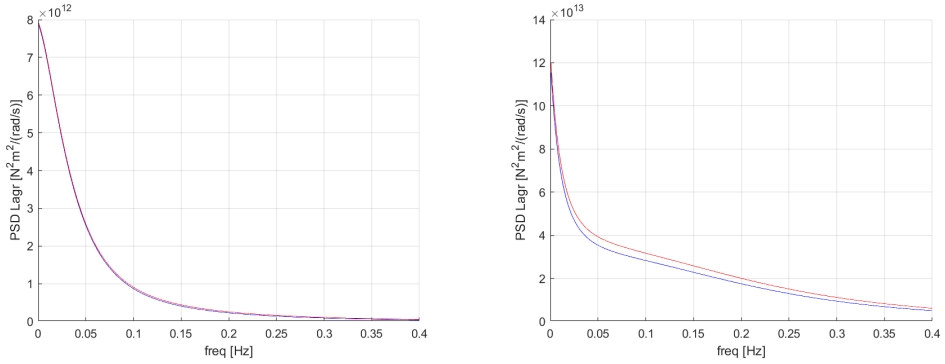

(a) Mode 3H **(b)** Mode 6V

Figure 3.111: PSD of the Lagrangian of the generated wind for mode 3H and 6V

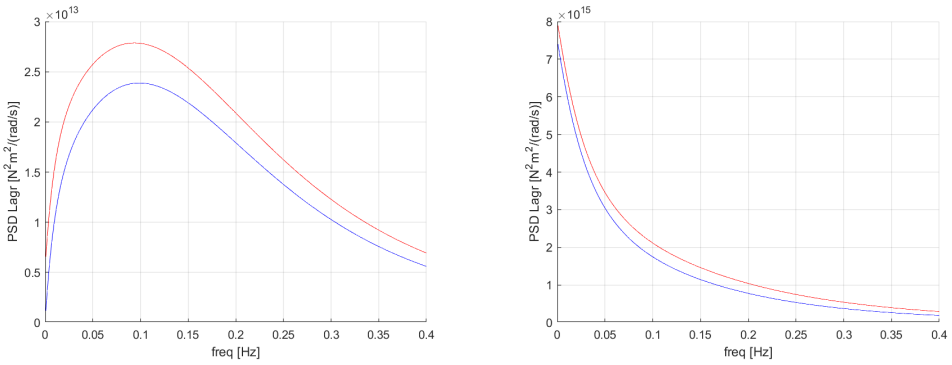

(a) Mode 7V **(b)** Mode 1T

Figure 3.112: PSD of the Lagrangian of the generated wind for mode 7V and 1T

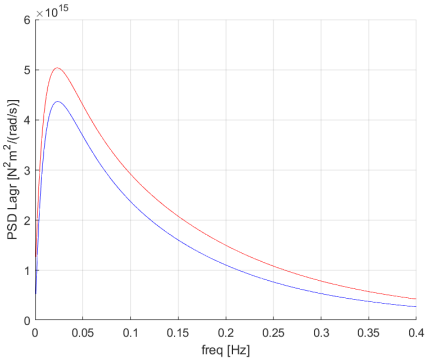

Figure 3.113: PSD of the Lagrangian of the generated wind for mode 2T

As we expected for each mode the recorrelated curve is higher in terms of amplitude of respective the *strip assumption* case, in the whole considered frequency range. The modes whose curves are superimposed are the ones that are mainly influenced by the drag contribution, that based on considerations made by previous researchers (i.e. Kimura et al.) have been computed by means of the *strip assumption*.

The convergent number of sections for 65 m/s wind velocity

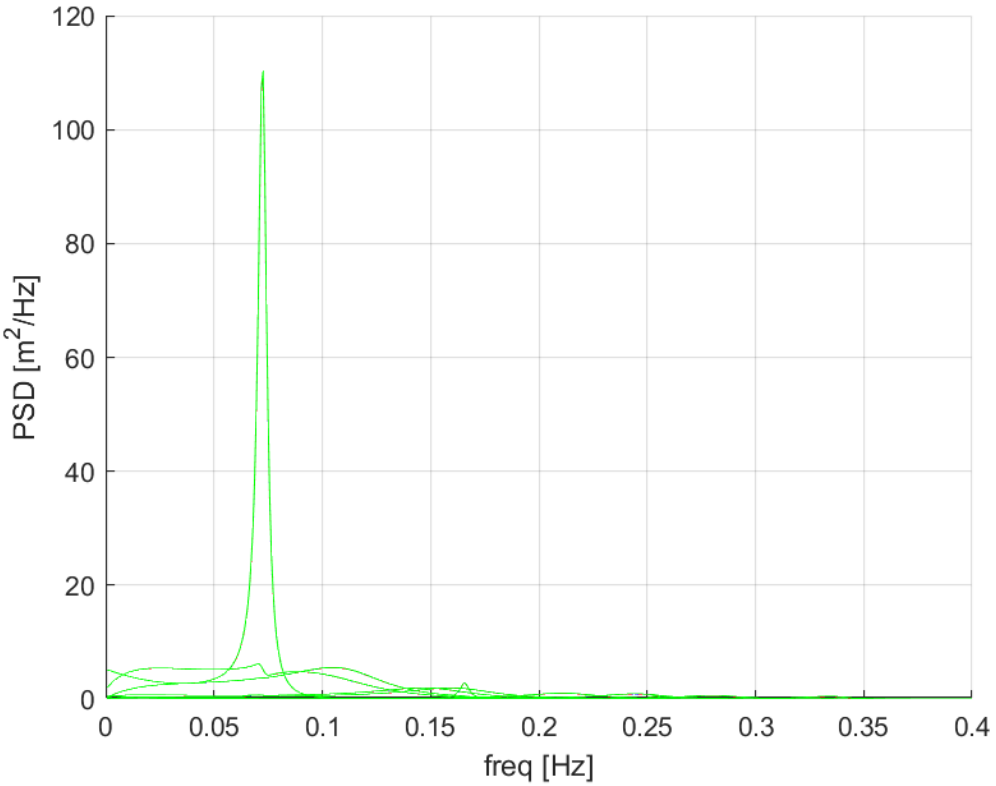

Figure 3.114: PSD of the displacement of the deck for each vibration mode changing number of sections: 82 sections (green line), 164 sections (blue line), 328 sections (red line).

In order to study the dynamic behaviour of the Braila bridge deck, it was initially divided in 82 sections. In order to apply the span - wise coherence function it was necessary to find the number of sections into divide the bridge for which the dynamic response did not change. In figures 3.114 and 3.115 it is possible to recognize that the convergent number of sections is 328. In order to have a better representation, in figure 3.115, the contribution of the first mode of vibration has been cancelled.

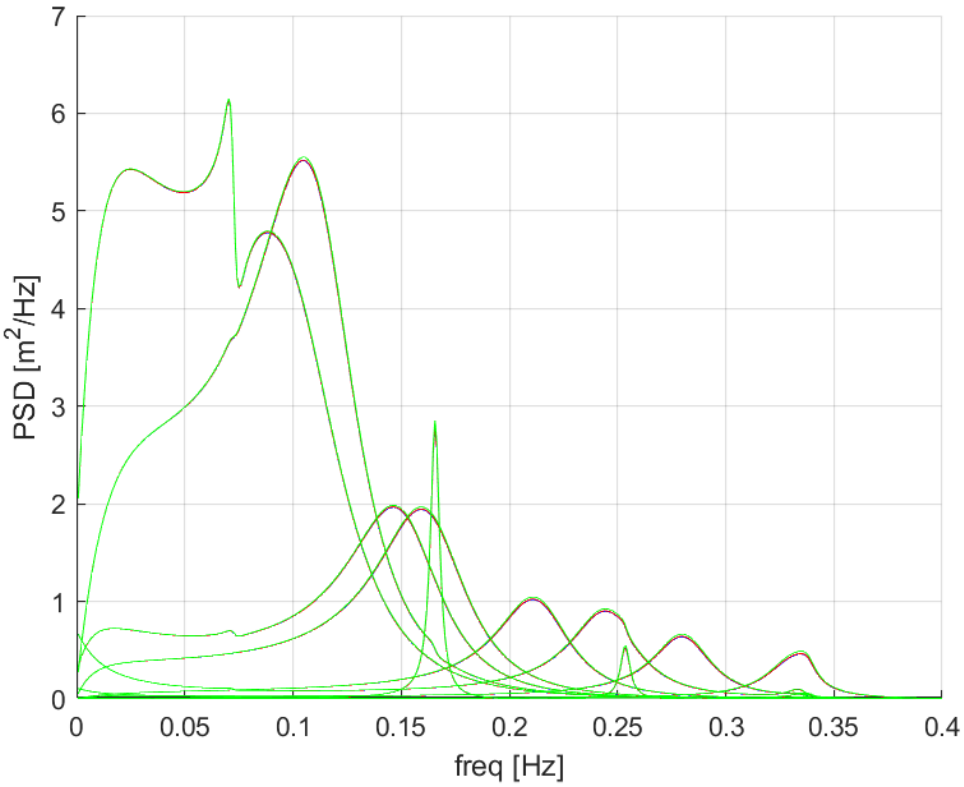

Figure 3.115: PSD of the displacement of the deck for each vibration mode except 1st changing number of sections: 82 sections (green line), 164 sections (blue line), 328 sections (red line).

Effect of the span-wise coherence on the bridge response for 65 m/s wind velocity

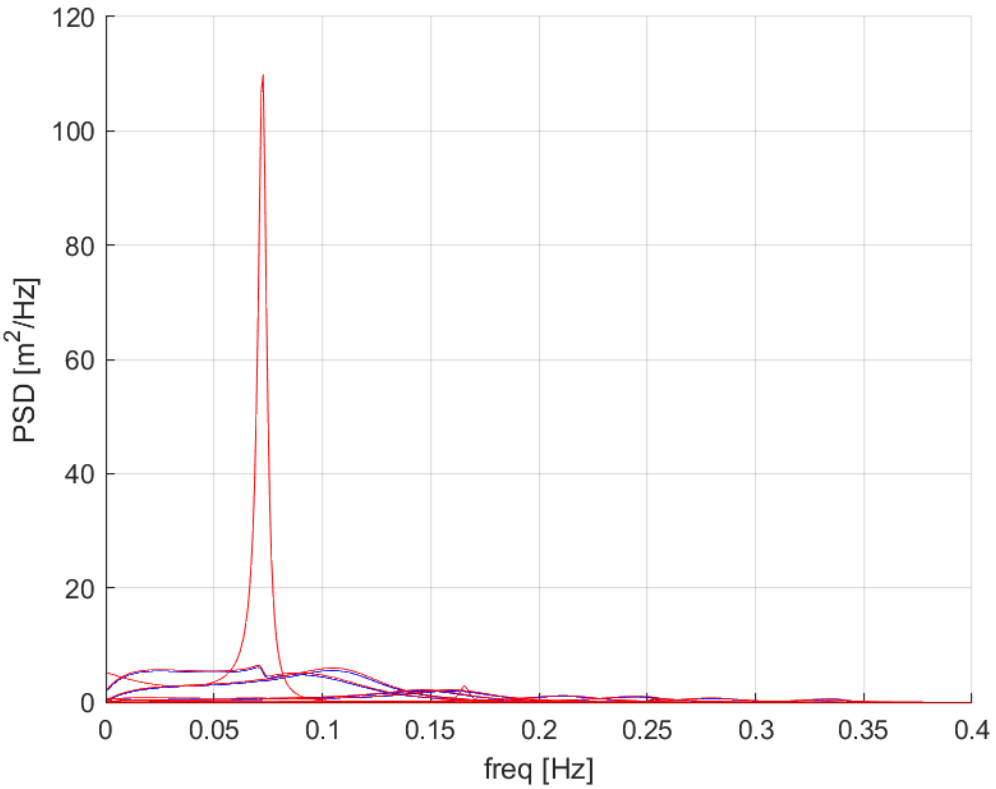

Figure 3.116: PSD of the displacement of the deck for each vibration mode with the span-wise coherence (red line) or the strip assumption (blue line).

In figure 3.116 and 3.117 it is possible to recognize the modal displacement of the Braila deck for each vibration mode. In picture 3.118 it is possible to see the modal acceleration of the deck. In figures 3.119, 3.120, 3.121 we can watch the accelerations along y, z and ϑ for sections $S2$, $S3$, $S4$.

All the plots described above have been performed using a number of sections equal to 328 (convergent number).

It is clear that the effect of recorrelation of buffeting forces is more important in correspondence of the peaks of resonance, than it is an effect that has to be considered during the design of the bridge and in its fatigue life. As we expected in all the cases mentioned above the *strip assumption* produces an underestimation of the results, that in certain cases could be quite big and it has to be taken into account. Passing from 50 m/s to 65 m/s it is possible to see that we have a similar effect of recorrelation between the two speeds. In the conclusion of this work a comparison between the case of 328 sections with span-wise coherence of the buffeting forces and the one characterized by each section of length equal to B (deck width) and 1.5 B considering the *strip assumption* will be made.

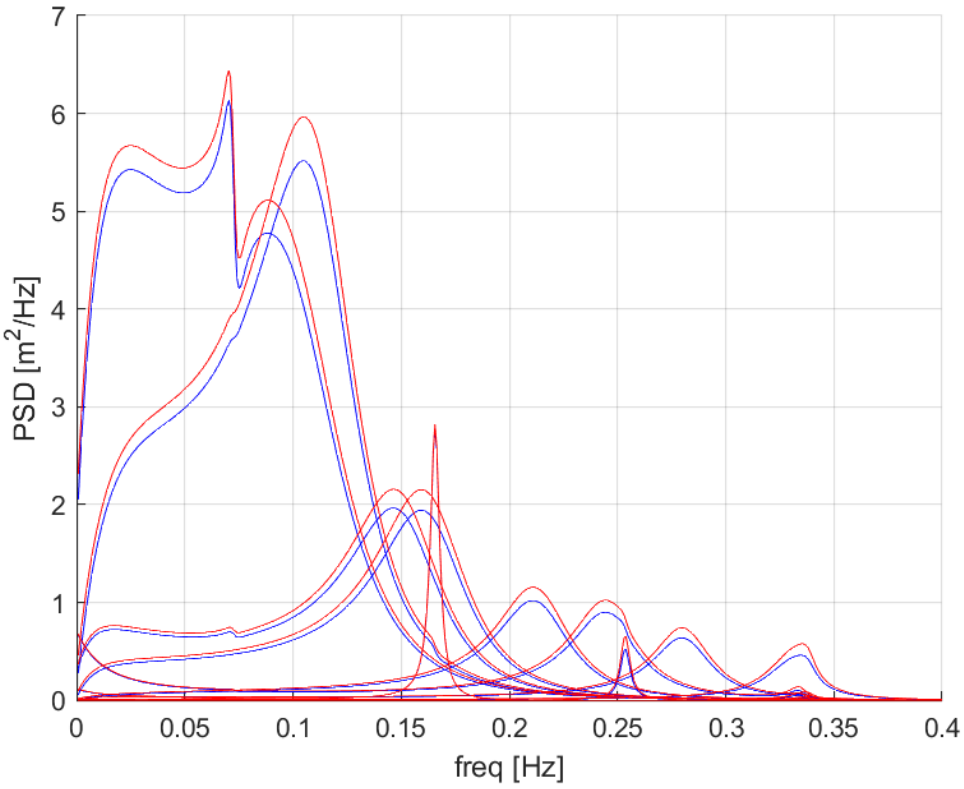

Figure 3.117: PSD of the displacement of the deck for each vibration mode except 1st with the span-wise coherence (red line) or the strip assumption (blue line).

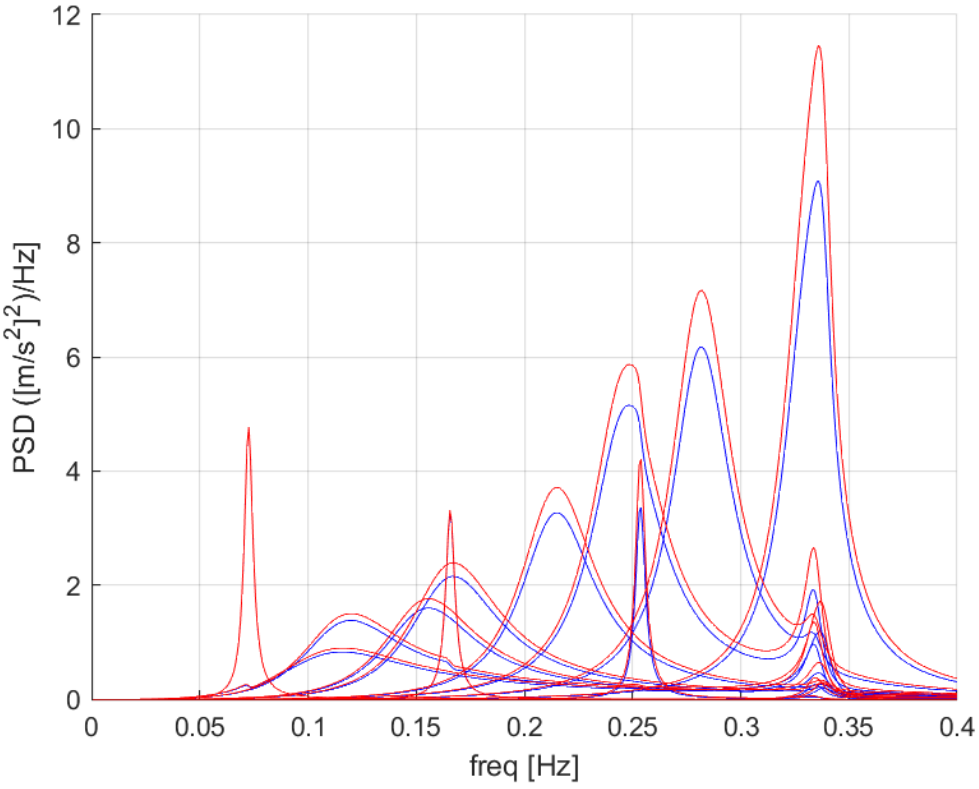

Figure 3.118: PSD of the modal acceleration of the deck with recorrelation (red line) or strip assumption (blue line).

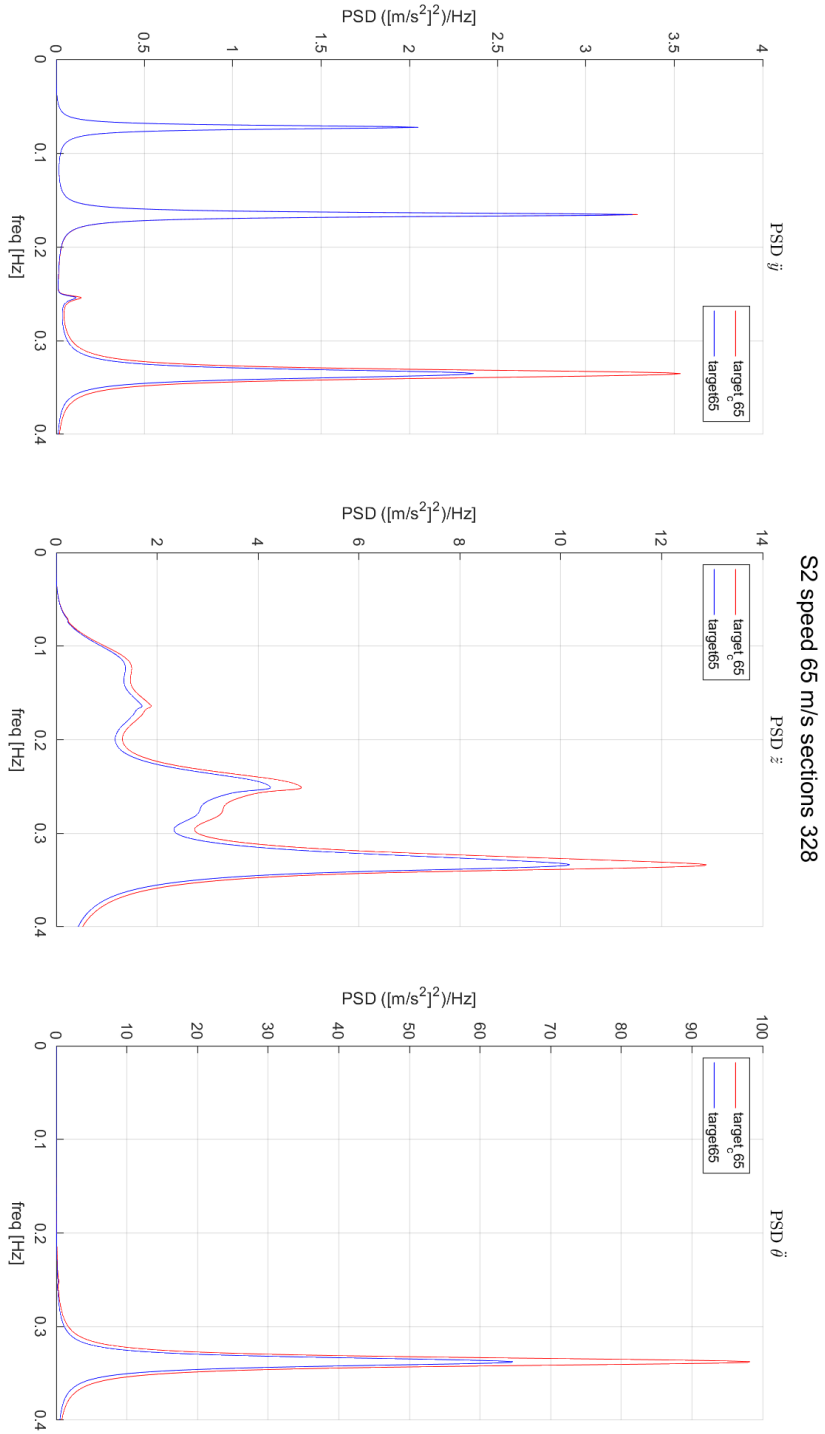

Figure 3.119: PSD of the acceleration along y, z and ϑ for section S2.

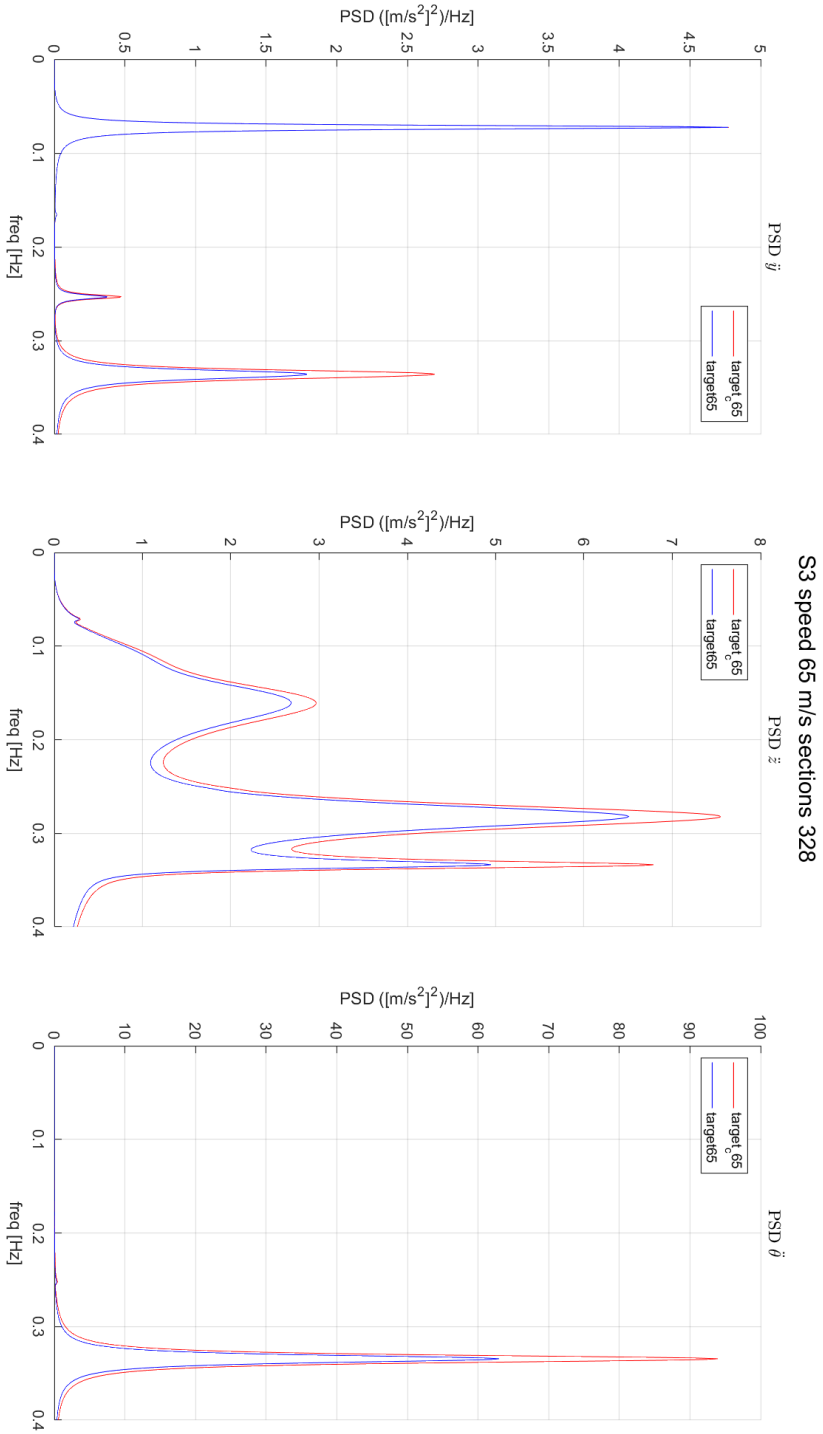

Figure 3.120: PSD of the acceleration along y, z and ϑ for section S3.

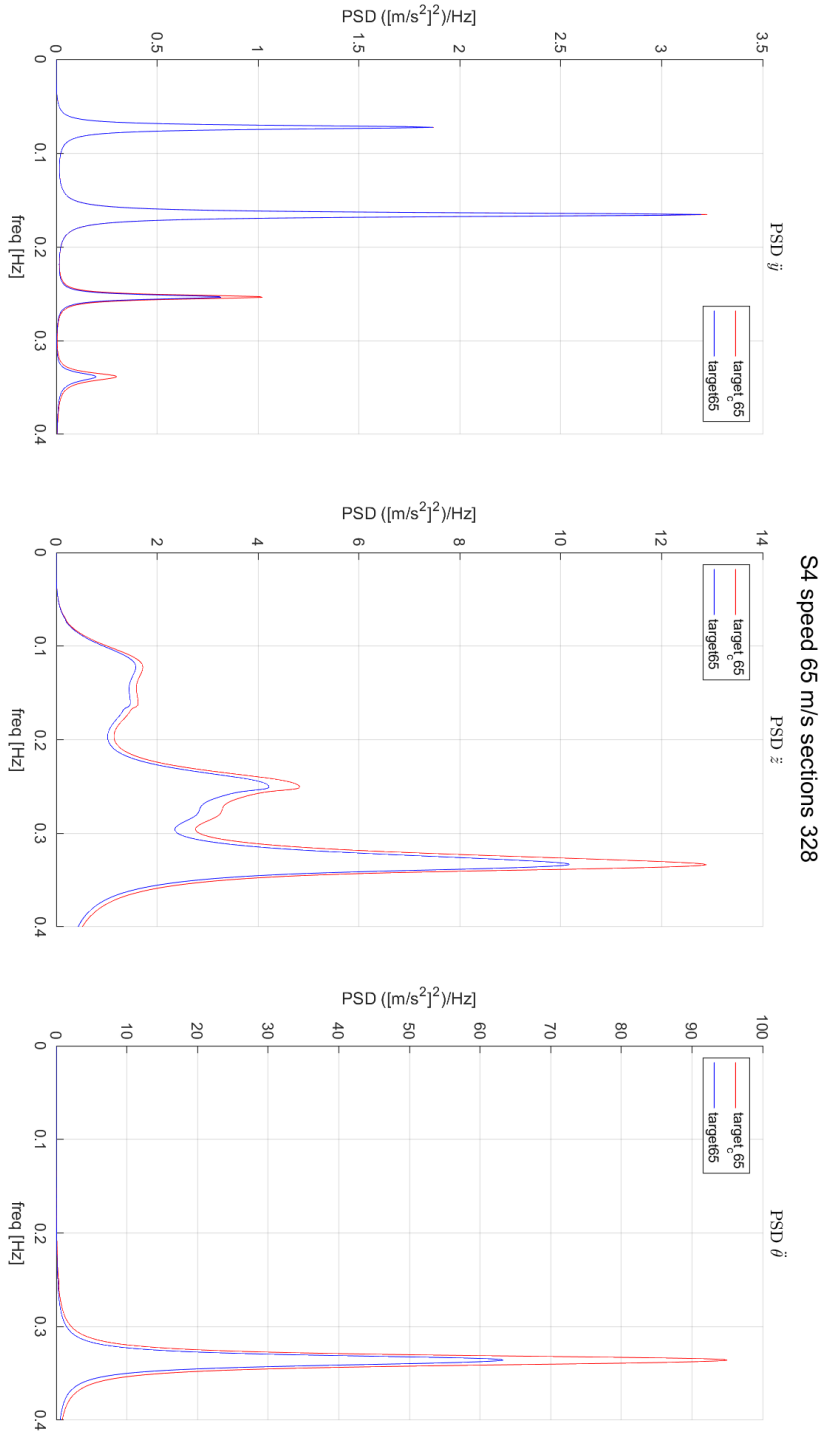

Figure 3.121: PSD of the acceleration along y, z and ϑ for section S4.

Conclusions

In this last part I want to compare the response of the Braila deck considering 328 sections with the span-wise coherence (with both the adapted Larose G. and Jakobsen J. representation) with the one characterized by a length of each section equal to the deck width B (62 sections) and equal to $1.5B$ (41 sections) both with the *strip assumption*. I am going the repeat the comparison for each considered wind speed $\overline{U}$ = 20 m/s (figure I and II), 50 m/s (figure III and IV), 65 m/s (figure V and VI).

The choice of considering 62 sectors in the discussion is due to the fact that nowadays is common practice to use a length of each section similar to the deck width B. It is well known that it represents a good approximation. I have taken into account the case characterized by 41 sectors ($1.5B$) in order to understand in which range I can find the number of sections in which I can divide my Bridge, considering the *strip assumption*, that well approximates the behaviour with the convergent number of sections (328) with the span-wise coherence of the buffeting forces.

In addition I have made a comparison between the two span-wise normalized cross spectra representations in terms of modal acceleration of the Braila deck for each wind velocity (20 m/s figure VII, 50 m/s figure VIII, 65 m/s figure IX).
There is a good agreement between the Larose G. adapted model and Jakobsen J. one at every wind speed considered. The differences between the two representation decreases passing from 20 m/s to 65 m/s. Larose G. adapted model slightly underestimate the modal acceleration with respect to the Jakobsen J. one.

Looking at figures I II, III, IV, V and VI it is possible to recognize which is the number of sections that well approximate the behavior of the curves with the span-wise recorrelation of the buffeting forces for both Larose G. and Jakobsen J.:

- 58 sections ($1.08B$) for 20 m/s wind speed
- 54 sections ($1.16B$) for 50 m/s wind speed
- 41 sections (1.5B) for 65 m/s wind speed

These values have been computed interpolating the relative distance between the three curves. I have to notice that these three values are affected by the high reduced frequency content that was not estimated well, initially, in the original representations. The value of sections depends on frequency, wind velocity and specific conditions of the site.

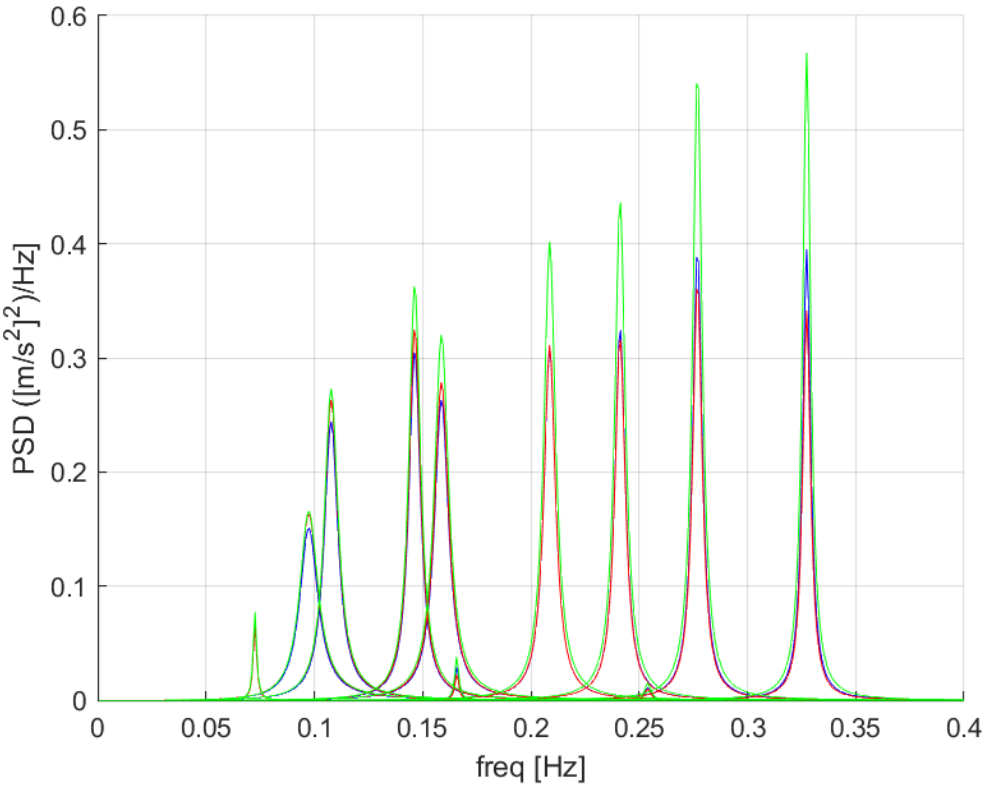

Figure I: PSD of the modal acceleration with Jakobsen J. recorrelation (red line) or strip assumption with 62 sections (blue line B) and 41 (green line $1.5B$) at 20 m/s.

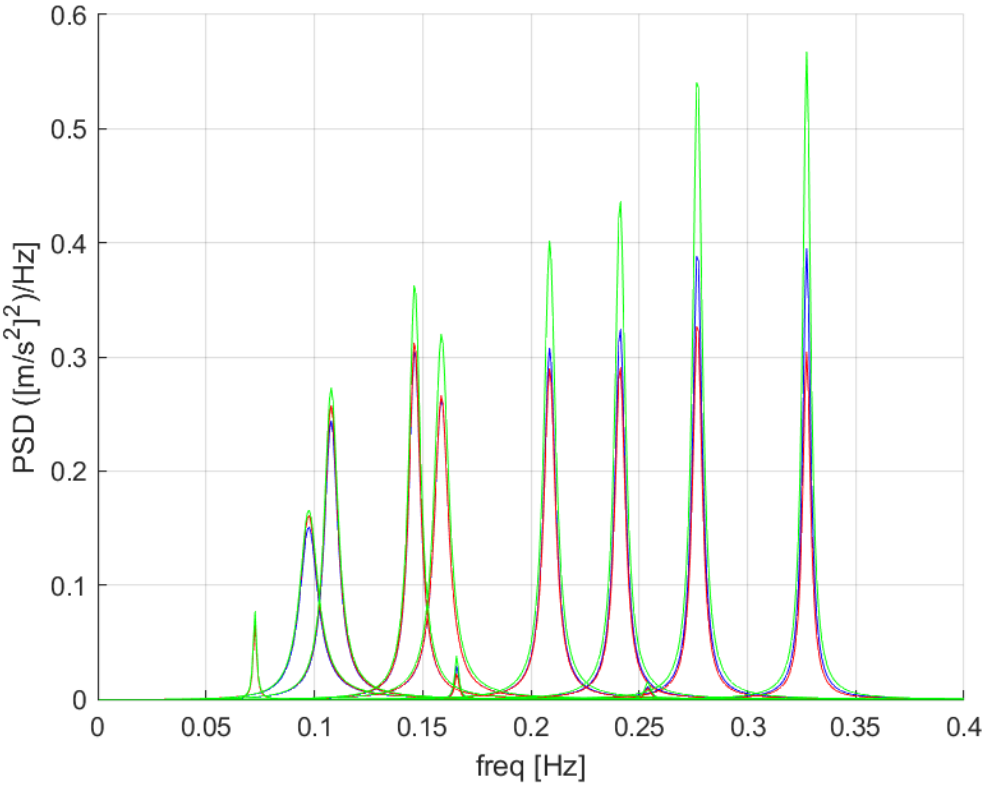

Figure II: PSD of the modal acceleration with Larose G. recorrelation (red line) or strip assumption with 62 sections (blue line B) and 41 (green line $1.5B$) at 20 m/s.

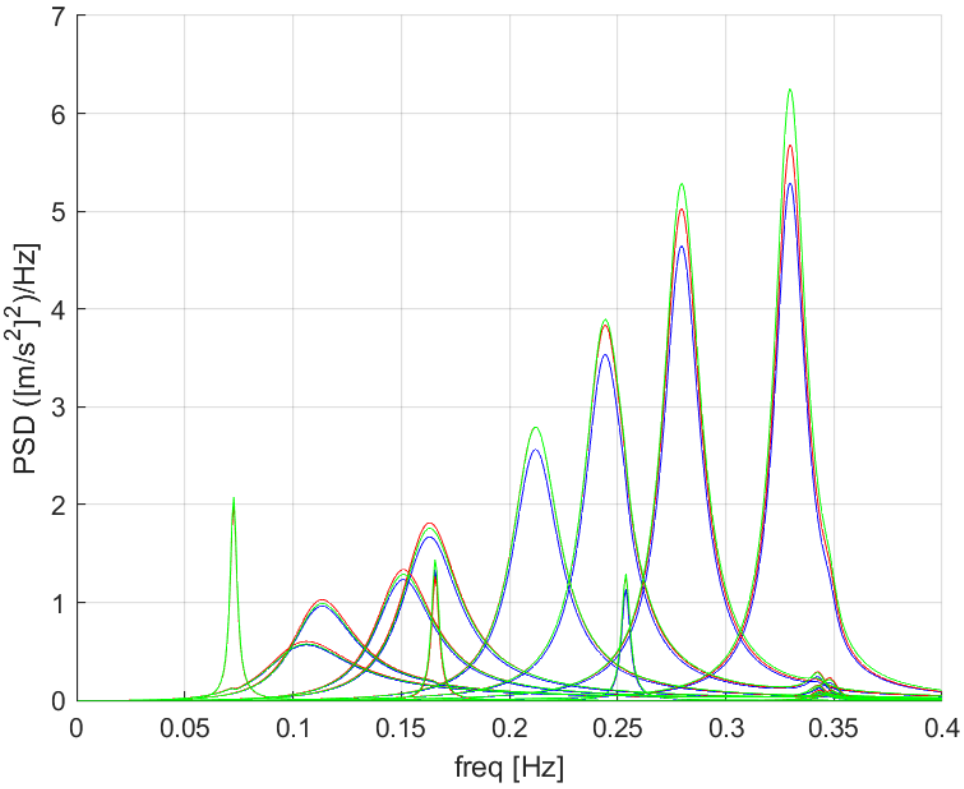

Figure III: PSD of the modal acceleration with Jakobsen J. recorrelation (red line) or strip assumption with 62 sections (blue line B) and 41 (green line $1.5B$) at 50 m/s.

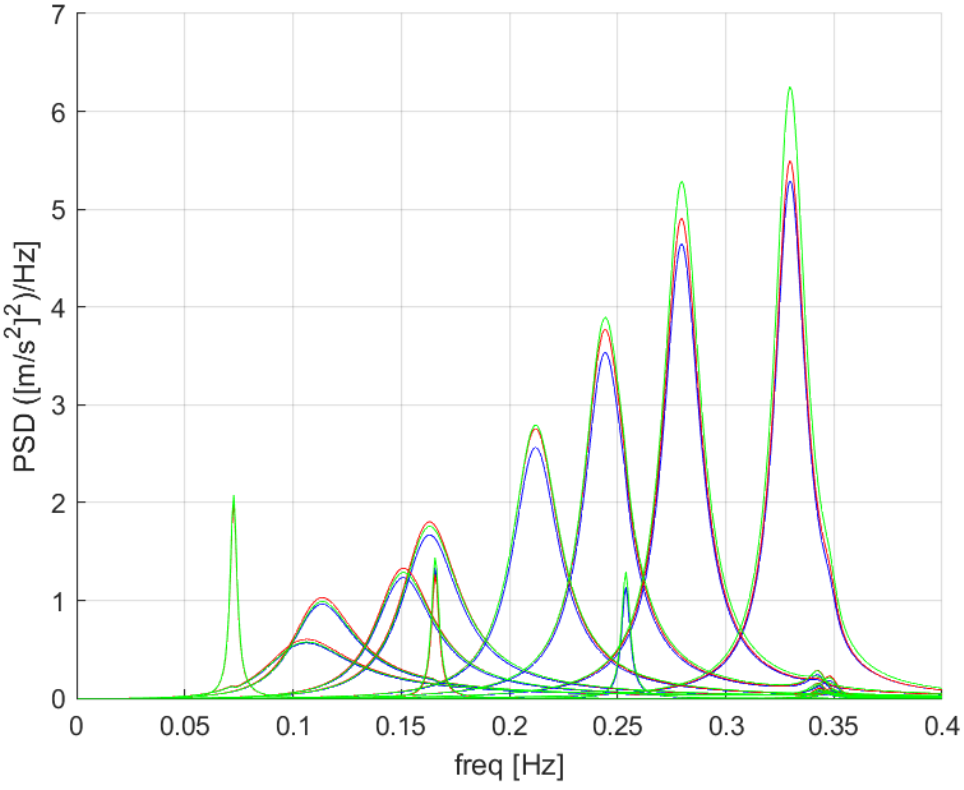

Figure IV: PSD of the modal acceleration with Larose G. recorrelation (red line) or strip assumption with 62 sections (blue line B) and 41 (green line $1.5B$) at 50 m/s.

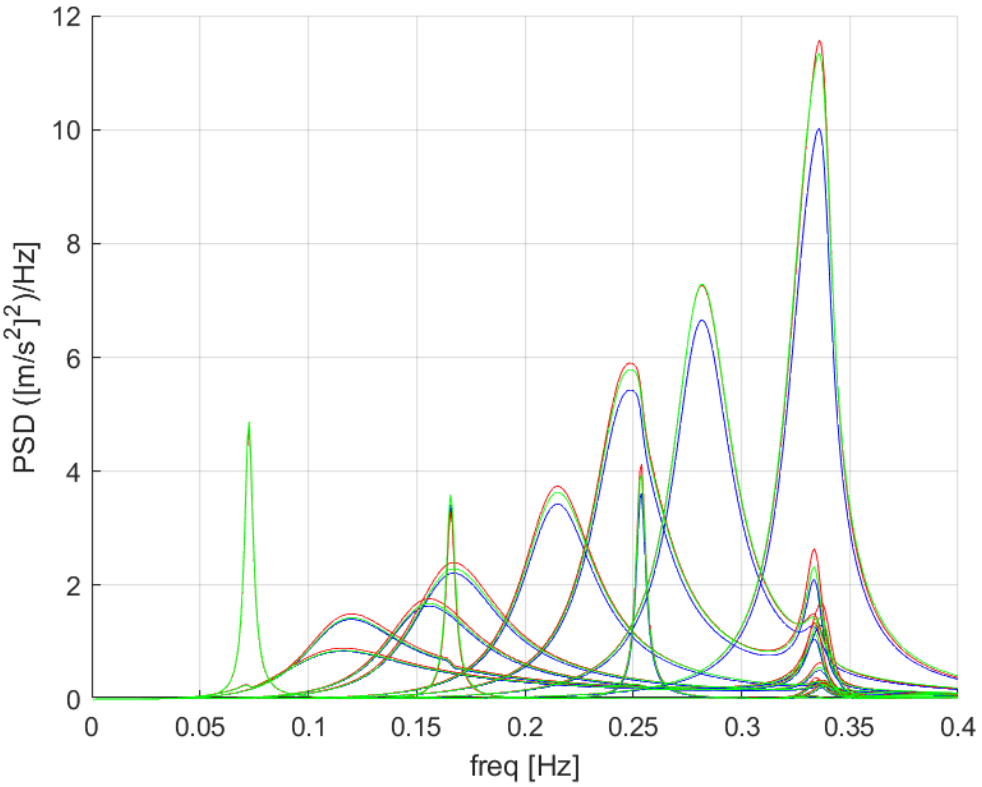

Figure V: PSD of the modal acceleration with Jakobsen J. recorrelation (red line) or strip assumption with 62 sections (blue line B) and 41 (green line $1.5B$) at 65 m/s.

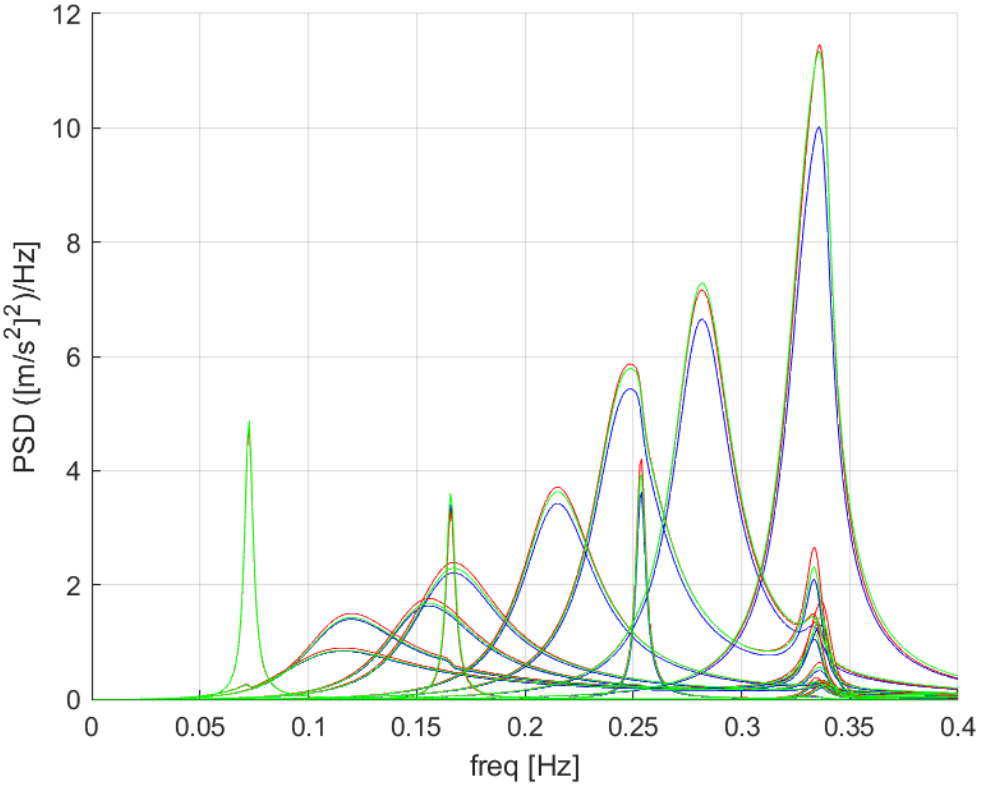

Figure VI: PSD of the modal acceleration with Larose G. recorrelation (red line) or strip assumption with 62 sections (blue line B) and 41 (green line $1.5B$) at 65 m/s.

Comparison among the two adapted models of Larose and Jakobsen

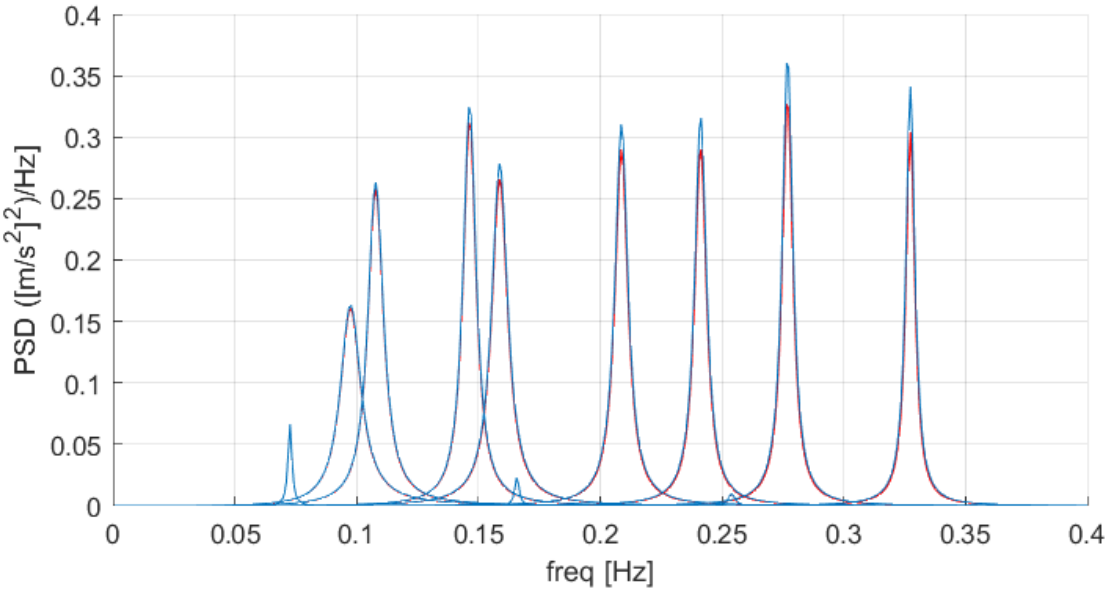

Figure VII: PSD of the modal acceleration with Larose G. recorrelation (red line) or Jakobsen J (green line) at 20 m/s.

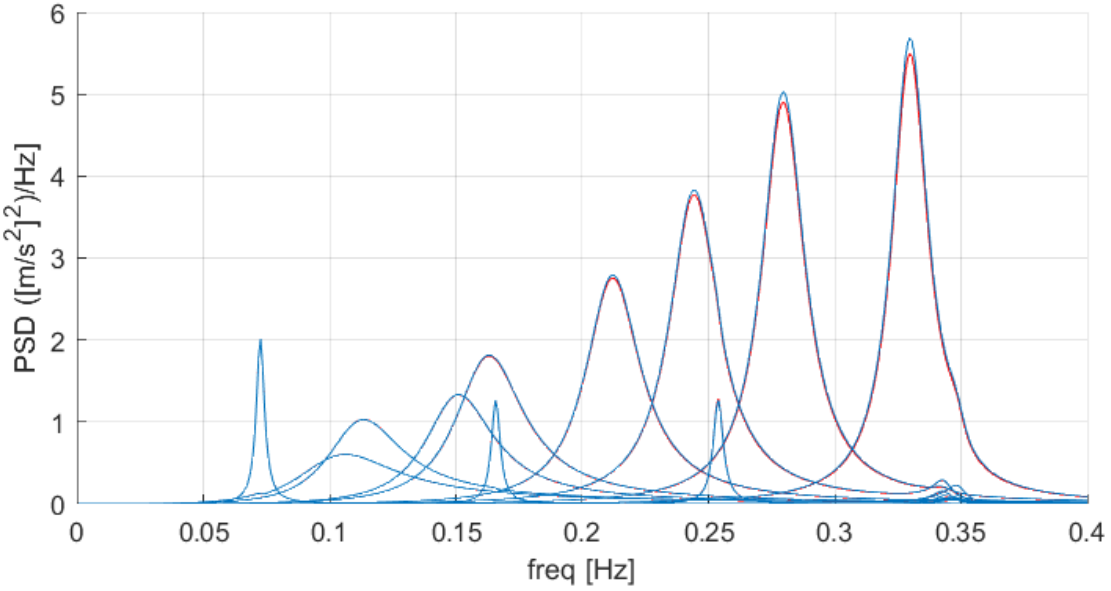

Figure VIII: PSD of the modal acceleration with Larose G. recorrelation (red line) or Jakobsen J (green line) at 50 m/s.

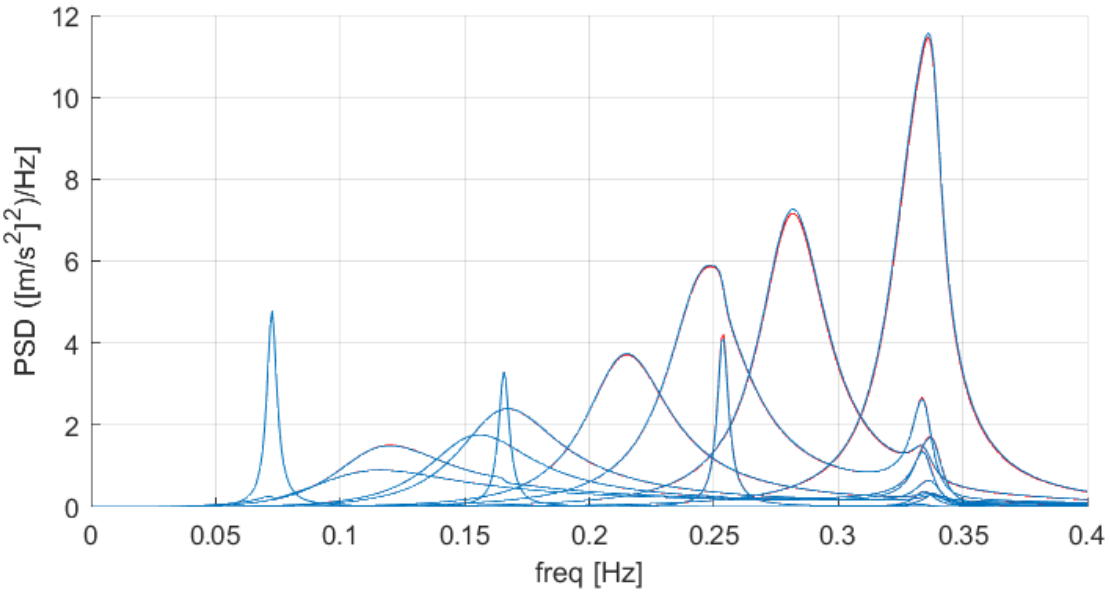

Figure IX: PSD of the modal acceleration with Larose G. recorrelation (red line) or Jakobsen J (green line) at 65 m/s.

Future developments

In order to deeply study the effect of recorrelation on bridges, it is necessary, by means of wind tunnel testings in the wind velocity range of the buffeting, to evaluate a new span-wise coherence function on a bridge deck section, specifically taking into account of the high frequency content. The next step is to compare the new span-wise coherence function with the previous ones of Larose G. and Jakobsen J. in order to validate the results. A further step is to repeat the study that I made for the Braila bridge with the new normalized co-sprectrum function and to implement it for the case of different bridges. This has to be performed in order to study the dependence of the recorrelation on:

- The specific wind conditions of the site
- The interested frequency range
- The geometry of the deck.

A CFD study would also be feasible and possible. In addition the recorrelation of the buffeting forces, being higher in correspondence of the resonance peaks, has to be investigated in the fatigue design of the bridge.

Appendix A

Wind action on Long Span Bridges

A.1 Introduction

The action of the wind produces static and dynamic loads on multiple types of structures and vehicles, such as bridges, buildings, high voltage cables, cars, freight and high-speed trains and many others.

In this work I will focus only on long span bridges, specifically the Braila bridge which is under construction in Romania. I make reference to the longest bridges because longer is the Bridge, worst is the problem related to wind effect. For short bridges the main problems are related to road and railway traffic.

We can have two types of long span bridges: cable stayed bridges and suspension bridges. The former have maximum lengths of the order of 1000m while the latter can exceed 1500m. The increase in length has the effect that the bridge becomes more and more flexible and its natural frequencies take on ever smaller values, until they are easily excitable by the wind.

The Braila bridge is the longest suspended bridge that is constructed in Romania, has a length of 1974m and is therefore a long span bridge for which the wind-structure interaction is very important and must be analyzed in detail.

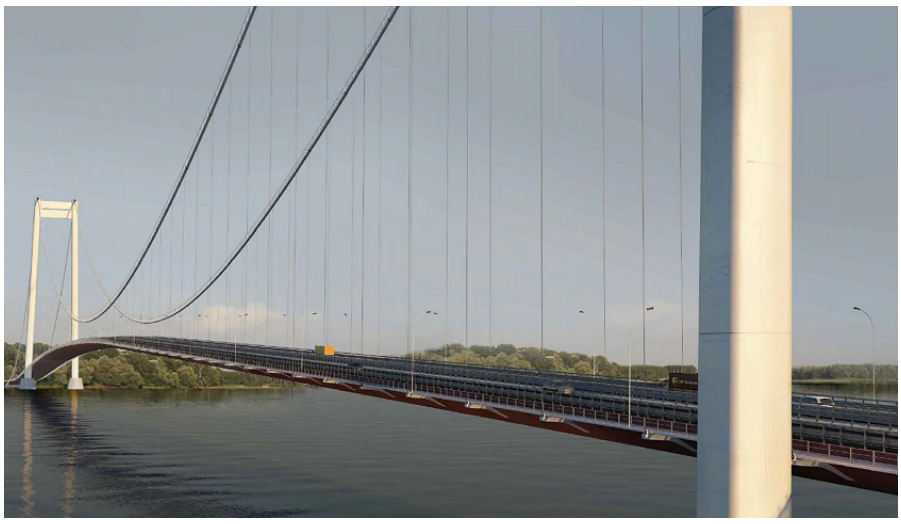

Figure I: Rendering of the Braila Bridge

A.2 Fluid-structure interaction

The wind can be schematized mainly by three components, namely the mean speed velocity and two turbulence components. Depending on the component considered, static or dynamic loads can occur.
The action of the wind takes place through aerodynamic forces, specifically the lift, the drag and the aerodynamic moment.

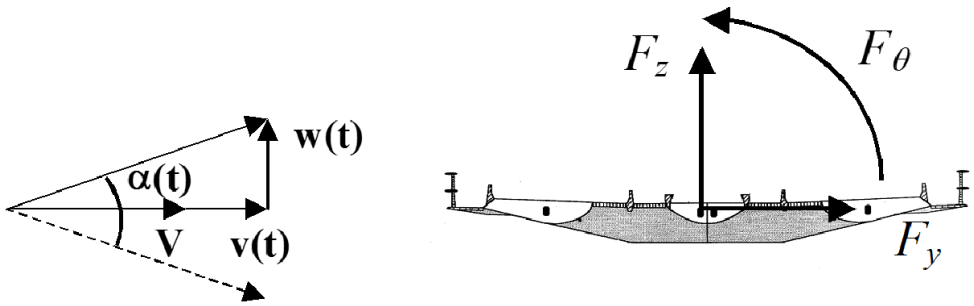

Figure II: Components of the wind action and aerodynamic forces

The most sensitive part of a bridge to the wind is the deck. These aerodynamic forces can be defined on a generic deck section as follows:

$$F_L = \frac{1}{2}\rho S V^2 C_L(\alpha) \tag{A.1}$$

$$F_D = \frac{1}{2}\rho S V^2 C_D(\alpha) \tag{A.2}$$

$$M = \frac{1}{2}\rho S V^2 C_M(\alpha) \tag{A.3}$$

Where ρ is the density of the air, V is the wind velocity, S is the deck upper surface and B is a reference body dimension usually the deck chord. The aerodynamics coefficient are $C_L(\alpha)$, $C_D(\alpha)$, $C_M(\alpha)$, and are a function of the angle of attack of the wind, which under the hypothesis of small displacements and speeds can be defined as:

$$\alpha = \vartheta + \psi = \vartheta + \frac{\omega - B_1\dot{\vartheta} - \dot{z}}{V + u - \dot{y}} \tag{A.4}$$

These coefficients are a function of the type of the deck that we are considering.
The problems that the wind generates on bridges can be divided into two macro categories:

- Static Problems due to average wind speed velocity,that are function of the angle attack

- Dynamic Problems due to turbulence components u, v, w and of the motion of bridge itself under aerodynamic forces.

A.2.1 Static Problem

Static loads are due only to the effect of the average wind speed and not to turbulence. They are a function of the aerodynamic coefficients C_L, C_D, C_M and the angle of attack α. An example of a very important static load for bridges is that to which the towers are subjected, or more specifically the tower foundations.

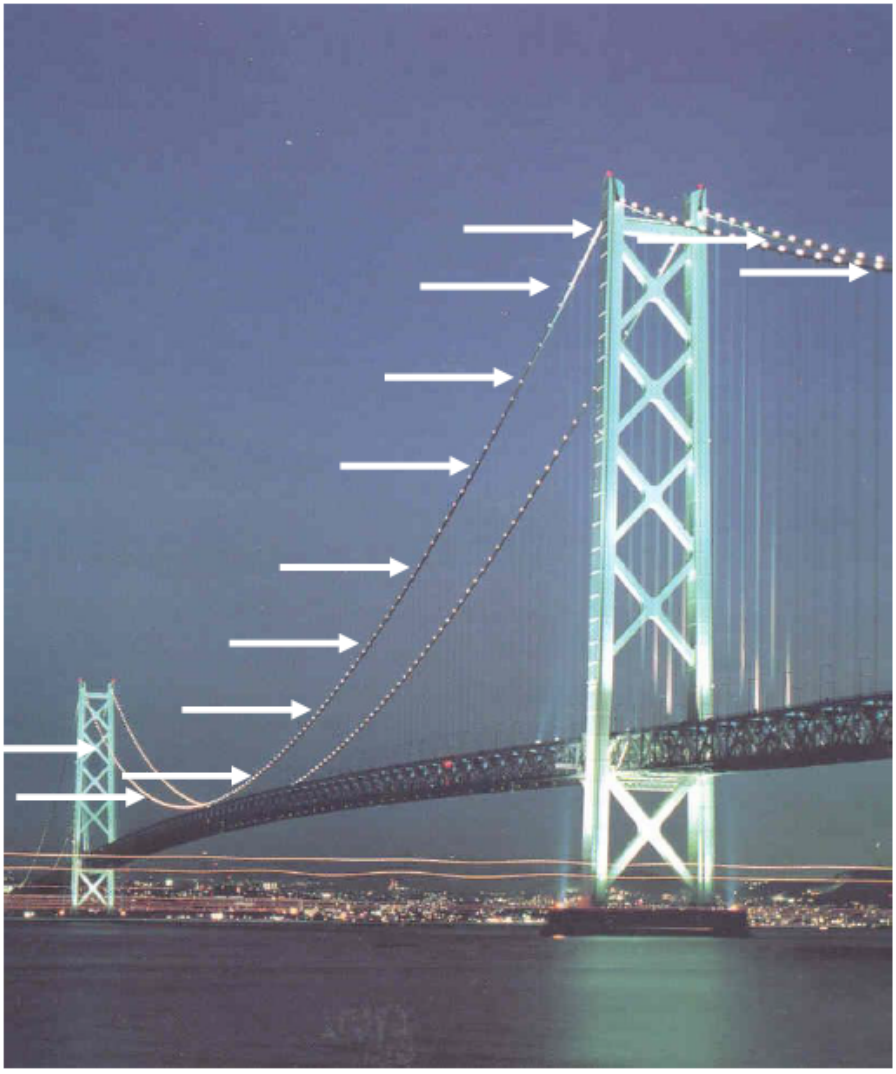

Figure III: Load transfer on Akashi Bridge

The load from the deck is transferred, through the hangers, to the main cables and finally to the top of the towers producing a huge overturning moment on the tower foundations. In order to reduce this effect, it is important to minimize the deck drag. One of the aims of the static analysis is find the equilibrium position around which is possible to linearize the aerodynamic forces.

To summarize, in order to take the static problem under control, during the design of a long span bridge, it is important to keep the drag coefficient as low as possible.

A.2.2 Dynamic Problem

They are due to the turbulent nature of the wind and to the motion of the bridge induced by the aerodynamic forces (aeroelastic problem). The main dynamic issues that we can have are :

- One d.o.f instability : we can experience this kind of issue, for example, when the derivative of the $C_M(\alpha)$ with respect to the incident angle α is lower than zero [14] (Takoma bridge).

- Flutter instability : It happens in the bridges of nowadays because they have a deck section that is of airfoil type [15], it can be single box or multi-box. With multi-box, like in Messina [16] Bridge we are able to have an higher flutter critical speed. It happens when we have the coupling of the first vertical mode and the first torsional mode, and the the resulting motion is a combination of the two.

- Buffeting : it is the result of the motion of the bridge due to the incoming turbulence. It is always present, not only in bridges, and there is not a way in order to avoid that.

- Vortex Shadding : The main problems for this type of instability are related to the towers and the deck. All decks are affected by vortex shadding. This problem is linked with the separation of flow from upstream edge of the deck to produce a vortex that moves downstream.

Figure IV: Takoma bridge collapse due to one d.o.f. instability

The wind forces can be expressed in terms of equivalent damping and stiffness matrices that can lead to the types of instability mentioned above. Usually the behaviour of long span bridges is linked to the wind velocity:

- When we are at null wind speed the damping contribution is only due to the structural part
- Increasing the speed, we have the contribution of the aerodynamic damping and for this reason it becomes larger
- A further increase of the velocity will cause a reduction in the overall damping. The velocity at which we have negative damping is called flutter velocity.

The solution, when we design a bridge, is to put the wind in favour of the bridge, in order to insert into the system a positive equivalent damping contribution and to design the bridge in order to have an high critical flutter velocity. Large vibrations can lead to fatigue problems and decrease of comfort when we are crossing the structure.

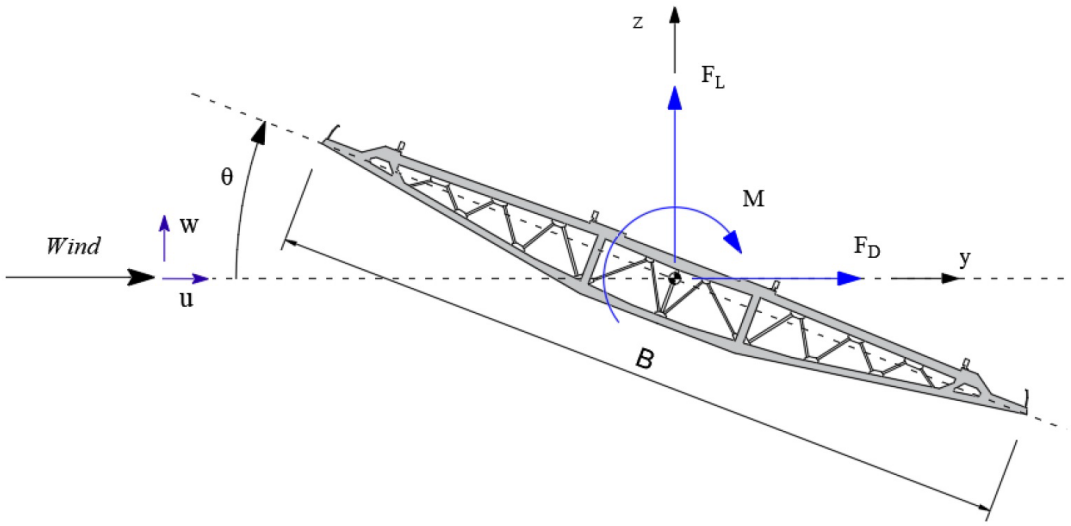

Figure V: Aerodynamic forces acting on a deck section

A.3 Wind description

Before going into the specifics of the various approaches to study the response of the structures under the action of the wind, it is important to know how the wind itself is described.

When the wind approaches the earth's surface, the frictional forces caused by the wind-earth interaction are growing more and more. Because of this, the wind becomes turbulent and changes according to space and time.

It is possible to define as "gradient height", the height z_g where the effects of frictional forces are negligible.

In wind engineering, the part of the atmosphere of our interest, where the structures subject to the action of the wind are immersed, is located below the z_g and is called the Atmospheric Boundary Layer (ABL). The ABL extends typically to 500-1000 m above the ground [17] [18].

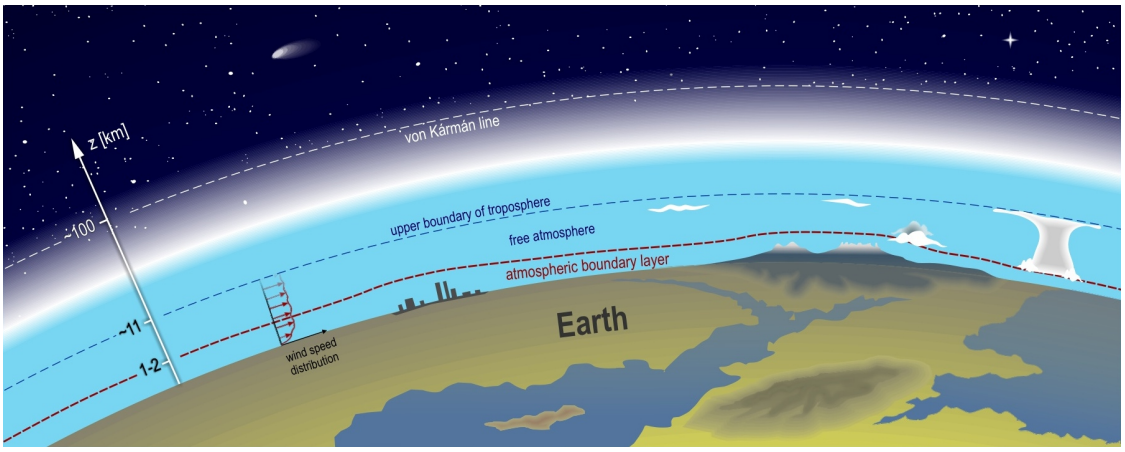

Figure VI: Atmospheric Boundary layer on surface Earth

The wind in this zone behaves randomly both in space and in time, therefore in order to know its characteristics it is necessary to refer to the analysis of large databases of anemometric records, that are taken in different places of the world for many years. Another facility in order to record useful datas is the weather station. The weather station is equipped in order to measure temperature, barometric pressure, humidity, wind speed and direction and amount of precipitations.
Its main aim is to provide weather forecast, while anemometers (Figure VII) are able mainly to measure the wind speed.

Wind measurements are commonly taken at a standard height of 10 m, in locations far from obstacles that could affect the measurement.

Due to the random nature of the wind, the repetition of measurements in the same areas leads to different results, however there are common characteristics that can be highlighted in long term measurements in the boundary layer. This suggests that an empirical model could be developed.

In Figure VIII it is possible to have a look to a six hour time history taken at 128 m from the ground on the Messina strait.

Figure VII: Rotating cup anemometer

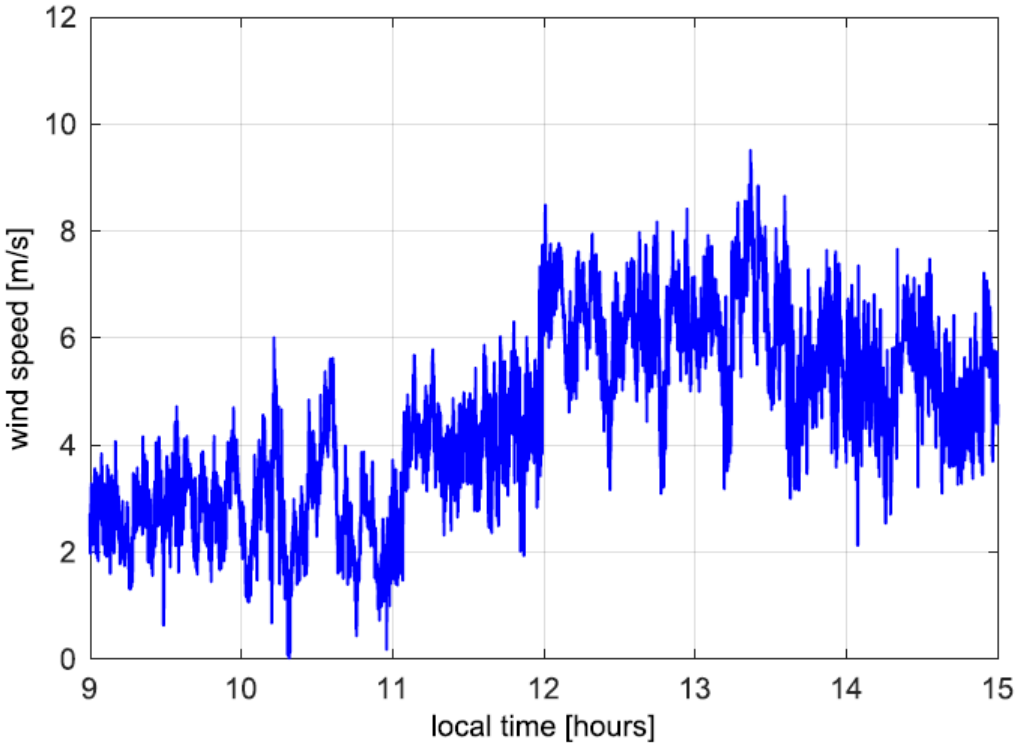

Figure VIII: Wind speed measures taken at Messina strait

The following characteristics can be highlighted [18]:

- The wind speed varies irregularly due to its turbulent nature.
- There is a change in the average speed over the course of a day.
- There are limited oscillations around the average speed and this is a characteristic of turbulence.
- The oscillations cover a very wide frequency range.

As is known, turbulence is a random signal therefore it requires an appropriate set of statistical parameters in order to describe it, statistical methods must be used.

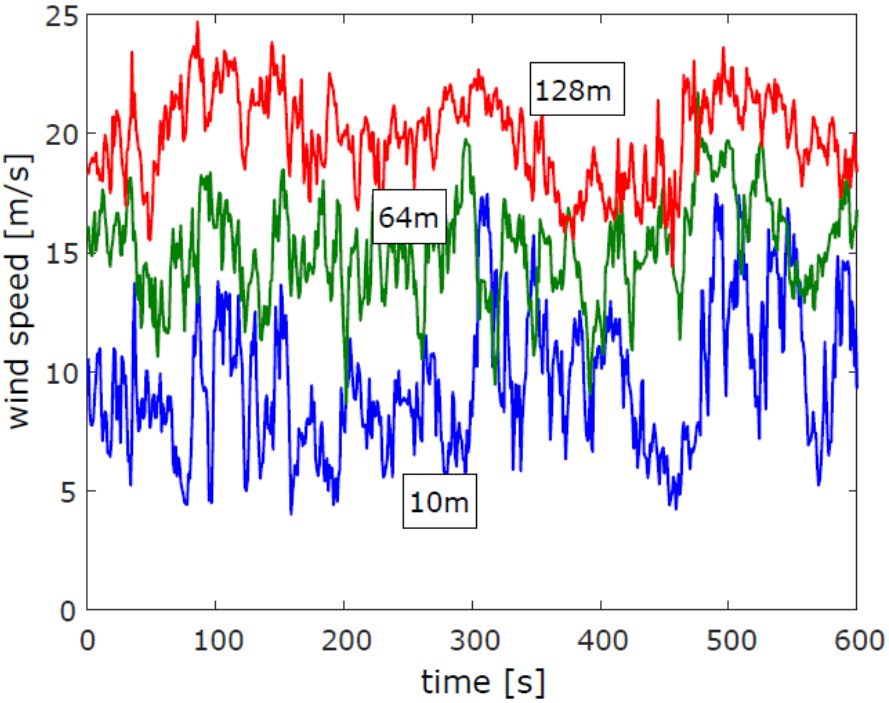

Figure IX: Wind speed measures taken at different heigths at Messina strait

Consequently, from the analysis of multiple time history taken at different height in the same place (Figure IX), the following characteristics can be highlighted:

- The average wind speed rise, increasing the height from ground
- There is some similitude between the pattern of the gusts at all height. It is because of the spatial correlation of the wind turbulence.

The data recorded by the anemometers contain both "global" informations related to the wind climate, and "local" informations related to the Atmospheric Boundary Layer. This is due to the fact that the wind contains contributions related to various characteristic scales of the phenomena.

The first to notice this was Van Der Hoven, who in 1957 developed the first wind spectrtum that was based on the data recorded at Brookhaven, NY [19].

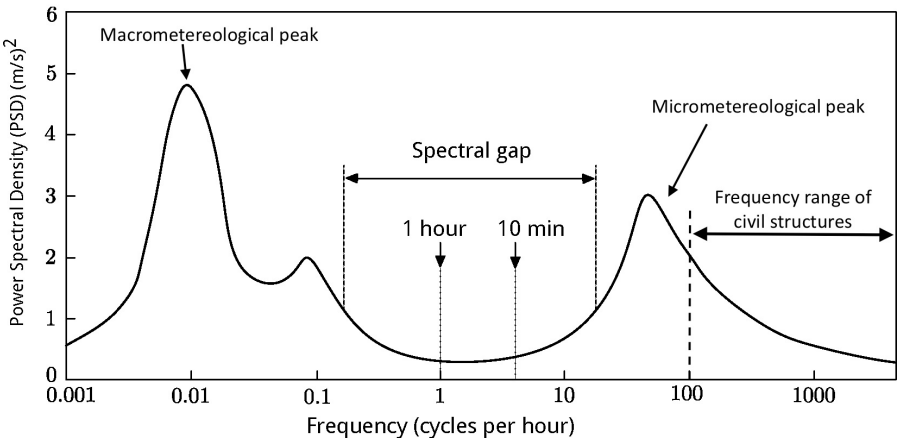

Figure X: Van der Hoven wind spectrum

Van der Hoven spectrum is represented in Figure X and it features three main energy peaks. The explanation of these peaks is the following:

1. The leftmost peak is at 0.01 Hz and It is because of the movement of fully developed weather systems. It is named macrometereological peak.

2. The second peak is in correspondence of 0.1 Hz (24 Hours period). It shows how wind speed increases during the day, and decreases during the night.

3. The rightmost peak is called micro-metereological peak (close to 100 Hz) and it contains a set of higher frequencies related to the turbulence in the ABL that are in the interval 10 minutes to less than 3 seconds.

4. The absence of wind speed variation is the central zone of Van Der Hoven's spectrum is called spectral gap. It separates the fluctuations associated with wind climate and the ones associated with wind turbulence

To summarize the macro-meteorological peak is caused by the movement of large pressure systems and it is related to the variations of the mean wind speed. These variations have a low frequency and correspond only to static effects of buildings. High frequency fluctuations, or the ones associated to the micro-meteorological peak, are associated to the Atmospheric Boundary Layer fluctuations. They are caused by the wind turbulence. These fluctuations are in the frequency range of civil structures and for this reason they are very important for wind engineering. When we make the design of a structure, in the site, it is important to define the average wind speed, the turbulence and its correlation.

A.3.1 Mean wind speed profile

The spectral gap represents the boundary between the frequencies associated with the average flow (at the left of the gap) and those associated with the turbulent flow (at the right of the gap).

Usually the wind speed is calculated over a period of 10 minutes (EUROCODE) or 1 hour.

The average wind speed and its slow speed fluctuations produces only static effect on structures. The Atmospheric Boundary Layer is heavily influenced by frictional forces caused by interaction with the ground. Therefore we expect the surface roughness of the soil to be an important parameter. The average wind speed is affected by the surface roughness that can be defined by the parameter z_0, called aerodynamic roughness parameter. It is related to the dimension and spacing of roughness elements. There are various formulations of the average wind profile.

Logarithmic profile

The first model of the average wind is represented by the Logarimic profile:

$$U(z) = \frac{u^*}{\kappa} \ln \frac{z}{z_0} \tag{A.5}$$

- u^* is the *friction velocity*. It is not a physical velocity but an abstraction introduced for introducing the shear stress in the dimension of a velocity.
- $\frac{1}{\kappa}$ is a constant of proportionality that is named *Von Karman constant*, its value is around 0.4.

The logarithmic profile represents the physical formulation of average wind speed in ABL . If we compare it with the real profile of the wind it is a good approximation up to 200m.

Power Law profile

An emprirical formulation that is used in North America is represented by the *Power Law* profile :

$$U(z) = U_{ref} \left(\frac{z}{z_{ref}} \right)^{\alpha} \tag{A.6}$$

- U_{ref} is the wind velocity at the reference height z_{ref}
- α is the power law exponent that changes, varying the terrain type. It usually ranges from 0.12 – 0.30.

It and can be linked to the aerodynamic length parameter z_0 by this formulation :

$$\alpha \cong \left(\frac{1}{\ln \frac{z}{z_{ref}}} \right) \tag{A.7}$$

Eurocode

Eurocode proposes a formulation of the mean wind that is based on the *Logarithmic profile* described before:

$$\begin{cases} U(z) = V_b k_r \ln\left(\frac{z}{z_0}\right) & z_{min} \leq z \leq 200\text{m} \\ U(z) = U(z_{min}) & z \leq z_{min} \end{cases} \tag{A.8}$$

Where :

- V_b is the basic wind velocity that depends on the wind climate and it is evaluated a 10 m above the ground, considering a terrain category .
- k_r is the terrain factor that that takes into account the aerodynamic roughness parameter z_0.

The aerodynamic roughness length parameter is reduced to consider only five different terrain categories that are highlighted in Figure XI and Figure XII:

Terrain category		z_0 m	z_{min} m
0	Sea or coastal area exposed to the open sea	0,003	1
I	Lakes or flat and horizontal area with negligible vegetation and without obstacles	0,01	1
II	Area with low vegetation such as grass and isolated obstacles (trees, buildings) with separations of at least 20 obstacle heights	0,05	2
III	Area with regular cover of vegetation or buildings or with isolated obstacles with separations of maximum 20 obstacle heights (such as villages, suburban terrain, permanent forest)	0,3	5
IV	Area in which at least 15 % of the surface is covered with buildings and their average height exceeds 15 m	1,0	10

Figure XI: Terrain categories and parameters according to Eurocode

The difference with the physical formulation is that we removed the friction velocity u^* and we introduced basic wind speed V_b and terrain factor k_r. The friction velocity u^* has the dimension of a velocity strictly speaking but it's more related to surface stresses. On the contrary the basic wind velocity V_b is a speed that has a physical meaning and can be measured. Every code has additional formulation in order to take into account of additional parameters such as :

1. Obstacles are very close each other ($zero - plane\ displacement\ d$)
2. Changes in surface roughness
3. Directionality effects
4. Topography effects.

Additional effects can be taken into account depending on the specific location.

Terrain category 0

Sea, coastal area exposed to the open sea

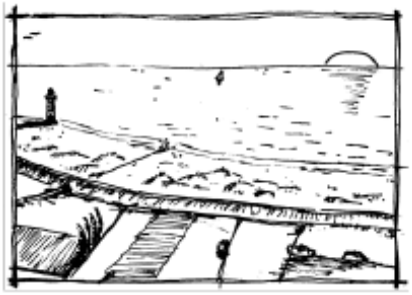

Terrain category I

Lakes or area with negligible vegetation and without obstacles

Terrain category II

Area with low vegetation such as grass and isolated obstacles (trees, buildings) with separations of at least 20 obstacle heights

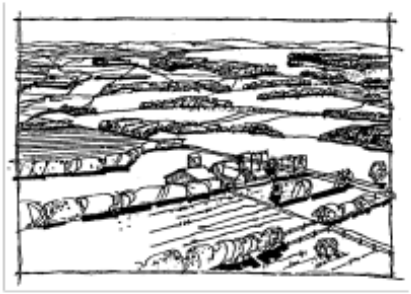

Terrain category III

Area with regular cover of vegetation or buildings or with isolated obstacles with separations of maximum 20 obstacle heights (such as villages, suburban terrain, permanent forest)

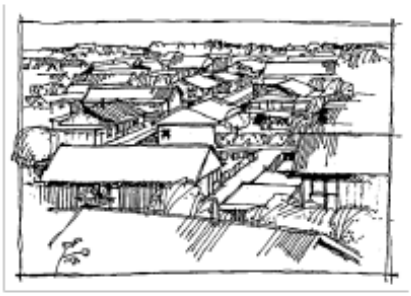

Terrain category IV

Area in which at least 15 % of the surface is covered with buildings and their average height exceeds 15 m

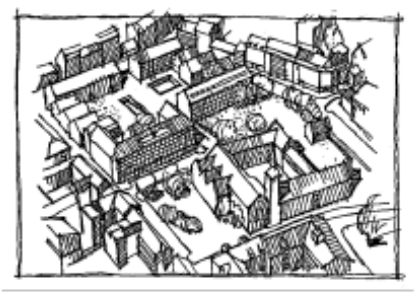

Figure XII: Terrain categories description according to Eurocode

A.3.2 Wind Turbulence

Turbulence is associated with high frequency phenomena, located at the right of the *spectral gap*. It is composed of three components u, v and w respectively, longitudinal, lateral and vertical components.

Turbulence is associated with high frequency oscillations (micrometeorological) and these fluctuations are in the frequency range of civil structures. Therefore they can be easily excited by this phenomenon. How we can measure the fluctuations associated to the turbulence? The oscillations due to turbulence represents a random phenomena and for this reason we have to use a statistical approach.

Turbulence intensity

In the *Atmospheric Boundary Layer* the standard deviation σ of wind speed decreases with the height and it is near to zero in correspondence of the height where the friction effects are zero z_g (gradient height). Despite this, up to 200 meters, it is possible to consider that σ remains more or less constant. Therefore it is possible to define a dimensionless parameter called *turbulence intensity* which can be defined for each turbulence component as the ratio of the standard deviation of the turbulence component considered divided by the average speed, both calculated at the same height :

$$I_u(z) = \frac{\sigma_u(z)}{U(z)} \tag{A.9}$$

$$I_v(z) = \frac{\sigma_v(z)}{U(z)} \tag{A.10}$$

$$I_w(z) = \frac{\sigma_w(z)}{U(z)} \tag{A.11}$$

- $\sigma_u(z)$, $\sigma_v(z)$, $\sigma_w(z)$ are the standard deviation of the turbulence components u, v, w
- $U(z)$ is the average wind speed

It is possible to consider a link to the turbulence intensity along the longitudinal direction and the roughness parameter z_0:

$$I_u(z) = \frac{1}{\ln\left(\frac{z}{z_0}\right)} \tag{A.12}$$

It can be clearly seen that the turbulence rises as the roughness increases and decrease with the height above the ground [20].

In addition is possible to link the different components of the turbulence intensity in this way :

$$I_v(z) = 0.75 I_u \tag{A.13}$$

$$I_w(z) = 0.5 I_u \tag{A.14}$$

Eurocode proposes the same forumulation for the along wind turbulence intensity

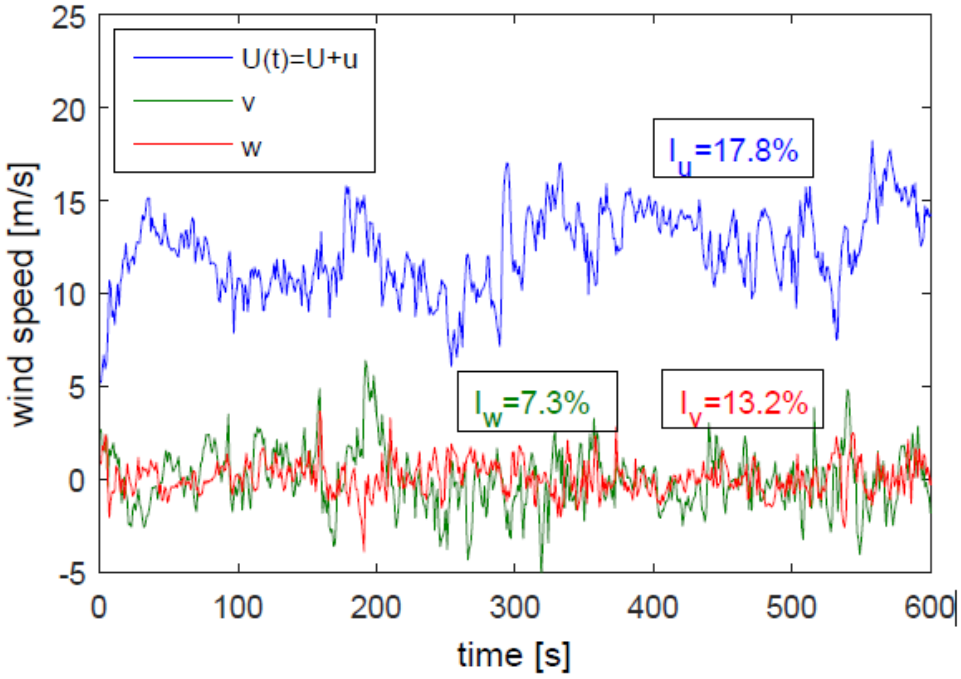

Figure XIII: Turbulence intensity components measured at the Messina strait over a period of 10 minutes, measured at 64 m height

Integral length scales

An indicator used to describe the spatial coherence of the turbulence is given by the *Integral length scales* [20]. They represent the mean dimension of a gust in a given direction. The integral length scale along the longitudinal direction x for the turbulence component u can be defined as:

$$L_u(x) = \int_0^\infty R_u(r_x) dr_x \tag{A.15}$$

- $R_u(r_x)$: is the cross correlation of two different points separated along x (means wind speed direction) of a distance r_x and measured simultaneously.

In a similar way we can define the matrix of the *Integral length scales* for turbulence components u, v, w along x, y, z directions:

$$\text{for longitudinal turbulence component } u \qquad L_u^x \; L_u^y \; L_u^z \tag{A.16}$$

$$\text{for lateral turbulence component } v \qquad L_v^x \; L_v^y \; L_v^z \tag{A.17}$$

$$\text{for vertical turbulence component } w \qquad L_w^x \; L_w^y \; L_w^z \tag{A.18}$$

Usually we have measures taken in a point for a long time. Considering the *Taylor* hypothesis (1938) of frozen turbulence we can calculate the longitudinal scale of turbulence taking into account the measures recorded in one point. By means of the auto-correlation $R_u(\tau)$ is possible to compute the time scale T:

$$T_u(z) = \int_0^\infty R_u(z, \tau) d\tau \tag{A.19}$$

According to the Taylor's hypothesis the frozen turbulence is carried by the mean with speed and then:

$$L_u^z = T_u(z)U(z) \tag{A.20}$$

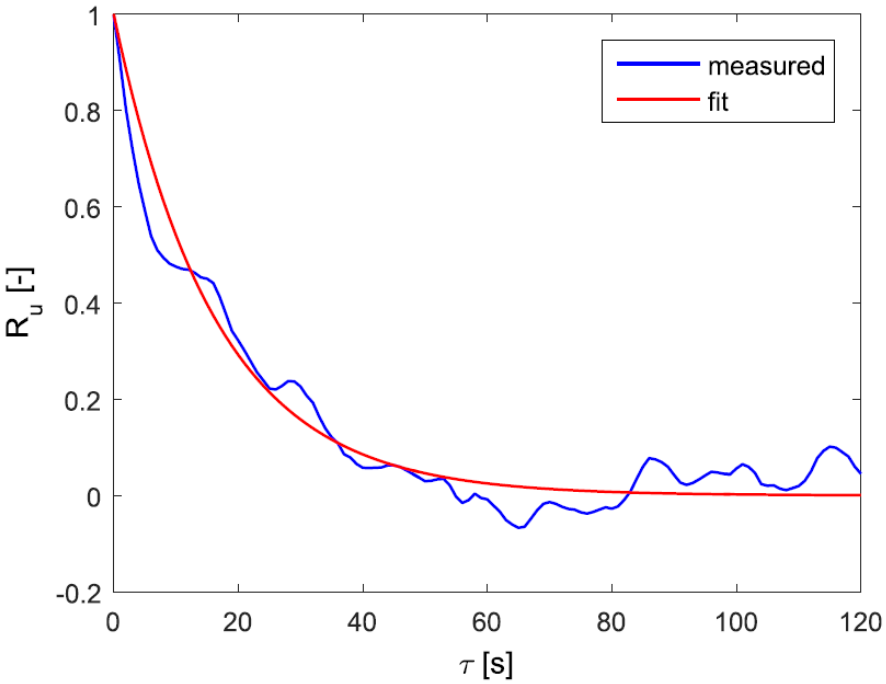

Figure XIV: Autocorrelation function of the u turbulence component

In *Eurocode*, as we expected , there is a dependence of the integral length scale on the height and terrain roughness :

$$L_u^x(z) = 300\left(\frac{z}{200}\right)^{\alpha} \tag{A.21}$$

where α is :

$$\alpha = 0.67 + 0.05\ln(z_0) \tag{A.22}$$

The other length scale components could expressed as a function of the longitudinal one :

$$L_v^x \approx 0.25L_u^x \qquad L_w^x \approx 0.1L_u^x \tag{A.23}$$

$$L_u^y \approx 0.3L_u^x \qquad L_u^z \approx 0.2L_u^x \tag{A.24}$$

Commonly we are interested in the components along the x axis, because it is the direction of the mean wind and for this reason they are generally bigger and the most important ones.

Power spectral density

The power spectral density explains how the wind energy is distributed along different frequencies, normalized by the frequency resolution. It represents a one-point analysis. Why is important to give a description of the energy introduced at different frequencies? Because if we are dealing with dynamics of the structures, if the wind energy is placed in correspondence of one the natural frequencies of the construction, this is responsible of dynamic effects.

Many formulations have been introduced in literature. *Von Karman* proposed the equation for u component [21]:

$$\frac{f \cdot S_u(f)}{\sigma_u^2} = \frac{4\left(\frac{fL_u^x}{U}\right)}{\left[1 + 70.8\left(\frac{fL_u^x}{U}\right)^2\right]^{\frac{5}{6}}} \tag{A.25}$$

and for i $= v, w$

$$\frac{f \cdot S_i(f)}{\sigma_i^2} = \frac{4\left(\frac{fL_I^x}{U}\right)\left(1 + 755.2\left(\frac{fL_i^x}{U}\right)^2\right)}{\left[1 + 283.2\left(\frac{fL_i^x}{U}\right)^2\right]^{\frac{11}{6}}} \tag{A.26}$$

Where :

- $S_u(f)$ $S_v(f)$ $S_w(f)$ are respectively the power spectal density of the turbulence components u, v, w.

In order to normalize the frequency It is possible to define the $non-dimensional\ frequency$ as :

$$f^* = \frac{fL_u^x}{U} \tag{A.27}$$

Another PSD formulation is the one given by EUROCODE :

$$\frac{f \cdot S_u(f)}{\sigma_u^2} = \frac{6.8\left(\frac{fL_u^x}{U}\right)}{\left[1 + 10\frac{fL_u^x}{U}\right]^{\frac{5}{3}}} \tag{A.28}$$

We can observe in Figure XV that this formulation is very similar to the one given by *Von Karman*. From the plot it is clear that most of the energy of the wind is introduced at low frequencies. If the natural frequencies of our structures are in this range, as it commonly happens we could have dynamic amplification in the wind induced response.

Cross spectral density and coherence

We are interested in defining the cross spectral density and the coherence if we want to make a multiple point analysis, or in other words if we want to evaluate the statistical dependence between two points P and Q spaced in y direction at a frequency f.

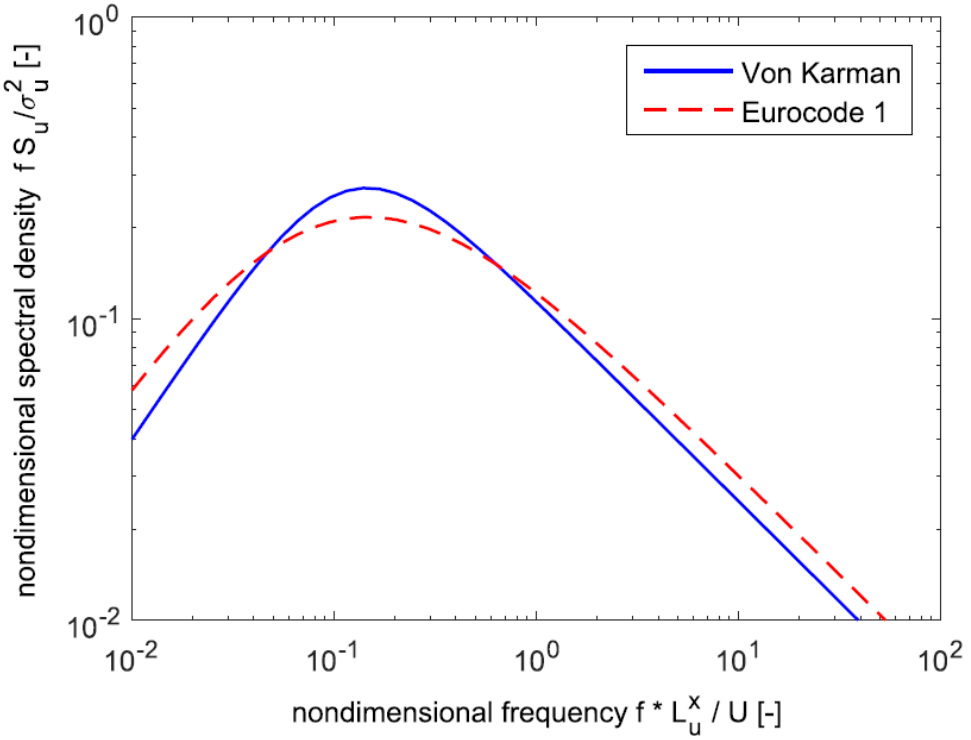

Figure XV: Wind speed measures taken at different heigths at Messina strait

The *coherence* is defined as :

$$\gamma_{uu}^2 = \frac{|S_{uu}(P,Q,f)|^2}{S_{uu}(P,f) \cdot S_{uu}(Q,f)} \tag{A.29}$$

- $S_{uu}(P,f)$ and $S_{uu}(Q,f)$ are the power spectral density evaluated in points P and Q.
- $S_{uu}(P,Q,f)$ is the cross spectral density functions between points P and Q.

Coherence is a real quantity that is in between zero and one, while *Cross spectral density* is in general a complex quantity described by modulus and phase. The formulation of *root coherence* by *Davenport* [20] is given by:

$$\gamma_{uu}(\Delta y, f) = \exp\left[-\left(-C_y \frac{\Delta y f}{U}\right)\right] \tag{A.30}$$

Where:

- C_y is a non dimensional decay constant ($C_y = 10$).

In a similar way it is possible to define the other coherence components, considering different coherence decay parameters. The major limitation of *Davenport* formulation is given by the fact that this considers value close to the unit for small frequencies but this is not exact if we consider large separations (Δy).

A.4 Deck aerodynamics

After describing with which statistical methodologies it is possible to describe the wind, it is necessary to introduce how we can evaluate the dynamic effects that the wind causes on a structure under consideration. To do this, a section of deck subjected to the action of a turbulent wind will be considered below.

There are multiple approaches, with a different level of detail, in order to evaluate the dynamic response of the deck, among all that capable of fully explaining the physics of the problem is represented by the *Quasi Steady Theory* (*QST*) [22] [23]. The *QST* theory is able to reproduce in a complete way the aerodynamic forces acting on a deck section function of its motion and the wind turbulence, if the reduced velocity :

$$V^* = \frac{V}{fB} \qquad \text{is higher than} > \text{10-15} \tag{A.31}$$

- V is the average wind speed
- B is the reference dimension of the body
- f is the frequency of the motion

The reduced velocity could be seen as the ratio between f_p and f_m where f_m is the vibration frequency of the motion, and f_p is $\frac{1}{T_p}$ and T_p $\frac{B}{V}$, the time needed by the fluid particle to move through the deck width B.

If the condition on V^* is satisfied then you can use as aerodynamic forces the ones that you really measure statically, because statically the frequency of motion is going to zero, or, in another way the aerodynamic forces are not influenced by the frequency of the motion.

With these premises it is possible to write the motion equation as:

$$[M_s]\ddot{x} + [R_s]\dot{x} + [K_s]x = F_a(\dot{x}, x, t) \tag{A.32}$$

- $F_a(\dot{x}, x, t)$ are the aerodynamic forces which are a function of the motion of the bridge in terms of displacements, speed and time

Several approaches can be considered in order to define the $F_a(\dot{x}, x, t)$ and the QST is one of them.

In the following we will consider a deck section under the wind action taking into account only u and w turbulence components and the first three modes of the deck, respectively the vertical (z), horizontal (y) and torsional (ϑ), A modal approach will be considered. The *QST* considers the same aerodynamic coefficients that are measured on static models in wind tunnels, considering the motion in terms of V_{rel} that is the relative velocity of the fluid with respect to the body.

The aerodynamic forces in Figure XVI can be described as:

$$F_L = \frac{1}{2}\rho S V_{rel}^2 C_L(\alpha) \tag{A.33}$$

$$F_D = \frac{1}{2}\rho S V_{rel}^2 C_D(\alpha) \tag{A.34}$$

$$M = \frac{1}{2}\rho S V_{rel}^2 C_M(\alpha) \tag{A.35}$$

Where :

- $C_L(\alpha)$, $C_D(\alpha)$, $C_M(\alpha)$ are the static aerodynamic coefficients.
- α is the angle between the relative wind velocity and the deck during its movement.

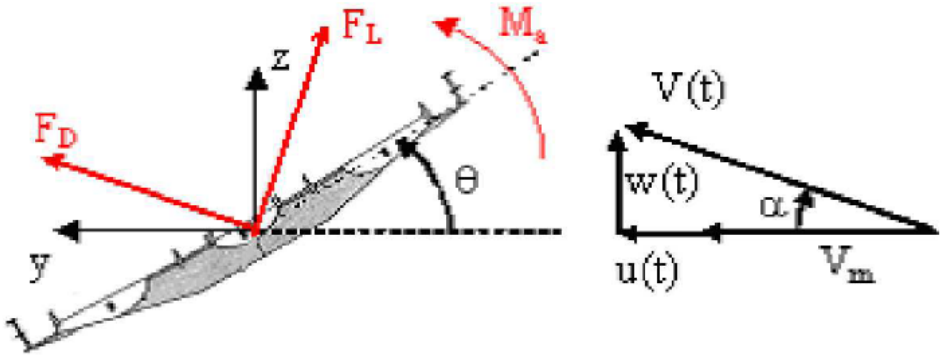

Figure XVI: Aerodynamic forces acting on a deck section

Knowing this it is possible to define the horizontal component of the speed of point P belonging to the deck as:

$$V_{P,y} = \dot{y} \tag{A.36}$$

And the vertical as :

$$V_{P,z} = \dot{z} + \overline{PG}\dot{\vartheta} \tag{A.37}$$

As a result considering different points P we will experience different relative velocities. Our choice of the reference point is the one at a distance B, upwind the deck centre G. This distance will be defined experimentally in the *corrected quasi steady theory* ($QSTC$).

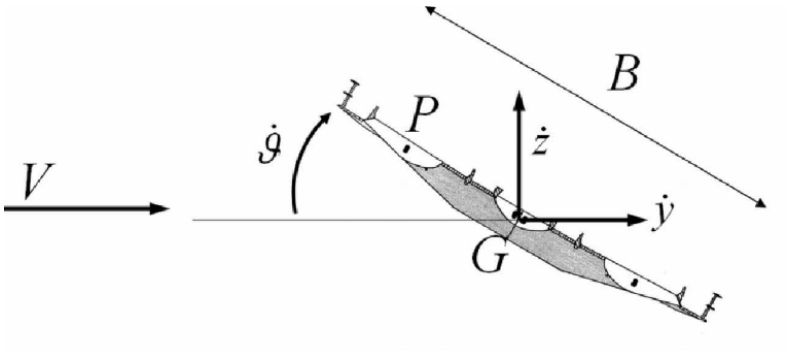

Figure XVII: Deck velocity components

Then we can define the relative velocity components along y and z direction in this way for the reference point we have chosen :

$$V_{Rel,y} = V_y - \dot{y} \tag{A.38}$$

$$V_{Rel,z} = V_z - \dot{z} - B_1\vartheta \tag{A.39}$$

- V_y and V_z are the horizontal and vertical components of the incoming relative wind

Considering that the wind is characterized by:

1. V_m average wind speed
2. u, v turbulence components

We can define V_{rel}^2 as :

$$V_{Rel}^2 = (V_m + v - \dot{y})^2 + (w - \dot{z} - B_1\dot{\vartheta})^2 \tag{A.40}$$

Where ψ is the angle of attack of the relative wind speed :

$$\psi = \arctan \frac{w - \dot{z} - B_1\dot{y}}{V_m - v - \dot{\vartheta}} \tag{A.41}$$

ψ is changing in time for two reasons:

1. Turbulence is changing in time
2. Motion of the body is changing in time

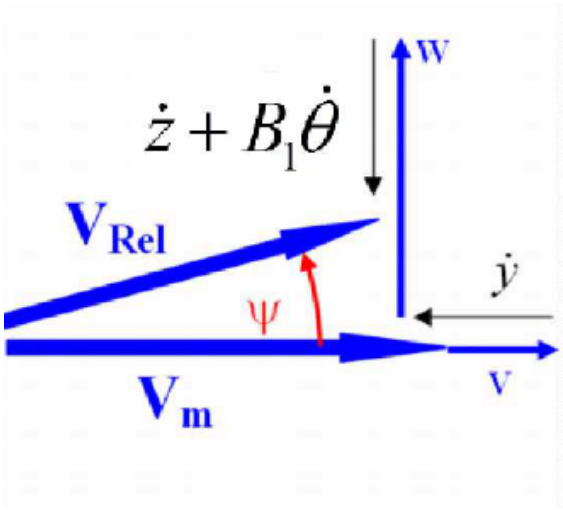

Figure XVIII: Definition of relative wind speed V_{rel}

The aerodynamic forces acting on the Deck section can be defined according to the QST theory as:

$$F_L = \frac{1}{2}\rho S V_{rel}^2 C_L(\alpha) \tag{A.42}$$

$$F_D = \frac{1}{2}\rho S V_{rel}^2 C_D(\alpha) \tag{A.43}$$

$$M = \frac{1}{2}\rho S V_{rel}^2 C_M(\alpha) \tag{A.44}$$

and α is defined as:

$$\alpha = \psi + \vartheta \tag{A.45}$$

The angle α represents the angle of attack between the relative velocity and the deck.

The problem can be modelled as in Figure XIX where the elastic links have the same stiffness and damping of the first vibration modes.

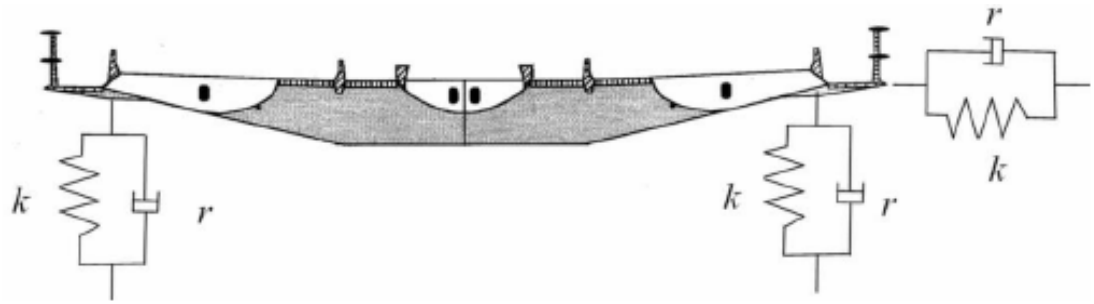

Figure XIX: Deck model with concentrated damping and stiffness elements

The equations of motion of the system are :

$$m_y\ddot{y} + r_y\dot{y} + k_y y = F_D\cos\psi - F_L\sin\psi = F_Y \tag{A.46}$$

$$m_z\ddot{z} + r_z\dot{z} + k_z z = F_D\sin\psi + F_L\cos\psi = F_z \tag{A.47}$$

$$J_G\ddot{\vartheta} + r_\vartheta\dot{\vartheta} + k_\vartheta\vartheta = F_M = F_\vartheta \tag{A.48}$$

Where:

- m_y, m_z and J_z are the modal masses and the modal moment of inertia.
- r_y, r_z e r_ϑ and k_y, k_z and k_ϑ are the respective damping e stiffness of the first three modes of vibration.

The equation is fully non linear and this approach is in condition to give the aerodynamic forces function of the incoming turbulence and the motion.

If we replace the expression of the aerodynamic forces found previously we obtain the equations:

$$m_y\ddot{y}+r_y\dot{y}+k_y y=\frac{1}{2}\rho S\big((V_m+v-\dot{y})^2+(w-\dot{z}-B_1\dot{\vartheta})^2\big)(C_D(\alpha)\cos\psi-C_L(\alpha)\sin\psi) \tag{A.49}$$

$$m_z\ddot{z}+r_z\dot{z}+k_z z=\frac{1}{2}\rho S\big((V_m+v-\dot{y})^2+(w-\dot{z}-B_1\dot{\vartheta})^2\big)(C_D(\alpha)\sin\psi+C_L(\alpha)\cos\psi) \tag{A.50}$$

$$J_G\ddot{\vartheta}+r_\vartheta\dot{\vartheta}+k_\vartheta\vartheta=\frac{1}{2}\rho S\big((V_m+v-\dot{y})^2+(w-\dot{z}-B_1\dot{\vartheta})^2\big)C_M(\alpha) \tag{A.51}$$

This formulation is called *Corrected Quasi steady theory* (*QSTC*) and the term that takes in consideration a specific characteristic length of body B_1 changes for each component of the aerodynamic forces (B_{1y}, B_{1z}, $B_{1\vartheta}$). Taking into account the $\underline{X}$ vector that contains the physical displacements,

$$\underline{X}=\begin{pmatrix}x\\y\\z\\\vartheta\end{pmatrix}$$

We can rewrite the equations (A.49) (A.50) (A.51) in matrix formulation:

$$[M_s]\underline{\ddot{X}}+[R_s]\underline{\dot{X}}+[K_s]\underline{X}=\underline{F}_A\big(\underline{X},\underline{\dot{X}},V_m,v(t),w(t)\big) \tag{A.52}$$

This approach is able to reproduce in a non linear way the response of the bridge, under the assumption of high reduced velocity (V^*>15).

Linearized Quasi Steady Corrected theory (QSTC)

The main aim of this analysis is to linearize the equation of the *QSTC* in order to obtain the equivalent stiffness matrix K_{AERO} and damping matrix R_{AERO} due to the aerodynamic forces.

There are more sophisticated models based on nonlinear equations or numerical integration with explicit or implicit methods. With these complex models, you can grasp every detail, but you don't understand the physics of the problem. On the contrary with the linear theory is sufficient to look if some conditions on the matrices R_{AERO} and K_{AERO} is verified in order to have a stable system, but the results are valid only for small displacements. In other words with the linearised equation of motion we are able to deeply understand the physics of the problem. The vector containing the aerodynamic forces F_A is in general function of the bridge motion ($\underline{X}$, $\underline{\dot{X}}$), the wind speed (V) and turbulence components $\underline{b}$:

$$\underline{F}_A=\begin{pmatrix}F_y\\F_z\\F_\vartheta\end{pmatrix}\qquad\underline{X}=\begin{pmatrix}y\\z\\\vartheta\end{pmatrix}\qquad\underline{\dot{X}}=\begin{pmatrix}\dot{x}\\\dot{x}\\\dot{\vartheta}\end{pmatrix}\qquad\underline{b}=\begin{pmatrix}u\\w\end{pmatrix}$$

Starting from the static deformation reached under mean wind speed as equilibrium position :

$$\underline{X}_0=\begin{pmatrix}y_0\\z_0\\\vartheta_0\end{pmatrix}\qquad\underline{\dot{X}}=\begin{pmatrix}0\\0\\0\end{pmatrix}\qquad\underline{b}=\begin{pmatrix}0\\0\end{pmatrix}$$

Under the iphotesys of small obscillations of the deck and turbulent fluctations close to the equilibrium values, it is possible to lineayze the aerodynamic forces in this way:

$$\underline{F}_A(\underline{X},\dot{\underline{X}},\underline{b}) = \underline{F}_A(\underline{X}_0,\dot{\underline{X}}_0,\underline{b}_0) + \left.\frac{\partial F_A}{\partial \underline{X}}\right|_0 (\underline{X}-\underline{X}_0) + \left.\frac{\partial F_A}{\partial \dot{\underline{X}}}\right|_0 \dot{\underline{X}} + \left.\frac{\partial F_A}{\partial \underline{b}}\right|_0 \underline{b} \quad \text{(A.53)}$$

Those three partial derivatives modify the natural frequencies of the system and consequently influence the stability itself. Recalling the expression of the aerodynamic forces found in $QSTC$:

$$F_y = \frac{1}{2}\rho V_{rel}^2 BL(C_D(\alpha)\cos\psi + C_L(\alpha)\sin\psi) \quad \text{(A.54)}$$

$$F_z = \frac{1}{2}\rho V_{rel}^2 BL(C_D(\alpha)\sin\psi + C_L(\alpha)\cos\psi) \quad \text{(A.55)}$$

$$F_\vartheta = \frac{1}{2}\rho V_{rel}^2 B^2 L C_M(\alpha) \quad \text{(A.56)}$$

It is needed the linearization of the aerodynamic forces (A.54) (A.55) (A.56) around y_0, z_0 and ϑ_0, defining:

$$\begin{cases} \overline{y} = y - y_0 \\ \overline{z} = z - z_0 \\ \overline{\vartheta} = \vartheta - \vartheta_0 \end{cases}$$

And we obtain:

$$\psi = \frac{w - B_1\dot{\overline{z}} - B_1\dot{\overline{\vartheta}}}{V} \quad \text{(A.57)}$$

$$\alpha = \overline{\vartheta} + \psi \quad \text{(A.58)}$$

$$\sin\psi = \psi \quad \text{(A.59)}$$

$$\cos\psi = 1 \quad \text{(A.60)}$$

$$V_{rel}^2 = V_m^2 + 2V_m v - 2V_m\dot{y} \quad \text{(A.61)}$$

$$\alpha_0 = 0 \quad \text{(A.62)}$$

$$C_D(\alpha) = C_{D0} + \left.\frac{\partial C_D}{\partial \alpha}\right|_0 (\alpha) = C_{D0} + K_D\alpha \quad \text{(A.63)}$$

$$C_L(\alpha) = C_{L0} + \left.\frac{\partial C_L}{\partial \alpha}\right|_0 (\alpha) = C_{L0} + K_L\alpha \quad \text{(A.64)}$$

$$C_M(\alpha) = C_{L0} + \left.\frac{\partial C_M}{\partial \alpha}\right|_0 (\alpha) = C_{M0} + K_M\alpha \quad \text{(A.65)}$$

Neglecting high order terms and subdividing the contribution of the aerodynamic forces into static $\underline{F}_{aero,st}$ and dynamic $\underline{F}_{aero,dyn}$:

$$\underline{F}_{aero,st} = \frac{1}{2}\rho S V_m^2 \begin{pmatrix} C_{D0} \\ C_{L0} \\ BC_{M0} \end{pmatrix} \tag{A.66}$$

$$\begin{aligned} \underline{F}_{aero,dyn} = \frac{1}{2}\rho S V_m^2 \begin{bmatrix} 0 & 0 & K_D \\ 0 & 0 & K_L \\ 0 & 0 & K_M \end{bmatrix} \overline{X} \\ - \frac{1}{2}\rho S V_m \begin{bmatrix} 2C_{D0} & (K_D - C_{L0}) & B_{1y}(K_D - C_{L0}) \\ 2C_{L0} & (K_L + C_{D0}) & B_{1z}(K_L - C_{D0}) \\ 2C_{M0}B & BK_M & B_{1\vartheta}BK_M \end{bmatrix} \dot{\overline{X}} \\ + \frac{1}{2}\rho S V_m \begin{bmatrix} 2C_{D0} & (K_D - C_{L0}) \\ 2C_{L0} & (K_L + C_{D0}) \\ 2C_{M0}B & BK_M \end{bmatrix} \underline{b} \end{aligned} \tag{A.67}$$

The dynamic contribution of aerodynamic foces $\underline{F}_{aero,dyn}$ can be rewritten in a compact way as :

$$\underline{F}_{aero,dyn} = -[K_{aero}]\overline{X} - [R_{aero}]\dot{\overline{X}} + [A_m]\underline{b} \tag{A.68}$$

Then the linearized equation of motion can be rewritten as:

$$[M_s]\ddot{\overline{X}} + ([R_s] + [R_{aero}])\dot{\overline{X}} + ([K_s] + [K_{aero}])\overline{X} = [A_m]\underline{b} \tag{A.69}$$

Where the $[M_s]$ $[K_s]$ $[R_s]$ are respectively the modal structural mass, damping and stiffness matrices and they are diagonal:

$$[M_s] = \begin{bmatrix} m_y & & \\ & m_z & \\ & & J \end{bmatrix} \qquad [R_s] = \begin{bmatrix} r_y & & \\ & r_z & \\ & & r_\vartheta \end{bmatrix} \qquad [K_s] = \begin{bmatrix} k_y & & \\ & k_z & \\ & & k_\vartheta \end{bmatrix}$$

$[K_{aero}]$ and $[R_{aero}]$ are the equivalent stiffness and damping matrices due to aerodynamic forces. The $[K_{aero}]$ and $[R_{aero}]$ multiplied respectively for the velocity vector $\dot{\overline{X}}$ and stiffness vector $\overline{X}$ are responsible of the aerodynamic forces function of the motion, while $[A_m]$ multiplied by the vector of the turbulence components $\underline{b}$ defines the aerodynamic forces because of the incoming turbulence.

The matrix $[K_{aero}]$ changes the natural frequency of the system with respect the ones computed in absence of the wind excitation, while $[R_{aero}]$ changes the system overall damping. Depending on the terms inside these two matrix is possible to meet the $one - degree$ of freedom and $flutter$ instability. But in order to verify the stability of the system we need to compute the *homogeneous* equation.

A.5 Aerodynamic forces identification through wind tunnel tests

Until now we have studied the aerodynamic forces using the *Quasi steady theory*, but this approach is valid when the reduced velocity V^* is high enough. We have to define the forces due to incident wind also in case of low reduced velocity. For this reason it is necessary to the define through wind tunnel testing drag, lift and moment as a function of y, z, ϑ, and u, w turbulence components.

Matrices $[K_{aero}]$ and $[R_{aero}]$ contain so called *flutter derivatives*, while the matrix $[A_m]$ is called *admittance matrix*.

A.5.1 Flutter derivatives identification

We can consider two methods in order experimentally define *flutter derivatives* or forces identification as a function of the bridge motion:

1. Free motion method
2. Forced motion method

The main difference between the two approaches is that the second is much reliable but is more expensive.

Free motion method

During the wind tunnel tests the deck sectional model, linked to an elastic supporting systems, is let free to vibrate under the V_m wind action. The response of the system to fixed initial condition is recorded.

Flutter derivatives are defined by comparing the response of the structure under the action of the mean wind V_m and the one in still air. Excitation of torsional and vertical modes have to be considered in order to define properly *flutter derivatives*.

Forced motion method

As explained above, this method is more reliable and expensive with respect the previous one. A deck sectional model is forced to vibrate by means of hydraulic or electromagnetic actuators (Figure XX) and then the response to this forced motion is computed.

The aerodynamic forces, as previously said, are non linear function of the motion of deck:

$$F_y = F_L = \frac{1}{2}\rho V^2 S C_L\left(\underline{X}, \underline{\dot{X}}, V_m, \underline{b}\right) \tag{A.70}$$

$$F_z = F_D = \frac{1}{2}\rho V^2 S C_D\left(\underline{X}, \underline{\dot{X}}, V_m, \underline{b}\right) \tag{A.71}$$

$$F_\vartheta = F_M = \frac{1}{2}\rho V^2 S B C_M\left(\underline{X}, \underline{\dot{X}}, V_m, \underline{b}\right) \tag{A.72}$$

Figure XX: Forced motion testing on a deck sectional model

There are many formulation of *flutter derivatives* changing university or country [24], the *PoliMi* notation of *flutter derivatives* is given by:

$$F_y^{se} = \frac{1}{2}\rho V^2 BL\left(-p_1^*\frac{\dot{z}}{V} - p_2^*\frac{B\dot{\vartheta}}{V} + p_3^*\vartheta + p_4^*\frac{\pi}{2V_\omega^{*2}}\frac{z}{B} - p_5^*\frac{\dot{y}}{V} + p_6^*\frac{\pi}{2V_\omega^{*2}}\frac{y}{B}\right) \quad \text{(A.73)}$$

$$F_z^{se} = \frac{1}{2}\rho V^2 BL\left(-h_1^*\frac{\dot{z}}{V} - h_2^*\frac{B\dot{\vartheta}}{V} + h_3^*\vartheta + h_4^*\frac{\pi}{2V_\omega^{*2}}\frac{z}{B} - h_5^*\frac{\dot{y}}{V} + h_6^*\frac{\pi}{2V_\omega^{*2}}\frac{y}{B}\right) \quad \text{(A.74)}$$

$$M^{se} = \frac{1}{2}\rho V^2 B^2 L\left(-a_1^*\frac{\dot{z}}{V} - a_2^*\frac{B\dot{\vartheta}}{V} + a_3^*\vartheta + a_4^*\frac{\pi}{2V_\omega^{*2}}\frac{z}{B} - a_5^*\frac{\dot{y}}{V} + a_6^*\frac{\pi}{2V_\omega^{*2}}\frac{y}{B}\right) \quad \text{(A.75)}$$

Where:

- $V_\omega^* = v^*/2\pi$
- p_i^* = Flutter derivatives of the drag force (i = 1, ..., 6)
- h_i^* = Flutter derivatives of the lift force (i = 1, ..., 6)
- a_i^* = Flutter derivatives of the pitching moment (i = 1, ..., 6)

Grouping (A.73) (A.74) (A.75) in compact matrix form it is possible to define K_{aero} and R_{aero} matrices containing the *flutter derivatives* :

$$[K_{aero}] = -\frac{1}{2}\rho BLV^2 \begin{bmatrix} p_6^* \frac{\pi}{2V_\omega^{*2}} \frac{1}{B} & p_4^* \frac{\pi}{2V_\omega^{*2}} \frac{1}{B} & p_3^* \\ h_6^* \frac{\pi}{2V_\omega^{*2}} \frac{1}{B} & h_4^* \frac{\pi}{2V_\omega^{*2}} \frac{1}{B} & h_3^* \\ a_6^* \frac{\pi}{2V_\omega^{*2}} \frac{1}{B} B & a_4^* \frac{\pi}{2V_\omega^{*2}} \frac{1}{B} B & a_3^* B \end{bmatrix} \tag{A.76}$$

$$[R_{aero}] = -\frac{1}{2}\rho BLV^2 \begin{bmatrix} p_5^* \frac{1}{V} & p_1^* \frac{1}{V} & p_2^* \frac{B}{V} \\ h_5^* \frac{1}{V} & h_5^* \frac{1}{V} & h_2^* \frac{B}{V} \\ a_5^* \frac{1}{V} B & a_1^* \frac{1}{V} B & a_2^* \frac{B}{V} \end{bmatrix} \tag{A.77}$$

Flutter derivatives are function of the frequency of the motion, but also of the static equilibrium around which wind tunnel tests are done. The frequency of the motion is in general expressed in terms of reduced velocity $V^* = \frac{V}{fB}$

A.5.2 Aerodynamic admittance function

The best way to compute this matrix by means of wind tunnel testing is to identify the aerodynamic forces as a function of a well defined wind turbulence by means of an *active turbulence generator*. This device generates the w vertical component of turbulence that has a sinusoidal shape, while the deck position is fixed, and in this condition the forces are measured. It is necessary the definition of the transfer function between the turbulence and the measured forces in order to define the coefficients of the admittance matrix.

In 1962, Davenport [3] [4] presented a model for computing fluctuating wind loads on structure immersed in the *atmospheric boundary layer*. The *admittance functions* are responsible of converting the air flow properties in wind loads on the structure. According to the Davenport's approach, buffeting forces acting on a section of the deck of length L are defined in this way:

$$[\underline{F}_{buff}] = \begin{Bmatrix} F_y \\ F_z \\ M \end{Bmatrix}_{buff} = \frac{1}{2}\rho V^2 BL \begin{bmatrix} \chi_{yu}^* & \chi_{yw}^* \\ \chi_{zu}^* & \chi_{zw}^* \\ B\chi_{\vartheta u}^* & B\chi_{\vartheta w}^* \end{bmatrix} \begin{Bmatrix} \frac{u}{V} \\ \frac{w}{V} \end{Bmatrix} \tag{A.78}$$

Where:

- $\chi^*(f^*)$ are the complex admitance function
- $f^* = \frac{fB}{V}$

Considering only the turbulence fluctuations related to the w component we can define the associated aerodynamic forces as:

$$F_y = \frac{1}{2}\rho V^2 BL \left[Re(\chi_{yw}^*)\frac{\omega}{V} + iIm(\chi_{yw}^*)\frac{\omega}{V} \right] \tag{A.79}$$

$$F_z = \frac{1}{2}\rho V^2 BL \left[Re(\chi_{zw}^*)\frac{\omega}{V} + iIm(\chi_{zw}^*)\frac{\omega}{V} \right] \tag{A.80}$$

$$M = \frac{1}{2}\rho V^2 BL \left[Re(\chi_{\vartheta w}^*)\frac{\omega}{V} + iIm(\chi_{\vartheta w}^*)\frac{\omega}{V} \right] \tag{A.81}$$

The Davenport model is one of the formulations available in literature, but it is one of the most commonly used. The admittance matrix coefficients can be obtained through proper wind tunnel testing or using the QST values weighted by the Davenport adimittance in this way:

$$\chi^*_{yu} = 2C_D A(f^*); \quad \chi^*_{yu} = 2C_L A(f^*); \quad \chi^*_{\vartheta u} = 2C_M A(f^*) \tag{A.82}$$

$$\chi^*_{yw} = (K_D - C_L)A(f^*); \quad \chi^*_{zw} = (K_L + C_D)A(f^*); \quad \chi^*_{\vartheta w} = K_M A(f^*) \tag{A.83}$$

Where $A(f^*)$ is a real function responsible of weighting in frequency the QST values of the buffeting forces:

$$A(f^*) = \frac{2}{(7f^*)^2}(7f^* - 1 + e^{-7f^*}) \tag{A.84}$$

The trend of $A(f^*)$ as a function of the reduced frequency and velocity can be observed in figures XXI XXII

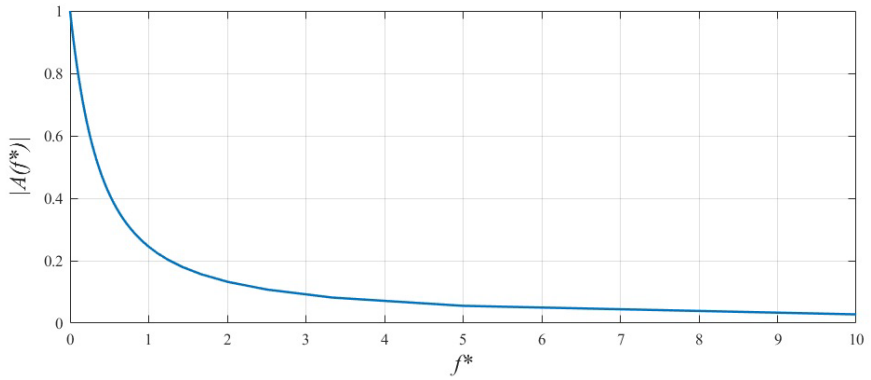

Figure XXI: $A(f^*)$ as a function of the reduced frequency

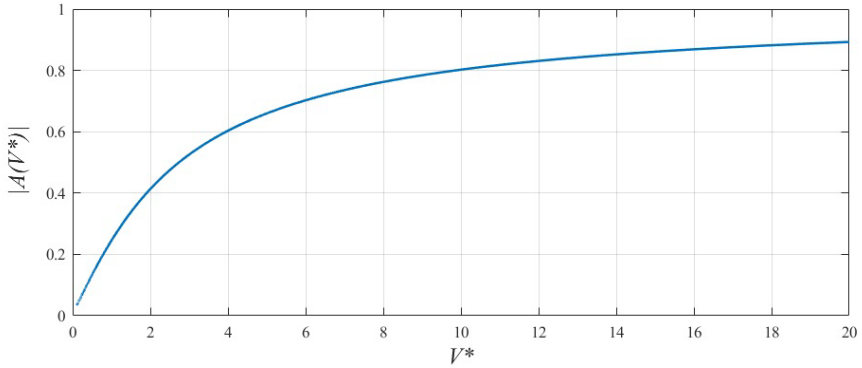

Figure XXII: $A(f^*)$ as a function of the reduced velocity

The admittance matrix can be defined as:

$$[A_m] = \frac{1}{2}\rho V^2 BL \begin{bmatrix} \chi^*_{yu} & \chi^*_{yw} \\ \chi^*_{zu} & \chi^*_{zw} \\ B\chi^*_{\vartheta u} & B\chi^*_{\vartheta w} \end{bmatrix} \tag{A.85}$$

Bibliography

[1] Guy L. Larose. "Experimental determination of the aerodynamic admittance of a bridge deck segment". In: 1999.

[2] Jasna B. Jakobsen. "Span-wise structure of lift and overturning moment on a motionless bridge girder". In: 1997.

[3] A. G. Davenport. "The response of slender, line-like structures to a gusty wind." In: *Proceedings of the Institution of Civil Engineers* 23.3 (1962), pp. 389–408.

[4] A. G. Davenport. "Buffeting of a Suspension Bridge by Storm Winds". In: 1962.

[5] Einar Strømmen. "Theory of Bridge Aerodynamics". In: (Jan. 2010).

[6] Guy Larose. "The dynamic action of gusty winds on long-span bridges". PhD thesis. Aug. 1997. ISBN: 87-7877-088-2.

[7] A. G. Davenport. "The spectrum of horizontal gustiness near the ground in high winds". In: *Quarterly Journal of the Royal Meteorological Society* 87.372 (1961), pp. 194–211. URL: https://rmets.onlinelibrary.wiley.com/doi/abs/10.1002/qj.49708737208.

[8] G. Naito. "Spatial structure of surface wind over the ocean". In: *Journal of Wind Engineering and Industrial Aerodynamics* 13.1 (1983), pp. 67–76. ISSN: 0167-6105. URL: http://www.sciencedirect.com/science/article/pii/0167610583901290.

[9] Masaru Kiya and Kyuro Sasaki. "Structure of a turbulent separation bubble". In: *Journal of Fluid Mechanics* 137 (1983), pp. 83–113.

[10] W.H. Melbourne. "Comparison of model and full-scale tests of a bridge and chimney stack". In: *Proc. of Int'l Workshop on Wind Tunnel Modelling, Maryland, USA*. 1982, pp. 637–653.

[11] E Hjorth-Hansen, A Jakobsen, and E Strømmen. "Wind buffeting of a rectangular box girder bridge". In: *Journal of Wind Engineering and Industrial Aerodynamics* 42.1-3 (1992), pp. 1215–1226.

[12] K. Kimura et al. "Characteristics of buffeting forces on flat cylinders". In: *Journal of Wind Engineering and Industrial Aerodynamics* 69-71 (1997). Proceedings of the 3rd International Colloqium on Bluff Body Aerodynamics and Applications, pp. 365–374. ISSN: 0167-6105. URL: http://www.sciencedirect.com/science/article/pii/S0167610597001694.

[13] Hamlyn Peter A.H. Irwin. "Wind tunnel and analytical investigations of the response of Lions' Gate Bridge to a turbulent wind". In: *National Research Council Canada june* (1977).

[14] G. Diana and F. Cheli. *Dinamica e vibrazioni dei sistemi meccanici*. Dinamica e vibrazioni dei sistemi meccanici v. 1, v.2. UTET Università, 1993. ISBN: 9788877502292. URL: https://books.google.it/books?id=aPBeAAAACAAJ.

[15] Xinzhong Chen, Ahsan Kareem, and Masaru Matsumoto. "Multimode coupled flutter and buffeting analysis of long span bridges". In: *Journal of Wind Engineering and Industrial Aerodynamics* 89.7 (2001). 10th International Conference on Wind Engineering, pp. 649–664. ISSN: 0167-6105. URL: http://www.sciencedirect.com/science/article/pii/S0167610501000642.

[16] F. Brancaleoni et al. *The Messina Strait Bridge: A Challenge and a Dream*. CRC Press, 2009. ISBN: 9781482266368. URL: https://books.google.it/books?id=1WG1DwAAQBAJ.

[17] N.J. Cook. *The Designer's Guide to Wind Loading of Building Structures: Part 2 : Static Structures*. Building Research Establishment report. Butterworths, 1990. ISBN: 9780408008716. URL: https://books.google.it/books?id=I0RSAAAAMAAJ.

[18] R.B. Stull. *An Introduction to Boundary Layer Meteorology*. Atmospheric and Oceanographic Sciences Library. Springer Netherlands, 1988. ISBN: 9789027727695. URL: https://books.google.it/books?id=eRRz9RNvNOkC.

[19] Isaac van der Hoven. "POWER SPECTRUM OF HORIZONTAL WIND SPEED IN THE FREQUENCY RANGE FROM 0.0007 TO 900 CYCLES PER HOUR". In: 1957.

[20] C. Dyrbye and S.O. Hansen. *Wind Loads on Structures*. Wiley, 1997. ISBN: 9780471956518. URL: https://books.google.it/books?id=fb7EQgAACAAJ.

[21] *Characteristics of atmospheric turbulence near the ground. Part 2*. Unknow. Oct. 1985.

[22] G. Diana et al. "Suspension bridge parameter identification in full scale test". In: *Journal of Wind Engineering and Industrial Aerodynamics* 41.1 (1992), pp. 165–176. ISSN: 0167-6105. URL: http://www.sciencedirect.com/science/article/pii/016761059290404X.

[23] Giorgio Diana et al. "Comparisons between wind tunnel tests on a full aeroelastic model of the proposed bridge over Stretto di Messina and numerical results". In: 1995.

[24] Alberto Zasso. "Flutter Derivatives: Advantages of a New Representation Convention". In: 1996.